Chimie des atmosphères planétaires : de la Terre à Titan , de Titan à la Terre primitive

Nathalie Carrasco

UNIVERSITE DE VERSAILLES
SAINT-QUENTIN-EN-YVELINES

HABILITATION A DIRIGER DES RECHERCHES

Dr Nathalie Carrasco
Maître de Conférences à l'Université de Versailles St Quentin
Discipline : Astronomie et Astrophysique

« Chimie des atmosphères planétaires : de la Terre à Titan , de Titan à la Terre primitive»

Soutenue le 5 janvier 2012 à l'Observatoire des Versailles Saint Quentin, site de Guyancourt

Membres du Jury :
Rapporteurs
- Pr. Marc Smith, Doyen de l'Université des Sciences de Houston
- Dr. Fabienne Poncin-Epaillard, Université du Maine
- Dr. Jean-Claude Guillemin, ENSC de Rennes

Examinateurs
- Pr. Philippe Bousquet, Président du jury
- Michel Viso, Responsable thématique d'exobiologie du CNES
- Pr. Guy Cernogora, tuteur

1. Introduction

La Terre et Titan, plus gros satellite de Saturne, (Figure 1) sont souvent comparés pour leurs similitudes atmosphériques : tous deux présentent en effet une atmosphère dense de l'ordre du bar de pression à la surface, majoritairement composée d'azote. La Terre se trouve dans des conditions de température et de pression compatibles avec les trois états physiques de l'eau, Titan avec ceux du méthane. Ils présentent donc tous deux des cycles d'évaporation-condensation-sublimation intenses, responsables du développement d'étendues liquides en surface, de nuages et de pluie. La présence de lacs (Stephan et al., 2010) et de phénomènes de pluies (Turtle et al., 2011) a ainsi été récemment confirmée par la mission Cassini. Les principales caractéristiques de ces deux corps sont reportées dans le Tableau 1.

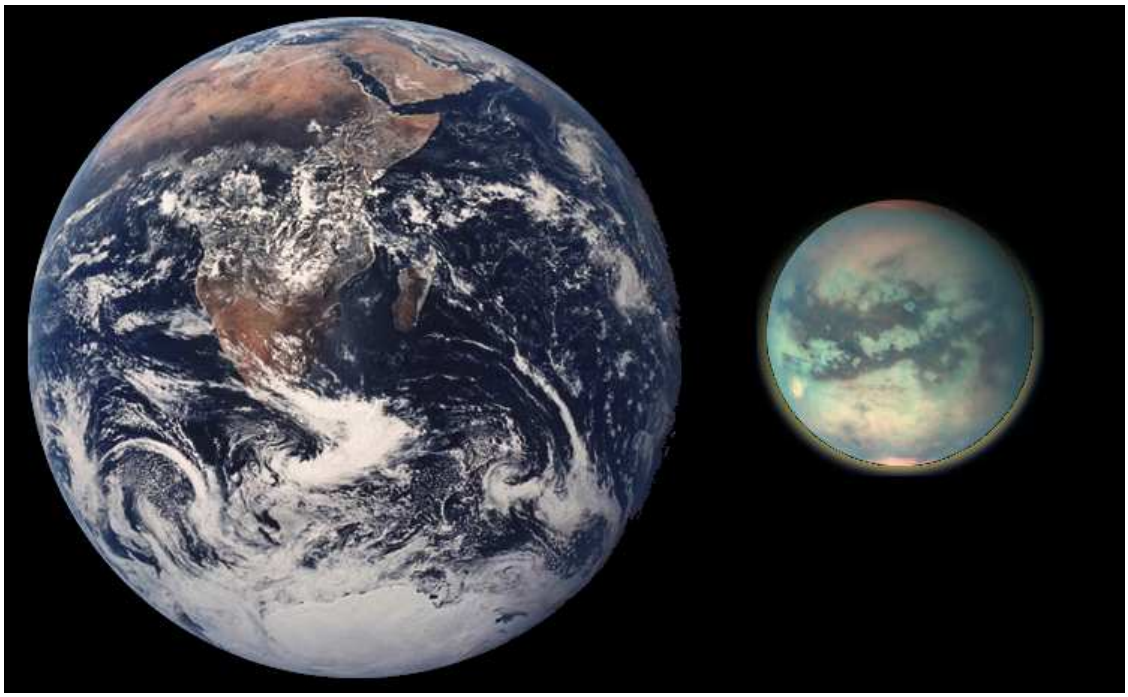

Figure 1: Comparaison de la Terre et de Titan. Copyright NASA.

Du point de vue de leur réactivité atmosphérique respective, une différence majeure les sépare : la présence sur le Terre d'oxygène atmosphérique issu de l'activité biologique. L'atmosphère de Titan, dénuée de dioxygène, est donc souvent suggérée comme un analogue froid d'une atmosphère primitive terrestre, avant que n'apparaisse la vie.
Sur Terre, nous nous intéressons donc à une chimie atmosphérique oxydante, indissociable de l'activité biologique. Sur Titan, nous considérons une chimie atmosphérique réductrice dénuée d'oxygène, d'intérêt prébiotique pour comprendre comment les processus chimiques atmosphériques peuvent former des matériaux complexes, potentielles briques pour l'apparition du vivant.

	Terre	Titan
Masse	5,9.1024 Kg	1,3.1023 Kg
Rayon	6378 km	2575 km
Distance au Soleil	1 u.a	9.5 u.a.
Température de surface	+15℃	**-** 180℃
Pression de surface	105 Pa	1.5 ×105 Pa
Composition Atmospherique	N_2 78,1 % O_2 20,9 %	N_2 98 %, CH_4 1.8 %

Tableau 1: Comparaison des principales caractéristique Terre - Titan.

Des expériences de recherche complémentaires m'ont permis d'aborder l'étude de la chimie atmosphérique de ces deux corps du système solaire avec des approches variées.
A l'occasion du M2-R et de la thèse j'ai travaillé sur la pollution atmosphérique terrestre par simulation expérimentale de laboratoire. Plus précisément j'ai étudié les vitesses et mécanismes de réactions d'oxydation de composés organiques émis dans l'atmosphère par des sources d'émission biotiques.
En post-doc, j'ai effectué une mobilité thématique vers un sujet de planétologie à des fins d'interprétation de données d'observation de la mission spatiale Cassini : l'étude de la réactivité en phase gazeuse dans l'ionosphère de Titan par modélisation numérique.
Enfin, en tant que Maître de Conférence depuis 2007, je développe les activités de chimie atmosphérique de Titan à l'UVSQ au LATMOS selon deux approches complémentaires : modélisation numérique/statistique et simulation expérimentale des brouillards organiques solides dans l'atmosphère de Titan.
Après une présentation du bilan scientifique de ces dix ans d'activité de recherche sur les réactivités atmosphériques planétaires, je développerai mes axes de direction de recherche envisagés pour les années à venir. Ils concernent l'étude de la chimie atmosphérique de Titan, ainsi que celle de l'atmosphère primitive terrestre. Ces travaux m'amèneront à poursuivre les co-encadrements de thèse de T. Gautier et de Z. Peng dans les deux années à venir sur la chimie de Titan, et à proposer une thèse en pleine direction sur la réactivité de la Terre primitive en septembre 2012.

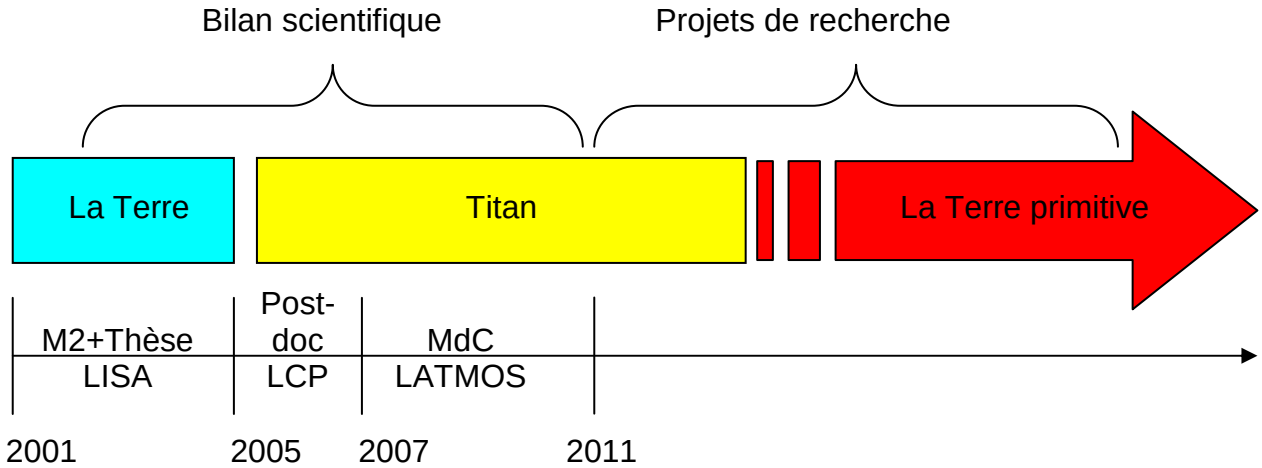

Figure 2: schéma de mon parcours et de mon projet de recherche.

Table des matières

2. Curriculum Vitae

2.1. Éléments de carrière

Carrière

Sep 2007 – Auj.	Maître de conférences, en section 34, Astronomie & Astrophysique, à l'Université de Versailles Saint-Quentin, au Laboratoire ATmosphères, Milieux, Observations Spatiales, dans l'équipe de Sciences Planétaires. • Recherche : réactivité chimique dans l'atmosphère de Titan. • Enseignement : Physique-chimie de l'Environnement de l'Observatoire de Versailles Saint Quentin (OVSQ), et responsable du parcours de Planétologie de l'UVSQ.
2007-2005	Position post-doctorale de 2 ans à l'Université de Paris-Sud 11 Orsay, « Laboratoire de Chimie-Physique », sous la responsabilité de Pascal Pernot. Supports financiers : 12 mois CNRS, 11 mois CNES. Sujet de recherche : modélisation de la réactivité ionosphérique de Titan et identification des processus clés responsables de la formation des molécules complexes détectées par Cassini.

Formation

Sep 2005 Sep 2002	Thèse de chimie atmosphérique au LISA (CNRS/Univ. Paris 7) Mention très Honorable avec les Félicitations du jury. « Simulation expérimentale de la réactivité atmosphérique de trois composés majeurs d'origine biotique », sous la direction de Patrick Carlier† et J-F. Doussin. + Monitorat Paris VII
2001	M2-R de « Chimie de la Pollution Atmosphérique et Physique de l'Environnement » de Paris 7. Stage au Laboratoire des Systèmes Atmosphériques (LISA), à Créteil, sur la cinétique d'ozonolyse de l'isoprène et du Methylbutènol. 1ère/20.
2001	Obtention de l'agrégation de sciences physiques - option chimie
2001-1998	Elève normalienne à l'Ecole Normale Supérieure de Cachan / obtention du Magistère de Physico-Chimie Moléculaire d'Orsay
1995-98	Classe préparatoire aux Grandes Ecoles. PCSI à Henri IV, Paris, et PC* à Fénelon, Paris

Compétences

Expérimentation	– Réacteur de Simulation Atmosphérique ; – Spectroscopie optique : spectroscopie d'émission dans l'UV-Vis pour l'analyse de plasma, FTIR pour l'analyse de phases gazeuse et solide ; – Spectrométrie de masse : analyse des neutres et ions *in-situ* et analyse *ex-situ* des aérosols
Modélisation	– Analyse et propagation des incertitudes par simulation Monte Carlo, et analyse de sensibilité dans des modèles physico-chimiques ; – Modélisation de systèmes cinétiques complexes

2.2. Bilan scientifique

2.2.1. Liste des publications dans des journaux de rang A

1. E. Sciamma-O'Brien; P.-R. Dahoo; E. Hadamcik; **N. Carrasco**; E. Quirico; C. Szopa; G. Cernogora (2011) Optical constants from 370 nm to 900 nm of Titan tholins produced in a low pressure RF plasma discharge, *Icarus*, soumis.

2. S. Plessis, **N. Carrasco**, M. Dobrijevic and P. Pernot (2011) Production of neutral species in Titan's ionosphere through dissociative recombination of ions, *Icarus*, soumis.

3. **N. Carrasco**, T. Gautier, Et. Es-sebbar, P. Pernot, G. Cernogora, (2011) Volatile products controlling Titan's tholins production, *Icarus*, soumis.

4. J. H. Westlake, J.H. Waite Jr., K.E. Mandt, **N. Carrasco**, J.M. Bell, B.A. Magee, J-E. Wahlund (2011) Titan's ionospheric composition and structure Part I:Photochemical modelling of Cassini INMS data. *JGR-Planets*. soumis.

5. J. H. Westlake, J.H. Waite Jr., D.T. Young, K.E. Mandt, B.A. Magee, F.J. Crary, **N. Carrasco** and J.-E. Wahlund (2011) Titan's ionospheric composition and structure Part II: Large ion composition and growth. *JGR-Planets*. soumis

6. S. Hörst, R. Yelle, A. Buch, **N. Carrasco**, G. Cernogora, O. Dutuit, E. Quirico, E. Sciamma-O'Brien, M. Smith, A. Somogyi, C. Szopa, R. Thissen, V. Vuitton (2011) Formation of Prebiotic Molecules in a Titan Atmosphere Simulation Experiment, *Astrobiology*, soumis.

7. P. Pernot, S. Plessis and **N. Carrasco** (2011) Probabilistic representations of partial branching ratios: bridging the gap between experiments and chemical models. *J. Phys.: Conf. Ser.*, 300: p. 012027

8. T. Gautier, **N. Carrasco**, A. Buch, C. Szopa, E. Sciamma-O'Brien, G. Cernogora (2011) Nitrile gas chemistry in Titan atmosphere, *Icarus*, 213(2) : pp. 625-635.

9. S. Plessis, **N. Carrasco** and P. Pernot (2010) Knowledge-based probabilistic representations of branching ratios in chemical networks: the case of dissociative recombinations, *Journal of Chemical Physics*, 133: 134110.

10. Z. Peng, M. Dobrijevic, E. Hébrard, **N. Carrasco** and P. Pernot (2010) Photochemical modeling of Titan atmosphere at the "10 percent uncertainty horizon", *Faraday Discussions*, 147(6)

11. V. Vuitton, J-.Y. Bonnet, M. Frisari, R. Thissen, E. Quirico, O. Dutuit, B. Schmitt, L. Le Roy, N. Fray, H. Cottin, E. Sciamma-O-Brien, **N. Carrasco** and C. Szopa (2010) Very high resolution mass spectrometry of HCN polymers and tholins, *Faraday Discussions*, 147(23)

12. E. Sciamma-O'Brien, **N. Carrasco**, C. Szopa, A. Buch, G. Cernogora (2010) Titan's atmosphere: an optimal gaz mixture for aerosol production ? *Icarus* 209, pp. 704–714.

13. P. Pernot, **N. Carrasco**, R. Thissen and I. Schmitz-Afonso (2010) Tholinomics - Chemical analysis of nitrogen-rich polymers. *Analytical Chemistry* 82(4), pp 1371–1380

14. B. Gans, L. Vieira-Mendes, S. Boyé-Peronne, S. Douin, G. Garcia, H. Soldi-Lose, B. Cunha de Miranda, C. Alcaraz, **N. Carrasco**, P. Pernot, D. Gauyacq (2010) Determination of the absolute photoionization cross section of CH_3 and I produced from a pyrolysis source, by combined synchrotron and VUV Laser studies. *J. Phys. Chem. A* 114, 9 : 3237–3246]

15. M. Dobrijevic, E. Hébrard, S. Plessis, **N. Carrasco**, P. Pernot, M. Bruno-Claeys. (2010) Comparison of methods for the determination of key reactions in chemical systems: Application to Titan's atmosphere. *Advances in Space Research* 45(1), p.77-91.

16. **N. Carrasco**, I. Schmitz-Afonso, J-Y. Bonnet, E. Quirico, R. Thissen, Odile Dutuit, A. Bagag, O. Laprévote, A. Buch, A. Giulani, Gilles Adandé, F. Ouni, E. Hadamcik, C. Szopa, G. Cernogora. (2009) Chemical characterization of tholins: Solubility, Morphology and Molecular Structure revisited. *J. Phys. Chem A* 113(42), p.11195-11203.

17. E. Hébrard, P. Pernot, M. Dobrijevic, **N. Carrasco**, A. Bergeat, K. M. Hickson, A. Canosa, S. Le Picard, and I. R. Sims (2009) How measurements of rate constants at low temperature increase the predictivity of photochemical models of Titan's atmosphere. *J. Phys. Chem A* 113(42) p.11227-11237.

18. **N. Carrasco**, S. Plessis, M. Dobrijevic and P. Pernot. (2008). Towards a reduction of the bimolecular reaction model for Titan ionosphere. *Int. J. Chem. Kinetics* 40(11): 699-709.

19. M. Dobrijevic, **N. Carrasco**, E. Hébrard and P. Pernot (2008) Epistemic bimodality and kinetic hypersensitivity in photochemical models of Titan's atmosphere. *Planetary and Space Science* 56(12): 1630-1643.

20. **N. Carrasco**, O. Dutuit, R. Thissen, C. Alcaraz, S. Plessis, V. Vuitton, R. Yelle and P. Pernot (2008) Sensitivity of a Titan ionospheric model to the ion-molecule reaction parameters. *Planetary and Space Science* 56(12) : 1644-1657.

21. **N. Carrasco**, E. Hébrard, M. Banaszkiewicz, M. Dobrijevic and P. Pernot.(2007) Influence of neutral transport on ion chemistry uncertainties in Titan ionosphere. *Icarus* 192:519-526.

22. **N. Carrasco** and P. Pernot (2007) Modeling of branching ratio uncertainty in chemical networks by Dirichlet distributions. *J. Phys. Chem. A* 111:3507-3512.

23. **N. Carrasco**, O. Dutuit, R. Thissen, M. Banaszkiewicz and P. Pernot. (2007) Uncertainty analysis of bimolecular reactions in Titan ionosphere chemistry model. *Planetary and Space Science* 55:141-157.

24. **N. Carrasco**, B. Picquet-Varrault and J.F. Doussin. (2007) Kinetic and mechanistic study of the reaction of sabinaketone with OH radicals. *International Journal of Chemical Kinetics* 39(7): 415-421.

25. **N. Carrasco**, J.F. Doussin, M. O'Connor, J.C. Wenger and B. Picquet-Varrault, R. Durand-Jolibois and P. Carlier (2007). Simulation studies of the atmospheric oxidation of 2-Methyl-3-Buten-Ol : reactions with hydroxy radicals and ozone under a variety of conditions. *Journal of Atmospheric Chemistry* 56(1): 33-55.

26. L. Chiappini, **N. Carrasco**, B. Temine, B. Picquet-Varrault , R. Durand-Jolibois, J.C. Wenger and J.F. Doussin (2006). Gaseous and Particulate Products from the Atmospheric Ozonolysis of a Biogenic Hydrocarbon, Sabinene. *Environmental Chemistry* 3(4): 286-296.

27. **N. Carrasco**, M.T. Rayez, J.C. Rayez and J.F. Doussin (2006). Experimental and theoretical study of the reaction of OH radical with sabinene. *Physical Chemistry and Chemical Physics* 8(27): 3211-3217.

28. **N. Carrasco**, J.F. Doussin, B. Picquet-Varrault and P. Carlier (2006). Tropospheric degradation of 2-Hydroxy-2-MethylPropanal, a photoxydation product of 2-Methyl-3-Buten-Ol: kinetic and mechanistic study of its photolysis and its reaction with OH radicals. *Atmospheric Environment* 40 (11): 2011-2019.

29. **N. Klawatsch-Carrasco**, J.F. Doussin and P. Carlier (2004). Absolute rate constants for the gas-phase ozonolysis of isoprene and methylbutenol. *International Journal of Chemical Kinetics* 36(3): 152-156.

2.2.2. Communications orales dans des conférences nationales et internationales

Par concision, seules les présentations que j'ai effectuées sont répertoriées ; pas les présentations dont je suis co-auteurs (idem à la section suivante, « communications affichées »).

1. N. Carrasco (janvier 2012) The active role of Nitrogen in the organic aerosol production in Titan's atmosphere, (**invitée**) Gordon Research Conference (GRC) on the Origin of Life, Galveston, Texas, USA.

2. N. Carrasco, E. Essebbar, T. Gautier, E. Sciamma-O'Brien, and G. Cernogora (octobre 2011) "An RF plasma experiment to simulate the production of Titan's atmospheric aerosols, EPSC-DPS, Nantes.

3. N. Carrasco, S. Plessis, P. Pernot (octobre 2011) "Production of neutral species in Titan's ionosphere through dissociative recombination of ions as measured by INMS" EPSC-DPS, Nantes.

4. N. Carrasco, (septembre 2011) "Nitrogen containing volatile products controlling Titan's organic aerosol production"; COST CM0805 WG3 group - Nitrogen in planetary systems: the early evolution of the atmospheres of terrestrial planets: the role of nitrogen. Barcelone, Espagne.

5. N. Carrasco, T. Gautier, G. Cernogora (avril 2011) Titan-like reactors to simulate globally the chemistry in Titan's atmosphere, (**invitée**) Fifth Workshop on Titan Chemistry, Hawaii, USA.

6. N. Carrasco (janv 2011) Simulation of Titan Photochemistry By SOLEIL VUV-EUV Beamline. SOLEIL Users' Meeting 2011, Polytechnique, Paris.

7. N. Carrasco, T. Gautier, A. Buch, C. Szopa, G. Cernogora (janv 2011) Gas phase chemistry in a plasma setup simulating Titan atmospheric reactivity, 18th Symposium on Application of Plasma Processes - Workshop on Plasmas as a Planetary Atmosphere Mimics, (**invitée**) Vrátna, Malá Fatra, Slovaquie.

8. N. Carrasco, T. Gautier, E. Sciamma-O'Brien, C. Szopa, G. Cernogora, A. Buch, P. Pernot. (sept 2010) Gaseous chemistry for a Titan's atmospheric plasma experimental simulation, EPSC, Rome

9. N. Carrasco, P. Pernot, C. Szopa, R. Thissen, and the orbitrap team (septembre 2010) High resolution mass spectrometry for Titan's aerosol analysis. EPSC, Rome.

10. N. Carrasco, G. Cernogora, C. Szopa, E. Hadamcik, J-J. Correia, E. O'Brien, T. Gautier, P. Pernot, A. Buch, R. Thissen, E. Quirico, V. Vuitton, O. Dutuit, I. Schmitz-Afonso (sept 2010) Structure polymérique des tholins de Titan, PNP, Brest.

11. N. Carrasco (juillet 2010) Processus de croissance des aérosols solides de Titan, « Chimie sur des poudres immergées dans des plasmas », Albi (**invitée**)

12. N. Carrasco, E. O'Brien, C. Szopa, G. Cernogora (2009) Titan's atmosphere: an optimized mixture for gas-particle conversion. 41st annual meeting of the Division for Planetary Sciences (DPS). Puerto Rico, EU.

13. N. Carrasco, P. Pernot, C. Szopa, G. Cernogora (2008) "Growth process of the organic matter in Titan upper atmosphere" 40st annual meeting of the DPS, Ithaca, EU.

14. N. Carrasco, E. Hébrard, M. Dobrijevic, P. Pernot (2007) "Uncertainty analysis in A Titan ionospheric chemistry model" Fifth International Conference on Sensitivity Analysis of Model Output, Budapest, Hongrie.

15. N. Carrasco, P. Pernot, M. Dobrijevic, E. Hébrard (2007) Uncertainty analysis in Titan ionospheric chemistry models, ESPC, Berlin, Allemagne.

16. N. Carrasco and P. Pernot (2007) "Uncertainty propagation and sensitivity analysis: providing insights for simulation of Cassini's INMS ions data", First Workshop on 'Titan - Observations, Experiments, Computations, and Modeling' Honolulu, Hawaï.

17. N. Carrasco (2005). "Atmospheric chemistry of methylbutenol: an important source of acetone in the troposphere". International Conference on Environmental Science and Technology. New Orleans, EU.

18. N. Carrasco (2004). "Etude du devenir troposphérique d'un composé biogénique majeur : le sabinène ». Journée de Cinétique et de Photochimie. Bordeaux.

19. N. Carrasco (2003). "Nouvelles données cinétiques et mécanistiques sur la réactivité atmosphérique de l'isoprène et du MBO ». Journée de Cinétique et de Photochimie. Orléans.

2.2.3. Communications affichées dans des conférences internationales

1. N. Carrasco, I. Schmitz-Afonso, R. Thissen, A. Buch, E. Hadamcik, C. Szopa, G. Cernogora (2009) « Chemical analysis of dust produced in a N_2 CH_4 RF plasma discharge », The 19th International Symposium on Plasma Chemistry, Bochum, Allemagne.

2. P. Pernot.; E. Hébrard; M. Dobrijevic.; N. Carrasco; Bergeat, A.; Hickson, K. M.; Canosa, A.; Le Picard, S.; Sims, I. R. (2009) "How Measurements Of Rate Constants At Low Temperature Increase The Predictivity Of Photochemical Models Of Titans's Atmosphere", DPS Puerto Rico, EU.

3. N. Carrasco, S. Plessis, P. Pernot (2007) "Towards a reduction of Titan ionospheric chemistry model", EPSC, Potsdam, Allemagne.

4. N. Carrasco, P. Pernot, E. Hébrard, M. Dobrijevic, (2006) "Comparison of two major sources of uncertainty in Titan ionospheric chemistry: neutral densities and ion-molecule reactions." EPSC, Berlin, Allemagne.

5. N. Carrasco, O. Dutuit, R. Thissen, M. Banaszkiewicz et P. Pernot, (2006) "Analyse des incertitudes sur les réactions bimoléculaires dans un modèle de chimie ionosphérique de Titan. » Colloque PNP, Nancy.

6. N. Carrasco, P. Pernot, E. Hébrard, M. Dobrijevic, (2006) "Comparison of two major sources of uncertainty in Titan ionospheric chemistry: neutral densities and ion-molecule reactions." ICAMDATA 05, Meudon.

7. N. Klawatsch-Carrasco, J.F. Doussin, B. Picquet-Varrault and P. Carlier (2005) "Atmospheric chemistry of methylbutenol : ozone and acetone production in the troposphere." EGS. Vienne, Autriche.

8. N. Carrasco, J. Doussin, G. Rea, J. Wenger and P. Carlier (2003). "Kinetics and mechanism of the gas-phase reaction of ozone with MBO." EGS. Nice.

2.2.4. Actions de diffusion scientifique

Année mondiale de la Chimie : Nathalie Carrasco, « La chimie dans l'atmosphère de Titan », Conférence invitée sur le thème « La chimie dans les Etoiles » au Parc aux Etoiles, Triel sur Seine dans les Yvelines. 30 septembre 2011.

Journal du cnrs : Nathalie Carrasco, « Atmosphère de Titan : une révélation surprise », p.13, n°252-253 Janvier-février 2011.

Journal du synchrotron SOLEIL : article de vulgarisation sur les travaux effectués par l'équipe sur plusieurs lignes de lumière en 2010-2011. http://www.synchrotron-soleil.fr/Soleil/ToutesActualites/2011/titan

Participation au projet « 1000 chercheurs parlent d'avenir » – à l'occasion de la fête de la Science 18-24 octobre 2010– projet de l'artiste Pierre Maraval, projection sur la façade du Panthéon de 1000 portraits de chercheurs accompagnés d'un message de leur vision d'avenir

Organisation d’une **formation des enseignants du secondaire** à la mesure de la qualité de l’air, dans le cadre des formations du rectorat de l’Académie de Versailles.

Séminaires invités:

N. Carrasco (novembre 2011) « La photochimie dans l'atmosphère de Titan: du laboratoire à la mission embarquée » Atelier du CNES sur la Photolyse en orbite, Paris.

N. Carrasco (juillet 2011) « Experimental simulation of the chemistry in the upper atmosphere of Titan », Séminaire invitée à la 36ème réunion de la section "Physique et Chimie Matière Diluée/ Sciences de l'Univers », Synchrotron Soleil, Saint Aubin.

N. Carrasco (mars 2010) « Experimental simulation of Titan atmospheric chemistry by the radio-frequency plasma device PAMPRE », séminaire invité au CIRES, Boulder, USA.

N. Carrasco (janvier 2011) « Experimental simulation of Titan’s atmospheric haze: chemical and physical analysis of nitrogen-rich solid organic matter », séminaire invité au IPFN, Lisbonne, Portugal.

N. Carrasco (janvier 2010) « La simulation atmosphérique de Titan par plasma radio-fréquence », séminaire inivité au LCP, Orsay.

2.3. Activités d'encadrement doctoral

2.3.1. Encadrement de stages de M2

J'ai encadré à 100% trois stages de M2 :

Duc Phu Quy Nguyen : stage de février à juin 2011.
M2 professionnel d'Analyses chimiques et biologiques de l'Université Paris Descartes.
Sujet de stage : « Caractérisation de l'azote dans différents mélanges gazeux par suivi en spectrométrie de masse ».
Q. Nguyen a travaillé cinq mois sur l'un de nos diagnostiques *in situ* sur l'expérience PAMPRE, le spectromètre de masse QMS 200 de Pfeiffer. Ses résultats ont permis de mettre en évidence des effets non linéaires inattendus sur la fragmentation de l'azote dans la source d'ions lorsque l'on travaille en gamme haute de pression de fonctionnement de l'instrument. Ces résultats nous éclairent sur certaines limites critiques d'utilisation de notre instrument.

Thomas Gautier : stage de mars à juin 2010.
M2 Recherche de Planétologie d'Ile de France, UVSQ.
Sujet de stage : « Étude des produits formés en phase gazeuse par simulation expérimentale de l'atmosphère de Titan ».
T. Gautier a effectué un très bon stage de M2-R, évalué par une note de 17,5/20 à la soutenance. T. Gautier poursuit ses recherches en thèse à l'UVSQ, en co-direction entre Pr. Pierre-Richard Dahoo et moi-même au LATMOS.
Ses résultats de M2, rédigés lors du premier semestre de sa thèse font l'objet d'une publication (Gautier et al., 2011).
T. Gautier a présenté ses résultats à un atelier et à une conférence internationale :

- T. Gautier, N. Carrasco, A. Buch, C. Szopa, E. Sciamma-O'brien, L. Hogrel, G.Cernogora (octobre 2010) Gaseous Chemistry induced by a CCP RF discharge in a N2-CH4 mixture. Poster. GEC, Paris.
- T. Gautier, N. Carrasco, A. Buch, E. Sciamma-O'brien, L. Hogrel, G. Cernogora (Mai 2010) Chimie induite par un plasma RF dans un mélange N_2-CH_4. Poster, SFP Plasma.

Tristan Fréjacques : stage de mars à juin 2009.
M2-R de Physique et Environnement d'Orsay.
Sujet de stage : « Simulation expérimentale de production d'aérosols de Titan : influence de la présence de dihydrogène dans la phase gazeuse ».
Cet étudiant normalien a effectué un très bon stage de recherche, évalué par une note de 17/20 lors de sa soutenance. Nous avons préparé ensemble un dossier de thèse, que l'ENS de Lyon a accepté de financer. M. Fréjacques a par ailleurs passé le concours d'entrée dans le corps des Ponts et Chaussée, où il a également été accepté. Ce dernier a choisi de s'orienter vers une carrière de gestion de l'Environnement.
Les résultats qu'il a obtenus au cours de ce stage ont permis de mettre en évidence le rôle de l'hydrogène comme inhibiteur de la croissance des aérosols dans le plasma réactif sur lequel nous travaillons. Ces travaux préliminaires ont par la suite été développés selon deux axes :

- Un axe basé sur la perturbation du plasma créée par la présence de dihydrogène dans le milieu réactionnel (travail en cours, en collaboration avec des modélisateurs Portugais, projet PICS décrit plus loin)
- Un axe basé sur la quantification du rendement de production d'aérosols en fonction de la quantité de méthane injectée, la dissociation du méthane étant

corrélée avec la présence d'hydrogène dans le milieu réactif (Sciamma-O'Brien et al., 2010).

2.3.2. Encadrement doctoral

J'ai co-encadré une thèse de sept. 2007 à sept. 2010 ; et suis co-encadrante de deux thèses en cours, débutées au premier semestre 2010.

Sylvain Plessis : sept-2007-sept 2010.
Bourse de l'ED de Chimie de Paris-Sud ED 470 d'Orsay en co-direction avec P. Pernot.
S. Plessis est actuellement en post-doc à Austin au Texas, au laboratoire PECOS (Predictive Engineering and Computational Sciences) pour travailler sur les incertitudes des modèles de pré-entrée atmosphérique de véhicules spatiaux.

Il a travaillé sur la « Modélisation probabiliste pour l'étude de l'influence des ions sur la composition des espèces neutres dans l'atmosphère de Titan : inversion bayésienne de spectres de masse INMS et représentation des recombinaisons dissociatives par distributions de Dirichlet imbriquées ».

Son travail a donné lieu à quatre publications (Carrasco et al., 2008b; Dobrijevic et al., 2010; Plessis et al., 2011; Plessis et al., 2010) et a été présenté à six conférences internationales :

- N. Carrasco, S. Plessis, M. Dobrijevic, P. Pernot (octobre 2011) EPSC-DPS, Nantes
- S. Plessis, N. Carrasco and P. Pernot, (septembre 2010) Knowledge-based probabilistic representations of branching ratios in chemical networks: dissociative recombinations in Titan's ionosphere, Présentation orale, EPSC, Rome, Italie.
- S. Plessis, P. Pernot, N. Carrasco and M. Dobrijevic, (juin 2010) Role of dissociative recombination in Titan's ionosphere: a reappraisal, Poster aux Faraday Discussions 147: Chemistry of the Planets, St-Jacut de la Mer.
- S. Plessis, N. Carrasco, P. Pernot (mai 2009) "Modelling Titan's ionosphere: towards a realistic ion-neutral coupled model" Présentation orale, European Geophysical Union, Vienne, Autriche.
- S. Plessis, P. Pernot, N. Carrasco. (septembre 2009) "Chemistry in Titan's ionosphere: contribution of dissociative recombination to an ion-neutral coupled model", Présentation orale, European Planetary Science Congress (EPSC), Potsdam, Allemagne
- N. Carrasco, S. Plessis, P. Pernot (2007) "Towards a reduction of Titan ionospheric chemistry model", EPSC, Potsdam, Allemagne.

Thomas Gautier : thèse démarrée en octobre 2010.
Bourse de l'ED Sciences et Technologies de l'UVSQ.
En co-direction avec P.-R. Dahoo et en co-tutelle avec l'Allemagne (laboratoire de plasma à Bochum).
« Simulation en laboratoire par plasma RF de la formation de particules solides d'intérêt astrophysique et prébiotique. »
Cette thèse est dans la continuité du stage de M2 de T. Gautier qui s'intéresse à la chimie prébiotique responsable de la production d'aérosols dans le réacteur PAMPRE.
Son travail a donné lieu pour cette première année de thèse à deux publications sur l'étude des produits en phase gazeuse (Carrasco et al., 2011; Gautier et al., 2011) et à des travaux sur l'analyse des solides produits que T. Gautier a présenté à trois conférences internationales :

- 63rd Gaseous Electronics Conference and 7th International Conference on Reactive Plasmas, Paris octobre 2010, 1 poster :
    - “Gaseous Chemistry induced by a CCP RF discharge in a N2-CH4 mixture”, T. Gautier, N.Carrasco, A.Buch, C.Szopa, E. Sciamma-O’brien, L. Hogrel, G.Cernogora.
- Origins, Montpellier, juillet 2011. 2 posters :
    - « Nitrile reactivity in Titan’s atmosphere », T. Gautier, N.Carrasco1 A.Buch, C.Szopa, E. Sciamma-O’Brien, G.Cernogora
    - « Prebiotic solid material from a Titanian atmospheric simulation”, T. Gautier, N.Carrasco, David Touboul, A.Buch, C.Szopa, I. Schmitz-Afonso
- European Planetary Science Congress, Nantes, septembre 2011, 2 posters
    - “Nitrile growth pattern in Titan's atmosphere”, T. Gautier, N. Carrasco, A. Buch, C. Szopa, E. Sciamma-O'Brien and G. Cernogor
    - “Far infrared properties of Titan's tholins”, T. Gautier, N. Carrasco, P. Dumas, J.-J. Correia, A. Giuliani and G. Cernogora

Zhe Peng : thèse démarrée en septembre 2010.
Bourse de l’ED de Chimie de Paris-Sud ED 470 d’Orsay
En co-direction avec P. Pernot.
« Influence du dépôt d'énergie sur la croissance moléculaire dans la photochimie de Titan. »
Cette thèse porte sur les réactions de photolyses d’intérêt pour Titan, basée à la fois sur la simulation expérimentale (expériences sur le réacteur APSIS, décrit plus loin dans le manuscrit et permettant d’effectuer des expériences de photo-ionisation sur une ligne de lumière du synchrotron SOLEIL) et sur la modélisation. En effet Z. Peng développe un modèle de chimie-transport en support à l’interprétation des résultats obtenus avec APSIS, et il travaille sur l’amélioration du module de photolyse d’un modèle de chimie ionosphérique de Titan.
Son travail a donné lieu à une publication cette année (Peng et al., 2010) et Z. Peng a participe à une conférence internationale pour la présentation de quatre travaux en cours :

- European Planetary Science Congress, Nantes, septembre 2011:
    - « APSIS: a Titan’s atmosphere simulation experiment using a continuous-spectrum UV synchrotron beamline » Z. Peng, T. Gautier, N. Carrasco, A. Giuliani, G. Cernogora, J.-J. Correia, A. Mahjoub, C. Szopa, P. Pernot, A. Buch and Y. Bénilan, Poster.
    - “Modeling of Atmospheric Photochemistry SImulated by Synchrotron setup”, Z. Peng, N. Carrasco and P. Pernot, Oral.
    - “Effects of uncertain photolysis parameters on predictions of Titan’s photochemistry models”, Z. Peng, F. Cailliez, N. Carrasco, E. Hébrard, M.Dobrijevic and P. Pernot, Poster.
    - “Impact of a new wavelength-dependent representation of methane photolysis branching ratios on the modeling of Titan’s atmospheric photochemistry”, Z. Peng, B. Gans, N. Carrasco, S. Lebonnois, D. Gauyacq and P. Pernot, Poster.

2.4. Participations à des projets et programmes scientifiques

2.4.1. Pilotage de projets français

Le travail expérimental nécessite des réponses régulières sur Appel d'Offre de projets scientifiques, autant pour le fonctionnement quotidien de l'expérience que pour les développements sous la forme de nouveaux équipements. Depuis mon recrutement en tant que Maître de Conférence UVSQ au LATMOS, j'ai initié, porté et assuré la **responsabilité scientifique** des six projets financés suivants :

- 1 projet concernant l'étude spécifique de la photochimie du méthane

PRES UniverSud 2008 : projet sur la photochimie du méthane financé par le PRES UniversSud Paris, en collaboration avec le LPPM (Orsay). Il s'agit d'un travail complémentaire entre expérimentation et modélisation afin de mieux déterminer les voies de dissociation du méthane par photolyse et leur impact dans un modèle de photochimie de Titan (Gans et al., 2009).

- 3 projets concernant des développements sur l'expérience Pampre (expérience décrite dans la partie 3.3.1)

PNP 2009 : étude des particules carbonées du système solaire d'intérêt en exobiologie. Ce projet a permis de d'étudier la conversion du méthane et de l'azote gazeux en particules organiques solides en précisant les mécanismes réactionnels par simulation expérimentale (Sciamma-O'Brien et al., 2010).
OPV 2008 : Ce projet a permis de développer un piège cryogénique pour concentrer les produits organiques volatiles formés dans le plasma réactifs afin de les analyser ex situ. Après des études préliminaires d'optimisation du piège et son utilisation, nous avons été à même de publier les résultats sur la composition de la phase gazeuse dans l'article Gautier et al., 2011.
ANR Jeune chercheur 2009-2012 : J'ai obtenu en sept. 2009 une ANR jeune chercheur d'une durée de 3 ans (2009-2012) pour développer nos connaissances de la réactivité atmosphérique de Titan avec le montage Pampre. Ce projet permet notamment de financer un nouvel équipement sur l'expérience : la spectroscopie d'absorption IRTF in situ, ainsi que le recrutement d'un post-doc sur deux ans (A. Mahjoub). Nous travaillons sur (i) caractériser la formation des produits en phase gazeuse, avec en particulier l'installation d'un nouveau diagnostique in situ de spectroscopie IRTF, (ii) caractériser le dépôt d'énergie dans le milieu réactionnel du à la décharge plasma radio-fréquence (coll. IST Lisbonne), (iii) comprendre les mécanismes de production et de complexification de la matière organique et conduisant à la formation de matière solide dans le plasma (coll. LPG Grenoble et LPL Arizona).

- 2 projets concernant le développement d'un nouveau réacteur afin de monter des expériences sur une ligne de lumière du synchrotron SOLEIL : le réacteur APSIS qui est décrit dans la partie 4.1.3.

PRES UniverSud 2009
CNES 2010
Ces deux financements complémentaires ont assuré la construction de l'intégralité du montage entre l'été et l'automne 2010 : le réacteur lui-même, son support, la ligne de gaz, toutes les jauges, ainsi que les raccordements sur la ligne de SOLEIL.
D'autre part, notre projet a été sélectionné deux fois pour allocation de temps de faisceau (automne 2010 et printemps 2011) par le comité de programme scientifique de SOLEIL. J'ai donc piloté deux campagnes d'expériences de ce nouveau réacteur sur une ligne de lumière UV-VUV du synchrotron SOLEIL.

2.4.2. Participation à des programmes internationaux

Participation à un programme PICS 2009-2011 du CNRS en collaboration avec un laboratoire de modélisation des plasmas au Portugal, afin d'étudier le dépôt d'énergie et les caractéristiques du plasma dans notre montage expérimental Pampre. La collaboration est établie entre le LATMOS, le GREMI (laboratoire plasma à Orléans) et l'IPFN (Institut de plasma et de fusion nucléaire à Lisbonne, Portugal).

Participation à un atelier international sélectionné par l'ISSI (Institut des Sciences Spatiales International, Berne, Suisse), avec le LCP (Orsay), le LAB (Bordeaux), le LMD (Jussieu), IAA (Grenade, Espagne) and SwRI (San Antonio, Texas, EU), pour une activité de modélisation des processus de chimie-transport atmosphérique de Titan.Il s'agit d'un groupe de travail international sur l'inter-comparaison des modèles 1D de photochimie atmosphérique de Titan (LCP Orsay, LMD Paris, LAB Bordeaux, IAA Grenade Espagne, SwRI San Antonio Texas US).

Mise en place d'une thèse en co-tutelle avec l'Université de Bochum pour T. Gautier. Obtention d'une bourse de la DAAD pour ses missions en Allemagne la première année, et participation à l'AO PROCOPE 2011 (en attente de réponse) pour financer la collaboration franco-allemande pendant les deux dernières années de sa thèse.

2.4.3. Participation à des comités d'évaluation scientifique :

2011-auj. **Expert pour la NASA** dans le comité d'évaluation scientifique des projets pour les appels d'offres NSPIRES.

2010-auj. **membre du comité de programme scientifique « Matière Diluée » du synchrotron SOLEIL**. J'ai été sollicitée en 2010 pour faire partie du comité scientifique d'évaluation des projets soumis à cette commission pour attribuer le temps de faisceaux de ce programme.

2010-auj. : **Expert pour la Région Aquitaine** dans le comité d'évaluation scientifique des projets régionaux.

2009-auj. : **Relecteur pour les journaux scientifiques** Planetary and Space Science et The European Physical Journal - Applied Physics.

2.5. Responsabilités administratives et d'enseignement

Responsabilité d'enseignement à l'UVSQ

- 2007-auj. : correspondante du parcours de planétologie de l'UVSQ : sélection des candidats, diffusion de l'information auprès des étudiants de l'UVSQ, entretiens individuels et participation aux Journées Portes ouvertes, et à des salons de l'étudiant. Responsabilité des inscriptions des étudiants dans cette filière.
- module de L3 de physico-chimie de l'atmosphère et des océans
- module de M1 de planétologie : crée par Hélène Massol (Orsay) et moi-même en 2008-2009 dans le cadre d'un partenariat PRES.
- module de M2 du parcours de Planétologie d'Ile de France
- De 2007 à 2010, j'ai organisé les interventions de conférenciers extérieurs (partenaires industriels) pour le master 2 professionnel QUALUB. Cette responsabilité impliquait la gestion du calendrier, et de l'ensemble des interactions avec les conférenciers (recherche de nouveaux partenaires/invitations/accueil).
- 2007-auj. : Responsabilité de la station de mesure de la qualité de l'air : j'ai notamment participé à deux appel d'offre IPSL pour équiper la station en instrument de mesure de la qualité de l'air intérieur (sonde COV et formaldéhyde) afin de monter un TP de niveau M1-M2 dédiés aux étudiants scientifiques de l'UVSQ et d'Orsay.

Responsabilité administrative à l'UVSQ

- 2010-auj. : membre du bureau d'évaluation des Primes d'Excellence Scientifiques pour les sections 34-35-36-37 à l'UVSQ
- 2008-auj. : participe à la sélection des ATER de l'UVSQ pour la section 34.

Responsabilités administratives au PRES UniverSud : 2009-2011

- Co-responsable du Pôle de Planétologie du PRES UniverSud, en binôme avec un collègue d'Orsay, E. Chassefière (directeur du laboratoire IDES). Cette charge de travail cette année s'est traduite par des réunions du bureau du pôle pour la centralisation et la gestion de l'évaluation des projets de recherche pour l'Appel d'Offre 2009, des réunions de coordination avec les responsables du PRES UniverSud et l'organisation du premier colloque de Bilan et Prospectives du pôle de Planétologie du PRES (22 janvier 2010, à Guyancourt).

3. Synthèse des travaux scientifiques

3.1. Thèse : Simulation expérimentale de réactions d'intérêt pour la troposphère

Mon travail de thèse s'est déroulé dans l'équipe "Réactivités Multiphasiques en Atmosphères Simulées" du Laboratoire Interuniversitaire des Systèmes Atmosphériques (LISA), sous la direction de J.F. Doussin et Guy Carlier. Il s'est inscrit dans une des thématiques de recherche de ce laboratoire, la réactivité physico-chimique des composés à l'état de traces en atmosphères réelles ou simulées.

3.1.1. Contexte scientifique

L'air est composé essentiellement d'azote (78 % en volume), d'oxygène (21 % en volume) et d'argon (0,95 %) mais il contient également une multitude d'espèces sous forme de traces gazeuses, liquides ou solides qui représentent quelques millièmes seulement en volume. Or, toute la réactivité chimique et les phénomènes de pollution de l'air proviennent de cette fraction infime de l'atmosphère.
Ces espèces traces sont d'origine biotique (émissions par la végétation, les océans, les volcans) ou sont produites par les activités humaines (cheminées d'usines, pots d'échappements).
Les produits sont émis directement dans l'atmosphère, comme les oxydes de carbone, les oxydes de soufre, les oxydes d'azote, les composés organiques volatils (COV). D'autres proviennent de la dégradation dans la basse atmosphère de ces mêmes produits, tels que l'ozone, les particules d'aérosol organiques et d'autres polluants photochimiques (aldéhydes, cétones, nitrates de peroxyacétyles).
L'ozone par exemple résulte de la dégradation des COV dans l'atmosphère en présence d'oxydes d'azote et de forte activité photochimique. La formation d'espèces secondaires peut nécessiter un certain temps durant lequel les masses d'air se déplacent. C'est pourquoi les pics de production d'ozone concernent souvent des zones plus étendues que les zones strictes d'émission de COV et d'oxyde d'azote. Ainsi, c'est dans la zone rurale autour des agglomérations que l'on trouve les niveaux d'ozone les plus élevés en cas de pic de production d'ozone. Au final, la qualité de l'air résulte d'un équilibre complexe entre les apports de ces composés et les phénomènes de dispersion et de transformation dans l'atmosphère.
Depuis le siècle dernier, seule la réactivité des espèces issues de l'activité humaine était prise en compte pour évaluer de la qualité de l'air sur un site. Or les composés d'origine biotique présentent eux aussi une forte réactivité vis à vis des polluants atmosphériques et sont susceptibles d'induire des productions d'ozone et d'autres polluants photochimiques dans la basse atmosphère. Je me suis intéressée dans le cadre de ma thèse à l'impact atmosphérique de la réactivité de trois composés biotiques : l'isoprène, le MBO et le sabinène, choisis notamment pour l'abondance de leurs émissions et la méconnaissance de leur devenir dans l'atmosphère.

3.1.2. Approche expérimentale

Il s'agissait d'un travail expérimental visant à comprendre les processus physico-chimiques qui se déroulent dans le réacteur complexe que constitue l'atmosphère terrestre.

J'ai utilisé différents outils expérimentaux de simulation atmosphérique qui permettent de modéliser au mieux les processus physico-chimiques dans l'atmosphère : les chambres de simulation atmosphérique du LISA (Créteil, France), du CRAC (Cork, Irlande) et d'EUPHORE (Valence, Espagne) et leurs panels de moyens analytiques associés (voir Figure 3).

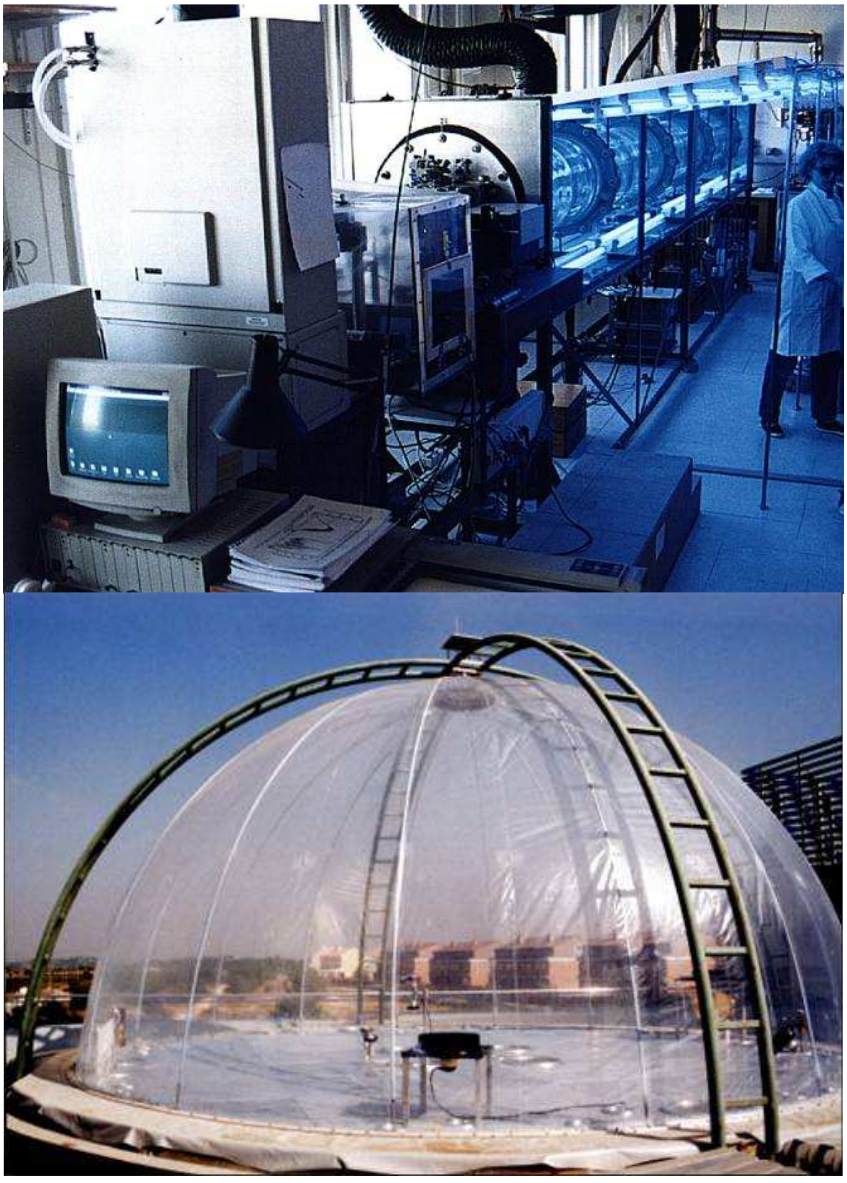

Figure 3: Chambres de simulation atmosphérique : (en haut) du LISA, Créteil, (en bas) d'EUPHORE, Valence.

Les chambres de simulation atmosphériques permettent de simuler expérimentalement les conditions atmosphériques dans des conditions de pression et de température contrôlées et ainsi d'étudier la cinétique et les mécanismes de dégradation en phase gazeuse de composés organiques volatiles (COV).
Je me suis intéressée à la réactivité en phase gazeuse d'une famille de composés organiques, les composés d'origine biotique (COVB), essentiellement de structure terpénique. L'étude de la réactivité de ces derniers n'est prise en considération que depuis une dizaine d'années. Elle est très mal représentée dans les modèles de chimie-transport actuellement utilisés. C'est pourquoi ce travail de thèse était essentiel pour mieux appréhender la contribution de la réactivité des COVB à l'ensemble des processus physico-chimiques qui se produisent dans la troposphère.

3.1.3. Exemple caractéristique de la démarche adoptée : le MBO

J'ai tout d'abord simulé expérimentalement la dégradation du MBO dans des conditions les plus réalistes possibles, dans la chambre de simulation d'EUPHORE (Valence) en téflon exposée directement au rayonnement solaire. Ces expériences regroupent tous les modes d'attaques du MBO simultanément ainsi que la dégradation de ses composés secondaires. Ces expériences, de type étude d'impact m'ont permis de quantifier les productions d'ozone, de produits organiques gazeux (Figure 4 :) et d'aérosols organiques secondaires (Figure 5) issus d'une photo-oxydation réaliste de ce composé.

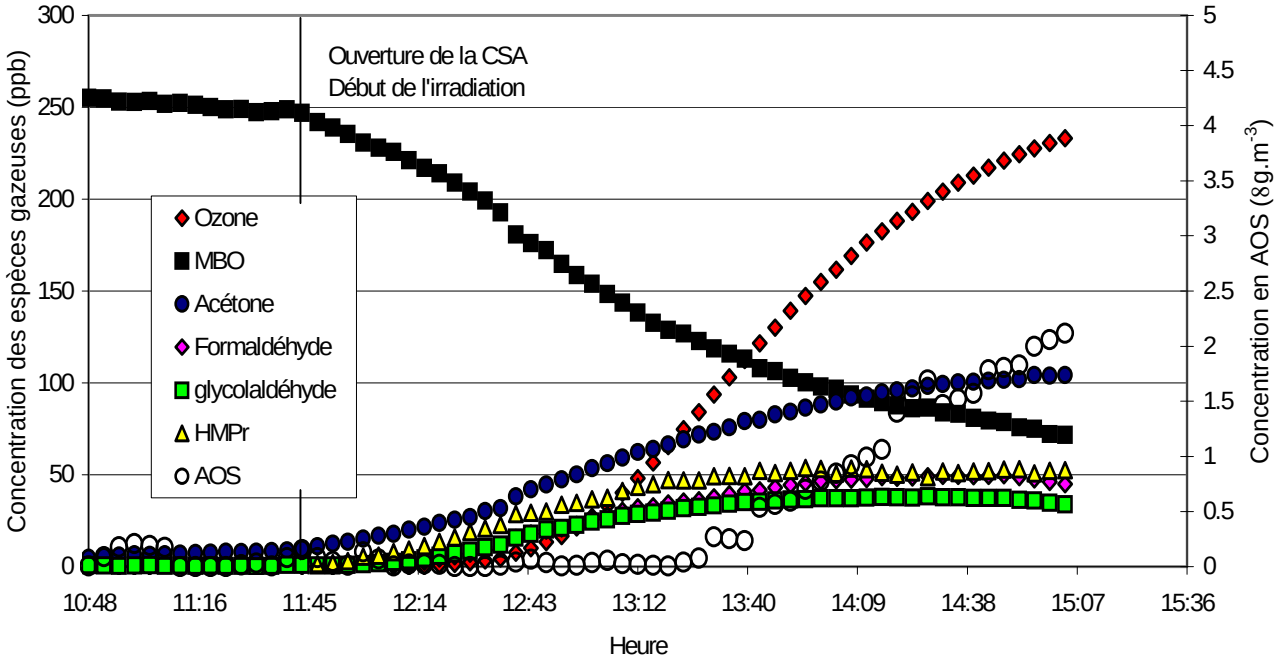

Figure 4 : Expérience de photo-oxydation réaliste du MBO (EUPHORE 19/05/03).

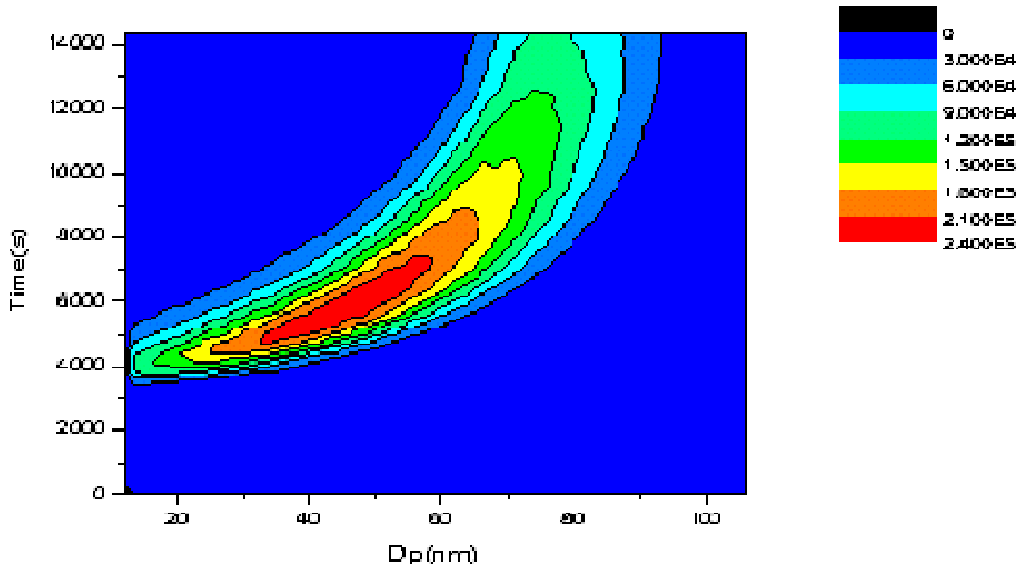

Figure 5 : Production d'aérosols organiques au cours de la réaction de photo-oxydation du MBO: nombre de particules produites par unité de volume (cm^{-3}) en fonction des classes de diamètre (nm) et du temps (s).

L'un de ses produits de réaction principal, l'Hydroxyméthylpropanal (HMPr) est un composé non commercial que j'ai été amenée à synthétiser en laboratoire pour le caractériser et le calibrer en spectroscopie d'absorption IR (Figure 6).

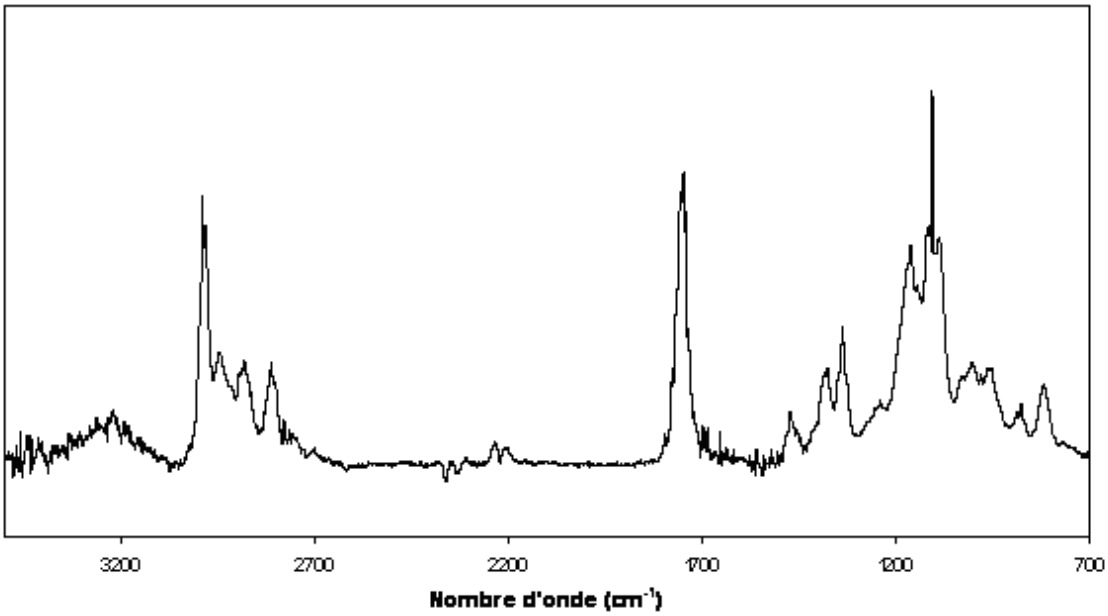

Figure 6:Spectre de référence de HMPr – 4,9 ×10^{13} molécule.cm^{-3} – L = 156 m – R = 0,7 cm^{-1}

J'ai par la suite, étudié les processus chimiques propres à la réactivité du MBO séparément, c'est-à-dire l'oxydation du MBO par OH et par l'ozone, dans les chambres de simulations du LISA (Créteil) et du CRAC (Cork).
Enfin, j'ai abordé les processus de dégradation propres au COV majeur issu de l'oxydation primaire du MBO, l'HMPr afin d'avoir une vue d'ensemble du devenir du MBO dans la troposphère.
Ce travail sur la réactivité du MBO et de son produit organique principal HMPr a ainsi donné lieu à trois publications indépendantes : la première sur la cinétique d'ozonolyse du MBO spécifiquement car cette détermination présentait une méthodologie innovante (détermination en absolu au lieu de relative), la seconde sur la réactivité complète du MBO

et la troisième sur la réactivité de HMPr. L'article sur la réactivité du MBO est donné en intégralité en fin de manuscrit parmi les cinq publications les plus significatives de mes travaux.

3.1.4. Bilan

Les résultats de cette thèse ont donné lieu à la publication de six articles dans des journaux internationaux (Carrasco et al., 2007a; Carrasco et al., 2006a; Carrasco et al., 2007d; Carrasco et al., 2006b; Chiappini et al., 2006; Klawatsch-Carrasco et al., 2004).
Ils ont de plus été utilisés dans la thèse de S. Moukhtar, 2005, intégrés dans le code du modèle de chimie-transport CHIMERE pour évaluer l'impact des COVB émis par les forêts vosgiennes sur la réactivité chimique afin de mieux simuler les épisodes de pollution photochimique mesurés pendant la campagne INTERREG III (Fossé-Rhénan, été 2003).
Au cours de cette expérience, je me suis formée à la simulation expérimentale de laboratoire pour les milieux atmosphériques, à la manipulation des flux de gaz, basse et haute pression, ainsi qu'aux méthodes d'analyse des mélanges gazeux complexes.

3.2. Post-doctorat : Modélisation de la chimie ionosphérique de Titan

Mon post-doc s'est déroulé au Laboratoire de Chimie Physique (LCP), auprès de Pascal Pernot dans l'équipe de chimie-théorique. Ce travail correspond à une mobilité thématique, me faisant passer de l'étude de la photochimie terrestre à celle de l'ionosphère de Titan, tout en changeant mes outils, pour aller de la simulation expérimentale de laboratoire à la modélisation numérique. J'ai travaillé en étroite collaboration avec P. Pernot, expert de l'analyse bayésienne des données et développant une plate-forme de codes, dédiée à l'étude de systèmes chimiques complexes (modèles cinétiques, traitement de données expérimentales, calculs de chimie théorique…). Nous avons adapté ensemble ces codes probabilistes d'analyse des données à la propagation des incertitudes et à l'analyse de sensibilité pour un modèle de chimie ionosphérique de Titan.

3.2.1. Contexte scientifique

La mission spatiale Cassini-Huygens apporte de très nombreuses données sur la composition de l'atmosphère de Titan. Ce satellite est doté d'une atmosphère dense d'azote et d'hydrocarbures et est soumis à des flux énergétiques intenses (photons+électrons), initiant une chimie atmosphérique complexe. Les molécules neutres de l'atmosphère de Titan sont partiellement ionisées dans la partie haute de l'atmosphère du fait du rayonnement solaire, très énergétique à ces hautes altitudes, et des électrons provenant de la magnétosphère de Saturne. Ce mélange d'ions et de molécules neutres forme un plasma ionosphérique au dessus de 900km d'altitude. Les premières mesures de composition en ions et en neutres ont été faites par l'instrument INMS - Ion Neutral Mass Spectrometer - de Cassini (Cravens et al., 2006). Une chimie ionique complexe a été révélée par cet instrument. Avant Cassini, la complexification organique était uniquement pressentie dans la stratosphère. Aujourd'hui on sait que la chimie des ions organiques lourds a un rôle essentiel dans la formation des aérosols, et l'on pense désormais que les noyaux de nucléation se forment dans l'ionosphère, avant de sédimenter vers les parties plus basse de l'atmosphère de Titan (Lavvas et al., 2009). (voir Figure 7).

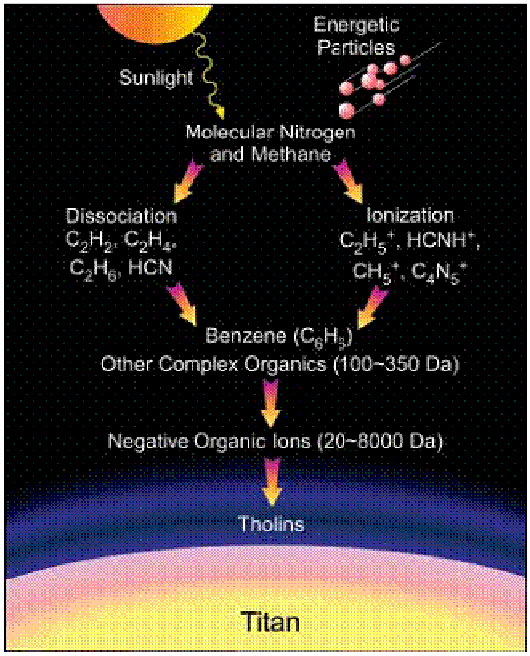

Figure 7 : Processus de formation des aérosols dans la haute atmosphère de Titan (Waite Jr. et al., 2007)

3.2.2. Outils de modélisation : propagation d'incertitude dans un modèle ionosphérique de Titan et analyse de sensibilité

La modélisation de systèmes cinétiques complexes nécessite le développement et une analyse détaillée des processus élémentaires les composant. Les réactions recensées dans ces modèles sont notamment paramétrisées par des sections efficaces, ou des constantes de vitesse et des rapports de branchement dans des gammes de températures ou d'énergie données. Ces paramètres sont préalablement déterminés expérimentalement, ou théoriquement, et sont affectés par des incertitudes. Ces dernières se propagent dans les modèles et affectent par conséquent les résultats des modèles.

La propagation d'incertitude par simulation Monte Carlo permet de quantifier ces incertitudes pour des systèmes complexes, même présentant des non-linéarités (voir Figure 8). Cet outil permet ainsi d'évaluer la fiabilité des prédictions du modèle. D'autre part, tenir compte des incertitudes sur les sorties des modèles permet de confronter les résultats de modèles aux résultats de mesures expérimentales. En effet, les différences ne sont significatives que si les barres d'incertitudes des résultats comparés ne se recouvrent pas. A fortiori ce travail permet de valider, ou d'invalider, l'ensemble des processus élémentaires invoqués dans la description du système. Quelques études ont d'ores et déjà été réalisées pour la combustion (Turányi et al., 2002), les plasmas (Bose et al., 2003) et la photochimie atmosphérique terrestre et planétaire (Dobrijevic et al., 2003; Smith et al., 2001). Le principe a été appliqué à un code de chimie ionosphérique, comme schématisé sur la Figure 8.

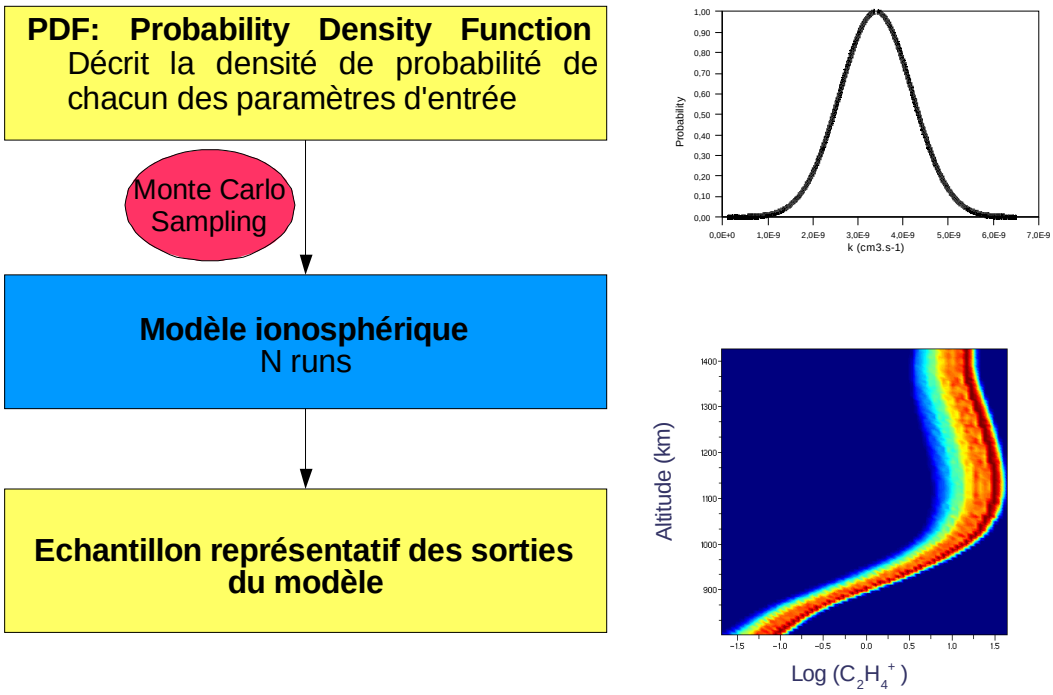

Figure 8: Principe de la propagation d'incertitude par tirages Monte Carlo.

L'analyse de sensibilité complète l'outil de propagation d'incertitudes en identifiant les paramètres clés qui contrôlent le système. Elle cartographie la réponse des prédictions vis à vis de la variabilité des paramètres d'entrée du modèle. Elle permet ainsi de mettre en évidence les paramètres cinétiques déterminants, auxquels les prédictions des modèles sont particulièrement sensibles. Or les déterminations expérimentales des valeurs des paramètres qui décrivent le système sont souvent longues et coûteuses. L'analyse de sensibilité constitue donc un outil précieux d'aide aux expérimentateurs pour prévoir leurs futurs efforts de campagnes de laboratoire. Les méthodes développées pour l'analyse de

sensibilité peuvent être très simples pour des systèmes simples, ou très complexes pour des systèmes non-linéaires à multiples paramètres. Elles donnent lieu à des développements continuels, notamment au cours des conférences internationales SAMO (International Conferences on Sensitivity Analysis of Model Outputs) qui se tiennent tous les 3 ans depuis 1995.

3.2.3. Exemple de résultat

Un premier travail fondateur (Carrasco et al., 2007b) a permis de simuler un spectre de masse des ions dans les conditions du survol T5 de Cassini, et de calculer ses incertitudes associées. Nous avons confronté le spectre de masse simulé à celui mesuré par l'instrument INMS, en tenant compte de leurs incertitudes respectives. Ceci a permis de quantifier les accords et désaccords entre modèle et mesure. Nous avons mis en évidence la performance du modèle pour la restitution des espèces de faibles masses (m/z < 50), mais aussi ses lacunes dans le domaine de la chimie des espèces ioniques plus lourdes mesurées par l'instrument INMS (m/z>50). Cet article a reçu un prix honorifique à l'EGU à Vienne en 2011 : celui des 50 articles de la période 2006-2011 les plus cités du journal Planetary and Space Science. Cette publication est fournie en fin de document, parmi les cinq articles les plus significatifs de mon travail.

J'ai effectué en complément un travail de simplification des schémas chimiques en collaboration avec P. Pernot (LCP Orsay) dans lequel j'ai sélectionné les réactions ion-molécule nécessaires et suffisantes pour déterminer le nombre de réactions minimales pour simuler intégralement le spectre de masse observé par Cassini lors du vol T5 à 1200 km d'altitude (Carrasco et al., 2008b, voir Figure 9). Ce travail a été réalisé en couplant plusieurs méthodes d'analyse de sensibilité.

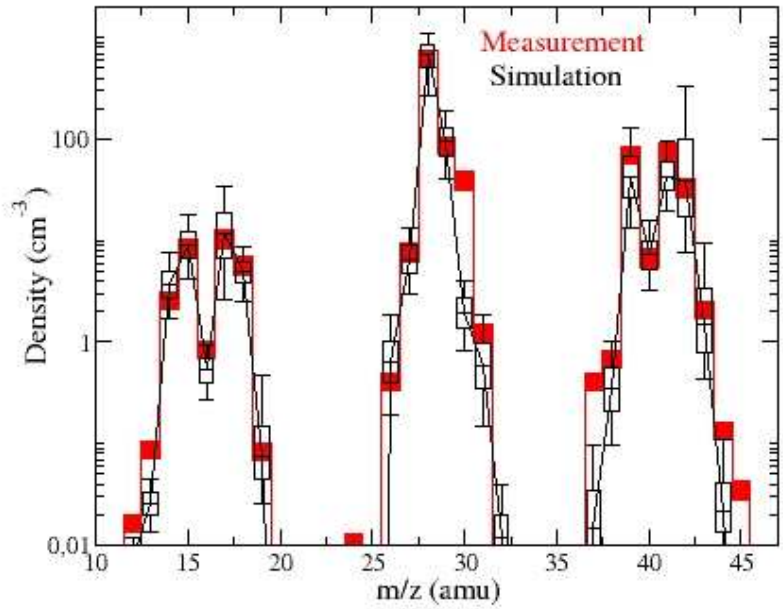

Figure 9 : Comparaison des spectres de masse des ions (rouge) mesuré par l'instrument INMS à 1200km lors du vol T5 ; (noir) simulé dans Carrasco et al., 2008b.

Ce travail montre que parmi 700 réactions ion-molécule, seules 35 sont nécessaires pour reproduire fidèlement le spectre mesuré par l'INMS de Cassini pour m/z < 50 u. Cette étude est partielle : elle n'a été effectuée qu'à une altitude, sur un spectre de Cassini. Néanmoins elle montre que malgré la complexité des mélanges, seules quelques processus clé sont dominants et contrôlent la réactivité ionosphérique.

Le travail préliminaire a ainsi été identifié (Waite Jr et al., 2009, Titan from Cassini-Huygens) comme une priorité pour la modélisation future de l'atmosphère de Titan, afin de mieux prédire les variations géographiques et saisonnières des composés atmosphériques principaux.

3.2.4. Bilan

Ce post-doc a donné lieu à l'écriture de six publications dans des journaux internationaux à comité de lecture (Carrasco et al., 2008a; Carrasco et al., 2007b; Carrasco et al., 2007c; Carrasco et Pernot, 2007; Carrasco et al., 2008b; Dobrijevic et al., 2008). Il a été pour moi l'occasion de développer une compétence en modélisation des systèmes atmosphériques, d'élargir mes connaissances de la réactivité en phase gazeuse en étudiant la réactivité des ions, et d'appréhender un outil original, la propagation d'incertitude par échantillonnage Monte Carlo, permettant l'évaluation des incertitudes sur les modèles et la quantification de la prédictivité des modèles.

3.3. Maître de Conférence à l'UVSQ

J'ai été recrutée en 2007 comme Maître de Conférences au Laboratoire ATmosphères Milieux et Observations Spatiales, au Département de Planétologie, dans l'équipe du Pr Guy Cernogora, Emérite aujourd'hui. Cette équipe a développé peu avant mon arrivée un réacteur plasma, optimisé pour la production de poudres organiques, analogues des aérosols atmosphériques de Titan (Szopa et al., 2006). Mon travail pendant ces quatre années a été de prendre en charge cette nouvelle activité, en collaboration avec Guy Cernogora. J'ai notamment travaillé à valider ce nouveau montage en confrontant ses résultats aux observations *in situ* de la mission Cassini.

3.3.1. Le réacteur PAMPRE :

Jusqu'à aujourd'hui, de nombreuses plateformes expérimentales ont été mises au point dans des laboratoires internationaux pour produire des tholins, *i.e.* des analogues d'aérosols de Titan. Certains d'entre eux utilisent les rayonnements UV comme source d'énergie (Bar-Nun et al., 2008; Tran et al., 2005). Néanmoins, en raison de la transmission limitées des fenêtres de quartz en deçà de 200 nm, l'azote de peut pas être dissocié dans ces montages. Dans ces derniers, on introduit donc des produits primaires détectés dans l'atmosphère de Titan, comme HCN et HC_3N, pour simuler la réactivité de l'azote dans le mélange réactionnel. Récemment, Imanaka et Smith, 2007 a montré la nécessité de dissocier l'azote moléculaire avec des VUV énergétiques pour initier des chaînes de réactions complexes. Ce domaine de longueur d'onde n'est accessible que dans la haute atmosphère de Titan : ionosphère et haute stratosphère. C'est pourquoi toutes les études récentes soulignent cette importance de la dissociation de l'azote moléculaire pour former des précurseurs pour les aérosols organiques de Titan.

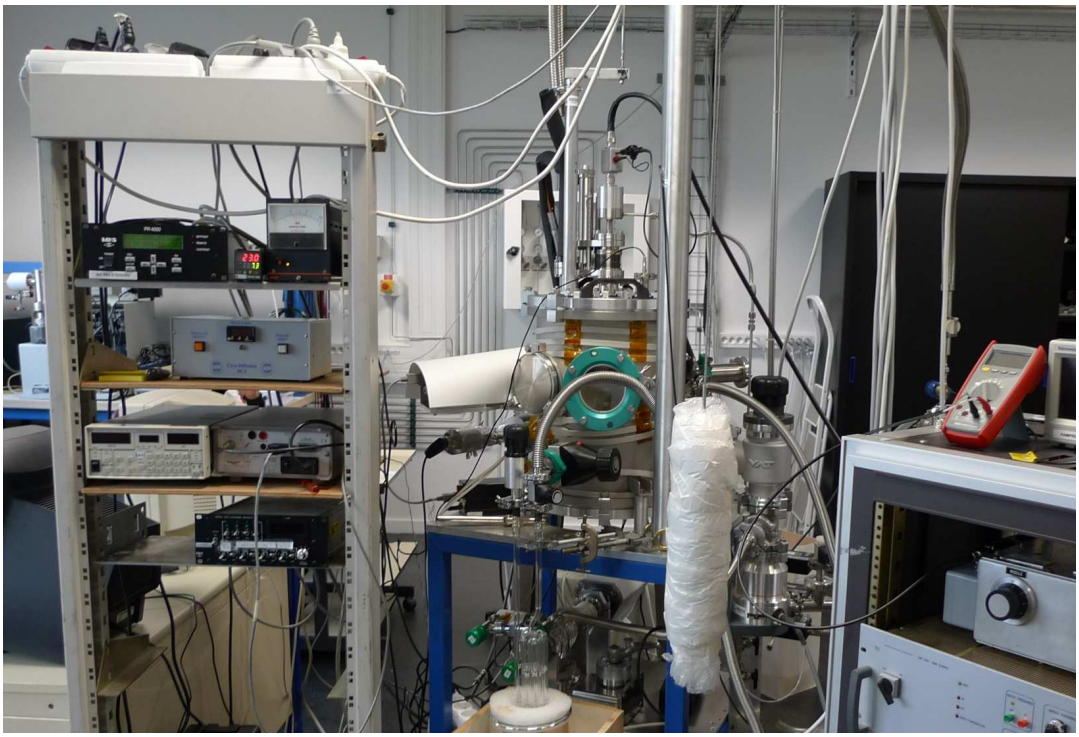

Figure 10: Installation PAMPRE au LATMOS.

D'autres expériences utilisent les décharges plasma comme source d'énergie, par exemple des décharges DC (Coll et al., 1999) ou RF couplées par induction (Imanaka et al., 2004). Dans ces décharges plasma, la quantité d'aérosols formés est plus importante qu'avec les montages photochimiques. Certaines de ces expériences ont pu produire les

échantillons sous forme de poudre, ou sous forme de films déposés sur des substrats. Ces films solides ne permettent de reproduire la morphologie des aérosols de Titan et le substrat peut influencer la chimie produisant les tholins.
Pour cette raison, l'équipe du LATMOS a développé un réacteur de simulation d'aérosols de Titan, appelé PAMPRE (Production d'Aérosols en Microgravité par Plasma Réactif, voir Figure 10), basé sur une technique de plasma radio-fréquence couplé capacitivement. Ce type de plasma est connu pour produire des particules solides en suspension dans la phase gazeuse, sans effet de parois avec le réacteur (voir Figure 11).

Figure 11 : Photo d'un plasma N_2-CH_4 dans la cavité reactive de PAMPRE ; la trace verte correspond à la diffusion par les poudres en suspension d'un laser vert à 532 nm.

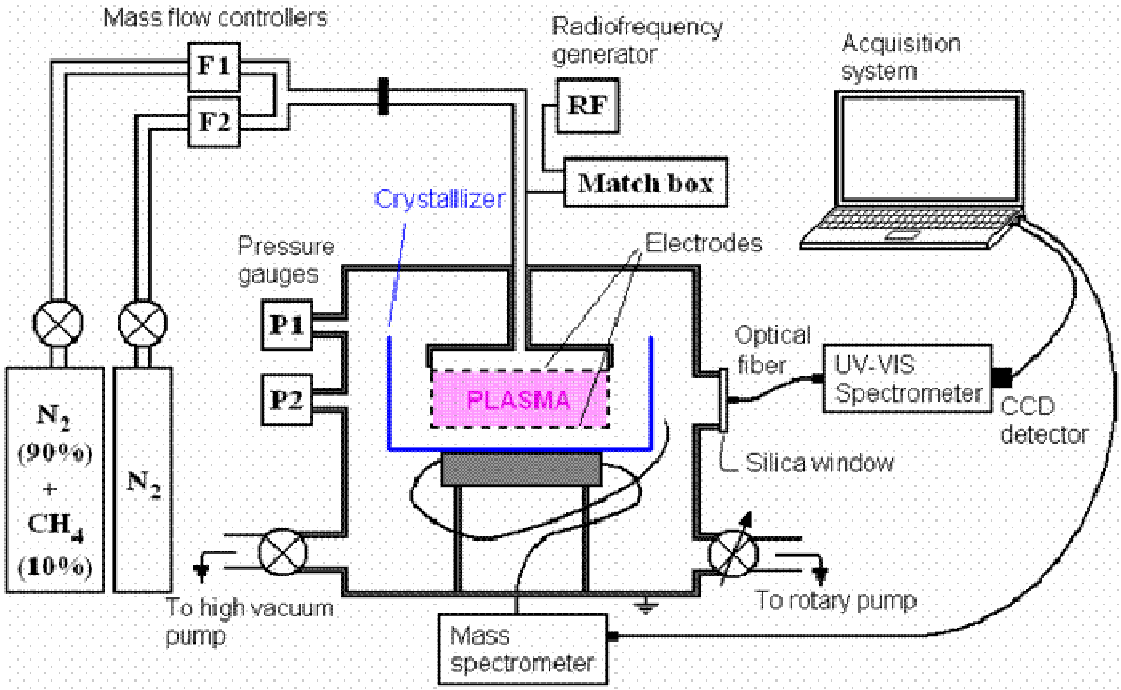

Figure 12 : Schéma de l'expérience PAMPRE.

Le réacteur est de forme cylindrique en acier inoxydable. Deux bouteilles (l'une d'azote pur, l'autre de mélange N_2-CH_4 à 10%) permettent d'ajuster la concentration de méthane du mélange gazeux initial N_2-CH_4 entre 0 et 10%. La décharge radio-fréquence dans la cavité plasma est assurée un générateur de fréquence 13,6 MHz de puissance réglable de 0 à 100W. La décharge a lieu entre deux électrodes couplées capacitivement, l'une polarisée (électrode du haut), l'autre reliée à la Terre. Elle est confinée latéralement par une cage métallique cylindrique reliée à la masse et de dimensions : 13,7 cm de diamètre et 5 cm de haut.

Le mélange gazeux est injecté continûment dans la cavité plasma au travers de l'électrode polarisée, et pompé par une pompe primaire, créant un flux gazeux uniforme au travers de la cavité plasma.
Entre deux expériences, la boîte à plasma et le cristallisoir dans lequel les poudres s'impactent sont nettoyés à l'éthanol. Le réacteur est étuvé et pompé en pompage secondaire avec une pompe turbomoléculaire (vide limite d'environ 2×10^{-6} mbar) plusieurs heures. Une fois le réacteur refroidi, un plasma d'argon d'environ une ½ heure assure le décapage des parois de la cavité plasma avant toute expérience.

3.3.2. Validation des tholins de PAMPRE comme analogues d'aérosols de Titan

L'adéquation entre les tholins de PAMPRE (voir Figure 13) et les aérosols de Titan est progressivement confirmée par l'identification de signatures communes aux deux matériaux.
Rannou et al., 2010 ont récemment identifié par exploitation des données de transmission tangentielles de l'instrument VIMS de Cassini une bande d'absorption IR à 3.4 μm caractéristique d'une signature de fonctions aliphatiques (modes de stretching de groupements $-CH_2-/-CH_3$) dans les aérosols de Titan. Il souligne le fait que cette bande est prédominante dans le même domaine spectral pour les tholins de PAMPRE et publiée dans l'article Quirico et al., 2008.

Figure 13 : Photo du dépôt et de la récolte de poudres dans le cristallisoir au bout de quelques heures d'expérience en plasma continu d'azote-méthane.

La transmission atmosphérique du rayonnement lointain infrarouge tellurique est aussi analysée par l'instrument CIRS de Cassini, qui a permis de mettre récemment en évidence des signatures spectrales des aérosols de Titan dans le moyen et le lointain infrarouge (Anderson et Samuelson, 2011; Vinatier et al., 2010).
Nous avons donc réalisé des mesures sur une ligne IR (moyen et lointain) du synchrotron SOLEIL en décembre 2010, en étendant les mesures sur les tholins dans le domaine spectral du lointain infra-rouge. Cette étude de confrontation des propriétés d'absorption infra-rouge avec les propriétés des aérosols de Titan est effectuée en collaboration avec des scientifiques travaillant sur les données CIRS (S. Vinatier, LESIA Meudon, et C. Anderson & R. Samuelson au Goddard Space Flight Center, Washigton DC, USA) (article en préparation.

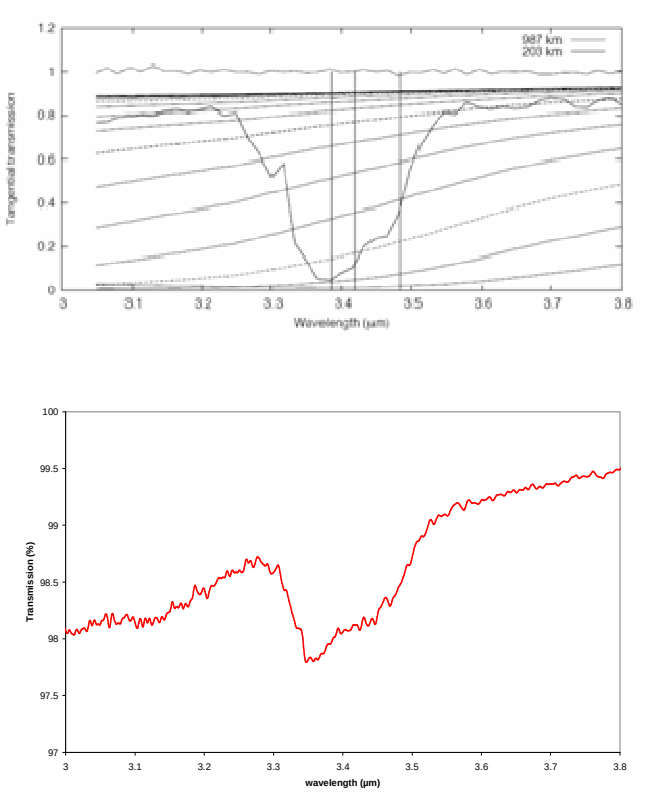

Figure 14 : (Bas) bande d'absorption infra-rouge à 3.4 µm d'un tholin de PAMPRE; (Haut) Même absorption mesurée par transmission tangentielle des aerosols de Titan par l'instrument VIMS de Cassini (Rannou et al., 2010).

Nous avons d'autre part mené un travail considérable sur l'analyse chimique des tholins de PAMPRE par spectrométrie de masse (Carrasco et al., 2009; Pernot et al., 2010) en collaboration avec l'Institut des Substances Naturelles (Gif Sur Yvette), le Laboratoire de Chimie-Physique (Orsay), le Laboratoire Génie des Procédés et Matériaux (Ecole Centrale, Chatenay Malabry) et le Laboratoire de Planétologie de Grenoble.

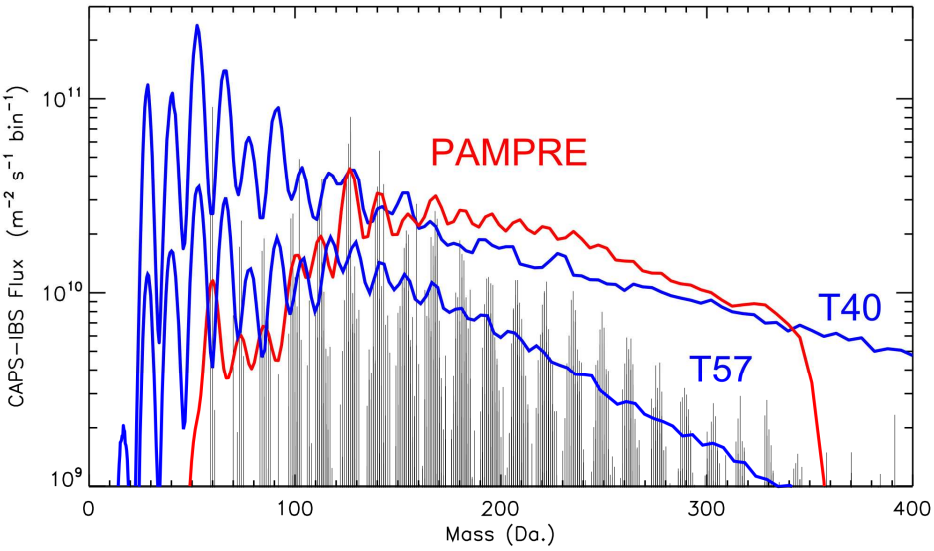

Figure 15: (Bleu) Spectres de masse mesuré par CAPS-IBS lors des survols T40 et T57 de Cassini à 1015km d'altitude. (Noir) Spectre de masse des tholins de PAMPRE à haute résolution (Pernot et al., 2010). (Rouge) Spectre de masse des tholins, avec une résolution dégradée, identique à celle de CAPS-IBS.

Ces travaux ont permis de montrer une grande similitude entre les spectres de masse des ions lourds, m/z > 100, mesurés par l'instrument CAPS-IBS de Cassini dans l'ionosphère de Titan et ceux des tholins de PAMPRE (Westlake et al., 2011). Ceci suggère des processus identiques dans l'ionosphère de Titan et dans le plasma de PAMPRE pour la formation des espèces organiques lourdes (voir Figure 15).

3.3.3. Validation de la composition gazeuse, neutre et ionique

En installant un spectromètre de masse in situ sur l'expérience en 2007, et en développant également un système de piège cryogénique sur l'expérience en 2009, nous avons commencé à travailler sur la compréhension de l'évolution du mélange gazeux avec l'allumage du plasma.

Le travail publié dans Gautier et al., 2011 a permis de mettre en évidence une croissance au sein d'une famille de nitriles (les mono-nitrile saturés) en accord quantitatif avec les concentrations relatives observées dans l'atmosphère de Titan (voir Figure 16). Ces résultats montrent que même si les concentrations absolues des produits formés ne sont pas les mêmes dans le plasma de PAMPRE et dans le plasma naturel que constitue l'ionosphère de Titan, les évolutions relatives entre produits d'une même famille sont comparables. L'expérience de laboratoire va donc nous permettre de comprendre les processus de croissance, voire d'identifier et de prédire la production de nouveaux composés dans l'atmosphère de Titan, en dessous du seuil actuel de détection des instruments de Cassini. L'article correspondant est fourni en annexe parmi les cinq publications les plus significatives de ce travail.

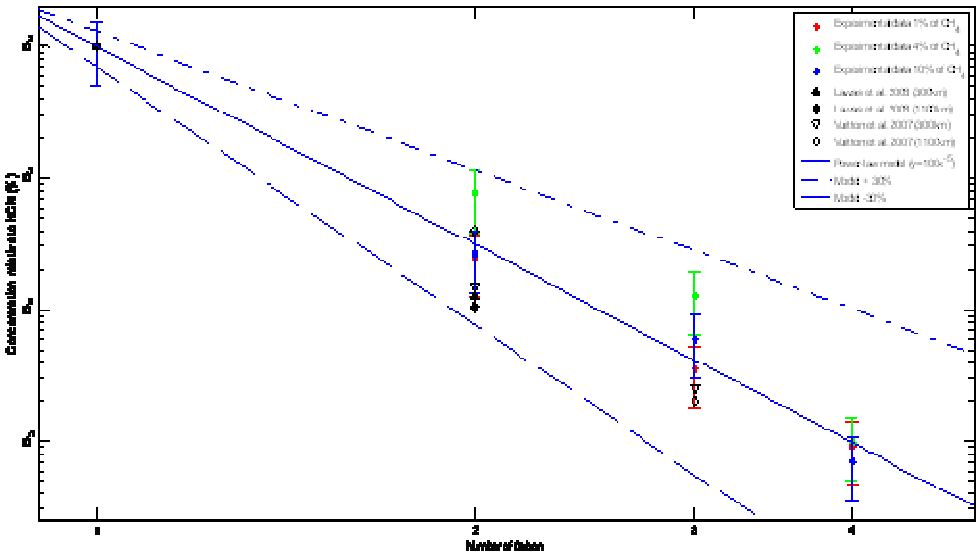

Figure 16 : concentration relative des nitriles en fonction du nombre de carbones dans les molécules. Les points rouge, vert et bleu représentent les points expérimentaux de différentes expériences menées sur PAMPRE. Les courbes bleues représentent la modélisation en loi de puissance de ces points expérimentaux. Les autres symboles (noirs et blancs) représentent les données d'observations de Cassini tirées d'observations CIRS à 300 km et INMS à 1100 km (Vuitton et al., 2007), ainsi que du modèle de Lavvas et al., 2008.

Les ions formés dans un plasma RF d'un mélange 50-50 d'azote-méthane, dans un plasma d'azote pur et dans un plasma de méthane pur sont mesurés par spectrométrie de masse par Mutsukura, 2001 et comparés et analysés par Carrasco et al., 2011 (voir Figure 17). Les ions de masse supérieure à 20 u dans le plasma de mélange sont très différents des ions formés dans les plasmas de méthane et d'azote purs : il s'agit d'ions organiques ayant incorporés de l'azote $C_xH_yN_z^+$, notamment des nitriles et des imines protonés. Ces ions majoritaires sont les mêmes que les ions majoritaires de l'ionosphère de Titan

mesurés par l'instrument INMS, confirmant dans un plasma de laboratoire la nature et la richesse du mélange ionique détecté *in situ* par Cassini.

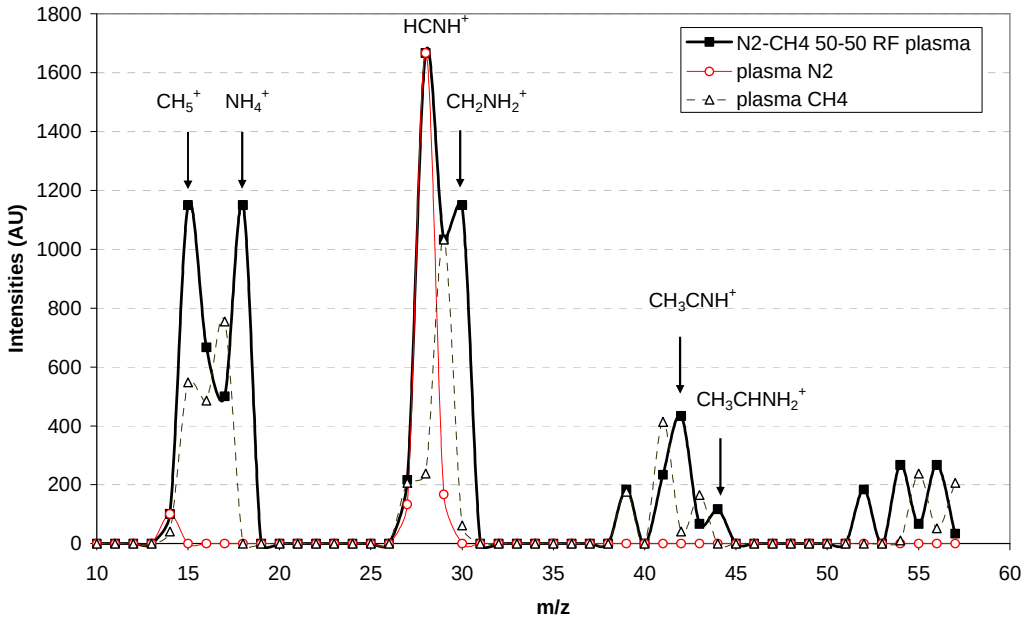

Figure 17 : Spectres de masse des ions mesurés dans un plasma RF d'azote pur, de methane pur et d'un mélange 50-50 d'azote-méthane (Carrasco et al., 2011)

3.3.4. Bilan

Ces travaux d'analyse des produits en phase gazeuse et en phase condensée, ainsi que la confrontation de ces résultats aux observations de Cassini ont donné lieu à huit publications (Carrasco et al., 2011; Carrasco et al., 2009; Gautier et al., 2011; Hörst et al., 2011; Pernot et al., 2010; Sciamma-O'Brien et al., 2010; Vuitton et al., 2010; Westlake et al., 2011) et un travail de revue est en préparation. Ces quatre années d'expérience sur PAMPRE m'ont permis de me former sur les technologies plasma, de m'apporter une approche complémentaire pour l'étude de l'ionosphère de Titan de celle de la modélisation abordée en post- doc, et de développer un réseau de collaboration indispensable pour progresser sur la compréhension de la composition chimique des tholins.

4. Projets scientifiques

4.1. Chimie organique complexe dans l'atmosphère de Titan

L'ionosphère de Titan est un réacteur naturel complexe révélé par la mission Cassini-Huygens, et où se couplent des processus mal connus neutres et ioniques, en phase gazeuse et en phase hétérogène et dont les couplages et rétroactions constituent un chantier important de la recherche sur Titan.

4.1.1. Contexte scientifique international

Jusqu'à aujourd'hui, très peu d'informations directes ont pu être collectées sur les aérosols atmosphériques de Titan. Les données disponibles proviennent des missions Voyager, Pioneer et Cassini-Huygens qui ont confirmé une morphologie de type micro-sphères de quelques dizièmes de micromètres, agrégées en fractales de quelques dizaines de micromètres dans la stratosphère (Tomasko et al., 2005). L'instrument ACP de la sonde Huygens a permis de mettre en évidence des noyaux solides dans l'atmosphère de Titan, relarguant du cyanure d'hydrogène et de l'ammoniac par pyrolyse (Israel et al., 2005). Ce résultat est compatible avec un noyau organique contenant des groupes fonctionnels amine et nitrile. L'instrument CAPS sur l'orbiteur Cassini a également détecté des molécules lourdes dans la haute atmosphère, qui pourraient constituer les précurseurs des aérosols détectés plus bas dans la stratosphère. L'orbiteur Cassini continue de sonder régulièrement l'atmosphère de Titan et d'accumuler des données (voir Waite Jr. et al., 2007; Westlake et al., 2011; Yelle et al., 2010). Néanmoins, ces données sont difficiles à analyser et à interpréter en l'absence de standards de comparaison pour de tels matériaux organiques.
Concernant la composition gazeuse de l'atmosphère de Titan, les molécules neutres majoritaires sont aujourd'hui bien caractérisées à partir des observations, mais les composés traces à l'origine de la formation des aérosols ne sont pas détectables avec les techniques en vol sur l'orbiteur Cassini. Différents scenarii chimiques sont développés dans les modèles atmosphériques pour expliquer ces productions dans la stratosphère (Lavvas et al., 2008; Lebonnois et al., 2002; Wilson et Atreya, 2003) et Lavvas et al., 2009 ont montré que la couche d'aérosols détachée était compatible avec une sédimentation d'espèces formées dans la haute atmosphère. Néanmoins les précurseurs gazeux ne sont pas clairement identifiés. Les mesures récentes des instruments INMS et CAPS de l'orbiteur Cassini montrent une chimie ionique complexe dans la haute atmosphère, certainement un facteur clé pour expliquer les processus de croissance organique dans l'atmosphère de Titan (Coates et al., 2007; Waite Jr. et al., 2007).

J'ai commencé un travail de longue haleine sur la chimie ionosphérique de Titan (voir expériences de post-doc et de Maître de Conférences à l'UVSQ) que j'envisage de poursuivre à court et moyen terme selon trois axes :

- **l'utilisation du réacteur plasma PAMPRE**; validé comme outil de simulation de la chimie ionosphérique de Titan (voir partie 3.3) pour reproduire et comprendre en laboratoire les processus responsable de la croissance organique,
- **le développement et l'utilisation d'un nouveau réacteur ionosphérique, APSIS**,
- **le couplage de la chimie des neutres et des ions positifs dans un modèle de chimie ionosphérique** développé conjointement avec P. Pernot (LCP, Orsay) et M. Dobrijevic (LAB, Bordeaux).

4.1.2. Simulation expérimentale de la chimie de Titan au moyen du dispositif plasma radio-fréquence PAMPRE

1.1.1.1. A court terme, l'influence de la basse température sur le système réactif

Jusqu'à présent, nous avons travaillé à température ambiante. Grâce à des contrats CNRS du programme Origine des Planètes et de la Vie et du Plan National de Planétologie, nous venons de développer et mettre en place en système de refroidissement efficace sur l'expérience, actuellement en phase de caractérisation et qui va nous permettre de travailler à l'avenir dans des conditions de température plus représentatives de l'atmosphère de Titan.

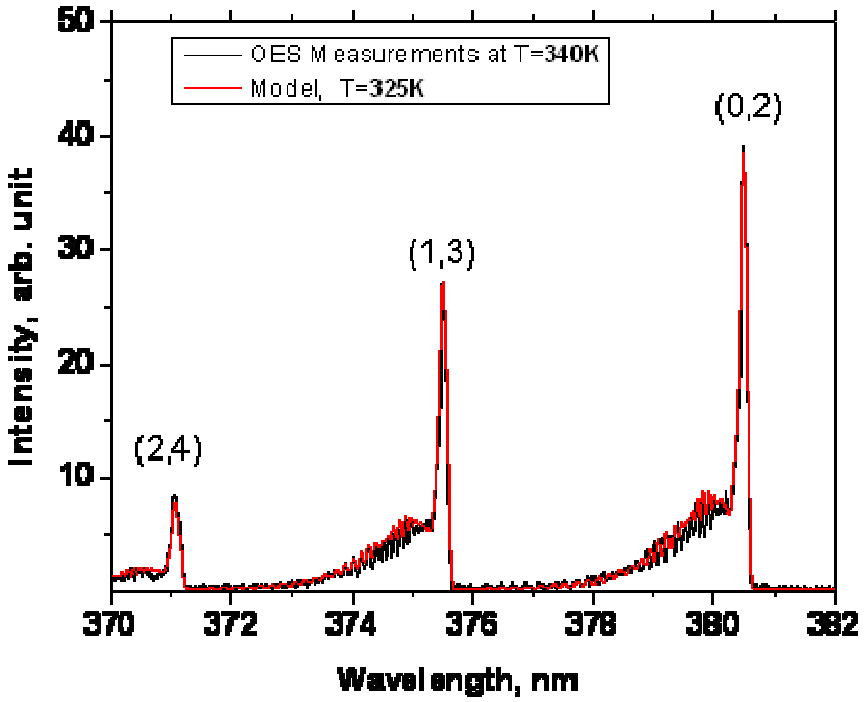

Figure 18 : Spectre UV d'un plasma N_2 (98%)-CH_4 (2)%

Le refroidissement s'effectue par une circulation d'azote liquide au contact de l'électrode supérieure. Le gaz est refroidi à la traversée de cette électrode, mais est aussi échauffé par le bombardement électronique du plasma (Alcouffe et al., 2010). Pour déterminer la température atteinte réellement par le gaz neutre, nous mesurons par spectroscopie optique d'émission les bandes d'émissions UV du second système positif de N_2 (SPS) émises depuis l'état $N_2(C)$: têtes de bandes à 371,0, nm (transition 2-4), 375,5 nm (transition 1-3) et à 380,5 nm (transition 0-2) (voir Figure 18). Un modèle de ces bandes d'émission a été développé au LISA, Créteil, par A. Jolly et permet de calculer ce même spectre, en considérant la fonction d'appareil et une température rotationnelle Tr. Un ajustement optimal des spectres mesurés et simulés permet d'évaluer cette température, qui est égale à la température de gaz neutre.
La Figure 19 présente la calibration obtenue entre la température de l'électrode et celle du gaz neutre, calculée par modélisation des bandes d'émission rovibroniques du second système positif de l'azote. L'efficacité du refroidissement d'atteindre une température du gaz neutre de l'ordre de 220K, au lieu des 340K atteints par échauffement du plasma lorsque le gaz est introduit dans le milieu réactionnel à température ambiante.

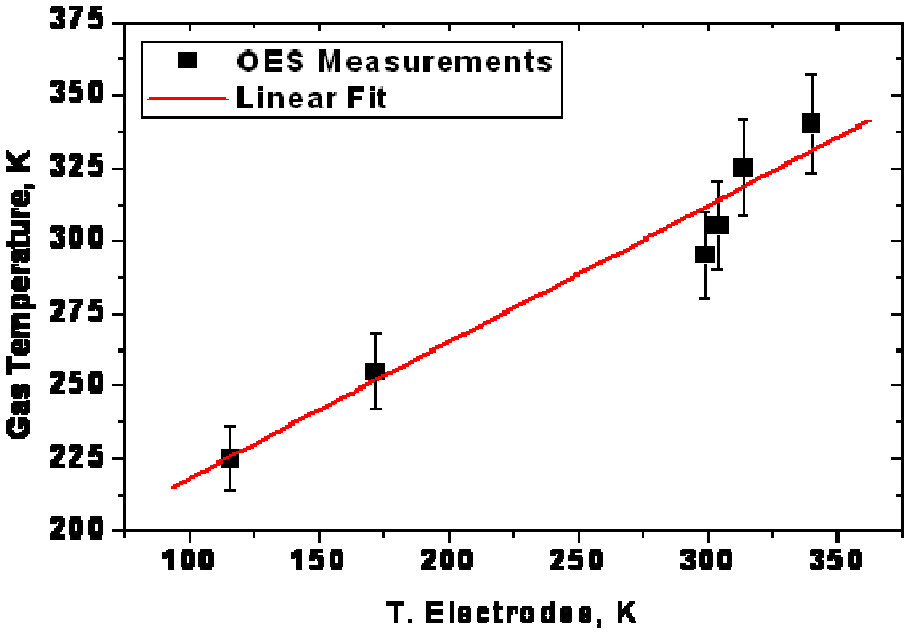

Figure 19 : Evolution de la température du gaz neutre en fonction des parois de la cavité plasma, refroidies par une circulation d'azote liquide.

Nous sommes donc capables de refroidir efficacement l'expérience jusqu'à une température représentative de l'ionosphère de Titan, et de travailler sur une gamme de température d'environ 100 K. Un pan du projet de recherche est d'étudier cette influence du refroidissement en température du gaz neutre sur la cinétique et les productions observées jusqu'à présent à température ambiante.
Pour avancer sur ce projet, je vais poursuivre le co-encadrement de thèse de T. Gautier pendant les deux prochaines années (fin prévue en octobre 2013),

1.1.1.2. A moyen terme : la caractérisation de l'énergie déposée dans le plasma radio-fréquence N_2-CH_4

Enfin, afin de quantifier et décrire les processus primaires qui initient les chaînes de réactions complexes, nous souhaitons prendre un soin tout particulier à la caractérisation de l'énergie déposée dans le plasma. Pour cela, une collaboration est mise en place avec trois universités portugaises (IST Lisbonne, FEUP Porto, Universidade do Minho à Braga) et le laboratoire GREMI à Orléans, initiée par un financement du programme PICS-CNRS 2009-2011.

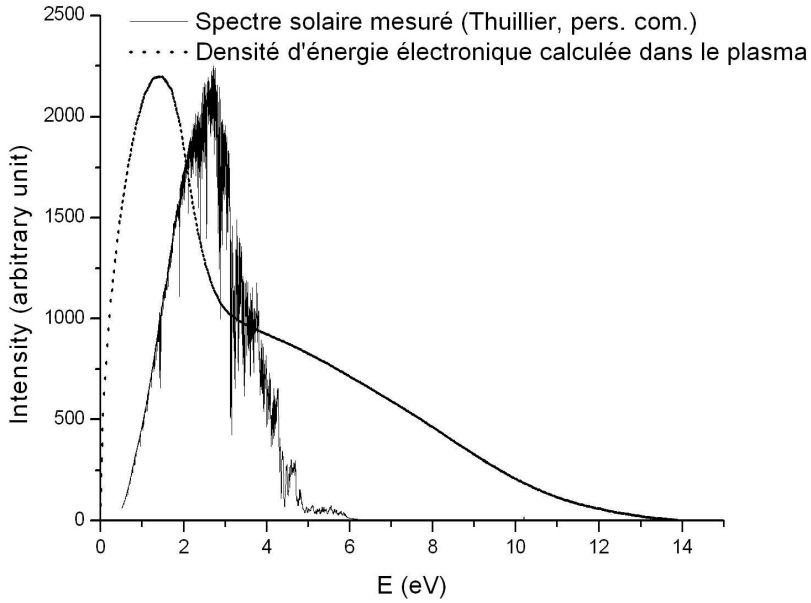

Figure 20 : EEDF du plasma DC d'azote-méthane de Bernard, 2004, compare au spectre solaire : courbe pleine : spectre solaire ; courbes pointillée : EEDF du plasma DC.

Les plasmas sont des milieux qui ne sont pas à l'équilibre thermodynamique ; la température des électrons est beaucoup plus élevée que la température des espèces neutres dans le gaz. Des atomes et des radicaux sont générés par collision électronique et forment des hydrocarbures lourds et des tholins. Du fait des collisions inélastiques des électrons, la fonction de distribution en énergie des électrons (EEDF) n'est pas une distribution de Maxwell et dépend des conditions expérimentales choisies (concentrations de méthane, pression, puissance, débit de gaz…).
Comme l'énergie de dissociation de l'azote est de 9,7 eV, seuls les électrons de la queue de la distribution en énergie permettent sa dissociation. Malheureusement, cette énergie effectivement déposée et permettant d'initier les processus n'est pas une donnée directement accessible. L'énergie globale effectivement absorbée par le milieu est très différente de la mesure de la puissance dépensée électriquement qui inclut de nombreuses pertes supplémentaires par effet Joule dans l'ensemble du montage expérimental. La détermination de l'EEDF nécessite donc un travail de modélisation du plasma. A partir de l'EEDF modélisée, nous pourrons déduire les premières étapes de la chimie dans le plasma.
Pour contraindre ce modèle, nous avons besoin de mesurer le maximum d'observables expérimentaux. C'est la raison pour laquelle l'ANR Jeune Chercheur dont je suis responsable finance un nouveau diagnostique IR-TF (InfraRouge à Transformée de Fourier). Ce dernier a été acheté et nous sommes en train de l'installer. Cet instrument nous permettra de caractériser la formation des produits gazeux et des poudres *in situ*. Avec l'ensemble de ces données, nous progresserons sensiblement sur la croissance des particules dans le volume du plasma, sur les mécanismes primaires impliqués lors du dépôt d'énergie dans le plasma et sur la chimie en phase gazeuse qui forme les précurseurs des aérosols organiques solides.
Cette tâche correspond au sujet de post-doc d'A. Mahjoub, recruté sur le financement ANR Jeune-chercheur CAT présenté partie 2.4.2 et dont le financement se terminera en septembre 2012. Pour poursuivre les recherches au-delà de 2012, nous envisageons avec mes collaborateurs portugais de déposer une thèse en co-tutelle, avec une direction principale portugaise.

1.1.1.3. A long terme : la chaîne réactionnelle complète depuis les composés primaires N_2-CH_4 jusqu'aux tholins

Mon projet à long terme vise à étudier de la chaîne complète de réactions, depuis la dissociation de l'azote et du méthane, jusqu'à la formation des produits gazeux et particulaires au moyen du montage expérimental PAMPRE.

Afin de comprendre la complexité chimique du brouillard organique solide observable dans l'atmosphère de Titan, je propose notamment de continuer le travail sur la caractérisation chimique et structurale des tholins (Carrasco et al., 2009; Pernot et al., 2010; Vuitton et al., 2010). Notons que l'article Carrasco et al. 2009 est fourni en annexe parmi les résultats les plus significatifs de ce travail. Ce travail interdisciplinaire nécessite des collaborations externes dans la mesure où le laboratoire LATMOS n'est pas un laboratoire de chimie analytique et ne dispose donc pas de beaucoup de matériel d'analyse chimique. Il va se poursuivre avec les collaborations déjà effectives (ICSN, Gif sur Yvette, LCP Paris, LGPM, Ecole Centrale Paris, LPG, Grenoble), mais également s'étendre à de nouveaux partenaires identifiés à l'UVSQ : l'ILV pour des mesures XPS (X-ray Photoelectron Spectroscopy) et le GEMAC pour des mesures SIMS (Secondary Ion Mass Spectrometry). Chaque analyse menée à son terme apportera des renseignements qui seront répertoriés et mis en partage sur la Banque de Données des Atmosphères Planétaires (BDAP) (http://bdap.ipsl.fr/pampre/).

4.1.3. Développement d'un nouveau réacteur simulant la photochimie dans l'atmosphère de Titan sur une ligne synchrotron de SOLEIL

Les montages plasma présentent l'avantage de reproduire en laboratoire un spectre énergétique d'électrons plus ou moins comparable au spectre solaire, et permettant en particulier la dissociation de l'azote moléculaire, essentiel pour la chimie atmosphérique de Titan. Le dépôt d'énergie se fait en volume et il est très efficace pour produire en quantité des poussières organiques, analogues des aérosols de Titan. Cependant, les processus d'impact électroniques caractéristiques des montages plasma ne sont pas strictement équivalents en termes de section efficace et de rapport de branchement aux processus de photo-dissociation.

Une expérience a été menée récemment sur un synchrotron aux Etats Unis par le groupe de Mark Smith à l'Université de Tucson, à des basses pressions, et en utilisant une lumière monochromatique dans le VUV. Les résultats de ce travail sont très prometteurs (Imanaka et Smith, 2007) pour la compréhension des processus chimiques complexes.

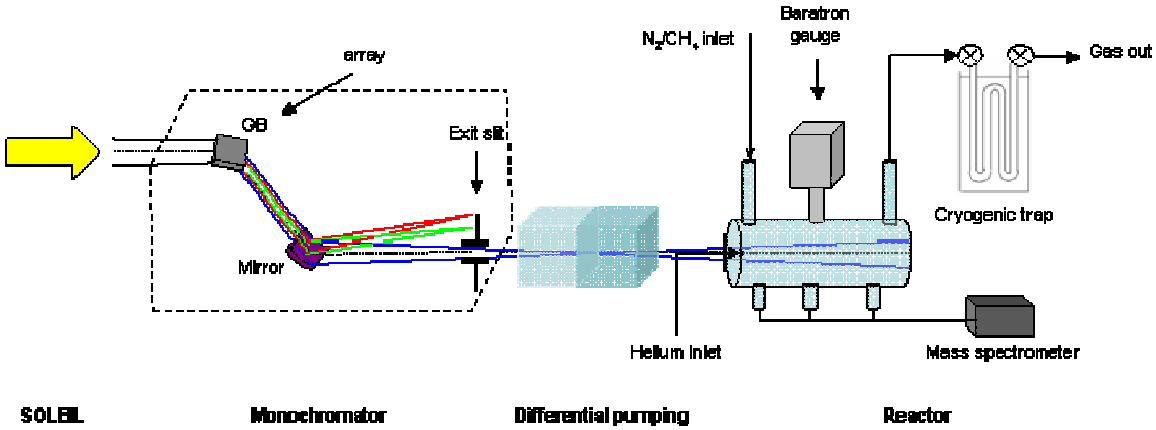

Figure 21 : Schéma du réacteur APSIS pour la ligne de lumière DISCO du synchrotron SOLEIL.

Avec une approche sensiblement différente, **nous avons développé un réacteur photochimique couplé avec le synchrotron SOLEIL : le réacteur APSIS, Atmospheric Photochemistry SImulated by Synchrotron** (voir Figure 21), grâce au financement du PRES-UniverSud et du pôle d'Exobiologie du CNES.
Le réacteur est opérationnel depuis l'automne 2010. Il s'agit d'un réacteur en inox de 50 cm de long, créé pour supporter une large gamme de pressions (de quelques dizièmes de mbar à 1 bar) dans un flux continu d'azote et de méthane, avec des concentrations de méthane ajustables, variant de 0 à 10%. Le haut du réacteur est amovible afin de collecter facilement les produits solides déposés sur les parois du réacteur. Un spectromètre de masse *in situ* permet de suivre l'évolution de la composition gazeuse dans le mélange à différentes positions dans le réacteur.

Ce montage expérimental permet d'effectuer des expériences dans des conditions aussi proches que possibles de celles de PAMPRE (P, T, débit, large spectre continu dans l'UV) en travaillant sur la seule ligne de lumière offrant ces conditions expérimentales : la ligne DISCO de SOLEIL dont le spectre comparatif à celui du Soleil est représenté Figure 22.

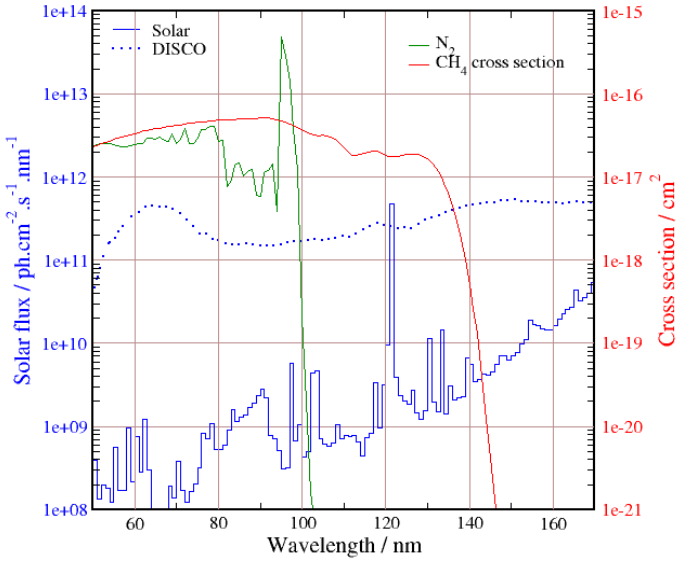

Figure 22 : Comparaison des spectres en énergie de DISCO et du Soleil.

Ce projet dont je suis responsable fédère cinq laboratoires d'Ile de France : le LATMOS, le LISA (Créteil), le LGPM (Centrale Paris, Chatenay Malabry), le LCP (Orsay) et le laboratoire DISCO du synchrotron Soleil (Saint Aubin).

L'utilisation du synchrotron pour initier les chaînes de réactions complexes permet de réaliser la première inter-comparaison électrons *vs.* photons entre un montage basé sur une technique plasma (PAMPRE) et un montage basé sur de la photochimie (APSIS) pour l'amorçage de la chimie globale issue de la dissociation de l'azote et du méthane. Cette étude comparative, permettra de mieux appréhender le rôle des processus primaires dans un contexte global de simulation de la chimie atmosphérique se produisant dans l'atmosphère de Titan. Ce projet long terme constitue à ma connaissance la première tentative d'une telle inter-comparaison plasma/photolyse pour la communauté des sciences planétaires.

Nous avons déjà obtenu sur appel d'offre (automne 2010, printemps 2011) deux sessions de temps de faisceau qui ont permis de tester l'installation, de faire des expériences préliminaires ainsi que d'obtenir une première série d'expériences en irradiation d'un mélange à 90-10% d'azote-méthane sur la ligne DISCO. Ces résultats préliminaires vont être présentés par Z. Peng à la conférence EPSC-DPS d'octobre 2011 (voir Figure 23).

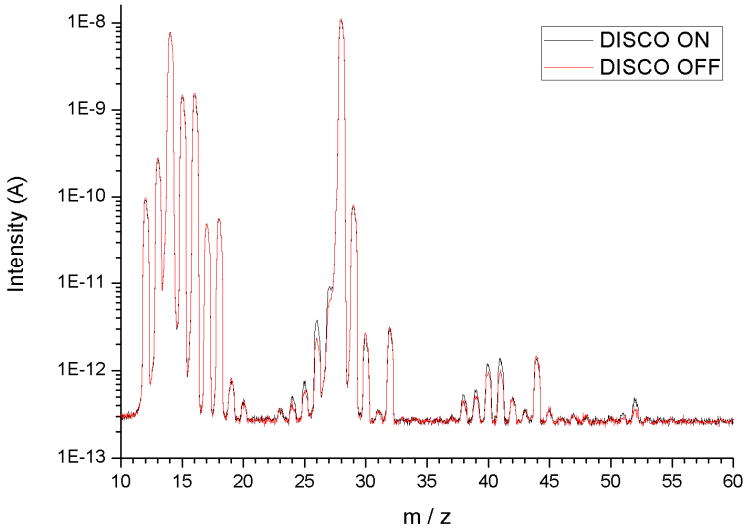

Figure 23 : Effet d'environ 1 h d'irradiation DISCO sur un mélange N_2-CH_4 90-10%.

D’autre part, pour compléter les expériences sur ce réacteur en dehors des temps de faisceaux accordés sur synchrotron, nous avons participé au printemps 2011 à un appel d’offre d’Excellence organisé par l’UVSQ, pour lequel nous sommes en attente du résultat. La sélection éventuelle de ce projet nous permettrait de compléter les expériences tout au long de l’année au LATMOS. En effet cela nous permettrait de remplacer au laboratoire la source de lumière synchrotron par une lampe à décharge plasma : nous serons dans les mêmes conditions environnementales, avec une source de lumière permettant comme sur DISCO de dissocier l’azote, mais à longueur d’onde discrète.

A court terme, pour avancer sur ce projet de photolyse d’un mélange gazeux simulant l’atmosphère de Titan avec des conditions physiques comparables aux conditions du réacteur PAMPRE, je vais poursuivre le co-encadrement de thèse de Z. Peng pendant deux ans (fin prévue octobre 2013). D’autre part, si l’équipe est sélectionnée sur l’appel d’offre d’Excellence de l’UVSQ 2011, nous serons à même de faire fonctionner le réacteur APSIS dans les locaux du LATMOS. Je pourrai dans ce cas proposer des stages de niveau L3, M1 ou M2 avec cet outil au cours des prochaines années.
A plus long terme, ce réacteur sera utilisé pour initier de nouveaux sujets de recherches liés à la photochimie atmosphérique, complémentaire de l’approche plasma du réacteur PAMPRE. Il permettra en particulier de simuler la réactivité dans des couches atmosphériques plus basses, préservées du rayonnement solaire ionisant de la haute atmosphère.

4.1.4. Couplage de la chimie des ions et de la chimie des neutres dans un modèle de chimie ionosphérique

Le travail de thèse de S. Plessis (Plessis, 2010), que nous avons co-encadré P. Pernot et moi-même a permis de mettre en évidence l'importance d'une famille de processus dont la description était négligée jusqu'à présent dans les modèles de chimie ionosphérique. Il s'agit des processus de recombinaison dissociative (RD) des ions avec les électrons de faible énergie de l'ionosphère. Ces processus sont très exothermiques et conduisent à la formation de plusieurs neutres, souvent avec rupture d'une liaison avec un hydrogène labile (processus dit à « perte de H »), mais également avec cassure de la chaîne carbonée de l'ion.
Un exemple de fragmentation est développé sur la Figure 24. B1 et B3 correspondent aux rapports de branchement entre les deux voies de fragmentation. B11 et B12 sont deux sous-rapports de branchement de la voie B1. L'exemple développé Figure 24 illustre ainsi le fait qu'au cours d'une expérience les produits peuvent être imparfaitement caractérisés, conduisant à des scénarii de répartition plus ou moins connue entre les deux sous-voies conduisant aux produits neutres P1 et P2.

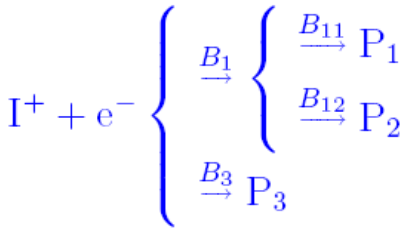

Figure 24 : Exemple de la fragmentation d'un ion par recombinaison dissociative avec un électron.

Les composés formés sont des espèces neutres souvent instables, difficiles à récupérer, identifier et quantifier en laboratoire. Les bases de données de ces recombinaisons dissociatives s'arrêtent donc au-delà des hydrocarbures à 4 carbones et très peu d'ions azotés ont été étudiés. La complexité des analyses expérimentales et leur incomplétude est illustrée Figure 25 sur l'exemple de lion $C_4H_9^+$.

Cette difficulté et cette méconnaissance expliquent que les modèles de chimie ionosphérique de Titan ont jusqu'à présent ignoré cette source de production d'espèces neutres dans l'ionosphère de Titan. Seuls des schémas « perte de H » ou légèrement améliorés (implémentation spécifique de quelques réactions de recombinaison dissociative pour expliquer des observations particulières) sont implémentés. C'est le cas par exemple du travail de Yelle et al., 2010 pour expliquer la formation d'ammoniac, ou encore de Wilson et Atreya, 2003 pour la formation de benzène, ces deux composés ayant été détectés en concentrations importantes par l'INMS de Cassini sans que les modèles de photochimie seuls puissent l'expliquer.

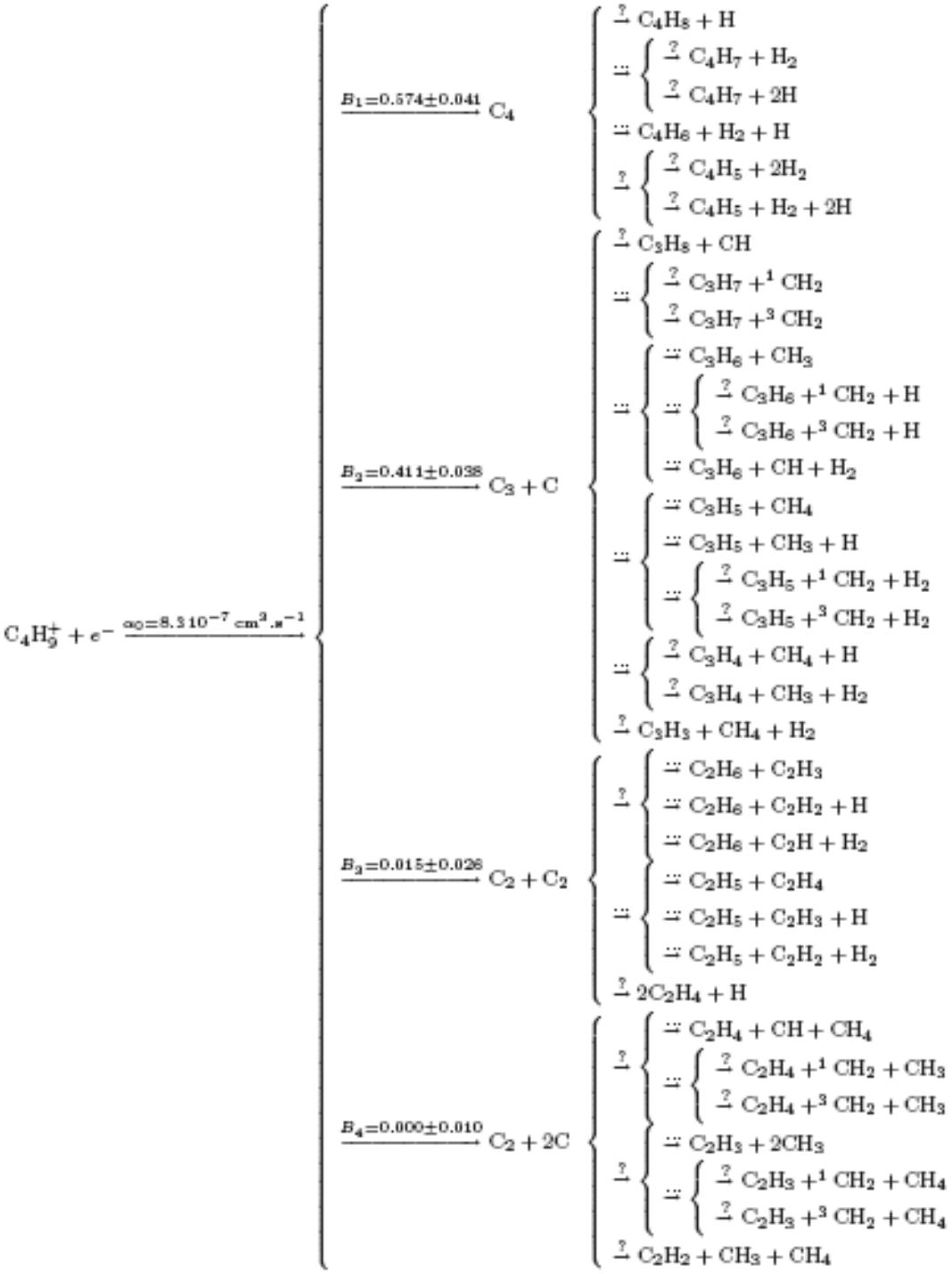

Figure 25 : Exemple du schéma de fragmentation de l'ion $C_4H_9^+$ par recombinaison dissociative.

Plessis et al., 2010 répertorient ainsi de manière exhaustive toutes les données existantes sur les rapports de branchement des DR pour lesquelles existent des déterminations expérimentales plus ou moins complètes et propose une méthode probabiliste pour tenir compte des incertitudes importantes sur ces rapports de branchement, tout en conservant fidèlement la structure imbriquée des déterminations expérimentales. Le détail de cet article est fourni en fin de document parmi les cinq publications les plus significatives de ce travail.

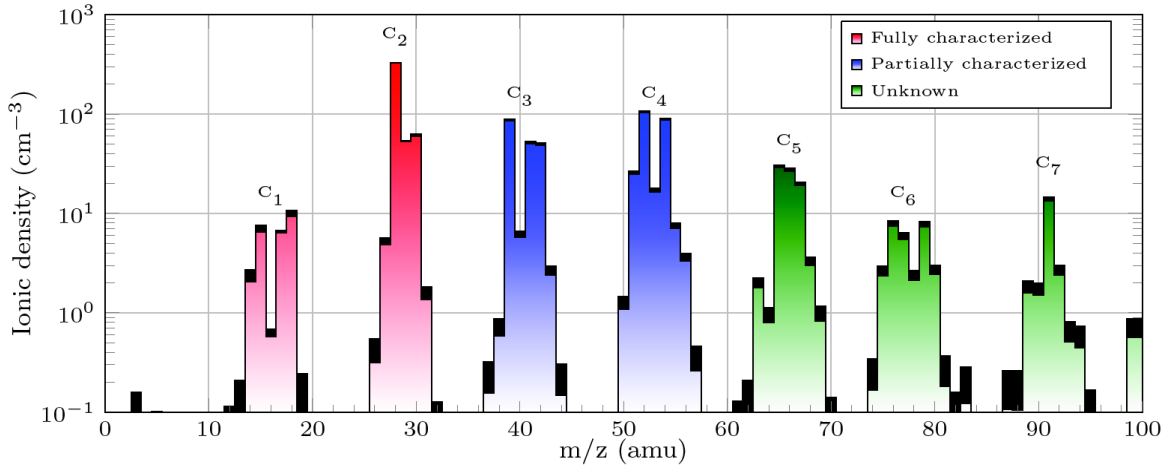

Figure 26 :Spectre de masse des ions mesuré par l'instrument INMS au cours du survol diurne T19 à 1100 km d'altitude. La couleur des blocs indique l'état des connaissances sur les produits neutres issus des recombinaisons dissociatives des ions identifiés.

Grâce à ce travail préliminaire, nous sommes capables de calculer pour l'atmosphère de Titan les flux de production de neutres dans l'ionosphère de Titan (Équation 1), issus des recombinaisons dissociatives des ions avec leurs concentrations effectivement mesurées par INMS (exemple de spectre de masse INMS reporté Figure 26).

$$\frac{\mathrm{d}\,[\mathrm{M}]}{\mathrm{d}t} = \sum_{r} \left[\alpha_0^{(r)} \times \left(\frac{T_e}{300} \right)^{\beta^{(r)}} \times [I^+]_r \times d_e \times \sum_{j=1}^{n_r} b_j^{(r)} \times \nu_{j,\mathrm{M}} \right]$$

Équation 1 : Calcul du flux de production de l'espèce neutre M par la RD r.
[M] est la concentration de l'espèce M,
α_0 est la constante de vitesse à 300 K ,
β_0 est paramètre puissance de la constante de vitesse en fonction de la température,
$[I^+]_r$ est la concentration de l'ion détruit par la RD r,
de est la concentration en électrons,
$b_j^{(r)}$ est le rapport de branchement de la voie j de r produisant M
$\nu_{j,M}$ est le coefficient stochiométrique de la voie j de r.

Nous les avons ensuite comparés aux flux des mêmes neutres issus du modèle photochimique de M. Dobrijevic, LAB Bordeaux. La comparaison des flux de production d'hydrocarbures est donnée Figure 27. Il montre que les flux issus RD des ions est souvent du même ordre de grandeur, voire plus important que les flux de production photochimiques (Plessis et al., 2011).

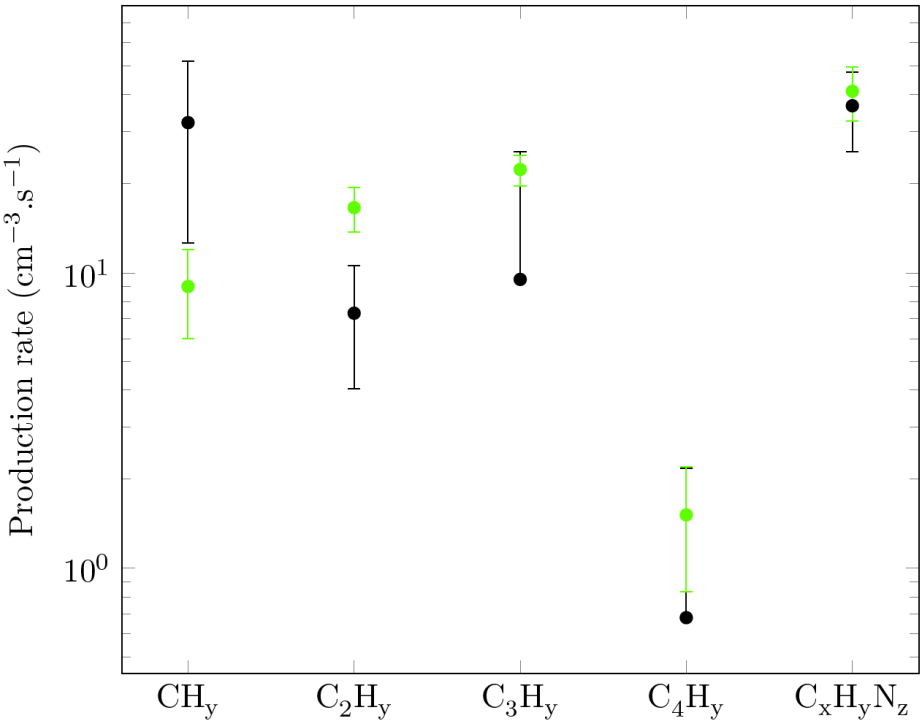

Figure 27 : Comparaison des vitesses de production de neutres à 1100 km. (Noir) Vitesse de production par le modèle photochimique ; (vert) vitesse de production par les recombinaisons dissociatives avec les densités ioniques mesurées par INMS au cours du survol T19 à 1100 km d'altitude.

Les conséquences de ce travail sont essentielles puisqu'elles mettent en évidence l'importance des processus de RD pour la production de neutres dans l'atmosphère de Titan. Carrasco et al., 2007c avaient dans une première étape identifié la grande sensibilité du modèle des ions à la description du bain de neutres servant à prédire les densités d'ions. Plessis et al., 2011 vont plus loin puisqu'ils remettent en question la notion même de bain de neutres pour les modèles de chimie ionosphérique. Si les flux de neutres sont fortement perturbés par les DR, on ne peut plus les considérer comme invariables devant la réactivité des ions. Ils montrent donc la nécessité de développer des modèles totalement couplés entre chimie des ions et chimie des neutres pour prédire des densités correctes d'ions et de neutres.

La suite à long terme de ce projet sur la modélisation de la chimie ionosphérique est donc de développer un modèle couplé ionosphérique en collaboration avec P. Pernot et M. Dobrijevic. Ce travail tiendra compte des incertitudes sur l'ensemble des paramètres réactionnels (constantes de vitesse, rapports de branchement, leurs dépendance en température, etc..) du modèle des ions comme du modèle des neutres.
De longue haleine, ce travail de couplage va être amorcé par Z. Peng, étudiant en première année de thèse en co-direction entre P. Pernot et moi-même (fin prévue en octobre 2013).

4.2. Vers la chimie de la Terre primitive

La chimie organique abiotique de l'atmosphère de Titan est la plus efficace connue dans le système solaire (Atreya, 2006). Il est courant d'extrapoler cette atmosphère à celle de la Terre primitive pour expliquer la croissance organique prébiotique sur la Terre ayant précédé et ou accompagné l'apparition de la vie : une atmosphère relativement réductrice essentiellement composée d'azote et de méthane. Dans le cas de Titan, l'azote moléculaire serait vraisemblablement issu de la photolyse de l'ammoniac primordial au cours de l'histoire de Titan (Atreya et al., 1978; Atreya et al., 2010). Le point déterminant est que le méthane est identifié comme le facteur clé de la croissance organique (Raulin, 2005) car le carbone est plus réactif sous sa forme la plus réduite CH_4 que sous sa forme la plus oxydée CO_2.

Néanmoins, la comparaison aux deux autres planètes telluriques nous suggère que l'atmosphère terrestre primitive était comme celles de Mars et Vénus massivement oxydée. Les scenarii les plus probables actuels proposent donc une atmosphère primitive de CO_2 et d'azote moléculaire. L'azote étant un composé relativement lourd, il n'a pas subi d'échappement et aurait donc été dans les mêmes abondances qu'aujourd'hui ~0,8 bar (Selsis et Parisot, 2005). La quantité de CO_2 reste délicate à prévoir notamment du fait des cycles complexes du CO_2 avec les émissions volcaniques et les sédimentations sous forme de carbonates. En l'absence d'autres gaz à effet de serre, une pression partielle de 0,2 bar de CO_2 aurait suffi à maintenir la température à 0°C avant -4 milliard d'années (Kasting, 1993). Cette atmosphère oxydante n'exclut néanmoins pas la présence de méthane : soit abiotique par différents processus (volcanisme primitif, capture de la nébuleuse primitive même faible, impacts météoritiques, chimie abiotique inconnue…) soit biotique une fois la vie émergeante.

L'importance avérée du méthane dans la croissance organique a conduit Trainer et al., 2006 à étudier en simulation expérimentale la formation d'aérosols organiques dans des mélanges CO_2-CH_4 et CO_2-CH_4-N_2. Leur dépôt d'énergie s'effectue par photolyse avec une lampe UV ne permettant pas la dissociation de l'azote. Ils simulent pourtant une atmosphère sèche correspondant à la haute atmosphère, là où donc l'azote doit être partiellement dissocié.
Forts de nos expériences appliquées à Titan en mélange N_2-CH_4 et N_2-CH_4-CO (Hörst et al., 2011), nous envisageons donc de travailler sur le même type de mélanges que Trainer et al., mais en utilisant les réacteurs PAMPRE (décrit dans la partie 3.3.1) et APSIS (décrit dans la partie 4.1.3) qui permettront d'étudier l'influence de la réactivité de l'azote sur ce système chimique. Ceci permettra de vérifier si comme dans Titan, la haute atmosphère sèche de la Terre primitive a pu produire des aérosols organiques d'intérêt prébiotique ensemençant par sédimentation les basses couches atmosphériques et la surface terrestre.

J'ai pour projet de déposer un sujet de thèse en pleine direction sur ce thème pour la rentrée de septembre 2012.

4.3. Conclusion et perspectives

Pour résumer, je souhaite caractériser la chaîne complète de processus chimiques atmosphériques de Titan depuis la dissociation des composés primaires en phase gazeuse, jusqu'à la formation du brouillard organique en suspension dans l'atmosphère, en utilisant et en développant des outils de modélisation et de simulation expérimentale. L'un des montages expérimentaux est déjà en activité et doit être amélioré (par installation de l'IR *in situ*, financement ANR jeune chercheur), un autre a été récemment développé et adapté à la ligne DISCO du synchrotron SOLEIL. En complément aux simulations expérimentales, la modélisation me permettra de mettre en évidence les processus clés de la chimie ionosphérique complexe de Titan.

Les processus physico-chimiques conduisant à la formation d'aérosols organiques dans des atmosphères planétaires extra-terrestres ne sont pas limités à Titan. Je souhaite étendre la méthodologie développée sur le cas d'étude de Titan à d'autres atmosphères comparables. L'atmosphère de Titan est aujourd'hui au cœur d'études intensives car une mission spatiale est en orbite autour de ce satellite et parce que Titan constitue un analogue glacé possible de la Terre primitive.

Une première étape raisonnable vers l'étude d'autres systèmes d'intérêt exobiologique, et dans la continuité de nos travaux sur l'atmosphère de Titan concerne l'atmosphère de la Terre primitive, pour laquelle des études en modélisation ont déjà activement démarré au LATMOS (E. Marcq et F. Leblanc), ainsi qu'à Bordeaux, dans l'équipe de Franck Selsis et de Michel Dobrijevic. Nous envisageons donc dans un futur proche de commencer un travail de simulation expérimentale complémentaire pour étudier la possibilité de croissance organique dans la haute atmosphère primitive.

Au delà des corps du système solaire, le défi scientifique de la prochaine décennie sera l'observation directe et la caractérisation des exoplanètes et de leurs atmosphères. Cette perspective enthousiasmante ouvre les portes d'un nouveau champ d'étude de la chimie atmosphérique pour des atmosphères qui, on peut le penser, contiennent des composés organiques. Récemment, on a ainsi rapporté la première détection de méthane dans une atmosphère d'exoplanète (Swain et al., 2008), initiant une ère de découvertes sur ces atmosphères lointaines.

Mon ambition à plus long terme est de simuler la chimie des atmosphères des exoplanètes au moyen de l'expérience PAMPRE et de la nouvelle expérience APSIS sur SOLEIL afin d'étayer les futures observations spectroscopiques de ces atmosphères. Ce projet est encore très prospectif et nécessite plus de contraintes observationnelles pour réaliser et choisir des mélanges d'intérêt pour la simulation de ces atmosphères. Néanmoins, dès que possible, ce travail revêtira un grand intérêt pour l'exobiologie et la recherche de matériaux organiques dans l'Univers.

5. Références bibliographiques

Alcouffe, G., et al., 2010. Capacitively coupled plasma used to simulate Titan's atmospheric chemistry. Plasma Sources Science and Technology 19**,** 015008.

Anderson, C. M., Samuelson, R. E., 2011. Titan's aerosol and stratospheric ice opacities between 18 and 500 µm: Vertical and spectral characteristics from Cassini CIRS. Icarus. 212**,** 762-778.

Atreya, S. K., 2006. Titan's Organic Factory. Science. 316**,** 843-845.

Atreya, S. K., et al., 1978. Evolution of a Nitrogen Atmosphere on Titan. Science. 201**,** 611-613.

Atreya, S. K., et al., Volatile Origin and Cycles: Nitrogen and Methane. In: R. H. Brown, et al., Eds.), Titan from Cassini-Huygens. Springer Netherlands, 2010, pp. 177-199.

Bar-Nun, A., et al., 2008. Titan's aerosols: Comparison between our model and DISR findings. Planetary and Space Science. 56**,** 708-714.

Bernard, J.-M., Simulation expérimentale de la chimie atmosphérique de Titan :
Suivi des espèces produites et comparaison à un modèle cinétique. Université Paris 7, 2004.

Bose, D., et al., 2003. Uncertainty and sensitivity analysis of gas-phase chemistry in a CHF_3 plasma. Plasma Sources Science and Technology. 12**,** 225-234.

Carrasco, N., et al., 2007a. Simulation studies of the atmospheric oxidation of 2-Methyl-3-Buten-Ol : reactions with hydroxy radicals and ozone under a variety of conditions. . *Journal of Atmospheric Chemistry*. 56**,** 33-55.

Carrasco, N., et al., 2006a. Tropospheric degradation of 2-Hydroxy-2-MethylPropanal, a photoxydation product of 2-Methyl-3-Buten-Ol: kinetic and mechanistic study of its photolysis and its reaction with OH radicals. . *Atmospheric Environment*. 40**,** 2011-2019.

Carrasco, N., et al., 2008a. Sensitivity of a Titan ionospheric model to the ion-molecule reaction parameters. . Planet. Space Sci. 56**,** 1644-1657.

Carrasco, N., et al., 2007b. Uncertainty analysis of bimolecular reactions in Titan ionosphere chemistry model. Planetary and Space Science. 55**,** 141-157.

Carrasco, N., et al., 2011. Volatile products controlling Titan's tholins production. in preparation.

Carrasco, N., et al., 2007c. Influence of neutral transport on ion chemistry uncertainties in Titan ionosphere. Icarus. 192**,** 519-526.

Carrasco, N., Pernot, P., 2007. Modeling of Branching Ratio Uncertainty in Chemical Networks by Dirichlet Distributions. The Journal of Physical Chemistry A. 111**,** 3507-3512.

Carrasco, N., et al., 2007d. Kinetic and mechanistic study of the reaction of sabinaketone with OH radicals. *International Journal of Chemical Kinetics* 39**,** 415-421.

Carrasco, N., et al., 2008b. Toward a reduction of the bimolecular reaction model for titan's ionosphere. International Journal of Chemical Kinetics. 40**,** 699-709.

Carrasco, N., et al., 2006b. Experimental and theoretical study of the reaction of OH radical with sabinene. . *Physical Chemistry and Chemical Physics*. 8**,** 3211-3217.

Carrasco, N., et al., 2009. Chemical Characterization of Titan's Tholins: Solubility, Morphology and Molecular Structure Revisited The Journal of Physical Chemistry A. 113**,** 11195-11203.

Chiappini, L., et al., 2006. Gaseous and Particulate Products from the Atmospheric Ozonolysis of a Biogenic Hydrocarbon, Sabinene. *Environmental Chemistry* 3 286-296.

Coates, A. J., et al., 2007. Discovery of heavy negative ions in Titan's ionosphere. Geophys. Res. Lett. 34**,** L22103.
Coll, P., et al., 1999. Experimental laboratory simulation of Titan’s atmosphere: Aerosols and gas phase. Planet. Space Sci. 47**,** 1331-1340.
Cravens, T. E., et al., 2006. Composition of Titan’s ionosphere. Geophysical Research Letters. 33**,** L07105.
Dobrijevic, M., et al., 2008. Epistemic bimodality and kinetic hypersensitivity in photochemical models of Titan's atmosphere. . Planet. Space Sci. 56**,** 1630-1643.
Dobrijevic, M., et al., 2010. Comparison of methods for the determination of key reactions in chemical systems: Application to Titan's atmosphere. Advances in Space Research. 45**,** 77-91.
Dobrijevic, M., et al., 2003. Effect of chemical kinetic uncertainties on photochemical modeling results : Application to Saturn's atmosphere. A&A. 398**,** 335-344.
Gans, B., et al., 2009. Determination of the Absolute Photoionization Cross Sections of CH_3 and I Produced from a Pyrolysis Source, by Combined Synchrotron and Vacuum Ultraviolet Laser Studies The Journal of Physical Chemistry A. 114**,** 3237-3246.
Gautier, T., et al., 2011. Nitrile gas chemistry in Titan atmosphere. Icarus. 213**,** 625-635.
Hörst, S., et al., 2011. Formation of Prebiotic Molecules in a Titan Atmosphere Simulation Experiment. Astrobiology. Revision.
Imanaka, H., et al., 2004. Laboratory experiments of Titan next term tholin formed in cold plasma at various pressures: implications for nitrogen-containing polycyclic aromatic compounds in previous termTitan next term haze Icarus. 168**,** 344-366.
Imanaka, H., Smith, M. A., 2007. Role of photoionization in the formation of complex organic molecules in Titan's upper atmosphere. Geophys. Res. Lett. 34**,** L02204.
Israel, G., et al., 2005. Complex organic matter in Titan's atmospheric aerosols from in situ pyrolysis and analysis. Nature. 438**,** 796-799.
Kasting, J. F., 1993. Earth's Early Atmosphere. Science. 259**,** 920-926.
Klawatsch-Carrasco, N., et al., 2004. Absolute rate constants for the gas-phase ozonolysis of isoprene and methylbutenol. . International Journal of Chemical Kinetics. 36**,** 152-156.
Lavvas, P., et al., 2009. The detached haze layer in Titan's mesosphere. Icarus. 201**,** 626-633.
Lavvas, P. P., et al., 2008. Coupling photochemistry with haze formation in Titan's atmosphere, Part II: Results and validation with Cassini/Huygens data. Planetary and Space Science. 56**,** 67-99.
Lebonnois, S., et al., 2002. Transition from Gaseous Compounds to Aerosols in Titan's Atmosphere. Icarus. 159**,** 505-517.
Mutsukura, N., 2001. Deposition of Diamondlike Carbon Film and Mass Spectrometry Measurement in CH4/N2 RF Plasma. Plasma Chemistry and Plasma Processing. 21**,** 265-277.
Peng, Z., et al., 2010. Photochemical modeling of Titan atmosphere at the "10 percent uncertainty horizon". Faraday Discussions. 147**,** 137-153.
Pernot, P., et al., 2010. Tholinomics: Chemical Analysis of Nitrogen-Rich Polymers. Analytical Chemistry. 82**,** 1371-1380.
Plessis, S., Modélisation probabiliste pour l’étude de l’influence des ions sur la composition des espèces neutres dans l’atmosphère de Titan : inversion bayésienne de spectres de masse INMS et représentation des recombinaisons dissociatives par distributions de Dirichlet imbriquées. Université Paris Sud, Orsay, 2010.
Plessis, S., et al., 2011. Production of neutral species in Titan's ionosphere through dissociative recombination of ions as measured by INMS. in preparation.

Plessis, S., et al., 2010. Knowledge-based probabilistic representations of branching ratios in chemical networks: The case of dissociative recombinations. The Journal of Chemical Physics. 133**,** 134110-21.
Quirico, E., et al., 2008. New experimental constraints on the composition and structure of tholins. Icarus. 198**,** 218-231.
Rannou, P., et al., 2010. Titan haze distribution and optical properties retrieved from recent observations. Icarus. 208**,** 850-867.
Raulin, F., Chimie prébiotique : expériences de simulation en laboratoire et "vérité terrain". In: M. Gargaud, et al., Eds.), L'environnement de la Terre prmitive. Presses Universitaires de Bordeaux, Bordeaux, 2005, pp. 343-360.
Sciamma-O'Brien, E., et al., 2010. Titan's atmosphere: An optimal gas mixture for aerosol production? Icarus. 209**,** 704-714.
Selsis, F., Parisot, J. P., L'atmosphère primitive de la Terre et son évolution. In: M. Gargaud, et al., Eds.), L'environnement de la Terre primitive. Presses Universitaires de Bordeaux, Bordeaux, 2005, pp. 217-233.
Smith, G., et al., 2001. Assessing effects of rate parameter changes on ozone models using sensitivity analysis. J. Phys. Chem. A. 105**,** 1449-1455.
Stephan, K., et al., 2010. Specular reflection on Titan: Liquids in Kraken Mare. GEOPHYSICAL RESEARCH LETTERS. 37.
Swain, M. R., et al., 2008. The presence of methane in the atmosphere of an extrasolar planet. Nature. 452**,** 329-331.
Szopa, C., et al., 2006. PAMPRE: A dusty plasma experiment for Titan’s tholins production and study. Planet. Space Sci. 54**,** 394-404.
Tomasko, M. G., et al., 2005. Rain, winds and haze during the Huygens probe's descent to Titan's surface. Nature. 438**,** 765-778.
Trainer, M. G., et al., 2006. Organic haze on Titan and the early Earth. Proceedings of the National Academy of Sciences. 103**,** 18035-18042.
Tran, B. N., et al., 2005. Photochemical processes on Titan: Irradiation of mixtures of gases that simulate Titan's atmosphere. Icarus. 177**,** 106-115.
Turányi, T., et al., 2002. Effect of the uncertainty of kinetic and thermodynamic data on methane flame simulation results. Phys. Chem. Chem. Phys. 4**,** 2568-2578.
Turtle, E. P., et al., 2011. Rapid and Extensive Surface Changes Near Titan's Equator: Evidence of April Showers. Science. 331**,** 1414-1417.
Vinatier, S., et al., 2010. Analysis of Cassini/CIRS limb spectra of Titan acquired during the nominal mission II: Aerosol extinction profiles in the 600-1420 cm-1 spectral range. Icarus. 210**,** 852-866.
Vuitton, V., et al., 2010. Very high resolution mass spectrometry of HCN polymers and tholins. Faraday Discuss. 147**,** 495-508
Vuitton, V., et al., 2007. Ion chemistry and N-containing molecules in Titan's upper atmosphere. Icarus. 191**,** 722-742.
Waite Jr, J. H., et al., High-Altitude Production of Titan’s Aerosols. In: R. H. Brown, et al., Eds.), Titan from Cassini-Huygens. Springer, 2009, pp. 201-214.
Waite Jr., J. H., et al., 2007. The Process of Tholin Formation in Titan’s Upper Atmosphere. Science. 316**,** 870-875.
Westlake, J. H., et al., 2011. Titan's Ionospheric Composition and Structure Part II: Large Ion Composition and Growth. Journal of Geophysical research. submitted.
Wilson, E. H., Atreya, S. K., 2003. Mechanisms for the formation of benzene in the atmosphere of Titan. Journal of Geophysical research. 108.
Yelle, R. V., et al., 2010. Formation of NH_3 and CH_2NH in Titan's upper atmosphere. Faraday Discussions. 147**,** 31-49.

6. Annexe : cinq publications les plus significatives des travaux

Carrasco, N., et al., 2007a. Simulation studies of the atmospheric oxidation of 2-Methyl-3-Buten-Ol : reactions with hydroxy radicals and ozone under a variety of conditions. . *Journal of Atmospheric Chemistry*. 56**,** 33-55.

Carrasco, N., et al., 2007b. Uncertainty analysis of bimolecular reactions in Titan ionosphere chemistry model. Planetary and Space Science. 55**,** 141-157.

Plessis, S., et al., 2010. Knowledge-based probabilistic representations of branching ratios in chemical networks: The case of dissociative recombinations. The Journal of Chemical Physics. 133**,** 134110-21.

Carrasco, N., et al., 2009. Chemical Characterization of Titan's Tholins: Solubility, Morphology and Molecular Structure Revisited The Journal of Physical Chemistry A. 113**,** 11195-11203.

Gautier, T., et al., 2011. Nitrile gas chemistry in Titan atmosphere. Icarus. 213**,** 625-635.

Available online at www.sciencedirect.com
ScienceDirect
Planetary and Space Science 55 (2007) 141–157
Planetary and Space Science
www.elsevier.com/locate/pss

Uncertainty analysis of bimolecular reactions in Titan ionosphere chemistry model

N. Carrasco[a], O. Dutuit[a], R. Thissen[a], M. Banaszkiewicz[b], P. Pernot[a,*]

[a]*Laboratoire de Chimie Physique, Bât. 349, UMR 8000 CNRS, Université Paris-Sud 11, 91405 Orsay cedex, France*
[b]*Space Research Centre, Bartycka 18A, 00-716 Warsaw, Poland*

Received 24 March 2006; received in revised form 14 June 2006; accepted 15 June 2006
Available online 7 August 2006

Abstract

We report about the first detailed uncertainty analysis concerning the kinetics parameters of the ion–molecule reactions included in a Titan's ionospheric chemistry model. Uncertainty propagation has been performed by Monte Carlo sampling. Different possible descriptions of the uncertainties on the rate constants are discussed and compared on the basis of our state of knowledge about ion–molecule reaction rates laboratory measurements. We propose also a new method for the treatment of branching ratios correlated uncertainties. We show that the uncertainty on branching ratios contribute significantly to the uncertainty on ion densities predicted by the chemistry model. Simulation of a mass spectrum for ionic species in Titan ionosphere at 1200 km of altitude and night-time chemistry has been performed and compared to the INMS mass-spectrum available on the website of the NASA ⟨http://photojournal.jpl.nasa.gov/catalog/PIA07865⟩], corresponding to Cassini's T5 flyby.

Keywords: Monte Carlo uncertainty propagation; Elicitation; Titan; Ionospheric chemistry; Branching ratio; Chemical rate constant; Mass spectrum

1. Introduction

Titan's dense and complex atmosphere is essentially made of nitrogen and methane but also of traces of numerous hydrocarbons (Broadfoot et al., 1981; Hanel et al., 1981; Samuelson et al., 1997). This atmosphere is exposed to solar extreme ultraviolet radiations and to a flux of energetic electrons from the magnetosphere of Saturn. Nitrogen and methane ionization initiates a complex chemistry in Titan's ionosphere between charged and neutral species producing big molecular ions. Between altitudes of 800 and 1400 km, the density of neutral species decreases from about 10^{11} to $10^{8}\,cm^{-3}$, while the density of ions peaks at a few $10^{3}\,cm^{-3}$ (Yelle et al., 1997). The temperature of the neutral bath is nearly constant, around 170 K. Ongoing flybys of Titan by the Cassini spacecraft are providing invaluable data on the rich chemical composition of the upper atmosphere and ionosphere. The complexity of its atmospheric chemistry makes it a challenging system for models.[1] Let us note that models are very helpful to unravel the mass spectra acquired by the ions and neutrals mass spectrometer (INMS) instrument for neutral and ionic species (Waite et al., 2004, 2005).

Earlier models of Titan's ionospheric chemistry were first concerned with the major ions identified such as $HCNH^+$, $C_2H_5^+$, CH_5^+ and HCN^+ (Ip, 1990; Keller et al., 1992). Keller et al. (1992) predicted the altitudes and the intensities of a peak electron density for zenith angles of 60° and 90° in good agreement with Voyager data (Bird et al., 1997). Since Roboz and Nagy (1994) reported that Titan's ionosphere below 1500 km was chemically controlled, models evolved towards an increase in chemical species and reactions, in order to build a realistic account of the chemistry. These refinements were made possible thanks to the vast amount of laboratory data gathered over the years. Several review articles by Anicich and collaborators (Anicich, 1993, 2003; Anicich and McEwan, 1997) report rate constants and product branching ratios for

*Corresponding author. Tel.: +33 1 69 15 54 28.
E-mail address: pascal.pernot@lcp.u-psud.fr (P. Pernot).

[1]A recent bibliography of over 500 references as of 2005/01/09 is available online (Minard, 2005).

0032-0633/$ - see front matter © 2006 Elsevier Ltd. All rights reserved.
doi:10.1016/j.pss.2006.06.004

numerous bimolecular ion–molecule reactions. Fox and Yelle (1997) built a model of Titan's upper atmosphere taking into account 38 neutral species and 35 ions, involved in more than 600 chemical processes. Keller et al. (1998) improved the model of Keller et al. (1992) by updating rate constant values and by adding new ion species (51 ions in total) in order to better describe the production of heavy hydrocarbons. In all these studies, neutral species were considered as a fixed bath in Titan's ionosphere. However, Keller et al. (1998) tested two different neutral atmospheres, as predicted by the neutral models of Yung et al. (1984) and Toublanc et al. (1995), and concluded that the ion densities strongly depend on the neutral atmosphere. This important correlation between ion and neutral reactivity has been accounted for by both Banaszkiewicz et al. (2000) and Wilson and Atreya (2004) who developed ion-neutral coupled models containing 33 neutrals/57 ions and 80 neutrals/33 ions, respectively.

Discrepancies between the outputs of the different models and between the outputs and available data are difficult to assess in the absence of quantified uncertainties. In particular, modelling the chemistry of planetary ionospheres involves numerous physical and chemical parameters, whose values are known from laboratory measurements with non-negligible uncertainty factors. These uncertainty sources should be accounted for in the modelling. Uncertainty quantification of model outputs is a recurrent issue in atmospheric or space chemistry (Thompson and Stewart, 1991; Stewart and Thompson, 1996; Dobrijevic and Parisot, 1998; Dobrijevic et al., 2003; Vasyunin et al., 2004; Wakelam et al., 2005, 2006) but few systematic studies have been reported for Titan atmosphere (Hébrard et al., 2005) and none for Titan ionosphere, to our knowledge. A sensitivity test by Keller et al. (1992) revealed that a 30% variability of ionization cross-sections, ion–molecule reaction rates, and neutral densities produced a similar perturbation of the equilibrium ion densities. Considering that the uncertainties on the input parameters are now known to be often higher than 30% (Anicich and McEwan, 1997; Hébrard et al., 2005) and that the uncertainties on the branching ratios of the ion–molecule reactions were not accounted for, the balance should certainly be worse. We focus in the present article on ion–molecule reactivity related uncertainties, in the case of the model of Banaszkiewicz et al. (2000). Uncertainty propagation is done by a Monte Carlo method.

Monte Carlo uncertainty propagation has been systematically used in recent studies of complex chemical systems (Dobrijevic et al., 2003; Vasyunin et al., 2004; Hébrard et al., 2005; Wakelam et al., 2005, 2006; Zádor et al., 2006). This approach requires the definition of a probability density function (pdf) from which one draws samples of input parameters. The pdf should be as representative as possible of the state of knowledge about these theoretically estimated or experimentally measured parameters. The 1993 and 1997 reviews by Anicich (1993) and Anicich and McEwan (1997), on which is based the model of Banaszkiewicz et al. (2000), provide preferred values k^0 for the rate constants, usually reported with their relative uncertainty x, and preferred values for the corresponding branching ratios, without uncertainty.

A first point which requires a closer examination is the absence of reported uncertainties for branching ratios. Moreover, as clearly stated by Zádor et al. (2005a), it seems that the correct treatment of branching ratios as correlated parameters for more than two channels has not yet been properly addressed in the literature about uncertainty propagation in complex chemical systems. At best, the different reactive pathways of a given reaction have been treated as uncorrelated. However, it is known that neglecting correlations between input parameters is a source of spurious output uncertainty (Hanson and Hemez, 2003). Hence this point is an important issue for every chemical system containing multiple channels with poorly known branching ratios. We address this issue here by using an adapted Dirichlet distribution.

The representation of rate constant uncertainty with log-normal distributions seems to be the present paradigm, regardless of the nature of the uncertainty. We would like to stress out that the appropriate type of uncertainty distribution might depend strongly on the experimental technique used or on the combination of results performed by a reviewer. Indeed, the initial and most delicate task in probabilistic uncertainty propagation is to design the pdf in input parameters space (Helton and Davis, 2000). This process, called *elicitation* (Garthwaite et al., 2005; Jenkinson, 2005), consists in building a pdf representative of one's state of knowledge about the parameters and taking into account all pertinent information.

The present paper addresses the following questions related to uncertainty propagation:

- Which type of pdf is best adapted to represent one's state of knowledge on rate constants of ion–molecule reactions?
- How do different choices of input pdf affect uncertainty propagation results?
- How does the uncertainty propagation on the branching ratios affect the uncertainties on the outputs in such a complex chemical scheme?

Uncertainty propagation of the ion–molecule chemistry performed on the model of Banaszkiewicz et al. (2000) is applied to the estimation of ion densities. The recent publication of ion mass spectra measured by the INMS instrument on Cassini during T5 flyby (Cravens et al., 2006) motivated the extension of our results to the uncertainty propagation for ion mass spectra.

2. Representation of uncertainty in chemistry model inputs

Uncertainty in input parameters $\boldsymbol{\theta}$ is represented with a joint pdf $p(\boldsymbol{\theta}|I)$. As it represents a state of knowledge about the possible values of the parameters, this pdf is

conditional to an ensemble of a priori information and hypotheses, noted I. Uncertainty propagation consists in calculating the transformation of the inputs pdf through the model $\mathbf{y} = f(\boldsymbol{\theta})$, resulting in a pdf for the outputs $p(\mathbf{y}|I)$. The formal equation for this process is (d'Agostini, 2003)

$$p(\mathbf{y}|I) = \int \mathrm{d}\boldsymbol{\theta}\, \delta(\mathbf{y} - f(\boldsymbol{\theta}))p(\boldsymbol{\theta}|I). \quad (1)$$

This multidimensional integral can be evaluated by collocation methods (e.g. polynomial chaos; Isukapalli and Georgopoulos, 2001) or by Monte Carlo methods. When the number of parameters increases, collocation methods are doomed by the "curse of dimensionality". As we deal here with more than 500 parameters, we did not retain such methods.

The standard uncertainty propagation Monte Carlo algorithm consists in drawing a representative sample from the inputs pdf $p(\boldsymbol{\theta}|I)$, and to evaluate the value of the output(s) for every element of this sample (Helton and Davis, 2000; Helton, 2005). Statistical summaries and approximations of the output pdf are then built from the output sample. Analysis of output uncertainty provides a basis for uncertainty analysis, i.e. identification of the contribution of each parameter (or group of parameters) to the total uncertainty, and for sensitivity analysis, i.e. identification of those parameters which are important/unimportant to the model (Saltelli et al., 2005).

2.1. Assignment of probability distributions to uncertain input parameters

When physical measurements are considered, the available information for assigning a probability distribution to an uncertain parameter is often limited to a published value and an associated uncertainty factor, or a set of those. The corresponding pdf is almost never specified, and has thus to be elicited. Standard procedures or good practice rules have been published for the reporting of uncertainties, as for instance in the NIST guide (Taylor and Kuyatt, 1994), but scientists rarely acknowledge their conforming to such standards. Two classes are commonly considered to qualify uncertainties (Taylor and Kuyatt, 1994):

- statistical or "type A" uncertainties, resulting from the analysis of repeated measurements by statistical methods, and for which are reported typically a preferred value (location parameter) and an uncertainty factor (dispersion parameter);
- epistemic or "type B" uncertainties, which integrate the relevant information. There is no standard reporting scheme in this case, but a recommended approach is to report lower and upper limits.

The main rules for uncertainty reporting do also differ between scientific communities, and the elicitator has to take this global context into account. In most favorable cases, it is possible to interview experts in the field of interest to explicit the meaning of the reported uncertainties.

Once the nature of the available data has been clarified, one has to build a probability distribution from this sparse information (e.g. preferred value and standard uncertainty). An infinity of pdf's are consistent with such information, and some additional criterion is required to select a unique solution. The Maximum Entropy principle can be used to obtain the least biased solution (Levine and Tribus, 1979). Symmetry principles and central limit theorems are also often invoked in this process. For instance, the product or ratio of a few positive independent random variables takes a log-normal distribution (Limpert et al., 2001; Smith, 2003) which is representative of many physical laws, and which has been extensively used in the context of chemical models (Stewart and Thompson, 1996; Fröhner, 2000; Turányi et al., 2002; Dobrijevic et al., 2003; Wakelam et al., 2005, 2006). When the only available information is a pair of limit values, symmetry and maximum entropy principles converge towards uniform distributions, which represent indifference about any particular value of the parameter within the imposed limits.

The particular cases of ion–molecule reaction rate constants and branching ratios are considered in the next sections.

2.2. Rate constants of ion–molecule reactions

Reference values for ion–molecule reaction rates (k^0) and their relative uncertainties (x), as reported by Anicich and McEwan (1997), often result from the integration of several experimental values covering a variety of experimental methods, with different uncertainty schemes. A consistent representation of uncertainty by probability distributions should consider that all reported preferred values and uncertainties do not necessarily represent the same state of knowledge. The different experimental techniques involved in ion–molecule rate constant measurements are:

- Flow tubes: Flowing after glow, selected ion flow tube (SIFT), drift tube (Adams and Smith, 1988),
- ion cyclotron resonance (ICR) mass spectrometry (Kemper and Bowers, 1988),
- guided-ion beams (Gerlich, 1992).

Flow tubes and ICR determine rate constants through kinetics measurements whereas guided-ion beams is used to measure reaction cross sections. In the following, we briefly review these methods with a focus on the corresponding uncertainty sources.

Flow tubes: With the flow tubes techniques, ions pass through a flow-tube in a constant flow of helium buffer gas. The neutral reactant is added downstream and the reaction occurs into the flow tube. SIFT and drift tube are an improvement of the more general flowing after glow techniques. They make it possible to select single ionic

species from the ion source and to inject them at low energy into the buffer gas flow. No measurement bias is reported for this method, and the reported uncertainties can be considered as of statistical origin. They are evaluated to about 20% by Adams and Smith (1976) for SIFT measurements and to about 30% by Bohme et al. (1969) for flowing after glow.

For studying ion–molecule reaction kinetics at very low temperatures ($T<200$ K), specific flow tubes techniques have been developed. The CRESU and the free jet flow reactor are described in details in Rowe and Parent (1995). Among the different instruments, Rowe and Parent (1995) give a particular attention to the CRESU technique (Cinétiques de Réactions en Ecoulements Supersoniques Uniformes) in which the carrier gas is cooled down by a supersonic expansion. The free jet flow reactor (Hawley et al., 1990) also uses a supersonic expansion as the cooling system. The experimental uncertainty range is evaluated to about 30% (Rowe et al., 1984).

ICR: In the case of ICR, the decrease of the parent ion intensity, due to its reaction with the neutral gas, is measured as a function of reactant gas pressure or as a function of time. According to various authors, the main source of (systematic) uncertainty is the accuracy of the neutral density measurement, which is estimated to about 5–10% (Anicich and Bowers, 1973; Huntress and Pinizzoto, 1973; Kim et al., 1977). The statistical reproducibility of the rate determination has also been studied by Anicich and Bowers (1973) and is evaluated to a minimum of 20%.

GIB: With the GIB technique, rate constants are calculated through the determination of the reaction cross section, and of the relative velocity of the collisional pair. When all the tests for proper ion collection, transmission and detection are carefully performed, typical statistical uncertainties for the total cross section are expected to be less than 5% (Teloy and Gerlich, 1974). Nevertheless, a remaining systematic error is estimated to 15–20% (Teloy and Gerlich, 1974; Ervin and Armentrout, 1985; Nicolas et al., 2002). A difference of 25% between SIFT and GIB results for the $N^+ + CO \rightarrow CO^+ + N$ reaction has been reported (Gerlich, 1986). Main uncertainty sources involve the measurement of the absolute pressure, the evaluation of the reactant ions path length, the influence of elastic collisions and of secondary reactions, and the differences in the collection and detection probabilities for reactant and for product ions (Teloy and Gerlich, 1974). The existence of an unknown bias in the determination of rate constants with the GIB technique means that the reported value k^0 is not specifically a *preferred* value. Indeed, any other value within an interval specified using error bars could be accepted.

2.2.1. Elicitation

In the reviews of Anicich (1993) and Anicich and McEwan (1997), multiple determinations with GIB, SIFT and ICR techniques are reported for almost all reactions taken into account in the model of Banaszkiewicz et al. (2000). In order to illustrate the elicitation process developed in this paper, we consider two examples of well-studied reactions particularly important for Titan ionosphere chemistry: $N^+ + CH_4$ and $N_2^+ + CH_4$.

The references and the preferred values considered by Anicich (1993) are reported in Table 1. There is not only a notable dispersion of the values obtained by different methods, but also for different measurements with similar techniques (e.g. 0.94 ± 0.20, 1.1 and 1.38 with SIFT). In the absence of a documented procedure, we infer that the evaluation of the preferred value may have been performed according to the following criteria:

(1) exclusion of the experimental results obtained at low temperature;
(2) the preferred value seems to correspond to the mean value between the lowest and the highest reported values;
(3) the confidence interval of 15% reported in both cases is a lower estimation of the interval defined by the lowest and the highest values.

The reported "preferred" values (k^0) and their associated relative uncertainty cover thus both systematic and statistical uncertainties and would correspond to a "type B" case. Moreover, interpretation of relative uncertainties (x) is not univocal, particularly with regard to their coverage factor. x is generally chosen subjectively to encompass some systematic uncertainties, in the sense that it defines a high confidence interval for k. Thus, it includes a subjective security factor, such that there is only a tiny probability for the parameter to be outside of the interval $[k^0(1-x), k^0(1+x)]$.

The shape of the distributions has yet to be defined. In the following, we consider two working scenarios: (1) the

Table 1
Original and reviewed (bold) reaction rates for two well-studied ion–molecule reactions

Reference	Method	k	Δk
$N^+ + CH_4$			
Rowe et al. (1985)	CRESU ($T = 8$ K)	0.82	0.25
Dheandhanoo et al. (1984)	DT	0.94	0.09
Adams et al. (1980)	SIFT	1.38	–
Tichy et al. (1979)	SIFT	1.1	–
Smith et al. (1978)	SIFT	0.94	0.20
Anicich et al. (1977)	ICR	1.35	0.13
Huntress (1977)	ICR	1.35	0.15
Anicich (1993)		**$1.15 \pm 15\%$**	
$N_2^+ + CH_4$			
Randeniya and Smith (1991)	($T = 8-15$ K)	1.9	0.9
Rowe et al. (1989)	CRESU ($T = 70$ K)	1.2	0.4
Smith et al. (1978)	SIFT	1.0	–
Smith et al. (1978)	ICR	0.98	–
Tichy et al. (1979)	ICR	1.3	–
Anicich (1993)		**$1.14 \pm 15\%$**	

Rate constants are in 10^{-9} cm^3 s^{-1}.

preferred value defines a maximum of the probability distribution (not necessarily the maximum itself, see below) and (2) there is a total indifference about any particular value within the confidence interval.

(1) *k^0 defines a maximum of the probability distribution*: In absence of any other information, and conforming with NIST recommendations (Taylor and Kuyatt, 1994) we should consider that "$k^0 \pm x\%$" defines a normal distribution centered on k^0 with a confidence interval such that

$$P(k \in [k^0(1-x), k^0 \times (1+x)]) \simeq 0.95. \quad (2)$$

This interval is symmetrical about k^0. We note that this specification of uncertainties for reaction rates is in contrast with the common practice in atmospheric or interstellar chemistry, where the positivity constraint on the rate constants is acknowledged by using a multiplicative uncertainty factor F (see e.g. Atkinson et al., 2004; Wakelam et al., 2006). In this case, a confidence interval is defined by

$$P(k \in [\mathrm{Med}(k)/F, \mathrm{Med}(k) \times F]) \simeq 0.95, \quad (3)$$

which preserves the positivity of k, independently on the value of F.[2] Note that this interval is asymmetric around the median value Med(k).

The log-normal pdf

$$p(k|\mathrm{Med}(k), F) = \frac{\sqrt{2/\pi}}{k \ln F} \exp\left(-2\left(\frac{\ln(k/\mathrm{Med}(k))}{\ln F}\right)^2\right) \quad (4)$$

is generally considered as appropriate for uncertainty analysis of chemical reactions (Stewart and Thompson, 1996; Fröhner, 2000; Turányi et al., 2002; Dobrijevic et al., 2003; Wakelam et al., 2005, 2006) although nothing about this is explicitly stated by the experts defining the reference values and uncertainties (Stewart and Thompson, 1996; Atkinson et al., 2004). This choice is often justified on statistical grounds from the positivity of the rate constants (violated by the normal distribution) and from the central limit theorem for multiplicative errors (formulae relating rate constants to sources of uncertainty involve mainly multiplications and divisions) (Smith and Futrell, 1974; Smith, 1992; Fröhner, 2000; Limpert et al., 2001).

In order to use a log-normal pdf, the information $\{k^0, x\%\}$ has to be recast in the form $\{\mathrm{Med}(k), F\}$. However, it is not possible to match simultaneously a location parameter (mean or median) and the 95% confidence interval limits. In the present case, it is reasonable to assume that the reference value is more carefully evaluated than the confidence interval and has to be preserved in the transformation. Assigning k^0 to the median value of the log-normal is generally chosen for the sake of convenience (Stewart and Thompson, 1996). Considering the properties of the log-normal distribution, this enables to separate both parameters, i.e. changing the value of F would not affect the value of the median $\mathrm{Med}(k) = k^0$, whereas it would affect the mean value ($\mathrm{Mean}(k) = k^0 \exp(\ln^2 F/8)$). We checked that those two options do not lead to significant differences in the uncertainty propagation, and retained the usual assignment of k^0 to the median. Matching the lower and upper limits of the 95% interval, leads to two possible values for F, namely $F = 1/(1-x)$ and $F = 1+x$. In order to guarantee the coverage of the interval, we choose the larger of both values, i.e. $F = 1/(1-x)$. It is to be noted that this might contribute somewhat to an over-weighting of large k values. Preliminary tests showed that for the values of x of interest, rarely above 0.5, this effect is not qualitatively remarkable.

A foreseeable inconvenience of the log-normal pdf is the absence of an upper limit. Some authors truncate the log-normal distribution within a given confidence interval (Zádor et al., 2005b). For ion–molecule reactions, excepted for charge transfer reactions, an upper limit would indeed be provided by the Langevin rate (Armentrout, 2003).

(2) *Total indifference about a specific value*: Another approach is to consider only limit values $\{k_{\min}, k_{\max}\}$ and to use a distribution reflecting the absence of a preferred value (all values within the interval are considered equally plausible). Considering that for large uncertainties such an interval is expected to cover a few orders of magnitude, we furthermore require that the distribution is uniform for the logarithm of the parameter, ensuring that the distribution is not biased towards large values of the parameter. This is verified by the log-uniform distribution

$$p(k|k_{\min}, k_{\max}) = \frac{1}{k \ln(k_{\max}/k_{\min})}. \quad (5)$$

If one considers, as stated above, that "security factors" are incorporated in the value chosen for x, the limits are defined by $k_{\min} = k^0 \times (1-x)$ and $k_{\max} = k^0 \times (1+x)$.

As an illustration, we display on Figs. 1 and 2 representative examples for a major ($N_2^+ + CH_4 \rightarrow CH_2^+ + NH_2$) and a minor ($H^+ + H_2 \rightarrow H_2^+ + H$) reaction. In the first case, we have a typical reaction with a low uncertainty factor ($x = 0.2$). We observe that the range covered by our elicitation of a log-uniform distribution is somewhat more contracted than for the log-normal, and that the shapes of both distributions are quite different. In the case of the second reaction, only an upper value for the reaction rate is known. A lower limit was defined as the sensibility threshold of the experimental technique. When the uncertainty factor is large, as in this case, both distributions become quite similar in shape, if not in range.

2.3. Uncertainties on the branching ratios

2.3.1. Experimental considerations

Uncertainties on branching ratios are not reported by Anicich (1993) or Anicich and McEwan (1997). In a paper

[2]The definition of F varies from author to author (Turányi et al., 2002; Dobrijevic et al., 2003; Atkinson et al., 2004) with ln F representing from 1σ to 3σ intervals. In this work, we follow the explicit recommendation by Atkinson et al. (2004) that $[k^0/F, k^0F]$ represents a 95% confidence interval, i.e. ln F represents a 2σ error bar on ln k.

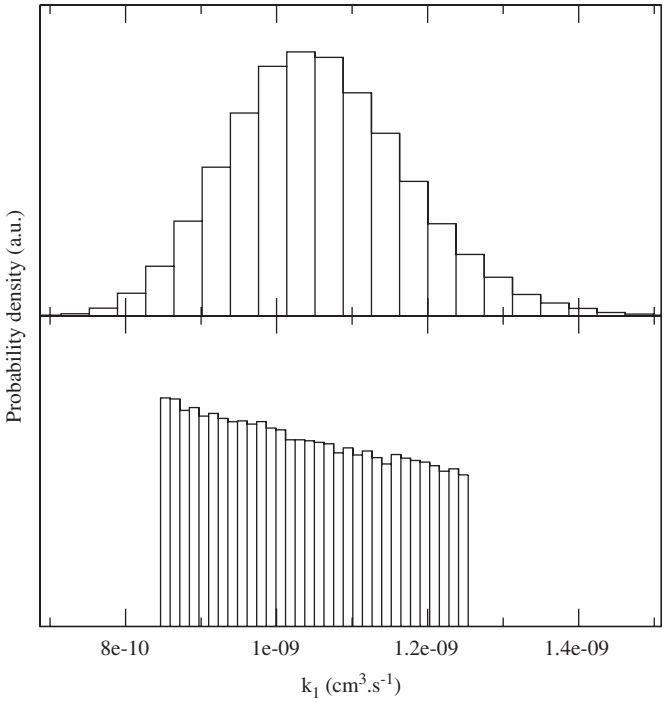

Fig. 1. Elicitation of the probability density function for the rate constant of the reaction $N_2^+ + CH_4 \rightarrow CH_2^+ + NH_2$ ($b_1 = 0.7$), with preferred value for the global rate $k^0 = 1.5 \times 10^{-9}$ and relative uncertainty $x = 0.2$. Comparison of probability densities for: (upper panel) a log-normal distribution ($k^0 b_1 = 1.05 \times 10^{-9}$, $F = 1.25$); (lower panel) a log-uniform distribution ($k_{min} b_1 = 0.84 \times 10^{-9}$, $k_{max} b_1 = 1.26 \times 10^{-9}$).

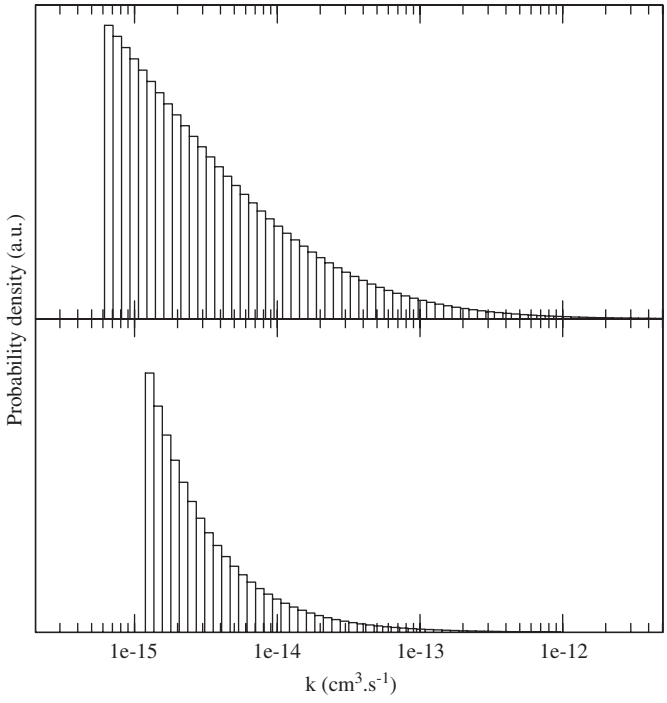

Fig. 2. Elicitation of probability density function for the rate constant of the reaction $H^+ + H_2 \rightarrow H_2^+ + H$. Comparison of probability densities for: (upper panel) a log-normal distribution ($k^0 = 5 \times 10^{-13}$, $F = 435$); (lower panel) a log-uniform distribution ($k_{min} = 1.2 \times 10^{-15}$, $k_{max} = 1.0 \times 10^{-12}$).

by McEwan et al. (1998), they are estimated to 5%. In order to evaluate more generally these uncertainties, we compared the values reported by different experts (and for different experimental techniques) for the same reactions as in Section 2.2.1.

Four pathways have been reported for the reaction $N^+ + CH_4$:

$$\begin{aligned} N^+ + CH_4 &\rightarrow CH_3^+ + NH \text{ (and/or } N + H) \ (b_1) \\ &\rightarrow CH_4^+ + N \ (b_2) \\ &\rightarrow H_2CN^+ + H_2 \ (b_3) \\ &\rightarrow HCN^+ + NH \ (b_4) \end{aligned} \quad (6)$$

and three pathways for the reaction $N_2^+ + CH_4$:

$$\begin{aligned} N_2^+ + CH_4 &\rightarrow CH_2^+ + N + H_2 \ (b_1) \\ &\rightarrow CH_3^+ + N + H \ (b_2) \\ &\rightarrow N_2H^+ + CH_3 \ (b_3). \end{aligned} \quad (7)$$

Values of the branching ratios measured by different groups are reported in Table 2 along with the relative discrepancies between these measurements and with the values reported in the review of Anicich (1993). The various studies on $N^+ + CH_4$ are in rather good agreement. Discrepancies vary between 15% and 36%. On the other hand, even for a well-studied reaction such as $N_2^+ + CH_4$, uncertainty on branching ratios can be much larger. The experimental determination of branching ratios can be subject to large errors due to the many perturbations that can blur the experimental results. Internal or kinetic energy of reactant ions are important parameters that can greatly affect branching ratio measurements. For instance, Alcaraz et al. (2004) showed that branching ratios for the reaction $N^+ + CH_4$ change a lot when N^+ reactant ions are in the ^1D metastable state or when they have some kinetic energy due to their formation from the N_2^+ or N_2^{++} dissociation. Temperature can also affect reaction branching ratios. In the case of the $N_2^+ + CH_4$ reaction, Randeniya and Smith (1991) measured at 30 K branching ratios, which differ by 10% from the room temperature ones. It can be much more important for very slightly endothermic reactions such as the formation of $C_2H_3^+$ in the $C_2H_2^+ + H_2$ reaction (see the discussion in the review paper from Armentrout and Baer, 1996). Another aspect is the possible mass overlaps and, therefore, the use of appropriate methods to decipher the various product ion assignments. For example, Nicolas et al. (2002) had to use deuterated and ^{15}N isotopes in their measurements, in order to clearly ascribe reaction products. Last but not the least, even for reactions exhibiting apparently small reaction rates, some reaction products may lead to secondary reactions, which are not easy to trace out. Experimentalists have therefore often to find a compromise between the precision on their determination of the total

Table 2
Comparison between branching ratios (b_i) determinations for the $N^+ + CH_4$ and the $N_2^+ + CH_4$ reactions

Reference	b_1	b_2	b_3	b_4
$N^+ + CH_4$				
Anicich et al. (2004)	0.38	0.03	0.15	0.44
McEwan et al. (1998)	0.53	0.05	0.10	0.32
Dheandhanoo et al. (1984)	0.52	0.06	0.09	0.33
Adams et al. (1980)	0.51	0.03	0.06	0.40
Tichy et al. (1979)	0.42	0.06	0.14	0.38
Anicich et al. (1977)	0.53	0.04	0.10	0.32
$\Delta b_i/(2\bar{b}_i)$	**15%**	**34%**	**36%**	**16%**
Anicich (1993)	**0.50**	**0.05**	**0.10**	**0.36**

Reference	b_1	b_2	b_3
$N_2^+ + CH_4$			
Nicolas et al. (2003)	0.07	0.88	0.05
McEwan et al. (1998)	0.05	0.80	0.15
$\Delta b_i/(2\bar{b}_i)$	17%	5%	50%
Anicich et al. (2004)	0.12	0.88	–
Randeniya and Smith (1991) (30 K)	0.20	0.80	–
Tichy et al. (1979)	0.11	0.89	–
Smith et al. (1978)	0.07	0.93	–
$\Delta b_i/(2\bar{b}_i)$	**52%**	**8%**	–
Anicich (1993)	**0.09**	**0.91**	–

The relative dispersion of the measurements and preferred values are in bold type.

reaction rates by increasing the pressure, and the risk to pollute the branching ratios in the presence of secondary reactions.

Moreover in the case of the reaction $N_2^+ + CH_4$, the ion product N_2H^+ has only been observed in the studies of McEwan et al. (1998) and Nicolas et al. (2003). Therefore the branching ratios are defined for three pathways in these two studies and for two pathways in the others. As a result, the branching ratios have a different meaning between both cases and cannot be directly compared. This underlines a recurrent difficulty for the treatment of the branching ratios, which vary with the detection of new products.

We expect that the uncertainties observed for these well-studied branching ratios is indeed a lower limit for the uncertainty on the branching ratios of less studied reactions. In the absence of additional information, we assigned a common relative uncertainty to all branching ratios reported in the reviews (Anicich, 1993; Anicich and McEwan, 1997). Levels of 25%, 50% and 75% are considered in the numerical applications. Note that it may seem awkward to assign the same relative uncertainty to all branching ratios of a given reaction. One would expect a better accuracy for major products. This issue is addressed in the next section.

In the case of unknown branching ratios for experimentally detected products (for instance for reactions $C^+ + HCN$, $CH_2^+ + N$, or $CN^+ + H_2$), it is reasonable to assume a uniform distribution of products with a large relative uncertainty. This would correspond to a situation where a very low detection sensitivity requires that all detected products are above a reasonably high density level, and consequently that they occur in approximately similar proportions. A 90% relative uncertainty, which excludes extreme ratios, is used for such reactions.

2.3.2. Elicitation

For a reaction with n product pathways, the partial reaction rates are expressed as $k_i = k * b_i$, where k is the global reaction rate, and b_i are branching ratios characterizing the proportion between the different product pathways. The b_i's are positive and normalized $\left(\sum_{i=1}^{n} b_i = 1\right)$, which means that they are correlated. The Dirichlet distribution represents the fluctuations of quantities independent of each other, under the condition that their sum remains fixed (Evans et al., 2000). As shown in the Appendix, this multivariate distribution can be uniquely parameterized from the estimated branching ratios ($\bar{b}_i$) and a relative uncertainty (x):

$$(b_1, \ldots, b_n) \sim \text{Dirichlet}\left(\hat{\gamma} \times \left(\bar{b}_1, \ldots, \bar{b}_n\right)\right), \tag{8}$$

where $\hat{\gamma}$ is a precision factor defined by a least squares equation

$$\hat{\gamma} = \frac{4}{x^2}\left(\frac{\sum_i \bar{b}_i(1-\bar{b}_i)}{\sum_i \bar{b}_i\sqrt{\bar{b}_i(1-\bar{b}_i)}}\right)^2 - 1. \tag{9}$$

An additional constraint

$$\hat{\gamma} \geqslant \left\{\min\left(\max\left(\bar{b}_1, 1-\bar{b}_1\right), \ldots, \max\left(\bar{b}_n, 1-\bar{b}_n\right)\right)\right\}^{-1} \tag{10}$$

is used to ensure the unimodality of the Dirichlet distribution. This distribution respects the average values, i.e. $\langle b_i \rangle = \bar{b}_i$, but it cannot reproduce a uniform relative uncertainty for all channels. The relative uncertainty for channel i

$$\hat{x}_i = 2\sqrt{\frac{(1/\bar{b}_i - 1)}{\hat{\gamma} + 1}} \tag{11}$$

has, however, the desirable property to be inversely related to the abundance of the product. As was underlined earlier, the uniform relative uncertainty (x) which is generally assigned to all branching ratios should be understood as an average uncertainty. The Dirichlet distribution contributes thus to distribute this uncertainty among channels in a more consistent manner.

Another interesting feature of the Dirichlet distribution is that, in the absence of any information on the branching ratios, it is possible to define a uniform distribution over the $(n-1)$ simplex by taking $\hat{\gamma}b_1 = \cdots = \hat{\gamma}b_n = 1$ in Eq. (8). A foreseeable use of this property is the introduction in the reaction scheme of still unobserved, but theoretically plausible pathways (for instance on the basis of their calculated exothermicity). Note that we

Table 3
Partial relative uncertainties resulting from a Dirichlet distribution elicited from two different global relative uncertainties

$\bar{b}_i$	$\hat{x}_i$	
	$x = 0.25$	$x = 0.75$
0.5	0.19	0.56
0.05	0.82	2.46
0.1	0.56	1.69
0.36	0.25	0.75

differentiate this case from the case discussed previously of observed but non quantified products ($b_1 = \cdots = b_n = 1/n$, $x = 0.9$).

Example. Let us consider the set of the four branching ratios (0.5, 0.05, 0.1, 0.36) relative to the reaction $N^+ + CH_4$. For a 25% relative uncertainty we estimate $\hat{\gamma} = 112$ (Eq. (9)). The corresponding "optimal" relative uncertainties $\hat{x}_i$ are shown in Table 3. For the same data with 75% relative uncertainty, the accuracy factor decreases to $\hat{\gamma} = 11.6$. In the latter case, we see that high relative uncertainties (up to 250%) are produced for the minor channels, whereas the accuracy of the major channels is well preserved. Considering that standard errors on branching ratios are rather gross estimates, this is quite acceptable for the present purpose.

3. Results and discussion

3.1. The model

In a coupled model of Titan's atmosphere and ionosphere, the stationary densities for ions are calculated by solving iteratively: (i) the ion equations with current neutral densities and (ii) the neutral equations with the production and loss terms estimated at step (i) (Banaszkiewicz et al., 2000). In the present paper, we focus on step (i) involving ion–neutral reactions in the absence of transport. The production terms of ions are due to ionization of neutral species by either solar photons or magnetospheric and secondary electrons, and to bimolecular and trimolecular reactions. Losses are due to recombination and chemical reactions.

Uncertainty sources in such chemical models are numerous and not necessarily very well quantified. We restrict the present study to parameters involved in bimolecular reactions, namely rate constants and branching ratios. The original model of Banaszkiewicz et al. (2000) involves 33 neutral and 57 ionic species, including two pseudo-ions representing heavy hydrocarbons (those $C_xH_y^+$ with $x \geqslant 3$ that are not explicitly included in the model) and heavy nitriles (those $C_xH_yN_z^+$ with $x \geqslant 3$ that are not explicitly included in the model). In order to simulate mass spectra in the 1–100 amu mass scale, as measured by the INMS apparatus on Cassini (Waite et al., 2004, 2005), we relaxed the definition of the pseudo-ions in order to explicitly estimate the density of ions with relevant masses (no new reactions are introduced). Therefore 42 additional product-ions, with the same recombination rate as the pseudo-ions, were explicitly accounted for: $C_2H_7^+$, CHN^+, CH_3N^+, CH_4N^+, C_3^+, $C_3H_8^+$, $C_3H_9^+$, C_2HN^+, $C_2H_2N^+$, $C_2H_3N^+$, $C_2H_4N^+$, $C_2H_5N^+$, C_4H^+, $C_4H_4^+$, $C_4H_6^+$, $C_4H_8^+$, $C_4H_9^+$, $C_2HN_2^+$, $C_3H_6N^+$,C_5H^+, $C_5H_2^+$, $C_5H_3^+$, $C_5H_4^+$, $C_5H_7^+$, $C_5H_9^+$, C_4N^+, C_4HN^+, $C_4H_2N^+$, $C_4H_4N^+$, $C_4H_5N^+$, $C_4H_6N^+$, $C_6H_2^+$, $C_6H_3^+$, $C_4N_2^+$, $C_4HN_2^+$, $C_5H_2N^+$, $C_5H_3N^+$, $C_5H_4N^+$, $C_5H_5N^+$, $C_7H_5^+$, $C_5HN_2^+$ and $C_6H_2N^+$.

Only reactions with rates available in the literature have been retained, on the basis of the comprehensive survey compiled by Anicich and McEwan (1997). The reaction scheme comprises 584 reactions, with 738 kinetic parameters (315 rate constants and 423 branching ratios). The distribution of those reactions with respect to the number of product pathways is the following: (1) 161, (2) 84, (3) 45, (4) 11, (5) 9, (6) 4 and (7) 1. Thus, about 50% of the 315 global reactions have multiple pathways, which points out the necessity of a consistent treatment of branching ratios uncertainty.

The densities of major ions, calculated for the nominal values of the parameters, are displayed in Fig. 3, for altitudes between 800 and 1400 km above Titan's surface, and are compared with the density profiles calculated by Banaszkiewicz et al. (2000). Specification of the pseudo-ions reveals two major ions which will be of relevance for construction of simulated mass-spectra: $C_5H_7^+$ and $C_5H_5N^+$. Significant concentrations of $HCNH^+$, $C_2H_5^+$, $C_3H_5^+$, $C_5H_5^+$ and $C_4H_3^+$ are predicted by this model. This is in good agreement with the significant contributions predicted by Keller et al. (1998): $HCNH^+$ for the mass 28 amu, $C_3H_5^+$ for the mass 41 amu, $C_4H_3^+$ for the mass 51 amu, $C_5H_5^+$ for the mass 65 amu, $C_5H_7^+$ for the mass 67 amu, and $C_5H_5N^+$ for the mass 79 amu.

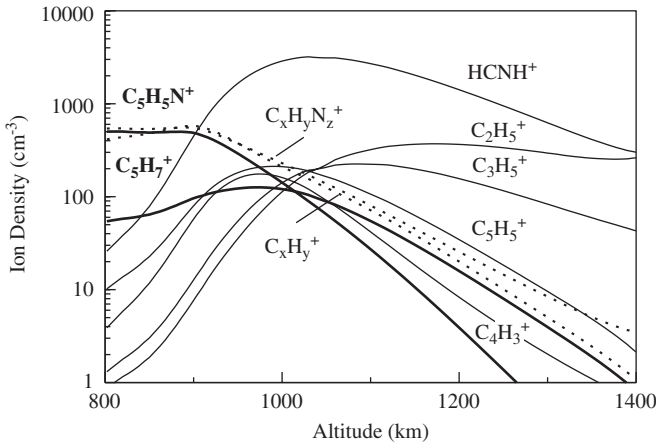

Fig. 3. Ion density profiles with and without specification of pseudo-ions in the model: (thin solid lines) common major ions; (thick solid lines) major former pseudo-ions; (dashed lines) $C_xH_yN_z^+$ and $C_xH_y^+$ pseudo-ions in the original model.

3.2. Simulation

The sampling for uncertainty propagation of the kinetic parameters has been performed by Monte Carlo simulation.

Inputs: Random numbers are generated by standard algorithms from the Ranlib library (Brown and Lovano, 1991). A sample of inputs is generated by a program independent of the chemical simulation code and stored in a file. This program reads the reference reactions database, containing all relevant parameters (stored as preferred values and relative uncertainties), and enables to select different elicitation schemes by keywords.

In order to preserve the intrinsic correlation of the Dirichlet distribution, partial reaction rates for a reaction with n pathways are produced following three steps:

(1) a global rate k is sampled from a log-uniform or log-normal distribution;
(2) the branching ratios are sampled from the Dirichlet distribution (Eq. (8)), by generating n independent Gamma deviates with shape parameters $\bar{b}_1\hat{\gamma},\ldots,\bar{b}_n\hat{\gamma}$ (Gelman et al., 1995);
(3) the partial rate constants are products of two random numbers $(k_i = kb_i)_1^n$.

The distributions are parameterized from the preferred values and the uncertainties reported in the review of Anicich and McEwan (1997). If an uncertainty value is not given, the preferred value is considered as being inaccurate, with a relative error of 60%. As uncertainty is not quantified for branching ratios in this review, three uncertainty classes (25%, 50% and 75%) have been tested. For a few reactions, branching ratios are not reported. In such cases the pathways are considered as equiprobable with an uncertainty of 90%.

As an example of input sample, we consider the three pathways of reaction (7). Fig. 4 represents samples for two limit cases, where either the branching ratios or the rate constant have been fixed to their nominal values (top panel, clear and dark dots, respectively). When the branching ratios are fixed, the sample lies on a straight line, whereas it lies in an hyperplane (simplex) when the rate constant is fixed. These are two extreme correlation patterns. When both items are let to fluctuate, the sample is more relaxed (bottom panel, clear dots), it's actual shape depending on their respective uncertainties.

Outputs: Monte Carlo uncertainty propagation needs very few modifications in the chemistry models. The chemistry code is slightly modified in order to implement a loop over the inputs sample and the storage of the outputs sample (ions densities at various altitudes) in a file. Output samples are treated by a series of independent codes to generate statistical summaries (mean, variance, quantiles…), probability density estimates (histograms or kernel estimation) and derived observables, such as mass spectra. The convergence of the outputs has been tested with 10^3, 10^4 and 10^5 samples. Cumulative density

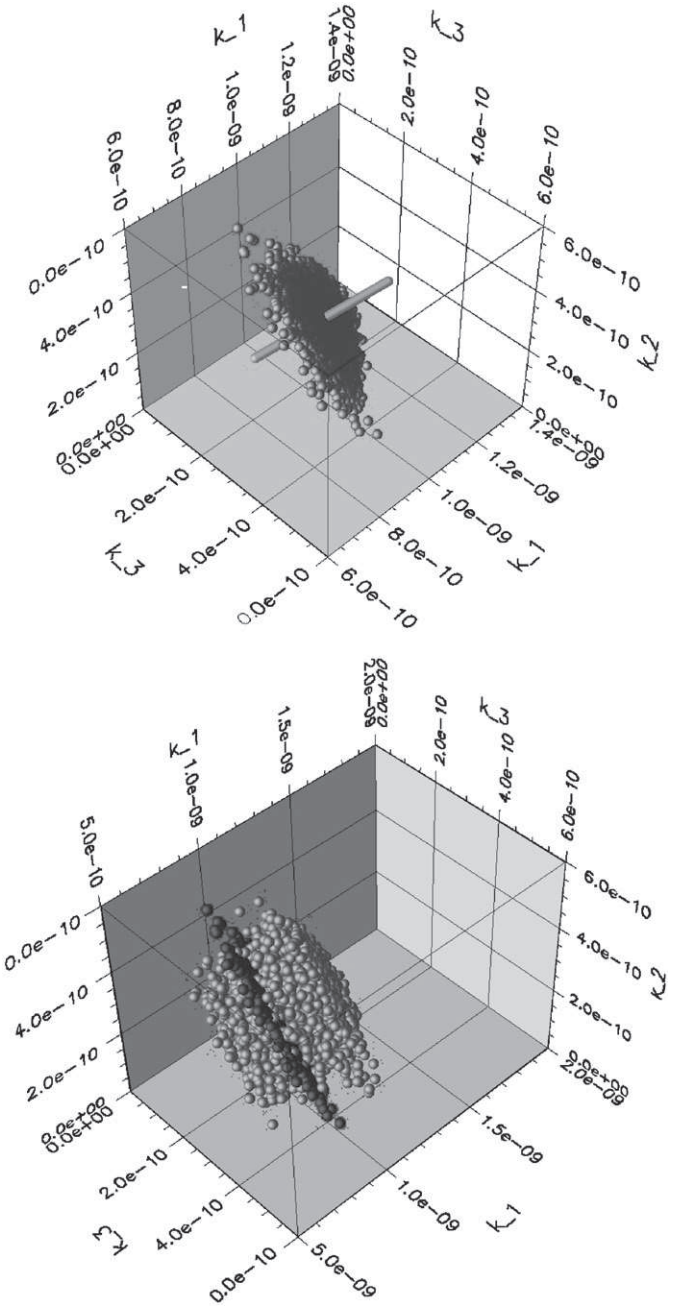

Fig. 4. Partial rates of reaction (7). The samples have been generated according the following scheme: (top panel, clear dots) fixed branching ratios and log-uniform distribution for k^0; (both panel, dark dots) fixed k^0 and Dirichlet distribution for the branching ratios; and (bottom panel, clear dots) log-uniform distribution for k^0 and Dirichlet distribution for the branching ratios.

functions used for this test were satisfyingly converged for 10^4 samples. Such runs need about one hour cpu time on a current tabletop computer.

3.3. Uncertainty propagation

3.3.1. Uncertainty propagation on rate constants

The usual way to elicit rate constants uncertainty is through log-normal distributions. Nevertheless we pointed

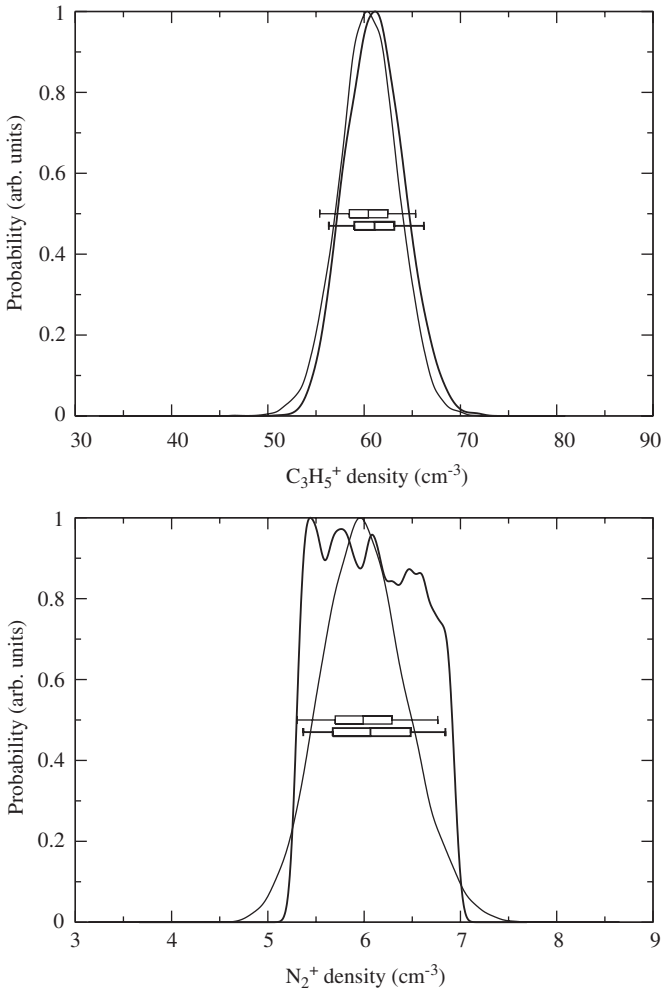

Fig. 5. $C_3H_5^+$ and N_2^+ density distributions at 1200 km obtained by uncertainty propagation with log-uniform (thick line) and log-normal (dotted line) rate constant uncertainties. Horizontal boxplots depict the 5/25/50/75/95 quantiles.

out earlier that a better adapted distribution to elicit ion–molecule rate constants is the log-uniform distribution, mainly because systematic errors are involved in most of the experimental measurements, and also because preferred values and uncertainties issued from a reviewing process pertain to a "type B" uncertainty. One of the main goals of this work is to evaluate the sensitivity of the calculated ion densities to the choice of the input distribution. Uncertainty propagations were performed for log-normal and log-uniform distributions. Examples corresponding to the ions $C_3H_5^+$ and N_2^+ at 1200 km are given in Fig. 5. These ions have been chosen for their different position in the reaction scheme:

- N_2^+ is a primary species, directly produced by electron impact and photo ionization, and essentially consumed by one major reaction, $N_2^+ + CH_4$;
- $C_3H_5^+$ is a late product in the reaction scheme, essentially coming from $C_2H_5^+ + C_2H_4$ (Nagy and Cravens, 1998), with $C_2H_5^+$ itself resulting from two successive reactions.

The shape of the outputs distributions can be strongly dependent on the choice of inputs distribution. With log-normal inputs, the outputs are likewise systematically log-normally distributed. With log-uniform inputs, the shape of the outputs distribution depends on the ion. At 1200 km, $C_3H_5^+$ density is well represented by a Gaussian distribution whereas N_2^+ density is akin to a log-uniform function. This difference is linked with the number of major reactions in which each ion is involved. Indeed, the central limit theorem forecasts that a sum of independent parameters (with any distribution) converges to a Gaussian distribution, and by the same way, that a product of independent parameters converges to a log-normal distribution (Cowan, 1998). Thus N_2^+ being a primary species with one major decay pathway, its pdf is very similar to the log-uniform distribution of the corresponding reaction rate $k(N_2^+ + CH_4)$. In contrast, $C_3H_5^+$ being a "late" ion, it's

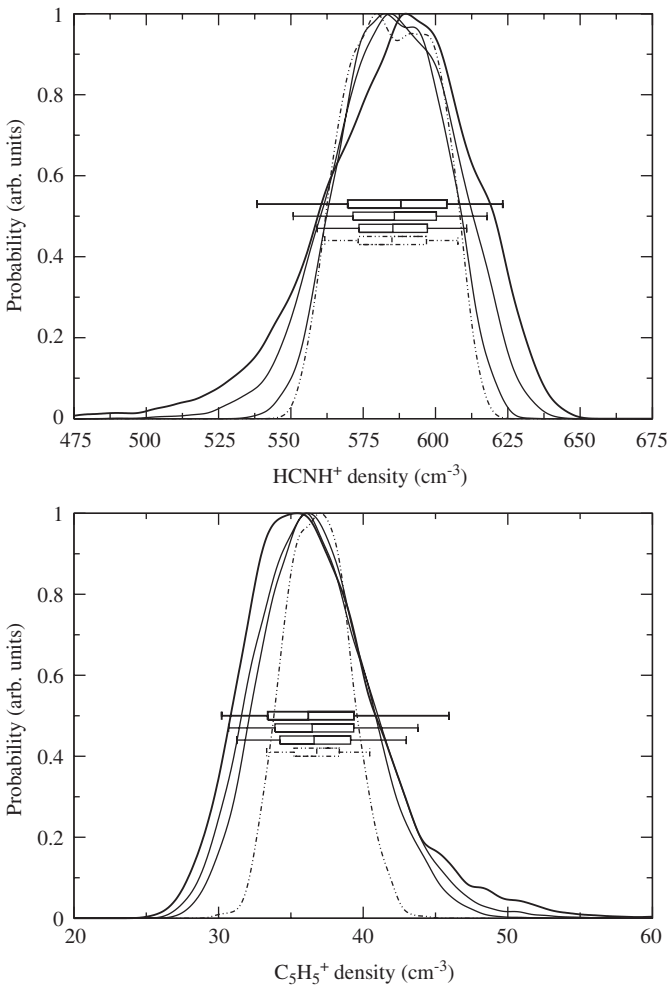

Fig. 6. $HCNH^+$ and $C_5H_5^+$ density distributions at 1200 km for night-time chemistry: with no (dashed line)/25% (thin line)/50% (normal line)/75% (thick line) relative uncertainty on the branching ratios. Horizontal boxplots depict the 5/25/50/75/95 quantiles.

density has a pdf that is nearly independent of the shape of individual reaction rates distributions.

Apart from this qualitative effect, both elicitation schemes provide essentially the same results for output uncertainty quantification. Moreover there is no computational issue in choosing between log-uniform and log-normal pdfs. As already stated, the log-uniform distribution is more consistent than the log-normal with the epistemic uncertainties affecting ion–molecule rate constants.

3.3.2. *Uncertainty propagation on branching ratios*

To quantify the effect of the uncertainties on the branching ratios, in addition to the uncertainty on the rate constants (modelled from now-on by log-uniform distributions), four cases were compared: no uncertainty, 25%, 50% and 75% relative uncertainty for all reactions, with a Dirichlet distribution. The distributions obtained in the case of two major ions $HCNH^+$ and $C_5H_5^+$ at 1200 km are plotted on Fig. 6 and the corresponding relative uncertainties $Q90/\overline{[ion]}$ are given in Table 4, with $Q90$ the width of the 90% confidence interval and $\overline{[ion]}$ the average density.

A progressive broadening of the output distribution with the increasing uncertainty on the branching ratios can be observed for $[HCNH^+]$. The Dirichlet distribution being asymmetric, an evolution of the pdf shape is also notable, giving some more weight to smaller concentrations for this ion. The pattern is different in the case of $C_5H_5^+$. The standard deviation on $[C_5H_5^+]$ strongly increases between the cases of no uncertainty and 25% uncertainty, then more progressively until 75%. The reason for this specificity is the presence of a poorly known reaction in the production scheme of $C_5H_5^+$. Indeed the reaction $C_3H_3^+ + C_2H_4$ has two pathways, producing $C_5H_5^+$ and $C_5H_7^+$. The branching ratios of this reaction are unknown and have consequently been assigned a 0.5/0.5 value, with 90% relative uncertainty (see Section 2.3.1). A large part of the uncertainty on $[C_5H_5^+]$ is consequently due to the large variability of these branching ratios.

In order to appreciate the effect of the branching ratios uncertainties, we computed histograms and sample cumulative density functions from the relative uncertainties of all ions densities, in the absence of branching ratios uncertainty, and in the case of a global 50% uncertainty, which we consider as the most realistic estimation (see Section 2.3.1). These are reported on Fig. 7 for night-time chemistry at 1000 km of altitude, on a logarithmic scale.

Table 4
Relative uncertainties, $Q90/\overline{[ion]}$ ($Q90$ is the width of the 90% confidence interval and $\overline{[ion]}$ the average density), for $HCNH^+$ and $C_5H_5^+$ at 1200 km as a function of the postulated uncertainty about branching ratios

	Uncertainty on b_i			
Ion	None	25%	50%	75%
$HCNH^+$	8%	9%	11%	14%
$C_5H_5^+$	20%	32%	36%	43%

Both distributions are peaked between 10% and 100%, but whereas uncertainties are all inferior to 100% when the branching ratios are fixed to their nominal value, about 40% of the ion densities have a relative uncertainty superior to 100% in the second case. Branching ratios appear thus to be a major source of uncertainty, and the estimated 30% of uncertainty on ion densities reported by Keller et al. (1992) appears quite optimistic for a large number of species.

We did not find a correlation between densities and relative uncertainties, indicating that the larger uncertainties cannot be assigned uniquely to minor ions. Nevertheless some tendencies related to the ion family can be seen on Fig. 8. Thus the explicitly developed pseudo-ions all (both hydrocarbons and nitriles) have large uncertainties, above 30%. The original nitriles treated in Banaszkiewicz et al. (2000) show a slight tendency of increasing

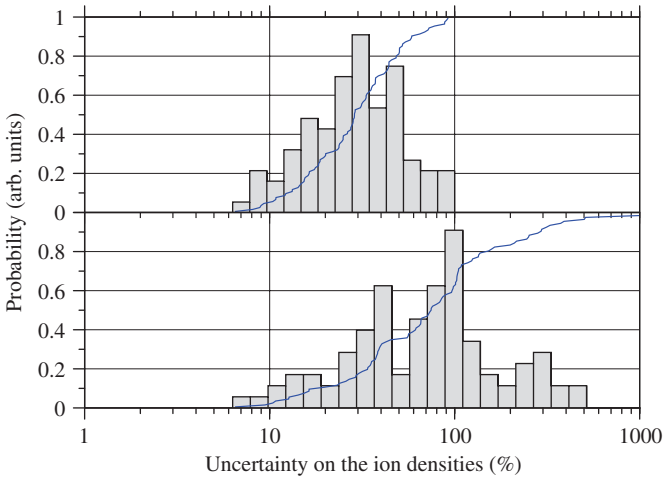

Fig. 7. Distribution of the uncertainties for all ions densities. The full line represents the sample cumulative density function. The simulations were performed by night-time chemistry at 1000 km of altitude for two cases of uncertainty on the branching ratios: (above) no uncertainty; (below) 50% relative uncertainty.

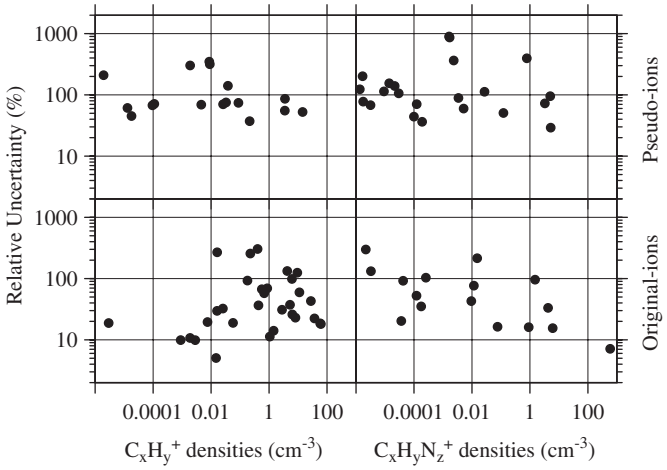

Fig. 8. Relative uncertainties versus ion densities at 1200 km of altitude by night-time chemistry.

Table 5
Uncertainty on the ten most abundant ions by night-time chemistry in Titan ionosphere at 1000, 1200 and 1400 km

1000 km		1200 km		1400 km	
Ions	$Q90/\overline{[Ion]}$ (%)	Ions	$Q90/\overline{[Ion]}$ (%)	Ions	$Q90/\overline{[Ion]}$ (%)
$HCNH^+$	20	$HCNH^+$	11	$HCNH^+$	23
$C_5H_5N^+$	50	$C_3H_5^+$	30	$C_2H_5^+$	26
$C_7H_7^+$	55	$C_2H_5^+$	30	CH_5^+	53
$C_5H_5^+$	56	$C_5H_5^+$	36	$C_3H_5^+$	28
$C_4H_3^+$	47	CH_5^+	68	CH_3^+	39
$C_5H_7^+$	89	$C_5H_7^+$	81	N_2^+	24
$C_3H_5^+$	32	$C_3H_3^+$	96	$C_2H_3^+$	52
$C_6H_7^+$	108	$C_4H_5^+$	195	CH_4^+	25
$C_4H_6N^+$	114	CH_3^+	38	$C_3H_3^+$	76
$C_2H_5^+$	39	$C_4H_3^+$	41	$C_2H_4^+$	239

$Q90$ is the width of the 90% confidence interval.

accuracy with the ion density: the most abundant ion $HCNH^+$ being also the most accurate one. Finally, the original hydrocarbons treated in Banaszkiewicz et al. (2000) are in general abundant, with a density often superior to $0.01\,cm^{-3}$, but their uncertainty shows a very large dispersion. It must be pointed out that many relatively abundant hydrocarbons present an uncertainty higher than 50%.

We calculated the uncertainty on the 10 most abundant ions (see Table 5) for 1000, 1200 and 1400 km of altitude and night-time chemistry:

- On the one hand the major component is common to the three altitudes: $HCNH^+$, which is also one of the most accurate compounds in the model, with a relative uncertainty of about 10–20%. The model is thus relatively well constrained for the most abundant ion in Titan ionosphere.
- On the other hand, numerous heavy species (and in particular some specified ex-pseudo-ions) with poorly known chemistry are among the most abundant ions at 1000 and 1200 km. Therefore their densities present large uncertainties. This highlights the necessity to improve the knowledge about the reactivity of these heavy compounds.

3.4. Mass spectra

Mass spectra are calculated with unit mass resolution from the ion densities estimated by the model, using the relative isotopic abundances found in Titan atmosphere: $D/H = 9 \times 10^{-5}$ (Mousis et al., 2002), $N^{14}/N^{15} = 194$[3] and $C^{12}/C^{13} = 95.6$ (Waite et al., 2005).

[3]Taken as the middle of the estimation interval $172 < N^{14}/N^{15} < 215$ (Waite et al., 2005) The fraction of the higher isotope is accordingly bracketed $0.0036 < N^{15}/(N^{14} + N^{15}) < 0.0058$. Considering that the number of nitrogen atoms in the nitriles of the model is small (1 or 2), this uncertainty source can be considered as irrelevant to the present work.

A mass spectrum was generated at the altitude 1200 km for night time conditions, in the ram side of Titan with a subram angle of 60°, in order to perform a qualitative comparison to the first INMS Cassini mass spectrum published on the website of the NASA (NASA/JPL/University of Michigan, 2005). As this was not the main purpose of this study, we did not attempt here to simulate further the specific conditions of the T5 flyby during which the INMS spectra were obtained.

Uncertainty bars on the simulated mass spectra presented on Fig. 9 have been calculated by uncertainty propagation with the following conditions: log-uniform distributions for the rate constants and Dirichlet distribution for the branching ratios, with an uncertainty of 50% for the documented values, and 90% for the unknown values. Calibration uncertainties have been added on the measured mass spectrum: 20% at low mass numbers and 50% at m/z of 50 or higher (Cravens et al., 2006).

Uncertainties on the simulated mass spectra are determined by the major ions for each mass. A large range of uncertainties is therefore observed, from $Q90/\overline{[HCNH^+]} = 11\%$ at $m/z = 28$, to $Q90/\overline{[C_4H_5^+]} = 195\%$ at $m/z = 53$.

In spite of the different conditions, the overall adequacy between simulated and measured spectra is quite satisfying for the lower masses (C1, C2, C3 and C4 ions). Considering the estimated uncertainties, there is a good agreement for a number of mass peaks. However, large discrepancies can be observed, especially in the case of the C5 ions which are overestimated. This difference will certainly not be corrected by taking additional uncertainty sources into account. On the basis of the rather good agreement for lower masses, we expect that the chemistry model will have to be updated and completed for these compounds, which are presently treated for most of them as terminal species. This will be a preliminary step to any meaningful quantitative comparison and it will require further laboratory experiments. For lower masses, a striking pattern is the systematic under-prediction of densities at masses 18, 30, 42 and 54. The recovery of these densities is

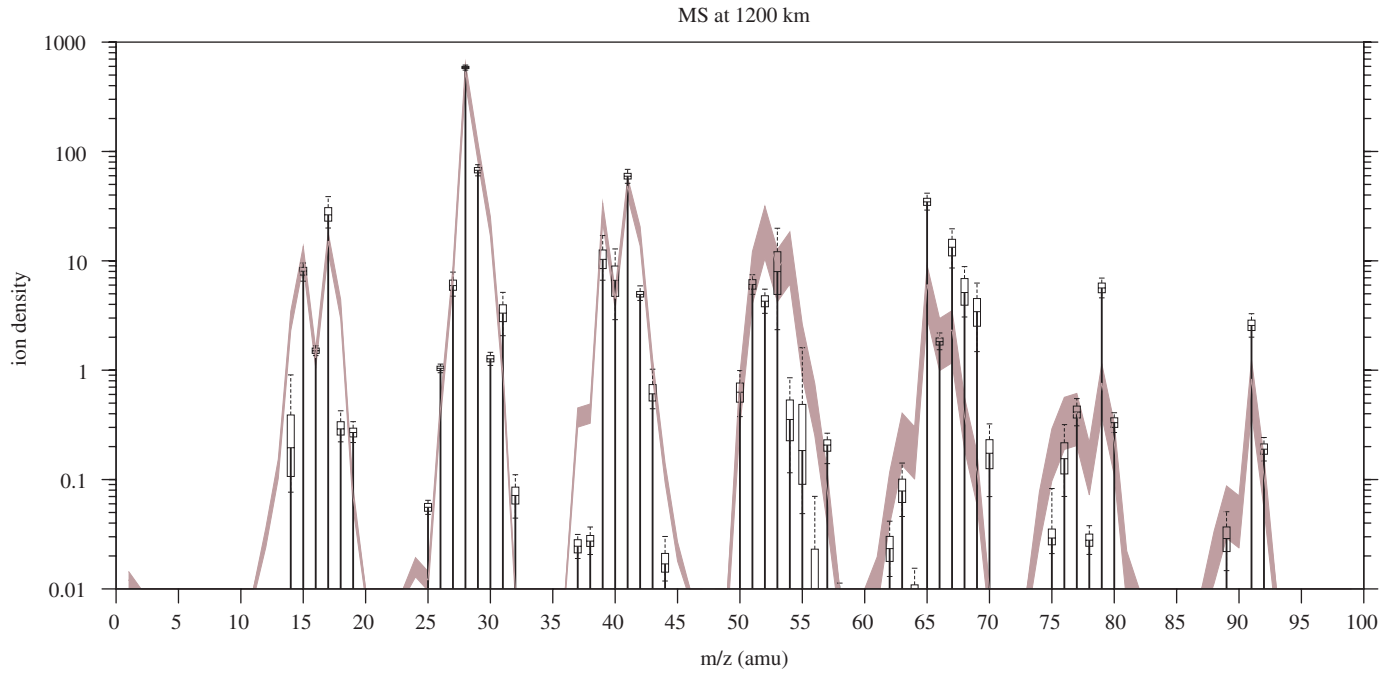

Fig. 9. Simulated (drop lines) and measured (envelope) mass spectra of Titan ionosphere at 1200 km of altitude by night time. Box-plots and error bars correspond to confidence intervals of 50% and 90% for the calculated mass spectrum. Vertical boxplots depict the 5/25/50/75/95 quantiles.

also beyond the uncertainties in the chemical parameters. Here again, it is likely that species, or even processes such as fragmentation of large ions (Cravens et al., 2006), are still lacking in the reaction scheme.

4. Conclusion

The results of uncertainty propagation of kinetics parameters on ion densities outputs have been reported for the model developed by Banaszkiewicz et al. (2000) for ion–molecule reactivity in the ionosphere of Titan. In comparison with the initial model, 42 pseudo-ions $C_xH_y^+$ and $C_xH_yN_z^+$ have been explicited in order to simulate mass-spectra in the 1–100 amu mass scale as measured by the INMS instrument of Cassini spacecraft.

Uncertainty propagations were performed by Monte Carlo sampling with probability distributions for the rate constants and branching ratios carefully adapted to the chemical data considered in the model. It was shown that a consistent way to describe the uncertainties on the rate constants for ion–molecule reactions reported in the review of Anicich and McEwan (1997) is through a log-uniform distribution. This choice has a qualitative impact on the probability distributions of the model outputs for primary species. As expected from the central limit theorem, the uncertainty distribution for the densities of species that occur after a series of reactions is rather insensitive to the specific choice of distribution for the individual reaction rates.

We propose a practical method to treat consistently uncertainties on branching ratios. To our knowledge, we provide here the first study of uncertainty propagation for such correlated parameters in the field of the modelling of complex chemical systems. In the case of our model of Titan's ionospheric chemistry, including the uncertainties on the branching ratios was shown to have a strong impact on the global uncertainty of the predicted ion densities. This study underlines the necessity of a database of evaluated branching ratio uncertainties. Meanwhile, the proposed method opens also the opportunity to treat reactions with totally unknown branching ratios, for instance on the basis of a list of pathways selected for their exothermicity. This subject will be developed in a forthcoming paper (Carrasco and Pernot, 2006).

As an illustration, we compared a simulated mass spectrum for night-time chemistry at 1200 km of altitude with an experimental mass spectrum measured by Cassini's INMS, available on the website of the NASA (NASA/JPL/University of Michigan, 2005). The shapes and orders of magnitude are globally in good agreement, which is very encouraging. However, the uncertainty bars do not overlap for a number of masses, especially in the C5 field. This indicates that adjustment of chemical parameters within their present uncertainty limits could not be a solution. In this article, the trajectory conditions of the T5 Cassini flyby were not precisely simulated. Considering the good agreement found for the C1, C2, C3 and C4 ions, we do not expect that a better simulation of the physical flyby parameters will correct the overestimation of the C5 group. Consequently, the chemical scheme needs to be completed for the production and loss of C5 ions, and other heavy ions. The chemistry of these species being practically unknown, new laboratory measurements of rate constants and branching ratios are a necessity, along

with recombination rates, most of which are presently estimated (Keller et al., 1992).

We propose here the preliminary steps for a more complete assessment of uncertainties in the simulation of Titan ionospheric chemistry. Other uncertainty sources will have to be quantified, such as the influence of considering rate constants values determined at 300 K (instead of 170 K in the ionosphere of Titan). Another source of expected major importance lies in the uncertainties on the simulated densities of neutral species (Hébrard et al., 2005). The list comprises also recombination rates, electron impact ionization and photo-ionization rates.

Once the different uncertainty sources for the present model will have been identified and quantified, the residual inadequacy between simulated and measured spectra will be decreased by further improvements to the chemical scheme. We plan in the near future to consider the sensitivity of the model predictions to presently ignored processes, such as the reactivity of excited states (in particular $N^+(^1D)$ (Alcaraz et al., 2004)), or the reactivity of doubly charged ions N_2^{++}, predicted recently to be present in Titan's ionosphere (Lilensten et al., 2005).

Although the complexity of Titan's ionospheric chemistry precludes any hope of establishing a fully detailed chemistry model, and considering that the INMS instrument will continue to produce invaluable data for many years, we foresee that considerable efforts, including new laboratory experiments, will be put into achieving a complete description of the processes involving ions with masses up to 100 amu.

More generally, we feel that the tools we developed in this study, and notably for the treatment of uncertain or unknown branching ratios, will be very helpful to modellers of complex chemical systems.

Acknowledgments

We gratefully thank EuroPlaNet for a grant to M.B. which enabled to practically initiate the present work. Part of M.B.'s work was also supported from the Polish State Committee for Scientific Research Grant 5 T12E 027 25. We acknowledge the support received from CNRS through a one year postdoctoral position for N.C.

Appendix A

A.1. The Dirichlet distribution

Although it has been only parsimoniously used in chemistry, the Dirichlet distribution is well known to represent the fluctuations of quantities independent of each other, under the condition that their sum remains fixed. In environmental modelling, it has been used to represent uncertainty in chemical composition (mole fractions) (Isukapalli, 1999; Isukapalli and Georgopoulos, 2001), or the partitioning of chemicals between different physical phases (Bates et al., 2003). Justifications for using this distribution can be, as above, its occurrence through ratios of Gamma or χ^2 distributions (Isukapalli, 1999; Isukapalli and Georgopoulos, 2001). It has recently been also derived with a random theory of dilution (Vlad et al., 2002), justifying its use for describing the distribution of chemicals after an infinite number of dilutions (geochemistry, nucleotide statistics…).

A.2. Properties

The Dirichlet distribution for a set of n numbers $\{b_i\}_{i=1}^n$ summing to 1, with parameters $\{\gamma_i\}_{i=1}^n$,

$$(b_1,\ldots,b_n)\sim\text{Dirichlet}(\gamma_1,\ldots,\gamma_n) \tag{12}$$

has for pdf

$$p\left(\{b_i\}_{i=1}^n|\{\gamma_i\}_{i=1}^n\right)=\frac{\Gamma(\gamma)}{\prod_{i=1}^n\Gamma(\gamma_i)}\prod_{i=1}^n b_i^{\gamma_i-1}, \tag{13}$$

where $\gamma=\sum_{i=1}^n\gamma_i$. The mean values, variances and covariances are

$$E(b_i)=\bar{b}_i=\frac{\gamma_i}{\gamma}, \tag{14}$$

$$\text{Var}(b_i)=\bar{b}_i(1-\bar{b}_i)/(\gamma+1), \tag{15}$$

$$\text{Cov}(b_i,b_j)=-\bar{b}_i\bar{b}_j/(\gamma+1)\ (i\neq j). \tag{16}$$

It can be seen that the Dirichlet distribution can only represent negative covariances which are the direct consequence of the normalization constraint. The marginals of the Dirichlet are Beta distributions

$$b_i\sim\text{Beta}(\gamma_i,\gamma-\gamma_i). \tag{17}$$

A.3. Elicitation

One way to estimate the parameters of the Dirichlet distribution is to select those that provide a good match between the marginal mean values and variances and the target data, i.e. $(\bar{b}_i,\sigma_i)_{i=1}^n$. This results in the following set of equations, for all $i=1,\ldots,n$:

$$E(b_i)=\frac{\gamma_i}{\gamma}=\bar{b}_i, \tag{18}$$

$$\text{var}(b_i)=\gamma_i(\gamma-\gamma_i)/(\gamma^2(\gamma+1)) \tag{19}$$

$$=\bar{b}_i(1-\bar{b}_i)/(\gamma+1) \tag{20}$$

$$=\sigma_i^2. \tag{21}$$

The constraint on the mean is directly satisfied by taking $\gamma_i=\bar{b}_i\gamma$, which leaves γ as the only parameter to be identified from the n marginal variances

$$\gamma=\frac{\bar{b}_i(1-\bar{b}_i)}{\sigma_i^2}-1\quad\text{for } i=1,\ldots,n. \tag{22}$$

In general, γ cannot satisfy to this set of equations, which underlines the fact that that the Dirichlet distribution is too rigid to represent any set of experimental uncertainties

(Aitchison, 1986). We propose here that a satisfactory solution can nevertheless be obtained by a least-squares procedure and we define the optimal γ value as

$$\hat{\gamma} = \underset{\gamma}{\operatorname{argmin}} \sum_i \left(\sigma_i - \left(\frac{\bar{b}_i(1-\bar{b}_i)}{\gamma+1} \right)^{1/2} \right)^2 \quad (23)$$

$$= \left(\frac{\sum_i \bar{b}_i(1-\bar{b}_i)}{\sum_i \sigma_i \sqrt{\bar{b}_i(1-\bar{b}_i)}} \right)^2 - 1. \quad (24)$$

By taking $\sigma_i = x\bar{b}_i/2$, one obtains an equation relating $\hat{\gamma}$ to the relative uncertainty x (see Eq. (9)). For large uncertainties, $\hat{\gamma}$ can become very small ($\hat{\gamma} \ll 1$), which is in agreement with the fact that the Dirichlet distribution becomes non-informative when all it's parameters become vanishingly small (Gelman et al., 1995). However, in such conditions, the Dirichlet and its Beta marginal distributions might become multimodal, with a concentration of probability mass at the borders/corners of the $(n-1)$-simplex. This behavior is not appropriate here, and we avoid it by defining a lower limit for $\hat{\gamma}$. The Beta distribution being bimodal when both it's parameters are smaller than 1, we require that $\hat{\gamma}\bar{b}_i \geqslant 1$ or $\hat{\gamma}(1-\bar{b}_i) \geqslant 1$ for all i. The lower limit is thus

$$\gamma_{\min} = \left\{ \min\left(\max\left(\bar{b}_1, 1-\bar{b}_1\right), \ldots, \max\left(\bar{b}_n, 1-\bar{b}_n\right) \right) \right\}^{-1} \quad (25)$$

and the optimal uncertainty factor is defined simultaneously by Eq. (23) and the condition $\hat{\gamma} > \gamma_{\min}$. The distribution for the branching ratios is accordingly approximated by

$$(b_1, \ldots, b_n) \sim \text{Dirichlet}\left(\hat{\gamma} \times \left(\bar{b}_1, \ldots, \bar{b}_n\right)\right). \quad (26)$$

The present parametrization of the Dirichlet distribution relies thus on n position parameters, provided by the reported values of the branching ratios $(\bar{b}_1, \ldots, \bar{b}_n)$, and on a single shape parameter $\hat{\gamma}$.

References

Adams, N., Smith, D., 1976. The selected ion flow tube (SIFT); a technique for studying ion-neutral reactions. Int. J. Mass Spectrom. Ion Phys. 21 (3–4), 349–359.

Adams, N., Smith, D., 1988. Techniques for the study of ion–molecule reactions, vol. XX. Wiley Interscience, New York.

Adams, N., Smith, D., Paulson, J., 1980. An experimental survey of the reactions of NH_n^+ ions ($n=0$ to 4) with several diatomic and polyatomic molecules at 300 K. J. Chem. Phys. 72 (1), 288–297.

Aitchison, J., 1986. The Statistical Analysis of Compositional Data. Monographs on Statistics and Applied Probability. Chapman & Hall, London.

Alcaraz, C., Nicolas, C., Thissen, R., Zabka, J., Dutuit, O., 2004. $^{15}N^+ + CD_4$ and $O^+ + {}^{13}CO_2$ state-selected ion–molecule reactions relevant to the chemistry of planetary ionospheres. J. Phys. Chem. A 108 (45), 9998–10009.

Anicich, V., 1993. Evaluated bimolecular ion–molecule gas phase kinetics of positive ions for use in modelling planetary atmospheres, cometary comae and interstellar clouds. J. Phys. Chem. Reference Data 22 (6), 1469–1569.

Anicich, V., 2003. An Index of the Literature for Bimolecular Gas Phase Cation–Molecule Reaction Kinetics. JPL Publication 03–19, pp. 1–1194.

Anicich, V., Bowers, M., 1973. Absolute ion–molecule rate constants from DRIFT cell ion cyclotron resonance spectroscopy. Int. J. Mass Spectrom. Ion Phys. 11, 329–344.

Anicich, V., McEwan, M., 1997. Ion–molecule chemistry in Titan's ionosphere. Planet. Space Sci. 45, 897–921.

Anicich, V., Huntress, W., Futrell, J., 1977. Ion cyclotron resonance studies of some reactions of N^+ ions. Chem. Phys. Lett. 47, 488–489.

Anicich, V., Wilson, P., McEwan, M., 2004. A SIFT ion–molecule study of some reactions in Titan's atmosphere. Reactions of N^+, N_2^+ and HCN^+ with CH_4, C_2H_2 and C_2H_4. J. Am. Soc. Mass Spectrom. 15, 1148–1155.

Armentrout, P., 2003. The Encyclopedia of Mass Spectrometry, vol. 1—Theory and Ion Chemistry. Elsevier, Amsterdam.

Armentrout, P., Baer, T., 1996. Gas-phase ion dynamics and chemistry. J. Phys. Chem. 100, 12866–12877.

Atkinson, R., Baulch, D., Cox, R., Crowley, J., Hampson, R., Hynes, R., Jenkin, M., Rossi, M., Troe, J., 2004. Evaluated kinetic and photochemical data for atmospheric chemistry: volume i—gas phase reactions of O_x, HO_x, NO_x and SO_x species. Atmos. Chem. Phys. 4, 1461–1738.

Banaszkiewicz, M., Lara, L., Rodrigo, R., Lopez-Moreno, J., Molina-Cuberos, G., 2000. A coupled model of Titan's atmosphere and ionosphere. Icarus 147, 386–404.

Bates, S., Cullen, A., Raftery, A., 2003. Bayesian uncertainty assessment in multicompartment deterministic simulation models for environmental risk assessment. Environmetrics 14, 355–371.

Bird, M., Dutta-Roy, R., Asmar, S., Rebold, T., 1997. Detection of Titan's ionosphere from Voyager 1 radio occultation observations. Icarus 130, 426–436.

Bohme, D., Dunkin, D., Fehsenfeld, F., Ferguson, E., 1969. Flowing after-glow studies of ion–molecule association reactions. J. Chem. Phys. 51 (3), 863–872.

Broadfoot, A., Sandel, B., Shemansky, D., Holberg, J., Smith, G., Strobel, D., McConnell, J., Kumar, S., Hunten, D., Atreya, S., Donahue, T., Moos, H., Bertaux, J., Blamont, J., Pomphrey, R., Linick, S., 1981. Extreme ultraviolet observations from Voyager 1 encounter with Saturn. Science 212, 206–211.

Brown, B., Lovano, J., 1991. Ranlib: Library of fortran routines for random number generation. Department of Biomathematics, M.D. Anderson Cancer Center, University of Texas, Houston.

Carrasco, N., Pernot, P., 2006. Modeling of branching ratio uncertainty in chemical networks by Dirichlet distributions., in preparation.

Cowan, G., 1998. Statistical Data Analysis. Oxford Science Publications, Oxford.

Cravens, T., Robertson, Jr. I., J.W., Kasprzak, W., Keller, C., Ledvina, S., Niemann, H., Luhmann, J., McNutt, R., Ip, W., De La Haye, V., Mueller-Wodarg, I., Wahlung, J., Anicich, V., Vuitton, V., 2006. The composition of Titan's ionosphere. Geophys. Res. Lett. 33, L07312.

d'Agostini, G., 2003. Bayesian Reasoning in Data Analysis: A Critical Introduction. World Scientific Pub. Co. Inc., Singapore.

Dheandhanoo, S., Johnsen, R., Biondi, M., 1984. Measured ion–molecule reaction rates for modelling Titan's atmosphere. Planet. Space Sci. 32 (10), 1301–1305.

Dobrijevic, M., Parisot, J., 1998. Effect of chemical kinetic uncertainties on hydrocarbon production in the stratosphere of neptune. Planet. Space Sci. 46, 491–505.

Dobrijevic, M., Ollivier, J.L., Billebaud, F., Brillet, J., Parisot, J., 2003. Effect of chemical kinetic uncertainties on photochemical modeling results: application to Saturn's atmosphere. Acta Astronaut. 398, 335–344.

Ervin, K., Armentrout, P., 1985. Translational energy dependence of $Ar^+ + XY \rightarrow ArX^+ + Y$($XY = H_2$, D_2, HD) from thermal to 30 eV cm. J. Chem. Phys. 83, 166–189.

Evans, M., Hastings, N., Peacock, B., 2000. Statistical Distributions, third ed. Wiley Interscience, New York.

Fox, J., Yelle, R., 1997. Hydrocarbon ions in the ionosphere of Titan. Geophys. Res. Lett. 24, 2179.

Fröhner, F., 2000. Evaluation and analysis of nuclear resonance data. JEFF Report 18, Nuclear Energy Agency and Organization for Economic Co-operation and Development.

Garthwaite, P., Kadane, J., O'Hagan, A., 2005. Statistical methods for eliciting probability distributions. J. Am. Stat. Assoc. 100, 680–701.

Gelman, A., Carlin, J., Stern, H., Rubin, D., 1995. Bayesian Data Analysis. Chapman & Hall, London.

Gerlich, D., 1986. Low energy ion reactions measured with guided beams. Electronic and Atomic Collisions. North-Holland, Amsterdam, p. 541.

Gerlich, D., 1992. Inhomogeneous RF Fields: A Versatile Tool for the Study of Processes with Slow Ions. Adv. Chem. Phys. LXXXII, 1–176.

Hanel, R., Conrath, B., Flasar, F., Kunde, V., Maguire, W., Pearl, J., Pirraglia, J., Samuelson, R., Herath, L., Allison, M., Cruikshank, D., Gautier, D., Gierasch, P., Horn, L., Koppany, R., Ponnamperuma, C., 1981. Infrared observations of the Saturnian system from Voyager 1. Science 212, 192–200.

Hanson, K., Hemez, F.M., 2003. Uncertainty quantification of simulation codes based on experimental data. In: Proceedings of the 41st AIAA Aerospace Sciences, Washington DC. AIAA, New York.

Hawley, M., Mazely, T., Randeniya, L., Smith, R., Zeng, X., Smith, M., 1990. A free jet flow reactor for ion/molecule reaction studies at very low energies. Int. J. Mass Spectrom. Ion Process. 97, 55–86.

Hébrard, E., Bénilan, Y., Raulin, F., 2005. Sensitivity effects of photochemical parameters uncertainties on hydrocarbon production in the atmosphere of Titan. Adv. Space Res. 36, 268–273.

Helton, J., 2005. Sampling-based methods for uncertainty and sensitivity analysis. In: Hanson, K.M., Hemez, F.M. (Eds.), Sensitivity Analysis of Model Output (SAMO 2004). Los Alamos National Laboratory, Los Alamos, pp. 221–229.

Helton, J., Davis, F., 2000. Sampling-based methods. Sensitivity Analysis, Wiley Series in Probability and Statistics. Wiley, New York, pp. 101–153.

Huntress, W., 1977. Laboratory studies of bimolecular reactions ions in interstellar clouds, comets, and in planetary atmospheres of reducing composition. Astrophys. J. Suppl. Ser. 33, 495–514.

Huntress, W., Pinizzoto, R., 1973. Product distributions and rate constants for ion–molecule reactions in water, hydrogen sulfide, ammonia, and methane. J. Chem. Phys. 59 (9), 4742–4756.

Ip, W., 1990. Titan's upper ionosphere. Astrophys. J. 362, 354–363.

Isukapalli, S., 1999. Uncertainty analysis of transport-transformation models. Ph.D. Thesis, Graduate School, New Brunswick, Rutgers, The State University of New Jersey.

Isukapalli, S., Georgopoulos, P., 2001. Computational methods for sensitivity analysis and uncertainty analysis for environmental and biological models. Technical Report EPA/600/R-01-068, US Environmental Protection Agency, Research Triangle Park, NC27711.

Jenkinson, D., 2005. The elicitation of probabilities—A review of the statistical literature. BEEP Working Paper, University of Sheffield.

Keller, C., Cravens, T., Gan, L., 1992. A model of the ionosphere of Titan. J. Geophys. Res. 97, 12117.

Keller, C., Anicich, V., Cravens, T., 1998. Model of Titan's ionosphere with detailed hydrocarbon ion chemistry. Planet. Space Sci. 46, 1157.

Kemper, P., Bowers, M., 1988. Techniques for the Study of Ion–Molecule Reactions, vol. XX. Wiley Interscience, New York.

Kim, J., Anicich, V., Huntress Jr., W., 1977. Product distributions and rate constants for the reactions of CH_3^+, CH_4^+, $C_2H_2^+$, $C_2H_3^+$, $C_2H_4^+$, $C_2H_5^+$, and $C_2H_6^+$ ions with CH_4, C_2H_2, C_2H_4 and C_2H_6. J. Phys. Chem. 81 (19), 1798–1805.

Levine, R., Tribus, M., 1979. The Maximum Entropy Formalism. MIT Press, Cambridge, MA.

Lilensten, J., Witasse, O., Simon, C., Solidi-Lose, H., Dutuit, O., Thissen, R., Alcaraz, C., 2005. Prediction of a N_2^{++} layer in the upper atmosphere of Titan. Geophys. Res. Lett. 32 (3).

Limpert, E., Stahel, W., Abbt, M., 2001. Log-normal distributions across the sciences: keys and clues. Bioscience 51, 341–352.

McEwan, M., Scott, G., Anicich, V., 1998. Ion–molecule reactions relevant to Titan's ionosphere. Int. J. Mass Spectrom. Ion Process. 172, 209–219.

Minard, R., 2005. A survey of data and publications relating to Titan atmospheric chemistry studies. ⟨http://psarc.geosc.psu.edu/TITAN/TitanChemBiblio.pdf⟩.

Mousis, O., Gautier, D., Cousténis, A., 2002. The D/H ratio in methane in Titan: origin and history. Icarus 159, 156–165.

Nagy, A., Cravens, T., 1998. Titan's ionosphere: a review. Planet. Space Sci. 46 (9/10), 1149–1155.

NASA/JPL/University of Michigan, 2005. PIA07865: Titan's upper atmosphere: A "factory" of hydrocarbons. INMS spectrum at 1200 km ⟨http://photojournal.jpl.nasa.gov/catalog/PIA07865⟩.

Nicolas, C., Alcaraz, C., Thissen, R., Zabka, J., Dutuit, O., 2002. Effects of ion excitation on charge transfer reactions of the Mars, Venus and Earth ionospheres. Planet. Space Sci. 50, 877–887.

Nicolas, C., Torrents, R., Gerlich, D., 2003. Integral and differential cross section measurements at low collision energies for the $N_2^+ + CH_4/CD_4$ reactions. J. Chem. Phys. 118 (6), 2723–2730.

Randeniya, L., Smith, M., 1991. Gas phase reaction rates of N_2^+ with CH_4, O_2, and n-H_2 at very low temperatures. J. Chem. Phys. 94 (1), 351–356.

Roboz, A., Nagy, A., 1994. The energetics of Titan's ionosphere. J. Geophys. Res. 99, 2087–2093.

Rowe, B., Parent, D., 1995. Techniques for the study of reaction kinetics at low temperatures: application to the atmospheric chemistry of Titan. Planet. Space Sci. 43 (1), 105–114.

Rowe, B., Dupeyrat, G., Marquette, J., Gaucherel, P., 1984. Study of the reactions $N_2^+ + 2N_2 = N_4^+ + N_2$ and $O_2^+ + 2O_2 = O_4^+ + O_2$ from 20 to 160 K by the CRESU technique. J. Chem. Phys. 80, 4915–4921.

Rowe, B., Marquette, J., Dupeyrat, G., 1985. Reactions of He^+ and N^+ ions with several molecules at 8 K. Chem. Phys. Lett. 113 (4), 403–406.

Rowe, B., Marquette, J., Rebrion, C., 1989. Mass-selected ion–molecule reactions at very low temperatures. The CRESUS apparatus. J. Chem. Soc. Faraday Trans. 2 85 (10), 1631–1641.

Saltelli, A., Ratto, M., Tarantola, S., Campolongo, F., 2005. Sensitivity analysis for chemical models. Chem. Rev. 105, 2811–2827.

Samuelson, R., Nath, N., Borysow, A., 1997. Gaseous abundances and methane supersaturation in titan's troposphere. Planet. Space Sci. 45, 959–980.

Smith, D., 2003. A demonstration of the lognormal distribution. Report ANL/NDM-156, Argonne National Laboratory.

Smith, D., Futrell, J., 1974. A new tandem mass spectrometer for the study of ion–molecule reactions. Int. J. Mass Spectrom. Ion Phys. 14 (2), 171–181.

Smith, D., Adams, N., Miller, T., 1978. A laboratory study of the reactions of N^+, N_2^+, N_3^+, O^+, O_2^+ , and NO^+ ions with several molecules at 300 K. J. Chem. Phys. 69 (1), 308–318.

Smith, M., 1992. State-selected and state-to-state ion–molecule reaction dynamics. Part 1-Experiment. Ion–Molecule Reaction Dynamics at Very Low Temperatures, vol. 82. Wiley, New York, pp. 183–251.

Stewart, R., Thompson, A., 1996. Kinetic data imprecisions in photochemical rate calculations: means, medians and temperature dependence. J. Geophys. Res. 101, 20935–20964.

Taylor, B., Kuyatt, C., 1994. Guidelines for evaluating and expressing the uncertainty of NIST measurement results. Technical Note 1297, National Institute of Standards and Technology, US Government Printing Office, Washington, DC.

Teloy, E., Gerlich, D., 1974. Integral cross sections for ion–molecule reactions. I—The guided beam technique. Chem. Phys. 4, 417–427.

Thompson, A., Stewart, R., 1991. Effect of chemical kinetics uncertainties on calculated constituents in a tropospheric photochemical model. J. Geophys. Res. 96, 13089–13108.

Tichy, M., Rakshit, A., Lister, D., Twiddy, N., Adams, N., Smith, D., 1979. A study of the reactions of the ground and metastable states of C^+, N^+, S^+ and N_2^+ at 300 K. J. Mass Spectrom. Ion Phys. 29, 231–247.

Toublanc, D., Parisot, J., Brillet, J., Gautier, D., Raulin, F., McKay, C., 1995. Photochemical modeling of Titan's atmosphere. Icarus 113, 2–26.

Turányi, T., Zalotai, L., Dóbé, S., Bérces, T., 2002. Effect of the uncertainty of kinetic and thermodynamic data on methane flame simulation results. Phys. Chem. Chem. Phys. 4, 2568–2578.

Vasyunin, A., Sobolev, A., Wiebe, D., Semenov, D., 2004. Influence of uncertainties in the rate constants of chemical reactions on astrochemical modeling results. Astron. Lett. 30 (8), 566–576.

Vlad, M., Tsuchiya, M., Oefner, P., Ross, J., 2002. Bayesian analysis with random chemical composition: renormalization-group approach to Dirichlet distributions and the statistical theory of dilution. Phys. Rev. E 65, 011112.

Waite, J., Lewis, W., Kasprzak, W., Anicich, V., Block, B., Cravens, T., Fletcher, G., Ip, W.-H., Luhmann, J., Mcnutt, R., Niemann, H., Parejko, J., Richards, J., Thorpe, R., Walter, E., Yelle, R., 2004. The Cassini ion and neutral mass spectrometer (INMS) investigation. Space Sci. Rev. 114 (1), 113–231.

Waite, J., Niemann, H., Yelle, R., Kasprzak, W., Cravens, T., Luhmann, J., McNutt, R., Ip, W.-H., Gell, D., De La Haye, V., Muller-Wordag, I., Magee, B., Borggren, N., Ledvina, S., Fletcher, G., Walter, E., Miller, R., Scherer, S., Thorpe, R., Xu, J., Block, B., Arnett, K., 2005. Ion neutral mass spectrometer results from the first flyby of Titan. Science 308 (5724), 982–986.

Wakelam, V., Selsis, F., Herbst, E., Caselli, P., 2005. Estimation and reduction of the uncertainties in chemical models: application to hot core chemistry. Acta Astronaut. 444, 883–891.

Wakelam, V., Herbst, E., Selsis, F., 2006. The effect of uncertainties on chemical models of dark clouds. Acta Astronaut. 451, 551–562.

Wilson, E., Atreya, S., 2004. Current state of modeling the photochemistry of Titan's mutually dependent atmosphere and ionosphere. J. Geophys. Res. 109, E06002.

Yelle, R., Strobell, D., Lellouch, E., Gautier, D., 1997. Engineering models for titan's atmosphere. ESA SP-1177, pp. 243–254.

Yung, Y., Allen, M., Pinto, J., 1984. Photochemistry of the atmosphere of Titan—comparison between model and observations. Astrophys. J. Suppl. Ser. 55, 465–506.

Zádor, J., Wagner, V., Wirtz, K., Pilling, M., 2005a. Quantitative assessment of uncertainties for a model of ethene oxidation using the European photoreactor (EUPHORE). Atmos. Environ. 39, 2805–2817.

Zádor, J., Zsély, I.G., Turányi, T., Ratto, M., Tarantola, S., Saltelli, A., 2005b. Local and global uncertainty analyses for a methane flame model. J. Phys. Chem. 109, 9575–9807.

Zádor, J., Zsély, I.G., Turányi, T., 2006. Local and global uncertainty analysis of complex chemical kinetic systems. Reliability Eng. System Safety 91, 1232–1240.

Chemical Characterization of Titan's Tholins: Solubility, Morphology and Molecular Structure Revisited†

N. Carrasco,*,‡ I. Schmitz-Afonso,§ J-Y. Bonnet,|| E. Quirico,|| R. Thissen,|| Odile Dutuit,|| A. Bagag,§ O. Laprévote,§ A. Buch,⊥ A. Giulani,#,∇ Gilles Adandé,|| F. Ouni,‡ E. Hadamcik,‡ C. Szopa,‡ and G. Cernogora‡

Université de Versailles St-Quentin, UPMC Univ. Paris 06 CNRS/INSU, LATMOS-IPSL, Route des Gâtines, 91371 Verrières le Buisson Cedex, France, Institut de Chimie des Substances Naturelles, CNRS, Bât. 27, Avenue de la Terrasse 91198 Gif-sur-Yvette Cedex, France, Laboratoire de Planétologie de Grenoble, CNRS, UJF, UMR 5109, BP 53, 38041 Grenoble Cedex 9, France, Laboratoire de Génie des Procédés et Matériaux, Ecole Centrale Paris, Grande Voie des Vignes - 92295 Chatenay-Malabry Cedex, France, SOLEIL, L'Orme des merisiers, Saint Aubin BP48, 91192 Gif sur Yvette Cedex, France, and Cepia, Institut National de la Recherche Agronomique (INRA), BP 71627, F-44316 Nantes Cedex 3 France

Received: May 20, 2009; Revised Manuscript Received: August 25, 2009

In this work Titan's atmospheric chemistry is simulated using a capacitively coupled plasma radio frequency discharge in a N_2-CH_4 stationnary flux. Samples of Titan's tholins are produced in gaseous mixtures containing either 2 or 10% methane before the plasma discharge, covering the methane concentration range measured in Titan's atmosphere. We study their solubility and associated morphology, their infrared spectroscopy signature and the mass distribution of the soluble fraction by mass spectrometry. An important result is to highlight that the previous Titan's tholin solubility studies are inappropriate to fully characterize such a heterogeneous organic matter and we develop a new protocol to evaluate quantitatively tholins solubility. We find that tholins contain up to 35% in mass of molecules soluble in methanol, attached to a hardly insoluble fraction. Methanol is then chosen as a discriminating solvent to characterize the differences between soluble and insoluble species constituting the bulk tholins. No significant morphological change of shape or surface feature is derived from scanning electron microscopy after the extraction of the soluble fraction. This observation suggests a solid structure despite an important porosity of the grains. Infrared spectroscopy is recorded for both fractions. The IR spectra of the bulk, soluble, and insoluble tholins fractions are found to be very similar and reveal identical chemical signatures of nitrogen bearing functions and aliphatic groups. This result confirms that the chemical information collected when analyzing only the soluble fraction provides a valuable insight representative of the bulk material. The soluble fraction is ionized with an atmospheric pressure photoionization source and analyzed by a hybrid mass spectrometer. The congested mass spectra with one peak at every mass unit between 50 and 800 u confirm that the soluble fraction contains a complex mixture of organic molecules. The broad distribution, however, exhibits a regular pattern of mass clusters. Tandem collision induced dissociation analysis is performed in the negative ion mode to retrieve structural information. It reveals that (i) the molecules are ended by methyl, amine and cyanide groups, (ii) a 27 u neutral moiety (most probably HCN) is often released in the fragmentation of tholin anions, and (iii) an ubiquitous ionic fragment at *m*/*z* 66 is found in all tandem spectra. A tentative structure is proposed for this negative ion.

1. Introduction

Titan, the largest satellite of Saturn, has a dense atmosphere composed of nitrogen (95 to 98%), methane, molecular hydrogen, and traces of hydrocarbons. Several nitrogen-bearing organic compounds such as hydrogen cyanide (HCN), cyanoacetylene (HC_3N), and cyanogen (C_2N_2) have been detected in its atmosphere.[1,2]

A further chemical growth, initiated by the activation of N_2 and CH_4 is at work, leading to strong interest and relevance for astrobiological questions. The atmospheric chemistry is so active that it eventually produces macroscopic particles that sediment slowly in the atmosphere, leading to the brownish haze permanently surrounding the satellite. These organic aerosols play an important role in the properties and evolution of Titan's atmosphere.[3] Indeed, aerosols absorb a significant fraction of the incoming sunlight, generating an antigreenhouse effect that cools down Titan's surface.[4] However, information on these aerosols composition, their formation, and their growth is still very limited due to the difficulty to perform observations of Titan's upper atmosphere from the Earth or from space probes.[5]

A complementary strategy to remote observations was developed. The study of Titan's aerosols was refined by producing analogous materials in laboratory, the so-called Titan tholins. The most efficient production methods are plasma discharges in gaseous N_2-CH_4 mixtures.[6−13] In the present work, the discharge is based on a radio frequency capacitively coupled plasma.[14]

† Part of the special section "Chemistry: Titan Atmosphere".
* Corresponding author. E-mail: nathalie.carrasco@latmos.ipsl.fr.
‡ Université de Versailles St-Quentin.
§ Institut de Chimie des Substances Naturelles CNRS.
|| Laboratoire de Planétologie de Grenoble, CNRS.
⊥ Ecole Centrale Paris.
SOLEIL.
∇ Institut National de la Recherche Agronomique.

10.1021/jp904735q CCC: $40.75
Published on Web 09/23/2009

In this work two different tholin samples have been generated by changing the relative abundance of N_2/CH_4 inlets in the plasma; either 98/2% (SA98) or 90/10% (SA90). They are similar to previous tholin production conditions[8,14−16] and representative of the methane molar fraction profile measured[17] in Titan's atmosphere.

The aim is very different from previous solubility studies[8,15,16] that were focused on a possible extrapolation of Titan's aerosols' solubilities with putative liquid interfaces on Titan's surface/subsurfaces or in atmospheric droplets. In this study, the aim is to know whether the laboratory analyses made on the easily accessible soluble fractions are representative or not of the bulk tholins. The choice of the solvent is thus decorrelated from any considerations about the actual solvatation processes on Titan's surface. It ensures that the tholins organic matter is significantly partitioned into two phases (soluble or insoluble fractions) to further investigate the morphology and chemical nature of both the solid and dissolved compounds through complementary analyses. To further characterize both soluble and insoluble phases, we first developed a new protocol to evaluate quantitatively the solubility of the samples and we measured the solubility of samples SA98 and SA90 in one polar (methanol) and in one nonpolar (toluene) solvent.

The fractions were further subjected to the following analytical methods:

• Scanning electron microscopy (SEM) was used to evaluate the effect of solubilization on the morphology of the samples.

• Infrared (IR) absorption spectroscopy was used to evaluate the potential chemical partitioning occurring in the SA90 and the SA98 samples when the soluble fraction was separated from the insoluble one.

• Atmospheric pressure photoionization (APPI) coupled with a hybrid quadrupole time-of-flight mass spectrometry (QTOF-MS) was used to evaluate the molecular composition of the soluble fraction of both samples. Further analysis by the tandem collision induced dissociation (CID) method led to structural information concerning the negatively charged ionic species present in the spectrum.

2. Experimental Methods

2.1. PAMPRE Experimental Setup and Tholins Production and Collection. The experimental set up named PAMPRE (French acronym for Production d'Aérosols en Microgravité par Plasma REactifs) was described in detail previously[14] and is summarized here briefly. The plasma is a radio frequency capacitively coupled plasma discharge produced at a 13.56 MHz frequency in a N_2-CH_4 gaseous mixture. The plasma is confined in a cylindrical cage shaped by a metallic grid of 138 mm in diameter and 45 mm length. In the plasma discharge, electrons dissociate and ionize N_2 and CH_4. This initiates chemical reactions and molecular growth producing hydrocarbons and nitrogen bearing molecules that eventually end up forming solid particles. The produced solid particles are negatively charged and maintained in levitation between the electrodes by electrostatic forces. The charge increases with tholin size. The N_2-CH_4 gaseous mixture is injected continuously into the plasma reactor, as a neutral flow oriented downward. This produces a neutral drag force, which can eject the solid particles out of the plasma discharge. The ejected tholins are trapped in a glass vessel surrounding the metallic cage. When sufficient amounts of tholins are produced (i.e., usually 8 h), the plasma is turned off; the reactor is thoroughly pumped to evacuate potential traces of HCN and other residual gases, then filled with N_2 to atmospheric pressure and opened for solid sample collection. Under usual conditions, about 0.5 cm^3 (∼100 mg) of solid material is produced in a run of 8 h. The tholins, which have the appearance of a very fine orange to brown powder, are deposited gently in the glass vessel without any interaction with the substrate. They are collected into microvials for ex-situ analyses.

In this work, the samples were obtained in the following operating conditions: a total pressure of 1 mbar, a flow rate of 55.0 ± 0.1 sccm, and an absorbed radio frequency power of 30 ± 2 W. Two different samples were produced by adjusting the relative flux of N_2 vs CH_4. The first sample (SA98) was produced with a gaseous mixture containing $2.00 \pm 0.06\%$ of methane, while the second sample (SA90) was produced with a mixture containing $10.0 \pm 0.2\%$ of methane. Experiments were performed at room temperature, which is not representative of Titan's atmosphere low temperature (100−200 K). The influence of temperature on kinetics and mechanisms is beyond this work but is a major concern for further studies on Titan's tholins.

2.2. Scanning Electron Microscopy. The morphology and size of the particles of both samples were investigated by field emission gun scanning electron microscopy (FEG-SEM). Aerosols were deposited on an aluminum plate and coated with a thin layer (20 nm) of gold to make their surface electrically conducting. Then, observations were achieved with an FEG-SEM (JEOL) equipped with an X-ray detector.[18]

2.3. Infrared Spectroscopy Analysis. Measurements by infrared spectroscopy were performed on the soluble and insoluble fractions of SA90 and SA98 samples, as well as on acid treated SA90. The sample for soluble fraction spectroscopy was produced as follows. The fine powder (a few milligrams) collected from the PAMPRE setup was put into a polypropylene microtube. Then 1 mL of methanol per mg of tholins was added, and the sample was sonicated for 30 min and centrifugated for 15 min at 800*g*. The slightly colored soluble fraction was then collected and deposited onto a BaF_2 window, by repeated sequences of droplets deposition and methanol evaporation. The pure sample, as well as the dried powder containing the insoluble fraction were also deposited and crushed between two BaF_2 windows. The final thin film samples were dried at ambient temperature under a low pressure of about 550 mbar for at least 2 h to evaporate the remnant methanol from the samples (soluble and insoluble). Measurements were performed with a micro-FTIR infrared microscope HYPERION3000 (Bruker Inc.) in the spectral range 4000−700 cm^{-1} with 4 cm^{-1} spectral resolution.

2.4. Mass Spectrometry: APPI. In this set of experiments, the samples were ionized by the atmospheric pressure photoionization (APPI) technique and analyzed by a hybrid quadrupole-time-of-flight mass spectrometer (Q-star pulsar *i* from Applied Biosystems) with a resolution of 0.15 u in the full mass range (from 50 to 1000 u). The photoionization of soluble fractions took place in the Photospray source (Applied Biosystems) fitted with a Krypton PKS 106 lamp that generates mainly 10.6 eV photons.

The extraction procedure was carried out on both SA98 and SA90 samples. First, 10 mg of tholins was dissolved in 10 mL of solvent (methanol or toluene). Each sample was stirred vigorously with a vortex for 1 h at room temperature and then filtered through a 0.2 μm Teflon membrane.

The extracted samples were injected into the mass spectrometer by the flow-injection analysis (FIA) method: 20 μL of solutions was loaded into an injection loop and next eluted with the base solvent at a flow rate of 200 μL min^{-1} for methanol and 150 μL min^{-1} for toluene. Toluene was used as dopant at 15 μL min^{-1} in methanol extracts. Operating

TABLE 1: Tholins Solubility (mg mL^{-1}) Obtained after Partial Dissolution of a Known Amount of Tholins in a Given Amount of Solvent[a]

	Coll et al.[8]	Sarker et al.[16]	this work	McKay[15]
operating conditions	2% CH_{42}	2%	2%	10% CH_4, 1150 mb
C/N ratio	2.8	1.8	2.3	5.5
solubility in	ND			
water		4.4	0.20	0.5
methanol	ND	ND	0.30	0.5
acetonitrile	4	ND	0.43	ND

[a] For each sample, the ratio of C/N retrieved from elementary analysis is indicated. ND: no data available.

parameters were heating temperature = 400 °C, ion source voltage = +1500 V or −1200 V, declustering potential = +10 V or −10 V, focusing potential = +40 V or −50 V (positive or negative potentials were adjusted to produce optimum flux of either positively or negatively charged ions, respectively). Tandem mass spectrometry experiments in negative ion mode were carried out with nitrogen as collision gas and collision energy at −20 or −35 V.

3. Results and Discussions

3.1. Solubility Properties of Tholins in Both Polar and Nonpolar Solvents. ***Comparison with the Protocol Previously Used in Tholins Solubility Studies.*** To compare the solubility properties of PAMPRE tholins with the already published literature, we first followed the protocol described in McKay,[15] which can be summarized into four steps: (i) mixing of a known quantity of tholins into a known amount of solvent; (ii) filtration of the cloudy solution; (iii) evaporation of the solvent; (iv) measurement of the mass of the remaining solid material. This method is the standard method to measure the solubility for a pure material as it usually refers to the concentration of the substance in a liquid that has reached equilibrium with the substance in solid phase (e.g., adding more solid no longer increases the concentration in the liquid phase, it just increases the solid's phase volume).

To do so, we measured with 10^{-2} mg precision, a well-defined amount of SA98 tholins (about 10 mg) and added 10 mL of solvent (methanol or toluene). The solution was then stirred vigorously with a vortex for 1 h at room temperature. The resulting cloudy mixture was filtered through a calibrated 0.2 μm Teflon membrane, known to be able to retain all solid material.[14] To measure the partitioning between insoluble fraction and soluble fraction, the solvent was removed from both fractions using a vacuum rotavapor. This operation was done at 30 °C to avoid tholin thermal degradation. The solid dry material was then weighted.

Table 1 presents a summary of the results and their comparison with those of McKay et al.,[15] Coll et al.,[8] and Sarker et al.[16] The conditions of tholin production in these studies are summarized in Table 2. In all these studies, solubility was supposedly achieved by a partial dissolution of the tholins samples in a given solvent.

The solubility found by McKay et al. has to be considered separately because in that case tholins were produced under very specific conditions: 10% of methane, and at a pressure slightly above atmospheric pressure. Their samples hence are specific because they contain much more carbon (C/N = 5.5) than the tholins analyzed in the other studies.

A surprising result is the low solubility in polar solvents of the PAMPRE tholins in comparison with the tholins produced by Coll et al.[8] and by Sarker et al.[16] (about 10 times less soluble). Indeed, the samples were produced almost in the same operating conditions (see Table 2): low pressure, about 2% CH_4 in the gaseous mixture and a gas residence time of a fraction of second. Moreover, the elemental compositions of the three tholins are quite similar: C/N = 2.3 for the PAMPRE samples, C/N = 2.8 for the tholins of Coll et al., C/N = 1.8 for the tholins of Sarker et al., suggesting the development of a similar chemistry within the plasma. This result allows us to realize that the so-called "solubility" used in the previous studies may not be a good indicator of the solubility properties for tholins. Indeed, these are nonhomogeneous solids, containing a huge amount of different compounds (as to be shown below by the APPI-TOF analysis, and as was shown by Sarker et al.[16]). Each one has its own solubility and according to the broad mass distribution observed by APPI-TOF analysis, a number of molecules may be still completely soluble in the used volume of solvent, whereas larger molecules may be at the saturation equilibrium since the very first microliter of solvent.

TABLE 2: Comparison of Plasma Reactors Operating Conditions for Tholins Production

experimental device	PAMPRE (this work)	Coll et al.[8]	Sarker et al.[16]
frequency	13.6 MHz	DC	60 Hz (mains)
length of the plasma path (mm)	45	250 + 250	450
diameter (mm)	138	18 and 9	supposed 10 or 18
pressure (mbar)	1	2	10
gas flow (sccm)	55	83	100
temperature (K)	ambiant	≈100−150	195
CH_4/N_2 (%)	2 and 10	2	0.5 to 8
gas residence time into the plasma (s)	≈0.7	≈0.3	≈0.3 or 1

Tholins can be compared with polymers.[19] The solubility of polymers and its measurement have been described by the Flory−Huggins theory in the early 40s.[20−23] This approach has also been followed by Raulin[24] for Titan. Three different cases are reported: (i) the polymer and solvent are totally immiscible over the entire composition range and will coexist as two distinct phases; (ii) the polymer and solvent are totally miscible, (iii) the polymer and solvent are partially miscible and a solution that contains such a polymer will separate into two phases containing different compositions of both components. In this case, phase equilibrium is hardly guaranteed, and quantitative evaluation is difficult. In the case of tholins, we are facing the third type of situation.

To confirm this hypothesis for our samples, we checked that a higher "solubility" could be obtained with the same tholins by adding systematically a supplementary amount of solid in a supposedly saturated solution (coexistence of solid and solution), showing that no stable value of solubility was reached with such a protocol for tholins.

We therefore extended the previous protocol to approach a satisfactory quantity to describe the solubility of the PAMPRE tholins. This was done in one polar and one nonpolar solvent.

Solubility Ratio and Average Solubility of the Soluble Part of PAMPRE Tholins. We propose that a better criterion to characterize and intercompare the solubility of the samples is (i) first to quantify the solubility ratio of the samples, i.e., the ratio between insoluble nucleus and soluble molecules, and (ii) quantify an average solubility of the soluble part itself, i.e., the maximum equilibrium concentration for the soluble material. The results are reported in Table 3 and illustrated in the case of SA90 in methanol in Figure 1.

(i) Solubility Ratio. Increasing concentrations of raw tholins in methanol were tested (up to 8 mg mL^{-1}) according to the

TABLE 3: PAMPRE Tholins Solubility Ratio and Average Solubility of the Soluble Fraction in Methanol and Toluene[a]

	solubility ratio (%)		average solubility (mg mL^{-1})	
solvent	SA98	SA90	SA98	SA90
methanol	19 ± 6	35 ± 5	2.5 ± 0.2	6.2 ± 0.6
toluene	3	5	ND	ND

[a] In the case of methanol extraction, measurements were repeated three or four times for solubility ratio determinations and twice for average-solubility determinations (reported uncertainty corresponds to the standard deviation). In the case of the toluene extraction, the low solubility of the samples and the viscosity of the solvent led to a difficult separation between the soluble and the insoluble fractions. The uncertainty on this determination is large for toluene and the protocol was not repeated more than once in this case.

protocol described above. Both insoluble and soluble fractions were retrieved. This allowed quantifying a mass ratio between the soluble mass and the total mass of the original sample.

A large mass ratio was found in methanol: 19 and 35% for SA98 and SA90, respectively, whereas the soluble fraction in toluene is only on the order of 3−5% of the total mass for both samples SA98 and SA90. The latter is hence close to the uncertainty on the values. This confirms the trend noticed by Coll et al. and McKay et al.[8,15] concerning the large affinity of tholins with polar solvents and a much lower one with nonpolar solvents. Following this, and according to the rule of thumb that "like dissolves like", tholins have a large content of polar molecules and, the fraction of nonpolar molecules is probably very limited, if it exists at all.

(ii) Average Solubility of the Soluble Fraction. A second step allowed us to determine the average solubility at saturation of the solution in methanol ("average" again because there is no guarantee that the soluble fraction is homogeneous; the so-called solubility refers here to the total concentration of all soluble compounds included in the tholins and not the concentration of a pure compound). The dried soluble fraction was partially dissolved in a limited amount of solvent to observe the coexistence of both a precipitate and a colored solution. The resulting mixture was filtered and the soluble part was then evaporated and weighted. Solubility at saturation was thus determined at 6.2 mg mL^{-1} for the SA90 sample and at 2.5 mg mL^{-1} for the SA98 sample.

Even in a polar solvent like methanol, most of the organic matter remains insoluble (65% for SA90 and 81% for SA98). The reason for such an amount of nonsoluble fraction within PAMPRE tholins comes likely from the growth process occurring in the plasma discharge. It seems that plasma processes using levitation allow the production of species containing long molecules, which are no longer soluble in any solvent. Hence tholins produced in PAMPRE consist in a limited fraction of polar molecules readily removable attached to a large and insoluble nucleus.

3.2. Analysis of the Remaining Insoluble Fraction by SEM (Scanning Electron Microscopy). The analysis by SEM of the integer samples SA98 and SA90 has been described in Hadamcik et al.,[18] showing a distribution of globally spherical grains, more or less regular, isolated or coalescent. In the same plasma conditions as the ones used for tholins production in the present work, a mean grain diameter of 315 ± 185 nm with diameters reaching 1400 nm for the largest detected grains has been measured for the SA98 sample, and a mean grain diameter of 595 ± 390 nm with diameters reaching 2500 nm for the largest detected grains for the SA90 sample (the uncertainty reported here is the half-maximum width of the Gaussian size grain distributions). More than one thousand grain diameters are measured on SEM images to obtain a good statistic of the size distributions. Each grain seems to be an aggregate with an apparent radial structure. The SA90 sample grains seem to be more porous than the grains of SA98.

After extraction and recovery of the insoluble fraction, as described in the previous section, a new snapshot of the samples was taken by SEM. The shape of the tholins is not modified by the previous liquid extraction and the sample shows again a Gaussian size distribution of spherical grains. Figure 2 shows some examples of the bulk tholins and their insoluble part. The surface appearance of the grains seems to be protected from the extraction process. The characteristic cauliflower feature of SA98 surface is, for example, also observable on the insoluble remaining grains. The average diameter of the grains is possibly reduced in comparison with the bulk sample: 290 nm instead of 315 nm for SA98 and 450 nm instead of 595 nm for SA90. This decrease is compatible with the mass loss of SA98 but is more important for SA90. After extraction, the SA90 sample seems to present more debris due possibly to the long mechanical stirring of grains which are on average bigger and maybe more fragile in SA90 than in SA98. The important size decrease of the insoluble part of SA90 may thus be explained by the contribution of these small fragments. The hypothesis of superficial smaller molecules is quite probable but needs to be confirmed by improving the precision on the average diameter of the particles.

The preservation of the tholins global structure despite the application of an efficient extraction stress (35% of the organic matter has been pulled out in methanol for sample SA90 for example) is in favor of a solid structure despite its important porosity.

The high porosity of the grains is confirmed by a solvent accessibility experiment, based on an acidic hydrolysis of the SA98 sample. The SA98 powder was exposed for 1 week at room temperature to a 12 mol L^{-1} HCl liquid solution. This exposition led to the attack of the terminating −CN functional groups. IR measurements revealed that this group fully disappeared in the spectra and therefore that any part of the tholins, soluble or insoluble, could be reached by the solvent (see Figure 3). On every IR spectra, the structure appearing between 2300 and 2400 cm^{-1} is the signature of atmospheric CO_2.

3.3. Comparison of Soluble and Insoluble Fractions in Methanol by IR Spectroscopy. The spectra of soluble, insoluble, and raw samples of SA90 and SA98 are displayed in Figure 4. The spectra are divided into four regions of

TABLE 4: Main Ionic Fragments and Neutral Mass Loss Observed for a Few Main Species by Collision Induced Dissociation Tandem Analysis of Negatively Charged Ions from Tholins Soluble Fraction in Methanol

	precursor (*m/z*)	collision energy (eV)	fragments (*m/z*)											neutral mass loss (u)
SA98	93	−20	65	66										28, 27
	117	−35	65	66			90							52, 51, 27
	141	−35	65	66	88	89	90			114				76, 75, 53, 52, 51, 27
SA90	117	−35	65	66										52, 51
	134	−35	65	66				92	107	119				69, 68, 42, 27, 15
	149	−35	65	66					107		122	134		84, 85, 42, 27, 15

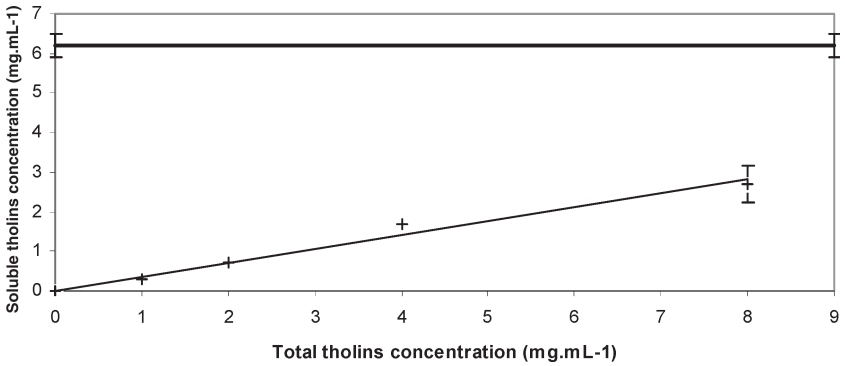

Figure 1. Determination of the soluble fraction and the average solubility of the soluble ratio for sample SA90 in methanol. The soluble ratio corresponds to the slope of the straight line. The average solubility (horizontal line) is obtained after evaporation of the solvent from the isolated soluble fraction; and resolubilization of the soluble sample in a minimum of solvent.

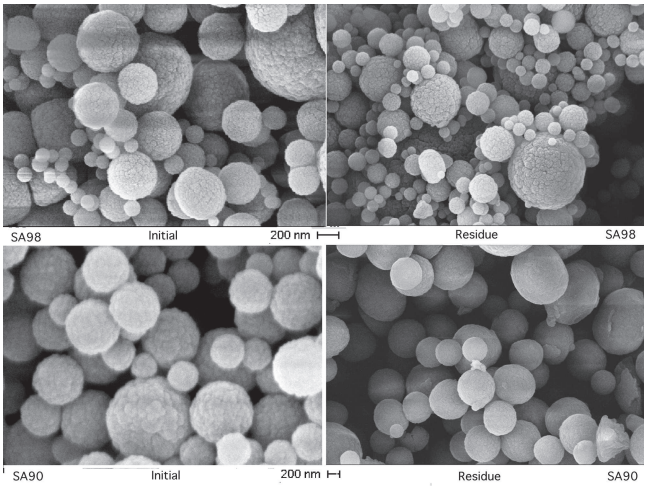

Figure 2. Electronic microscopy observations of tholins before (left) and after (right) extraction in methanol (top, SA98; bottom, SA90).

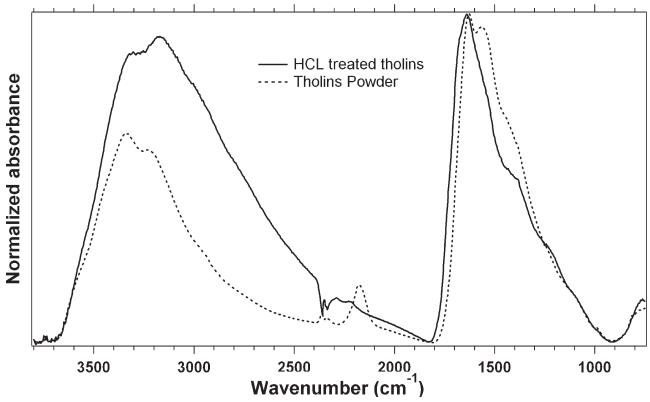

Figure 3. IR spectra of SA98 tholins before and after an HCl acid attack.

interest: region I (3000−3700 cm^{-1}), region II (2700−3000 cm^{-1}), region III (2000−2300 cm^{-1}), and region IV (900−1800 cm^{-1}).

The results are similar for SA98 and SA90. The three infrared spectra (bulk/insoluble/soluble fractions) exhibit only slight differences. Region I contains spectral features due to the symmetric and antisymmetric vibrational stretching modes of primary, and possibly secondary, amine functional groups.[25] The ratio of peak intensities of these bands is different between soluble and insoluble fractions. In region II, the intensities of the alkyl bands, with peaks at ∼2920 and ∼2960 cm^{-1} (symmetric and antisymmetric stretching modes of C−H in CH_2 and CH_3), are higher in the soluble fraction than in the insoluble one. This statement is confirmed by the more intense symmetric and antisymmetric bending modes of $-CH_2$ and $-CH_3$ peaking at 1380 and 1460 cm^{-1}, respectively (region IV). This suggests a higher content of aliphatic chains in the soluble fraction.

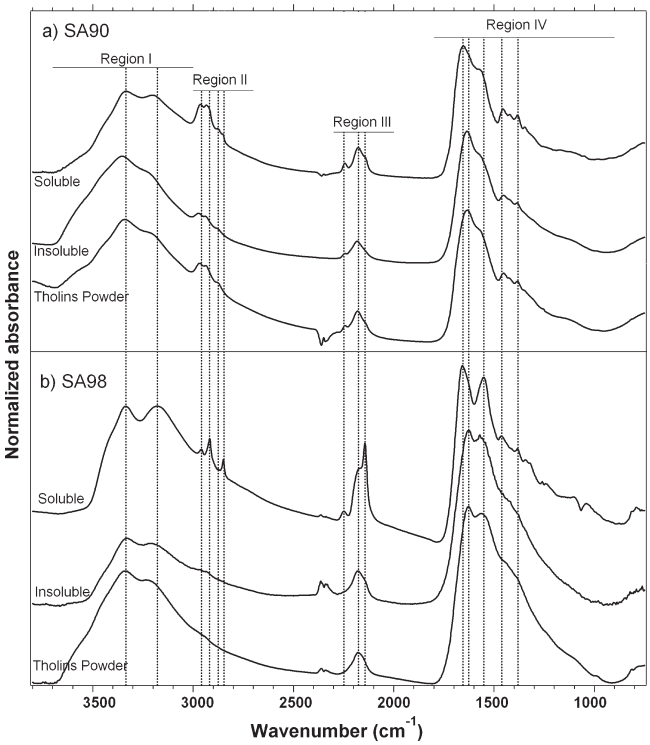

Figure 4. IR spectra of (a) the SA90 tholin and its soluble and insoluble fractions and (b) the SA98 tholin and its soluble and insoluble fractions. Band assignments are given in the text.

The broad and complex pattern at ∼2200 cm^{-1} also exhibits a slight evolution, as the weak band at 2240 cm^{-1} is more intense and better separated from the rest of the pattern in the soluble than in the insoluble fraction. This band can be confidently assigned to a cyanide functional group −CN (branched on an aliphatic group), whereas the broad structured pattern can be assigned to either conjugated nitriles and/or isocyanide. As unsaturation decreases with aliphaticity, these results would favor the former interpretation that there are fewer conjugated cyanides in the soluble fraction.

The spectral region IV exhibits spectral congestion. The broad band peaking at 1630 cm^{-1} in both the raw tholins powder and the insoluble fraction, is displaced at 1650 cm^{-1} in the spectrum of the soluble fraction. The other intense band peaks at ∼1560

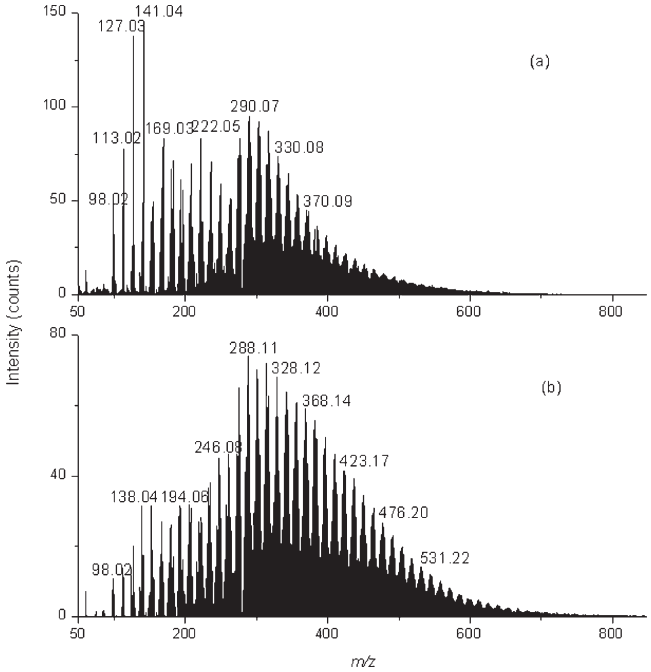

Figure 5. APPI mass spectra of tholins soluble fraction in methanol in positive ion mode: (a) SA98; (b) SA90. CH_4 inlet percentage effect on tholins composition.

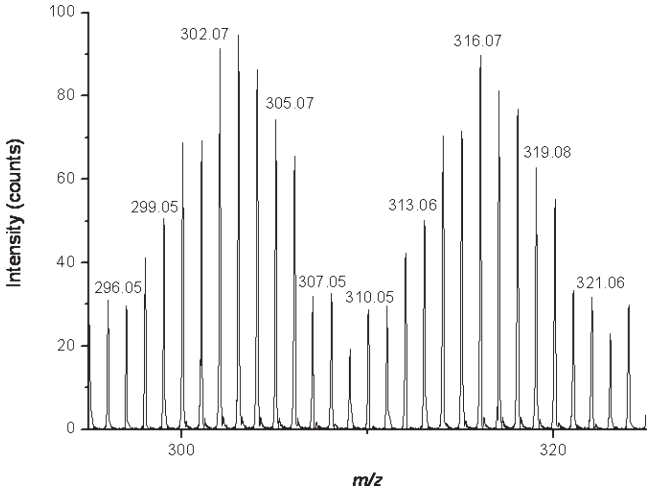

Figure 6. Enlargement of the APPI mass spectrum of sample SA98 between *m/z* 295 and 325.

cm^{-1} and shows no particular evolution in all the spectra. These bands involve the contribution of C═N groups, as imine and/or in N-bearing heteroaromatic or heterocyclic groups. Previous studies[16,26] showed that unsaturations were most probably located on nitrogen. No C═C bonds are thus expected in the IR spectra. However, the contribution of the scissors deformation of the $-NH_2$ amine group is expected to range between around 1650 and 1550 cm^{-1},[27] precluding a clear assignment of this spectral region.

To summarize this section, the infrared spectra of insoluble and soluble fractions of SA90 are very similar; the soluble fraction contains most, probably all, the functional groups that form the insoluble fraction. Hence, a study by mass spectrometry of the sole soluble fraction provides a valuable insight representative of all tholins.

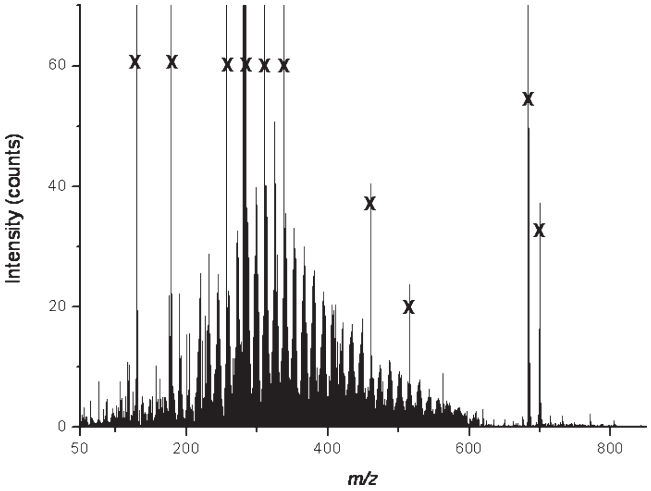

Figure 7. APPI mass spectrum of SA90 tholins soluble fraction in toluene in positive ion mode. Peaks labeled by and X are impurities also found in the blanks.

4. Analysis of the Soluble Fraction by Mass Spectrometry Analysis

4.1. Ionization Methods. The choice of the ionization method has been dictated by the aim to compare by mass spectrometry the molecular content of the soluble fractions resulting from solubilization in either methanol or toluene using the same ion source. While electrospray ionization (ESI) is not producing usable signals with nonpolar solvents such as toluene, atmospheric pressure photoionization (APPI) is.[28] APPI is a relatively recent method.[29] The technique is based on the irradiation of a heated atmospheric spray containing the solvent and the analyte molecules by EUV photons of known energy. Usually, when the solvent has an ionization potential higher than the photon energy, an additional solvent, referred to as the dopant in the following, is introduced concomitantly in the source. Direct photoionization of the solvent or photoionization of the dopant generates reactive ionic species, which can eventually ionize the analyte molecules. In the positive ion mode, this chemical ionization produces protonated molecules and radical cations upon proton transfer and charge transfer, respectively. In the negative ion mode, deprotonated molecules and radical anions can form by proton transfer, electron transfer, or electron attachment. This whole range of ionization mechanism is a further guarantee of the universal integral character of this ionization method, as it is able to reveal almost any type of analyte in the solution, independently of their chemical functionality. In this work, toluene extracts did not require any dopant, because the ionization potential of toluene is lower than the 10.6 eV photons of the lamp. For methanol extracts, there is the need to use a dopant. To allow proper comparison of the mass spectra recorded in toluene, the latter was used as a dopant.

4.2. Mass Spectra in Positive Ion Mode. Considering the solubility results, soluble fractions of both samples (SA98 and SA90) in methanol and in toluene were analyzed using APPI in the positive ionization mode.

For both SA98 and SA90 in methanol, the mass spectra show a complex spectrum (see Figure 5) containing a very large distribution of ions from $m/z = 50$ to m/z 800 (i.e., the full analysis range of the instrument), organized in regularly spaced clusters separated by 13 or 14 u. As can be seen in the spectra, the intensity of the observed features are quite different; increasing the CH_4 mixing ratio (SA90) favors the presence in the spectrum of heavier species. The spectra show peaks at every mass unit between *m/z* 100 and 800 (see a zoom between *m/z*

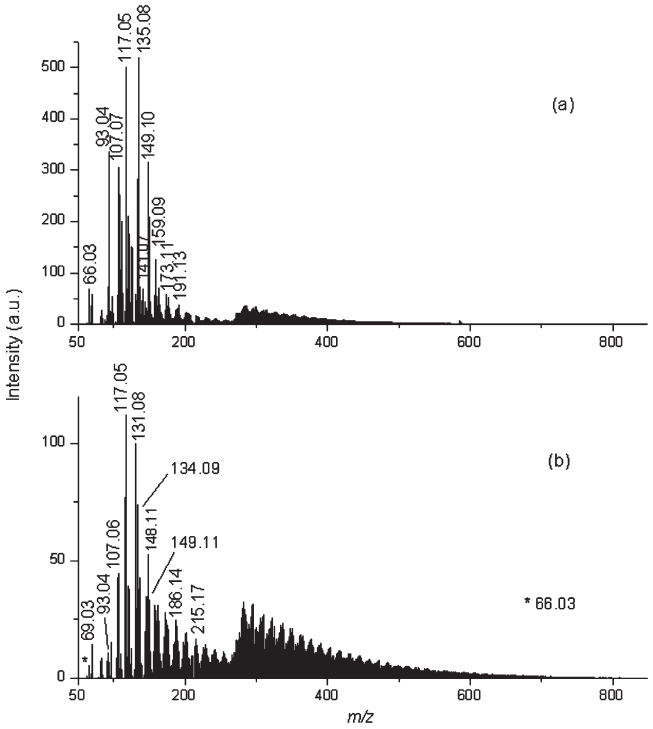

Figure 8. APPI mass spectra of tholins soluble fraction in methanol in negative ion mode: (a) SA98; (b) SA90.

295 and 325 in Figure 6). The resolving power of the time-of-flight analyzer is here insufficient to attribute unambiguously a peak to a single compound, since numerous species of same nominal mass can coexist inside each of the peaks.[16]

Similar clusters could be detected in the toluene soluble fraction (Figure 7), though at very low signal intensity. This not only confirms some very limited solubility of tholins in nonpolar solvents but also confirms a similar pattern in the extracted material in toluene and in methanol.

4.3. Negative Ionization Mode. Complementary results for methanol-extracted samples were obtained under APPI conditions in negative ionization mode. The versatility of the ion formation mechanisms upon APPI has shown to be particularly useful for the analysis of complex mixtures[30] and especially for the determination of nitrogen speciation.[31]

For both SA90 and SA98 soluble fractions, the mass spectra show a large distribution of ions from $m/z = 50$ to m/z 800, organized in regular clusters separated by 13 or 14 u (Figure 8) with a signal at each mass unit, as in positive ion mode. The irregularity in the continuum distribution observed around m/z 260 is due to an instrumental effect from the quadrupole transmission. Superimposed on this continuum, specific ions are observed at m/z 66, 93, 117, and 141 for SA98 (Figure 8a) and m/z 66, 117, 134, and 149 for SA90 (Figure 8b).

Such a peak distribution as observed in Figure 8 is indicative of a polymeric structure. Collision induced dissociation (CID) tandem mass spectrometry experiments have been carried out on some selected ions from the continuum (m/z 283, 284, 285, 297, 310) and on the low mass ions (m/z 66, 93, 117, 134, 141, and 149; see Table 4). The m/z 283, 284, and 285 set was chosen randomly and the fragmentation patterns of these species will

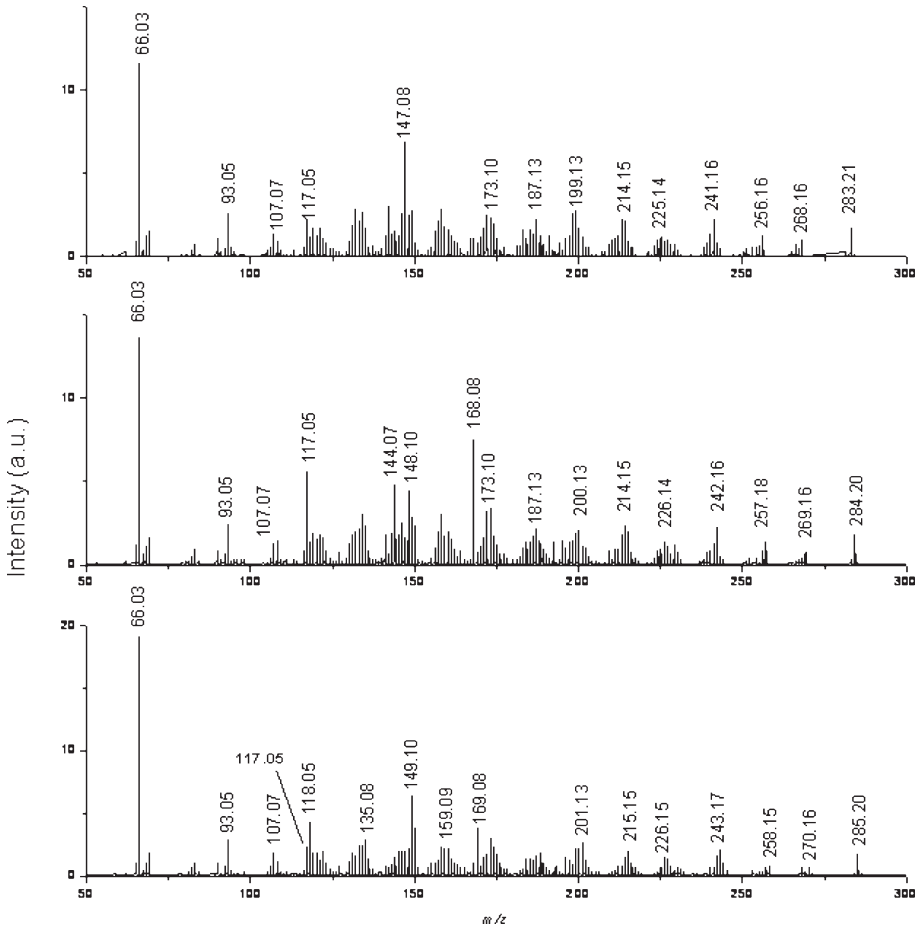

Figure 9. CID mass spectra for the peaks at m/z 283, 284, and 285 of SA98 in the negative ion mode.

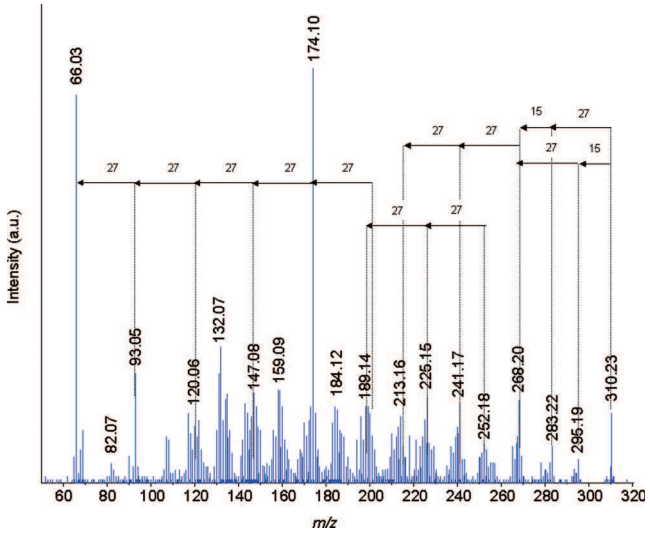

Figure 10. CID mass spectrum for the peak at *m/z* 310 of SA98 in the negative ion mode.

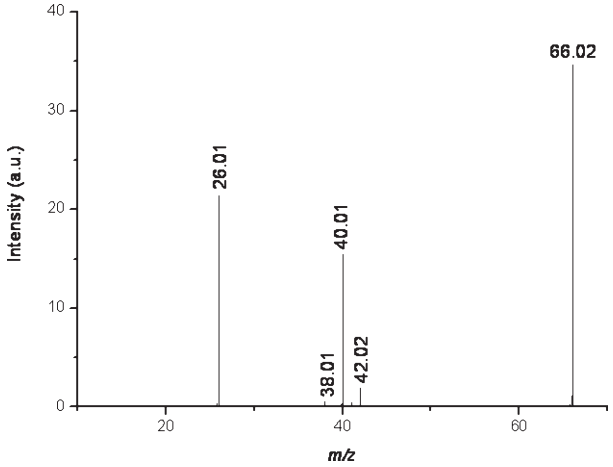

Figure 11. CID mass spectrum for the peak at *m/z* 66 of SA98 in the negative ion mode.

be analyzed by comparison. In the same trend of mind, CID of the *m/z* 310 ion will be analyzed with respect to the *m/z* 283 ion.

Figure 9 compares the MS/MS spectra obtained from the *m/z* 283, 284, 285 peaks.

These tandem mass spectra are overall very similar. The initial losses of 15, 17 and 27 u fragments, assigned respectively to neutral CH_3, NH_3, and HCN loss, appear as common features in all the spectra. This clearly indicates that the polymer chains are ended by a methyl, amine, or nitrile groups. It is noteworthy that these chemical functions have been identified by IR spectroscopy (see above). The spectra also show clusters of peaks separated by 13 or 14 u, similarly to full MS observations. Interestingly, several series of peaks connected together by 27 units may be found in the spectra. For example, in the CID spectra of the *m/z* 283 and 174 species we can find the following sequences:

$$283 \xrightarrow{-15} 268 \xrightarrow{-27} 241 \xrightarrow{-27} 214 \xrightarrow{-27} 187$$

$$174 \xrightarrow{-27} 147 \xrightarrow{-27} 120 \xrightarrow{-27} 93 \xrightarrow{-27} 66$$

In addition it is very likely that these series are enriched and complexified by intermittent incorporation of 15 u (CH_3) or 17 u (NH_3). Therefore, it seems that the soluble fraction of tholins is mostly made of associated nitrile moiety. To check this hypothesis, the *m/z* 310 ion has been analyzed by CID (see Figure 10). The higher mass fragments arise from a loss of 15 u from the precursor and from loss of 27 u to give the *m/z* 283 ion, which in turn may lose 15 to produce the *m/z* 268 species. Several series of 27 u losses may be identified in this spectrum, the most interesting one being the one connecting the *m/z* = 201 peak to the *m/z* 66 one through the base peak at *m/z* 174.

Finally, the most striking common feature of all the tandem mass spectra is the formation of an intense *m/z* 66 peak, whatever the precursor ion selected. Interestingly, the *m/z* 66, 93, 107, and 147 peaks are also observed in the full mass spectrum (see Figure 8). These species are found both in the mass spectra and in the CID spectra of all the selected compounds. This could indicate that they are sort of elementary blocks from which the polymerization might occur. Therefore, elucidation of the chemical structure of the *m/z* 66 ion, which seems to be the most fundamental of all these ions, appears especially important. The CID spectrum of the *m/z* 66 ion is displayed in Figure 11.

At the resolution of the instrument, this signal could correspond to the following formulas: $C_4H_4N^-$, $C_3H_2N_2^-$, $C_5H_6^-$ or $C_2N_3^-$. The $C_5H_6^-$ candidate may be ruled out considering the absence of nitrogen in the formula and the necessary presence of at least one unsaturation involving two carbon centers, which has been excluded by IR spectroscopy. The $C_4H_4N^-$ and $C_3H_2N_2^-$ formulas correspond to either five-member heterocyclic rings (such as pyrrole) or alkyl nitrile derivatives (such as allyl cyanide). Tandem mass spectra of the pure chemicals (pyrrole and allyl cyanide) have been recorded (in the same experimental conditions) to compare with the

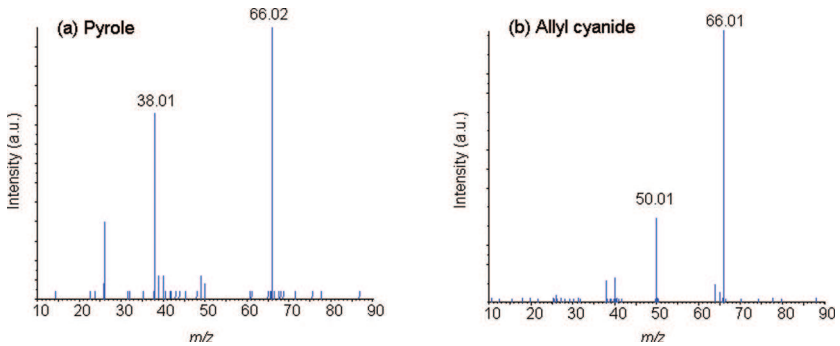

Figure 12. CID mass spectra for the $[M - H]^-$ precursors ions from pyrrole and allyl cyanide standards.

fragmentation pattern of the *m*/*z* 66 ion. As seen in Figure 12, the CID spectra of pyrrole and allyl cyanide are very different from that of the *m*/*z* 66 ion from tholins. The latter shows two main (and complementary) peaks at *m*/*z* 26 and 40, which are assigned to CN^- and CN_2^-, respectively. Therefore, the $C_2N_3^-$ formula appears to us as a good candidate. We propose the following tentative structure and suggest fragmentations as observed upon CID:

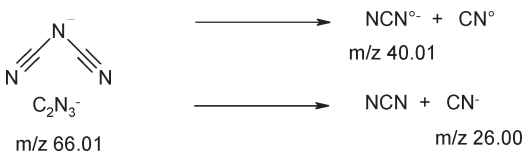

5. Conclusion

The complementary analyses performed in this work lead to a better understanding of the chemical structure of the tholins produced in the PAMPRE reactor. Both SA90 and SA98 samples are significantly soluble in the polar solvent methanol and almost nonsoluble in the nonpolar solvent toluene. Up to 35% of the organic matter was dissolved in the case of SA90 in methanol, which indicates the presence of a major insoluble fraction that constitutes the structural armature of the macroscopic material. Hence, a scanning electron microscope comparison of the samples was conducted and confirmed that almost no variation of the tholins structure took place, regardless of the removal of 35% of material as a soluble fraction in methanol. The IR transmission spectra revealed as well very similar chemical signatures for the soluble and the insoluble fractions (except an evolution of the ratio between aliphatic chains and nitrogen bearing unsaturated functions, such as cyanides). The soluble fractions in methanol and in toluene were finally scrutinized by mass spectral analysis. It highlighted complex but very organized and regular mass spectra, which are very similar in the toluene and methanol solutions, albeit very reduced in the toluene one. This final information is particularly important, as it validates the representative character of methanol extracts as probably containing the fraction of tholins that is sufficiently lightweight to be extracted, but not chemically different from the raw material. This will allow us in future to pursue our efforts in analyzing the soluble fraction. The study by mass spectrometry was pursued with the identification of a common fragmentation pattern by tandem collision induced dissociation analysis in the negative ion mode. A ubiquitous ionic fragment was found at *m*/*z* 66, attributed to the $C_2N_3^-$ pattern. The latter ion being also present as a major ion in the direct negative mass spectrum, it could possibly be an important building brick for the polymerization growth of the tholins. However the resolution of the mass spectrometer used for this study did not allow us to identify the thousands of compounds detected in the soluble fraction of the tholins. Further analysis, requesting for high resolution mass spectrometry are thus in preparation to solve this challenging question.

Acknowledgment. We acknowledge the French program for Planetology (PNP), the PRES UniverSud, the PID OPV, and the French space agency (CNES) for their financial support. We are grateful to Stephan Borensztajn (UPMC Univ Paris 06, UPR 15) for the SEM FEG images.

References and Notes

(1) Coustenis, A.; Achterberg, R. K.; Conrath, B. J.; Jennings, D. E.; Marten, A.; Gautier, D.; Nixon, C. A.; Flasar, F. M.; Teanby, N. A.; Bézard, B.; Samuelson, R. E.; Carlson, R. C.; Lellouch, E.; Bjoraker, G. L.; Romani, P. N.; Taylor, F. W.; Irwin, P. G. J.; Fouchet, T.; Hubert, A.; Orton, G. S.; Kunde, V. G.; Vinatier, S.; Mondellini, J.; Abbas, M. M.; Courtin, R. *Icarus* **2007**, *189*, 35.

(2) Cui, J.; Yelle, R. V.; Vuitton, V.; Waite, J. H., Jr.; Kasprzak, W. T.; Gell, D. A.; Niemann, H. B.; Müller-Wodarg, I. C. F.; Borggren, N.; Fletcher, G. G.; Patrick, E. L.; Raaen, E.; Magee, B. A. *Icarus* **2009**, *200*, 581.

(3) McKay, C. P.; Pollack, J. B.; Courtin, R. *Icarus* **1989**, *80*, 23.

(4) McKay, C. P.; Pollack, J. B.; Courtin, R. *Science* **1991**, *253*, 1 I I8.

(5) Israel, G.; Szopa, C.; Raulin, F.; Cabane, M.; Niemann, H. B.; Atreya, S. K.; Bauer, S. J.; Brun, J.-F.; Chassefière, E.; Coll, P.; Condé, E.; CosciaD. Hauchecorne, A.; Millian, P.; Nguyen, M.-J.; Owen, T.; Riedler, W.; Samuelson, R. E.; Siguier, J.-M.; Steller, M. R. S.; Vidal-Madjar C. *Nature* **2005**, *438*.

(6) Bernard, J.-M.; Coll, P.; Coustenis, A.; Raulin, F. *Planet. Space Sci.* **2003**, *51*, 1003.

(7) Cernogora, G.; Boufendi, L.; Coll, P. *Int. Symp. Plasma Chem. Proc.* **2001**, *4*, 2717.

(8) Coll, P.; Coscia, D.; Smith, N.; Gazeau, M. C.; Ramirez, S. I.; Cernogora, G.; Israel, G.; Raulin, F. *Planet. Space Sci.* **1999**, *47*, 1331.

(9) Imanaka, H.; Khare, B. N.; Elsila, J. E.; Bakes, E. L. O.; McKay, C. P.; Cruikshank, D. P.; Sugita, S.; Matsui, T.; Zare, R. N. *Icarus* **2004**, *168*, 344.

(10) Navarro-González, R.; Ramírez, S. I.; de la Rosa, J. P.; Coll, P.; Raulin, F. *Adv. Space Res.* **2001**, *27*, 271.

(11) Sagan, C.; Khare, B. N. *Nature* **1979**, *277*, 102.

(12) Sagan, C.; Thompson, W. R. *Icarus* **1984**, *59*, 133.

(13) Vanssay, E.; Gazeau, M.-C.; Guillemin, J. C.; Raulin, F. *Planet. Space Sci.* **1995**, *43*, 25.

(14) Szopa, C.; Cernogora, G.; Boufendi, L.; Correia, J.-J.; Coll, P. *Planet. Space Sci.* **2006**, *54*, 394.

(15) McKay, C. P. *Planet. Space Sci.* **1996**, *44*, 741.

(16) Sarker, N.; Somogyi, A.; Lunine, J. I.; Smith, M. A. *Astrobiology* **2003**, *3*, 719.

(17) Niemann, H. B.; Atreya, S. K.; Bauer, S. J.; Carignan, G. R.; Demick, J. E.; Frost, R. L.; Gautier, D.; Haberman, J. A.; Harpold, D. N.; Hunten, D. M.; Israel, G.; Lunine, J. I.; Kasprzak, W. T.; Owen, T. C.; Paulkovich, M.; Raulin, F.; Raaen, E.; Way, S. H. *Nature* **2005**, *438*, 779.

(18) Hadamcik, E.; Renard, J.-B.; Alcouffe, G.; Cernogora, G.; Levasseur-Regourd, A.-C.; Szopa, C. *Planet. Space Sci.* 2009. in press.

(19) Somogyi, A.; Oh, C.-H.; Smith, M. A.; Lunine, J. I. *Am. Soc. Mass Spectrom.* **2005**, *16*, 850.

(20) Flory, P. J. *J. Chem. Phys.* **1941**, *9*, 660.

(21) Flory, P. J. *J. Chem. Phys.* **1942**, *10*, 51.

(22) Huggins, M. L. *J. Chem. Phys.* **1941**, *9*, 440.

(23) Huggins, M. L. *J. Am. Chem. Soc.* **1942**, *64*, 1712.

(24) Raulin, F. *Adv. Space Res.* **1987**, *7*, 71.

(25) Quirico, E.; Montagnac, G.; Lees, V.; McMillan, P. F.; Szopa, C.; Cernogora, G.; Rouzaud, J.-N.; Simon, P.; Bernard, J.-M.; Coll, P.; Fray, N.; Minard, R. D.; Raulin, F.; Reynard, B.; Schmitt, B. *Icarus* **2008**, *198*, 218.

(26) Derenne, S.; Quirico, E.; Szopa, C.; Cernogora, G.; Schmidt, B.; Less, V.; McMillan, P. F. 39th Lunar and Planetary Science Conference, (Lunar and Planetary Science XXXIX), held March 10−14, 2008 in League City, Texas. LPI -Contribution No. 13912008.

(27) Rodil, S. E.; Ferrari, A. C.; Robertson, J.; Milne, W. I. *J. Appl. Phys.* **2001**, *89*, 5425.

(28) Robb, D.; Blades, M. W. *Anal. Chim. Acta* **2008**, *627*, 34.

(29) Robb, D. B.; Covey, T. R.; Bruins, A. P. *Anal. Chem.* **2000**, *72*, 3653.

(30) Mopper, K.; Stubbins, A.; Ritchie, J. D.; Bialk, H. M.; Hatcher, P. G. *Chem. Rev.* **2007**, *107*, 419.

(31) Purcell, J. M.; Rodgers, R. P.; Hendrickson, C. L.; Marshall, A. G. *J. Am. Soc. Mass Spectrom.* **2007**, *18*, 1265.

JP904735Q

J Atmos Chem (2007) 56:33–55
DOI 10.1007/s10874-006-9041-y

Simulation Chamber Studies of the Atmospheric Oxidation of 2-Methyl-3-Buten-2-ol: Reaction with Hydroxyl Radicals and Ozone Under a Variety of Conditions

N. Carrasco · J. F. Doussin · M. O'Connor · J. C. Wenger · B. Picquet-Varrault · R. Durand-Jolibois · P. Carlier

Received: 9 December 2004 / Accepted: 1 August 2006 /
Published online: 3 November 2006

Abstract This article presents a complete study of the diurnal chemical reactivity of the biogenic volatile organic compound (BVOC), 2-methyl-3-buten-2-ol (MBO) in the troposphere. Reactions of MBO with OH and with ozone were studied to analyse the respective parts of both processes in the global budget of MBO atmospheric reactivity. They were investigated under controlled conditions for pressure (atmospheric pressure) and temperature (298±2 K) using three complementary European simulation chambers. Reaction with OH radicals was studied in the presence of and in the absence of NO_x. The kinetic study was carried out by relative rate study using isoprene as a reference. The rate constant found for this reaction was $k_{MBO+OH} = (5.6 \pm 0.6) \times 10^{-11}$ molecule^{-1} cm^3 s^{-1}. FTIR spectroscopy, DNPH- and PFBHA-derivatisation analyses were performed for reactions with both OH radicals and ozone. In both reactions, the hydroxycarbonyl compound, 2-hydroxy-2-methylpropanal (HMPr) was positively identified and quantified, with a yield of $R_{HMPr} = 0.31 \pm 0.11$ in the reaction with OH, and a yield of $R_{HMPr} = 0.43 \pm 0.12$ and 0.84±0.08 in the reaction with ozone under dry (HR<1%) and humid conditions (HR=20%–30%). A primary production of two other carbonyl compounds, acetone $R_{acetone} = 0.39 \pm 0.22$, and formaldehyde $R_{HCHO} = 0.44 \pm 0.05$ was found in the case of the dry ozonolysis experiments. Under humid conditions, only formaldehyde was co-produced with HMPr as a primary carbonyl compound, with a yield of $R_{HCHO} = 0.55 \pm 0.03$. For the reaction with OH, three other carbonyl compounds were detected, acetone $R_{acetone} = 0.67 \pm 0.05$, formaldehyde $R_{HCHO} = 0.33 \pm 0.08$ and glycolaldehyde $R_{glycolaldehyde} = 0.78 \pm 0.20$. In addition some realistic photo-oxidation experiments were performed to understand in an overall way the transformations of MBO in the atmosphere. The realistic photo-oxidation experiments were conducted in the EUPHORE

N. Carrasco (✉) · J. F. Doussin · B. Picquet-Varrault · R. Durand-Jolibois · P. Carlier
LISA, Université Paris 12, 61 avenue du Général de Gaulle, 94010 Créteil Cedex, France
e-mail: carrasco@lisa.univ-paris12.fr

M. O'Connor · J. C. Wenger
Department of Chemistry and Environmental Research Institute, University College Cork, Cork, Ireland

outdoor simulation chamber. It was found that this compound is a weak secondary aerosol producer (less than 1% of the carbon balance). But it was confirmed that it is a potentially significant source of acetone, Δ[Acetone]/Δ[MBO]=0.45. With our experimental conditions ([MBO]$_0$=200 ppb, [NO]o=50 ppb), an ozone yield of $\Delta[O_3]/\Delta$[MBO]=1.05 was found.

Key words biogenic · hydroxyl radicals · 2-methyl-3-buten-2-ol · ozonolysis · photo-oxidation

1 Introduction

Biogenic volatile organic compounds (BVOCs), emitted by terrestrial and marine sources, account for around 90% of the global hydrocarbon emissions into Earth's atmosphere (Wayne 2000). Several thousand different BVOCs have been identified, including isoprene, the monoterpenes and sesquiterpenes, and some more recently detected oxygenated compounds such as 2-methyl-3-buten-2-ol (MBO) (Goldan et al. 1993). The world-wide emission rate of non-methane BVOCs is estimated to be 1,150 TgC year^{-1} (Guenther et al. 1995) and of the estimated 84 TgC year^{-1} of BVOCs emitted in the US, 30% are due to isoprene, 25% are due to terpenoid compounds and 40% are due to non-terpenoid compounds including MBO, which contributes 3.2 TgC year^{-1} (3.8%) (Guenther et al. 2000). Despite the apparently weak contribution of MBO to the BVOC budget in North America, several field studies report a very high abundance of MBO in the atmosphere. Goldan et al. 1993, for example, measured daytime concentrations of MBO eight times greater than those of isoprene on the mountain site of Niwot Ridge, in Colorado. It appears that MBO is probably emitted in large quantities by some specific types of trees and is therefore likely to play an important role in the chemistry of the troposphere.

The gas-phase degradation of MBO in the atmosphere can be initiated by reaction with hydroxyl (OH) radicals, nitrate radicals and ozone (Atkinson and Arey 2003). The reactions with OH radicals (Fantechi et al. 1998b; Ferronato et al. 1998; Alvarado et al. 1999; Papagni et al. 2001; Reisen et al. 2003; Imamura et al. 2004) and O_3 (Rudich et al. 1995; Grosjean and Grosjean 1995; Fantechi et al. 1998b; Alvarado et al. 1999; Klawatsch-Carrasco et al. 2004) have been reported a few times before. The major reaction products include acetone, which is of great atmospheric importance since that the photolysis of acetone is a significant source of HO_x radicals in the upper troposphere (Jaeglé et al. 2001; Jacob et al. 2002). Another major product, 2-hydroxy-2-methylpropanal (HMPr), has not been previously accurately quantified because it is not commercially available. However it has been previously synthesised and used as a standard to identify this product during field measurement campaign (Spaulding et al. 2002). In this work the reaction of MBO with OH radicals has been studied in the presence and absence of NO_x, and the reaction with O_3 has been studied under dry and humid conditions. Significant changes in the product distribution are observed under different reaction conditions, which may have important atmospheric implications. In addition, HMPr has been synthesised (Carrasco et al. 2006; Spaulding et al. 2002) and used to quantify its yield from the reactions and the possibility of secondary organic aerosol formation from the reactions of OH radicals and O_3 with MBO has also been investigated for the first time.

2 Experimental

2.1 Materials and methods

Experiments were carried out using three different atmospheric simulation chambers, at LISA (Créteil, France), CRAC (Cork, Ireland) and EUPHORE (Valencia, Spain). All three chambers have been described in detail elsewhere (Doussin et al., 1997; Thuener et al., 2004; Becker et al., 1996) and only brief details are provided here.

2.1.1 The LISA chamber

The chamber at LISA is a 0.98 m^3 cylindrical Pyrex evacuable reactor, equipped with a multiple-reflection optical system coupled to a Bomem DA8–ME FTIR spectrometer. The chamber was operated using synthetic air (80% N_2, 20% O_2) at atmospheric pressure and a temperature of 293±2 K. Between each experiment, the simulation chamber was cleaned by evacuating to a pressure of 10^{-3} mbar.

The hydroxyl radical reactions were performed using the photolysis (at 420 nm) of HONO or *n*-propyl nitrite as the radical source. Both precursors do not form compounds which are also products of the OH-initiated degradation of MBO (e.g., formaldehyde or acetone). The rate coefficient for the reaction of MBO with OH radicals was determined using the relative rate method with FTIR spectroscopy for chemical analysis. The initial reactant concentrations (in molecule cm^{-3}) were as follows: $[n-\text{propyl nitrite or HONO}] = 10 \times 10^{13}$, $[\text{MBO}] = 2.5 \times 10^{13}$. The ozone reactions were performed under dry conditions, with the relative humidity estimated to be <1%. Carbon monoxide was added as a scavenger for OH radicals. The initial reactant concentrations (in molecule cm^{-3}) were as follows: $[\text{MBO}] = 2.5 \times 10^{13}$, $[\text{O3}] = 5 \times 10^{13}$ and $[\text{CO}] = 2.5 \times 10^{17}$. During the reactions, the contents of the chamber were continuously monitored by FTIR spectroscopy using a path length of 156 m. Infrared spectra were obtained at a resolution of 0.5 cm^{-1} using a MCT detector and derived from the co-addition of 200 scans collected over 5 min.

2.1.2 The CRAC chamber

The chamber at CRAC is a cylinder made of FEP (fluorine–ethene–propene) foil (4.1 m long, 1.1 m diameter and 0.127 mm thickness) with a volume of 3.91 m^3. It is operated at 295±2 K using purified dry air at 0.1–1 mbar above atmospheric pressure. The chamber is equipped with a multiple reflection optical arrangement coupled to an FTIR spectrometer (BioRad Excalibur) for chemical analysis by *in situ* FTIR spectroscopy. The chamber is surrounded by 18 Philips TUV (40 W) lamps with an emission maximum at 254 nm and 18 Philips TL05 (40 W) lamps with an emission maximum at 360 nm. Between experiments the chamber is cleaned by flushing with the purified air at a flow rate of 0.15 $m^3\ min^{-1}$ for a minimum of 4 h.

The hydroxyl radical reactions were performed in the absence of NO using the photolysis of hydrogen peroxide (by the Philips TUV lamps) as the radical source. The initial reactant concentrations (in molecule cm^{-3}) were as follows: $[H_2O_2] = 7.5 \times 10^{13}$, $[\text{MBO}] = 2.5 \times 10^{13}$. The ozone reactions were performed under dry and humid conditions, with the relative humidity varying from 0.2% to 30%. Carbon monoxide was added as a scavenger for OH radicals. The initial reactant concentrations (in molecule cm^{-3}) were as follows: $[\text{MBO}] = 2.5 \times 10^{13}$, $[\text{O3}] = 5 \times 10^{13}$, $[\text{H2}O] = 150 - 19,500 \times 10^{13}?[H2O] = 150 - 19,500 \times 10^{13}$ and $[\text{CO}] = 2.5 \times 10^{17}$. During the reactions, the

contents of the chamber were continuously monitored by FTIR spectroscopy using a path length of (229.6±0.6) m. Infrared spectra were obtained at a resolution of 1 cm^{-1} using a narrow-band MCT detector and derived from the co-addition of 200 scans collected over 4 min. The number concentration and size distribution of aerosol particles produced during the experiments was determined by a scanning mobility particle sizer (TSI 3080) consisting of a condensation particle counter (TSI 3010) and a differential mobility analyser (TSI 3081). Particle size distributions were collected with a time resolution of 3 min.

2.1.3 The EUPHORE chamber

The EUPHORE chamber is a hemispherical reactor made of FEP foil with a volume of 204 m^3. It is operated at ambient temperature using purified dry air at 1–2 mbar above atmospheric pressure in order to stabilise the chamber against wind. To correct for the dilution of reactants and products, an inert tracer, SF_6 is added. The reactor is equipped with an FTIR spectrometer (Nicolet, Magna 550) coupled with a long-path absorption system (path length adjusted to 553.5 m) for monitoring the concentrations of gaseous reactants and products. The concentrations of O_3, NO_x and NO_y are monitored using automated analysers.

Two experiments on the reaction of OH radicals with MBO were performed in the presence of NO_x at the EUPHORE reactor in May 2003. The initial reactant concentrations (in molecule cm^{-3}) were, $[NO] = 0.06 \times 10^{13}$ and $[MBO] = 0.5 \times 10^{13}$, and $[NO] = 0.12 \times 10^{13}$ and $[MBO] = 0.5 \times 10^{13}$, for the first and second experiments, respectively. During the reactions, the contents of the chamber were continuously monitored by FTIR spectroscopy. Infrared spectra were obtained at a resolution of 1 cm^{-1} using a MCT detector and derived from the co-addition of 280 scans collected over 5 min. The number concentration and size distribution of aerosol particles produced during the experiments was determined by a scanning mobility particle sizer consisting of a condensation particle counter (TSI 3022A) and a differential mobility analyser (TSI 3081). Particle size distributions were collected with a time resolution of 3 min.

2.2 Chemical analysis

2.2.1 FTIR spectroscopy

Quantitative analysis was performed by subtraction of calibrated reference spectra of known compounds and subsequent integration of selected absorption bands for MBO and the reaction products. The Integrated Band Intensities (IBI) of spectral regions used during the subtraction procedures are given in Table I. For the indoor chamber studies, the formation yields of oxidation products were determined by simply calculating the initial slopes of the plots Δ[Product] vs. $-\Delta$[MBO]. For the EUPHORE experiments, the dilution had to be taken into account using the following method. For the reaction, MBO+OH $\rightarrow$ $Product_i$ ($\alpha_i k$), where α_i is the formation yield of $product_i$ and k is the rate coefficient and τ the measured dilution rate coefficient, formation yields were calculated as follows:

$$\frac{d[MBO]}{dt} = -\tau[MBO] - k[MBO][OH] \Rightarrow \alpha_i \frac{d[MBO]}{dt}$$

$$= -\alpha_i \tau[MBO] - \alpha_i k[MBO][OH] \frac{d[Product_i]}{dt} = -\tau[Product_i] + \alpha_i k[MBO][OH]$$

Table I IBI of the main IR absorption bands, values are given in $\log_e$

Compound	Main absorption band/cm^{-1}	IBI/$cm.molecule^{-1}$	Reference
MBO	820–1,067	$(1.43 \pm 0.03) \times 10^{-17}$	Klawatsch-Carrasco et al. (2004)
Acetone	1,260–1,150	$(1.02 \pm 0.02) \times 10^{-17}$	Picquet-Varrault et al. (2002)
Formaldehyde	3,000–2,630	$(1.33 \pm 0.06) \times 10^{-17}$	Picquet-Varrault et al. (2002)
Glycolaldehyde	3,020–2,620	$(1.87 \pm 0.17) \times 10^{-17}$	Private communication W. Mellouki, Orléans
Formic acid	1,840–1,704	$(5.91 \pm 1.15) \times 10^{-17}$	Barnes and Hjorth (2004)
	1,186–1,040	$(4.58 \pm 0.92) \times 10^{-17}$	
Formic anhydride	1,890–1,715	$(6.07 \pm 1.20) \times 10^{-17}$	Private communication I. Barnes
	1,144–853	$(8.08 \pm 2.44) \times 10^{-17}$	
HMPr	2,780–3,010	$(1.02 \pm 0.16) \times 10^{-17}$	Carrasco et al. (2006)

From these equations we obtain,

$$\alpha_{\mathrm{i}} = -\frac{\frac{\mathrm{d}[\mathrm{Product_i}]}{\mathrm{d}t} + \tau[\mathrm{Product_i}]}{\frac{\mathrm{d}[\mathrm{MBO}]}{\mathrm{d}t} + \tau[\mathrm{MBO}]}$$

τ was calculated for each experiment from the dilution rate of the tracer SF_6 and was found to be $5–7\times10^{-6}$ s^{-1}.

The errors quoted for the formation yields determined in this work represent twice the standard deviation arising from the least squares fit of the data and take into account the uncertainty in calibrations of the compounds.

2.2.2 PFBHA derivatization

During experiments performed in the CRAC chamber, carbonyl compounds were characterised by reaction with the derivatization agent, *O*-(pentafluorobenzyl)-hydroxyl amine (PFBHA) followed by GC–MS analysis (Yu et al., 1995; Destaillats et al., 2002). Air samples from the chamber were bubbled for 30 min at a flow rate of 0.13 l min^{-1} through two 10 ml glass impingers connected in series and filled with aqueous PFBHA solution (0.25 mg ml^{-1}). One drop of HCl (25%) was added to lower the solution pH to about 2. The impingers were immersed in a water–ice bath during sampling to increase the efficiency of the trapping process. Carbonyl compounds dissolved and reacted with PFBHA to form stable oximes. A column filled with KI crystals was inserted between the chamber and the sampling system to remove ozone and aerosols before the first impinger (only carbonyls in gaseous phase were trapped in PFBHA solution).

Samples were kept in the dark for approximately 16 h at room temperature to ensure complete derivatization. They were acidified with two to three drops of HCl (25%) just before the organic oximes were extracted with *n*-hexane and dried with anhydrous Na_2SO_4. One microlitre of the extract was analysed by a Varian GC–MS system (CP-3800 GC coupled to Saturn 2000 MS) using a CP–Sil8 fused silica capillary column (Varian, 30 m, 0.32 mm i.d., 0.5 μm film thickness). The injector temperature was held at 200°C until the analysis was finished. The oven temperature was programmed to maintain a temperature of 60°C for 5 min, then increased to 100°C at a rate of 4°C min^{-1}, and to 220°C at a rate of

15°C min^{-1}. The MS was operated in either EI or CI mode (using methane as the CI reagent gas) over the mass range 40 to 550.

2.2.3 DNPH-derivatization

In the EUPHORE chamber, carbonyl compounds were sampled on DNPH-cartridges for 30 min every hour with a flow of 1 l min^{-1} (Sep-Pak DNPH-Silica cartridges, plus-short body, 360 mg, by Waters). Ozone scrubber cartridges (LpDNPH ozone scrubber by Supelco) were used during sampling to avoid any artefacts caused by ozone and trapped hydrazones. The samples were eluted with 2 ml of acetonitrile (HPLC grade) distilled previously over DNPH. Twenty microliters of this elution was analysed using HPLC (HP Kayak AX Workstation) with a chromasil 100 C18 column (15 cm length, 4 mm i.d., 5 μm diam. particles) at ambient temperature, using the following mobile phase gradient profile: a flow of 1.5 ml min^{-1}, 1 min with A (60/40 H_2O/Acetonitrile), and 10 min with the linear gradient to B (40/60 H_2O/Acetonitrile) at the end.

2.3 Chemicals

Chemicals were obtained from the following sources and used without further purification; MBO (Aldrich, >98%), H_2O_2 (Aldrich, 30%), CO (BOC gases, >99%). Ozone was generated by flowing high purity O_2 through a silent discharge ozoniser (Kaufmann Umwelttechnik, GmBH, in LISA; Ozone Services GE60/M5000 in CRAC). HONO was synthesised from the dropwise addition of sulphuric acid to a diluted $NaNO_2$ solution (Taylor et al., 1980). *N*-propyl nitrite was synthesised prior to its use as described in Nash (1968) by adding diluted sulphuric acid dropwise to a mixture of propanol and $NaNO_2$.

3 Results and Discussion

In this part, results obtained in the LISA and in the CRAC are treated and compared to previous literature: the reaction of MBO with OH is studied in the presence and in the absence of NO_x and the reaction of MBO with ozone is studied in dry and in humid conditions.

3.1 Reaction of MBO with OH radicals

3.1.1 Kinetics

The rate constant for the reaction between MBO (1 ppm) and OH radicals was determined by relative rate technique (RR) using isoprene (500 ppb) as reference compound. Experiments were realised in LISA simulation chamber and concentrations were monitored by FTIR. Two different OH sources were used: OH radicals were obtained photolysing either HONO (two experiments) or *n*-propylnitrite (one experiment). Temperature and pressure were adjusted to 298±2 K and atmospheric pressure.

It was checked that both MBO and isoprene were stable in the chamber over the time scale of a typical experiment in different conditions: with light without OH radical sources, and without light with OH radical sources.

$$\begin{aligned} \text{MBO} + \text{OH} &\rightarrow \text{products } k_1 \\ \text{Isoprene} + \text{OH} &\rightarrow \text{products } k_2 \\ \text{Ln}\left([\text{MBO}]_o/[\text{MBO}]_t\right) &= k_1/k_2 \times \text{Ln}\left([\text{Isoprene}]_o/[\text{Isoprene}]_t\right) \end{aligned} \quad (1)$$

According to Equation (1), ratio k_1/k_2 is given by the slope of the plot $\text{Ln}([\text{MBO}]_o/[\text{MBO}]_t)$ vs. $\text{Ln}([\text{Isoprene}]_o/[\text{Isoprene}]_t)$ where $[\text{MBO}]_o$ and $[\text{Isoprene}]_o$ are the initial concentrations and $[\text{MBO}]_t$ and $[\text{Isoprene}]_t$ are varying concentrations during the reaction (see Figure 1). All experiments led to coherent results despite the use of two different OH sources. The uncertainty on ratio k_1/k_2 is given by the method described in Brauers and Finlayson-Pitts (1997), which takes into account errors in both [MBO] and [Isoprene] to calculate $\delta Y_{\text{MBO}}(t)$ and $\delta Y_{\text{Isoprene}}$, the errors in $Y_{\text{MBO}}(t)=\text{Ln}([\text{MBO}]_0/[\text{MBO}]_t)$ and in $Y_{\text{Isoprene}}(t)=\text{Ln}([\text{Isoprene}]_0/[\text{ Isoprene}]_t)$.

Knowing $k_2 = 1.01 \pm 0.10 \times 10^{-10}$ cm^3 molecule^{-1} s^{-1} (more recent IUPAC recommendation : IUPAC, http://www.iupac-kinetic.ch.cam.ac.uk/ (2005)) and the ratio k_1/k_2, k_1 value was deduced. Relative error on k_1 was obtained by adding relative errors on k_2 and on ratio k_1/k_2. The ratio k_1/k_2 was found equal to 0.56±0.02, giving a rate constant equal to $k_1 = (5.6 \pm 0.6) \times 10^{-11}$ cm^3 molecule^{-1} s^{-1} which was compared to previous data in Table II.

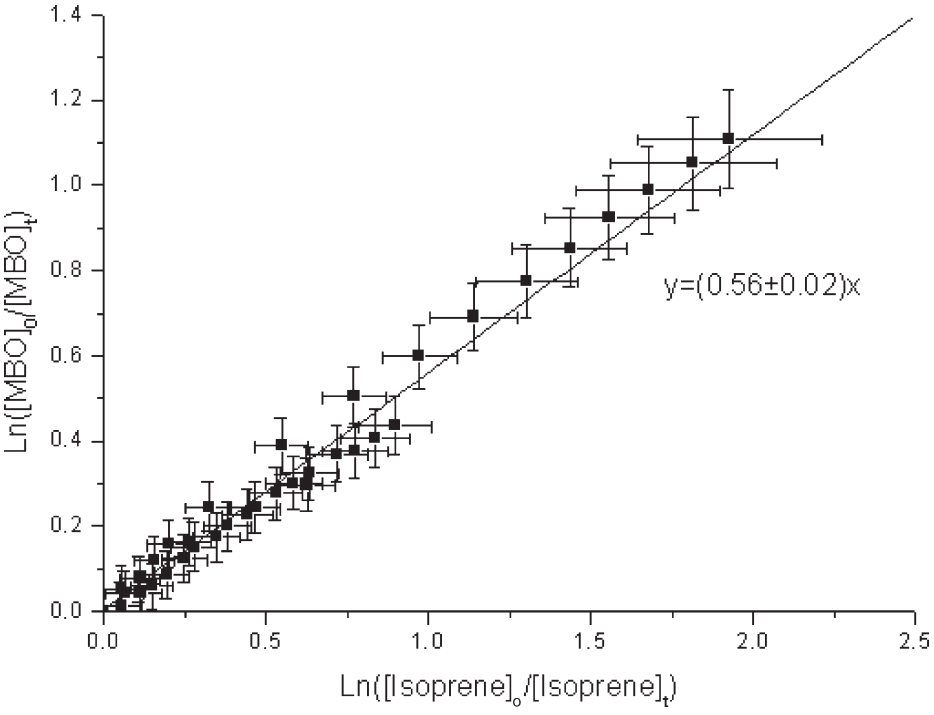

Figure 1 Relative decay of MBO *versus* Isoprene when exposed to OH radicals.

Table II Rate constant for the reaction between MBO and OH radicals – comparison with previous data

T (K)	$k_1 \times 10^{11}$ cm^3 molecule^{-1} s^{-1}	Reference	Method
298±2	5.6±0.6	This work	RR (Isoprene)
298±2	6.6±0.5	Imamura et al. (2004)	RR (*n*-butylether and propene)
296±2	5.7±0.1[a]	Papagni et al. (2001)	RR (1,3,5-trimethylbenzene)
295±1	6.4±0.5	Ferronato et al. (1998)	RR (Ethene)
	7.4±0.8		RR (Propene)
298±2	3.8±0.9	Fantechi et al. (1998a)	RR (Isoprene)
	4.3±1.8		RR (Propene)
298±1	6.4±0.6	Rudich et al. (1995)	PLP–LIF

[a] The error bar does not include the uncertainty in the rate constant for 1,3,5-trimethylbenzene.

This study is in agreement with the relative rate studies of Imamura et al., Papagni et al., and Ferronato et al., and the absolute rate study of Rudich et al., considering the error limits and despite differences in used methods. In this work, the used method is relative rate technique with isoprene as a reference at 298 K such as in the publication of Fantechi et al., However the value reported in their work is slightly lower than ours and than the other publications. Both them and us used the value of $k_{\text{Isoprene}+\text{OH}} = 1.01 \pm 0.10 \times 10^{-10}$ cm^3 molecule^{-1} s^{-1} given by Atkinson (1997). The only noticeable difference between our respective protocols was OH radical source: the group of Fantechi worked in absence of NO_x with H_2O_2 whereas we worked in presence of NO_x with HONO or *n*-propylnitrite. The energetic irradiation used to photolyse H_2O_2 may have induced an additional consuming of the reactants but no clear reason explains the lower value of Fantechi et al., in comparison to the other publications.

3.1.2 Mechanistic study of the gazeous phase

Six experiments were performed in LISA and in CRAC at 298±2 K to study the mechanism of MBO reaction with OH radicals. Different OH sources were chosen to compare MBO degradation in presence of NO_x: HONO and *n*-propylnitrite (which was chosen because its chemistry is not leading to common products with MBO (Meunier et al., 2003), in particular neither formaldehyde nor acetone), and in absence of NO_x:H_2O_2. It was checked that the mixture of MBO with the OH source was stable in the darkness and that no loss was observed before irradiation began. Four primary carbonyl compounds were

Table III Yields observed for the main carbonyl primary products in the reaction between MBO and OH radicals

Yields	Acetone	Formaldehyde	Glycolaldehyde	HMPr
n-Propylnitrite	0.67±0.08	0.45±0.06	0.83±0.17	0.33±0.11
HONO	0.66±0.04	0.35±0.03	0.66±0.10	0.27±0.06
(With NO, LISA)	0.62±0.04	0.34±0.03	0.86±0.10	0.37±0.08
	0.68±0.05	0.29±0.03	0.76±0.11	0.29±0.06
H_2O_2	0.91±0.28[a]	0.16±0.06	0.89±0.24	0.20±0.08
(Without NO, CRAC)	0.75±0.07	0.11±0.02	0.75±0.13	0.21±0.06

[a] This yield presents a large uncertainty due to the difficulty to quantify acetone by FTIR under high HR conditions. Indeed an important amount of water is co-introduced with H_2O_2.

observed and quantified, acetone, formaldehyde, glycolaldehyde and HMPr. Their respective formation yields are reported in Table III for each experiment. A typical plot of [Product] vs. −Δ[MBO], giving formation yields in the case of LISA- and CRAC-experiments, is traced on Figure 2. Yields were corrected by the secondary reactions HCHO+OH, Acetone+OH, Glycolaldehyde+OH (rate constants in IUPAC, http://www.iupac-kinetic.ch.cam.ac.uk/ 2005) and HMPr+OH (rate constant in Carrasco et al., 2006) as described in Atkinson et al., (1982). Thus formaldehyde and acetone yields increase with the extent of the reaction because of formation from HMPr+OH (Carrasco et al., 2006). Uncertainties given in the table correspond to the description made in the experimental part. Experiments with and without NO are averaged and compared to previous literature, respectively, in Table IV and in Table V.

In the presence of NO, our results are quite in good accordance with previous literature, considering their overall combined uncertainties, except for the lower production yield of HMPr found by Alvarado et al., (1999). They suspected that their procedure (derivatization/GC–FID analysis) was not 100% efficient for hydroxyl-containing compounds. Moreover, our study is the only one that presents a direct measurement of HMPr. As this compound is not commercially available, we synthesised it and calibrated its FTIR spectrum (Figure 3). Alvarado et al., (1999) attributed residual FTIR bands from O_3+MBO reaction, at around

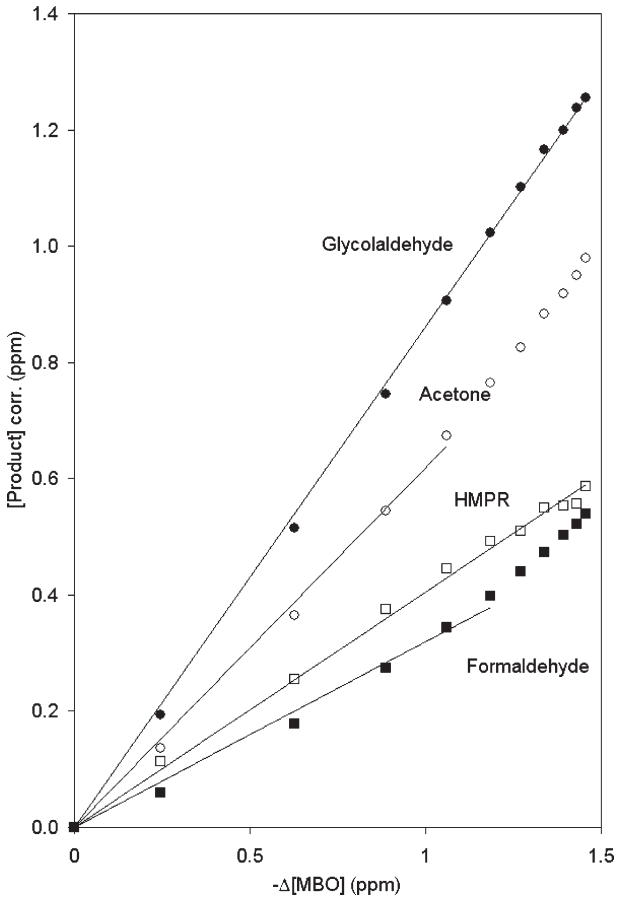

Figure 2 Formation of acetone, formaldehyde, glycolaldehyde and HMPr during a reaction between MBO and OH (coming from photolysis at 410 nm of HONO). Yields were corrected by the secondary reactions HCHO+OH, Acetone+OH, glycolaldehyde+OH (rate constants in IUPAC 2005) and HMPr+OH (rate constant in Carrasco et al., 2006) as described in Atkinson et al., (1982).

Table IV Product formation yields for the OH radicals – initiated reaction of MBO in the presence of NO_x

Product	Yields with NO_x	Reference	Technique
Acetone	0.67±0.05	This work	FTIR
	0.52±0.05	Ferronato et al. (1998)	FTIR
	0.58±0.04	Alvarado et al. (1999)	FTIR+GC
Formaldehyde	0.33±0.08	This work	FTIR
	0.35±0.04	Ferronato et al. (1998)	FTIR
	0.29±0.03	Alvarado et al. (1999)	FTIR
Glycolaldehyde	0.78±0.20	This work	FTIR
	0.50±0.05	Ferronato et al. (1998)	FTIR
	0.61±0.09	Alvarado et al. (1999)	FTIR
	0.67±0.11	Reisen et al. (2003)	SPME
HMPr	0.31±0.11	This work	FTIR
	0.19±0.07	Alvarado et al. (1999)	GC
	0.31±0.04	Reisen et al. (2003)	SPME

800, 1,150, 1,350 and 1,750 cm^{-1}, to HMPr absorption bands. These bands seem to be in good agreement with our HMPr spectrum considering the low plot resolution in their document. To quantify the HMPr production, Alvarado et al., (1999) and Reisen et al., (2003) adopted an indirect method, assuming HMPr response factor (respectively, for GC and for SPME) equal to the one of a similar compound. It must be pointed out that the approximation made in Reisen et al., (2003) leads to the same production yield than our direct measurement. Consequently, our study is the only one that uses the same technique for all the four carbonyl compounds detected. The four products observed account for 100% (within the experimental uncertainties) of the MBO reacted, so that we think that no other major compounds can be primary formed in the reaction of MBO with OH in the presence of NO.

However, Ferronato et al., (1998) and Reisen et al., (2003) suggest an additional production of hydroxynitrate because of IR absorption bands found at 1,290 or 1,670 cm^{-1} in their residual spectra. Moreover Reisen et al., (2003) observed ion peaks in their API-MS analyses indicating formation of molecular weight 165 dihydroxynitrates. These peaks were attributed to $(CH_3)_2C(OH)CH(ONO_2)CH_2OH$ and $(CH_3)_2C(OH)CH(OH)CH_2ONO_2$, coming from the RO_2+NO reactions. These products were not observed in our case. Indeed a

Table V Product formation yields for the OH radicals – initiated reaction of MBO in the absence of NO

Product	Yields without NO_x	Reference	Technique
Acetone	0.76±0.14	This work	FTIR
	0.141±0.002	Fantechi et al. (1998b)	FTIR
Formaldehyde	0.12±0.05	This work	FTIR
	0.093±0.033	Fantechi et al. (1998b)	FTIR
Glycolaldehyde	0.79±0.22	This work	FTIR
	0.280±0.028	Fantechi et al. (1998b)	FTIR
HMPr	0.21±0.07	This work	FTIR
	Detected	Fantechi et al. (1998b)	DNPH cartridges

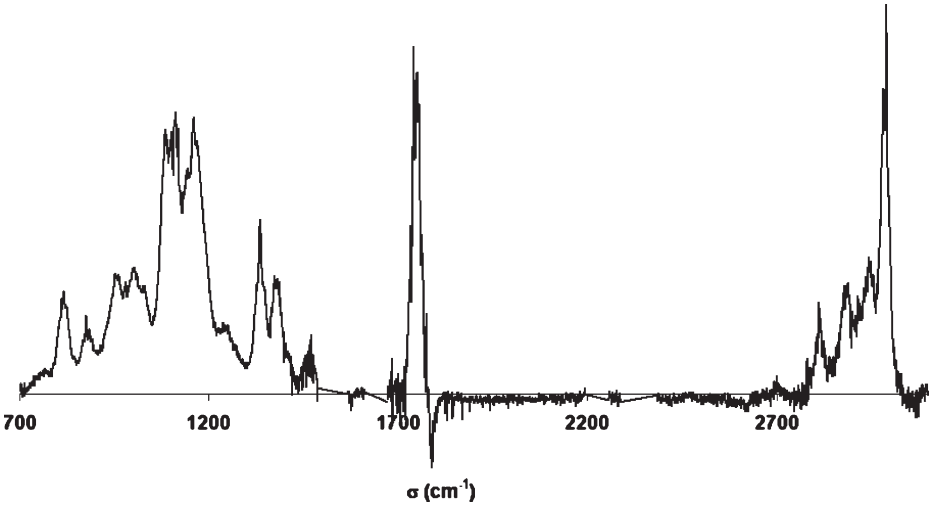

Figure 3 FTIR spectrum of HMPR between 700 and 3,000 cm^{-1}.

weak IR absorption was observed at 1,290 cm^{-1} when the OH source was *n*-propylnitrite, but this feature was not observed with HONO. The absence of the absorption band at 1,290 cm^{-1} when the OH source is HONO indicates that this absorption is rather an artefact due to the own reactivity of the nitrite than a specific product of the reaction MBO+OH.

In the absence of NO, we found higher formation yields than Fantechi et al., (1998b). Our measurements within the uncertainties are only in agreement for formaldehyde yield: R_{HCHO}=0.09, $R_{acetone}$=0.28 and $R_{glycolaldehyde}$=0.14 in the work of Fantechi et al., (1998b), vs. R_{HCHO}=0.12, $R_{acetone}$=0.79 and $R_{glycolaldehyde}$=0.76 in our case. Despite the use of the same technique, FTIR, was used yet. No clear reason can explain such a difference on acetone and glycolaldehyde yields. Fantechi et al., (1998b) detected HMPr with DNPH cartridges but could not quantified it. We found a yield of $R_{HMPr} = 0.21 \pm 0.07$ by FTIR, not inconsistent with the hypothesis that formaldehyde, $R_{HCHO} = 0.12 \pm 0.05$, and HMPr are coproduced.

A slight difference is noticeable between reactions with and without NO_x. In both case, within the uncertainties, acetone and glycolaldehyde are coproducted (as shown in Alvarado et al., (1999), and in Ferronato et al., (1998), as are formaldehyde and 2-hydroxy-2-methylpropanal., Nevertheless the yield of acetone and glycolaldehyde is around 0.65 in the presence of NO and around 0.75 in the absence of NO. Likewise the production yield of formaldehyde and 2-hydroxy-2-methylpropanal is around 0.35 in the presence of NO and around 0.15 in its absence. According to these measurements, the pathway that produces acetone and glycolaldehyde is preferred to the way that produces the two others co-products, formaldehyde and 2-hydroxy-2-methylpropanal, and this tendency increases in the absence of NO_x. This observation is in agreement with the mechanism with NO_x suggested in Rudich et al., (1995) and presented on Figure 4. Figure 5 represents a possible mechanism in the absence of NO_x. OH radical adds on the double bond C=C either on C_3 or on C_4 site, leading preferentially to the most substituted radical., HMPr and formaldehyde are common to both pathways. Therefore no more precise details such as branching ratios can be deduced from these production yields.

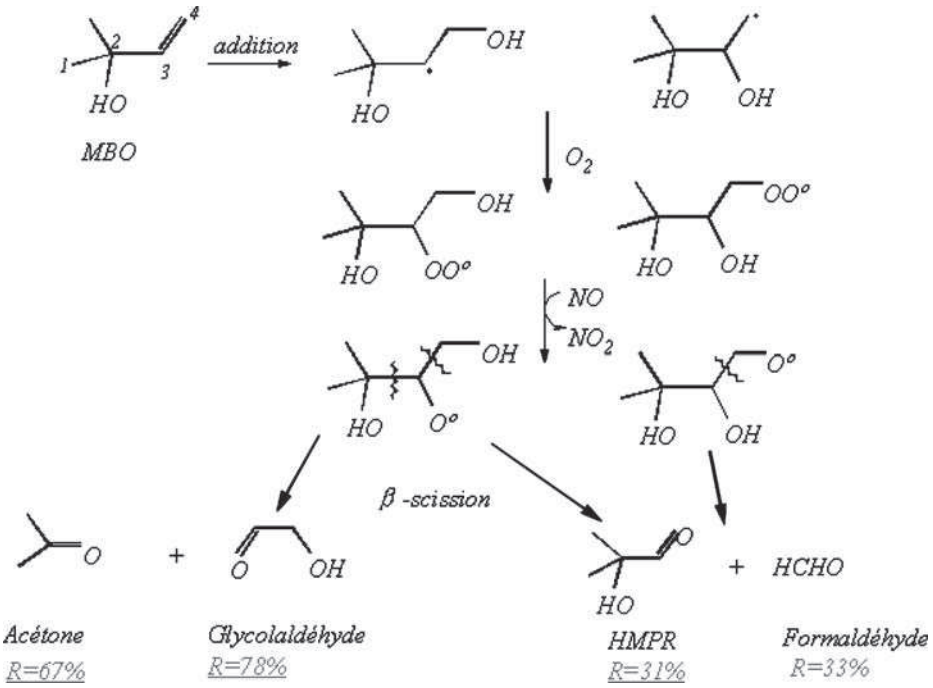

Figure 4 Oxidation scheme of MBO with OH radicals in the presence of NO_x.

3.1.3 Aerosol production

SMPS continuous sampling was proceeded in EUPHORE during experiments between MBO and OH (coming from photolysing H_2O_2). No significant secondary aerosol production was observed for this reaction.

3.2 Reaction of MBO with ozone

Absolute rate technique was employed in Klawatsch-Carrasco et al., (2004) to determine the kinetic rate constant of MBO ozonolysis. A value of $k_{O3+MBO} = (8.3 \pm 1.0) \times 10^{-18}$ cm^3 molecule^{-1} s^{-1} was found, in good agreement with the previous determinations of Grosjean and Grosjean (1994); Fantechi et al., (1998a), respectively, $k_{O3+MBO} = (10.0 \pm 0.3) \times 10^{-18}$ cm^3 molecule^{-1} s^{-1} and $k_{O3+MBO} = (8.6 \pm 2.9) \times 10^{-18}$ cm^3 molecule^{-1} s^{-1}. This work deals with the mechanistic study of the MBO+O_3 reaction. Twelve experiments of MBO ozonolysis, all in the presence of CO as OH-scavenger, were performed. Seven of them were realised in dry conditions (six in LISA and one in CRAC), and five in humid conditions (Relative Humidity between 20% and 30%, in CRAC), to study the influence of humidity on the mechanism.

3.2.1 Mechanistic study of the gazeous phase

3.2.1.1 PFBHA derivatisation: identification of Carbonyls PFBHA samples were taken in every experiment realised in the CRAC chamber to identify the carbonyl compounds formed, with the method described in the experimental part. Only three carbonyls are

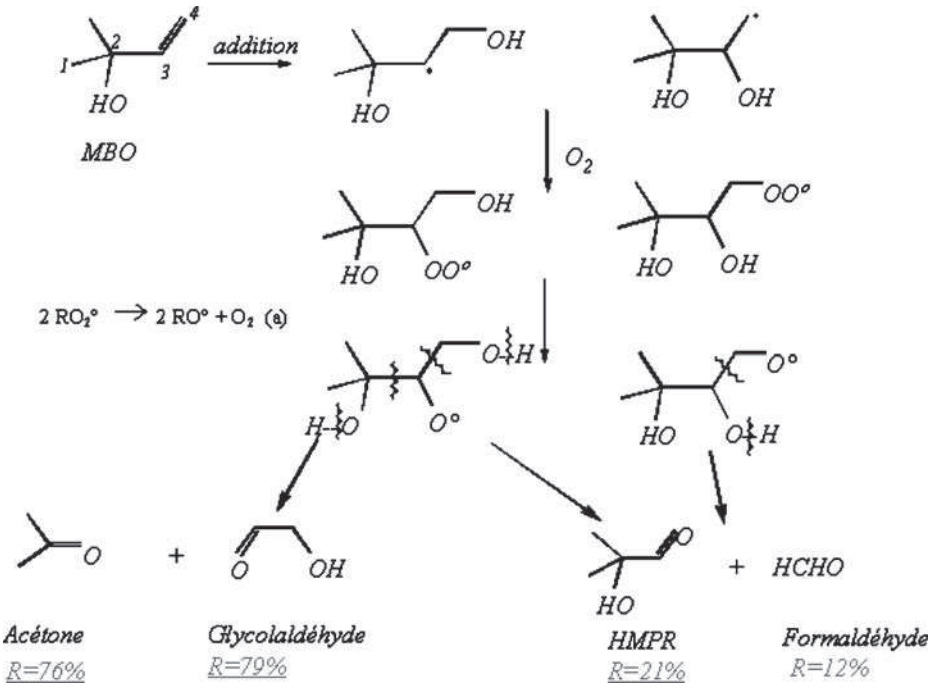

Figure 5 Oxidation scheme of MBO with OH radicals in the absence of NO_x. (a) Horie et al., (1990); Niki et al., (1982); Lightfoot et al., (1991); Wallington et al., (1989).

produced during MBO ozonolysis (see Figure 6). Formaldehyde and acetone were identified by comparison to standards in the same conditions. The third carbonyl compound has an $M+H^+$ fragment ion m/z=284. Its mass spectrum is consistent with HMPr derivative, but no standard was available when the samples were taken to confirm the time retention observed. However a very strong M-17=266 fragment ion peak indicates a probable presence of an OH group and the large m/z 59 ion peak is consistent with a typical fragment ion $(CH3)_2C^+$–OH. Reisen et al., (2003) used the same analytical

Table VI Formation yields of primary products during 12 experiments of MBO ozonolysis, seven under dry conditions and five under humid conditions

Experimental conditions	R_{HCHO}	R_{HMPR}	$R_{acetone}$	R_{HCOOH}	R_{FAN}	C-mass balance
HR=0% – LISA	0.44±0.03	0.36±0.08	0.13±0.02	0.09±0.03	0.10±0.04	0.49±0,09
HR=0% – LISA	0.53±0.04	0.51±0.10	0.41±0.03	0.15±0.03	0.21±0.10	0.83±0.13
HR=0% – LISA	0.46±0.04	0.48±0.10	0.36±0.04	0.14±0.03	0.15±0.04	0.75±0.13
HR=0% – LISA	0.38±0.04	0.44±0.08	0.60±0.04	0.12±0.06	0.22±0.06	0.78±0.12
HR=0% – LISA	0.38±0.04	0.61±0.12	0.64±0.04	0.18±0.04	0.23±0.07	1.03±0.15
HR=0% – LISA	0.45±0.04	0.38±0.10	0.40±0.03	0.12±0.03	0.17±0.05	0.69±0.12
HR=0% – CRAC	0.45±0.03	0.27±0.05	0.17±0.02	0.16±0.04	0.10±0.03	0.75±0.07
HR=20% – CRAC	0.58±0.05	0.84±0.16	–	–	–	0.79±0.14
HR=20% – CRAC	0.56±0.05	0.83±0.15	–	–	–	0.78±0.13
HR=30% – CRAC	0.55±0.04	0.88±0.16	–	–	–	0.81±0.14
HR=30% – CRAC	0.51±0.04	0.80±0.15	–	–	–	0.74±0.13
HR=30% – CRAC	0.54±0.04	0.86±0.16	–	–	–	0.80±0.14

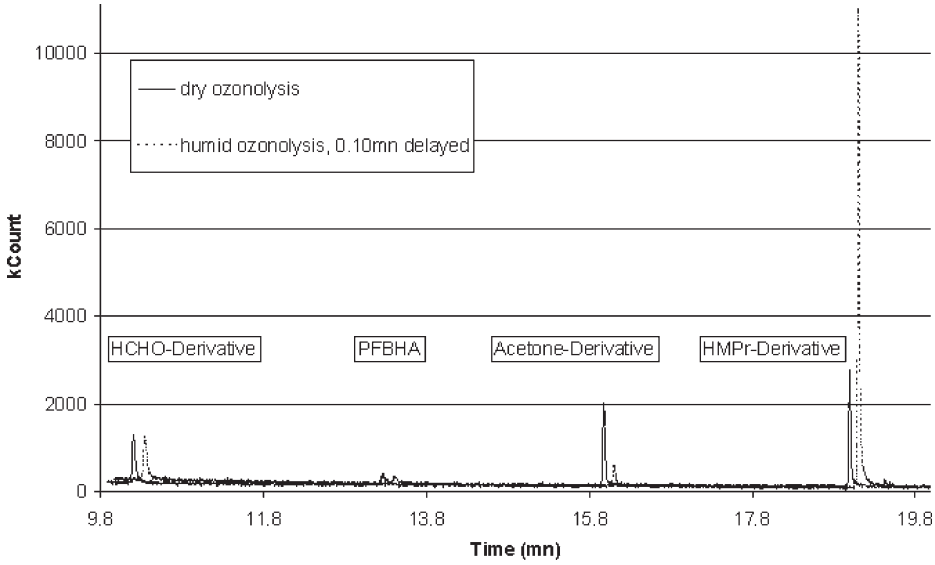

Figure 6 Chromatograms for MBO+ozone experiments in dry and in humid conditions. For a better visibility of the diagram, the plot of the humid experiment was 0.10 mn delayed.

technique in 2003 to study oxidation of MBO by OH and noticed a similar PFBHA-derivative. Typical chromatograms obtained in dry and in humid conditions are given in Figure 6. Even if the PFBHA-method is not quantitative, it is noticeable that the peak corresponding to HMPr-derivative is increasing in humid conditions compared to dry experiments, and that the acetone derivative is less important in humid than in dry conditions.

3.2.1.2 IRTF A typical plot of [Product] vs. $-\Delta$[MBO], giving formation yields in the case of LISA- and CRAC-experiments, is traced on Figure 7. Production yields of the primary products, formaldehyde, HMPr, acetone, formic acid and formic anhydride are reported for each experiment of ozonolysis in Table VI. Noticeable differences were observed between experiments in dry and in humid conditions. Primary formation of acetone, formic acid and formic anhydride is only observed in dry conditions and production yield of HMPr is very different according to the presence or not of humidity in the chamber. In both case, mass carbon balances are almost complete: 80% in humid conditions and around 75% in dry conditions. The use of CO as OH-scavenger prevented us from measuring CO and CO_2.

Previous studies reported in the literature (Alvarado et al., 1999; Fantechi et al., 1998b; Grosjean and Grosjean 1995) describe experiments essentially in dry conditions. However the Alvarado et al., (1999) experiments with GC analyses were probably carried out at (based on other reports from this group using Teflon chambers) a few percent humidity. Our formaldehyde yield is in good agreement with the work of Fantechi and Grosjean with a value around 45% but Alvarado found a value noticeably smaller. Under dry conditions, formaldehyde is coproducted with the larger Criegee intermediate and HMPr with the smaller one (see mechanism on Figure 7). This indicates that the larger Criegee Intermediate formation is not the preferred pathway during ozonolysis of MBO, on the contrary to previously studied dissymetrical Criegee intermediates (Horie and Moortgat 1991; Grosjean et al., 1994; Atkinson et al., 1995; Grosjean and Grosjean 1997, 1998). This

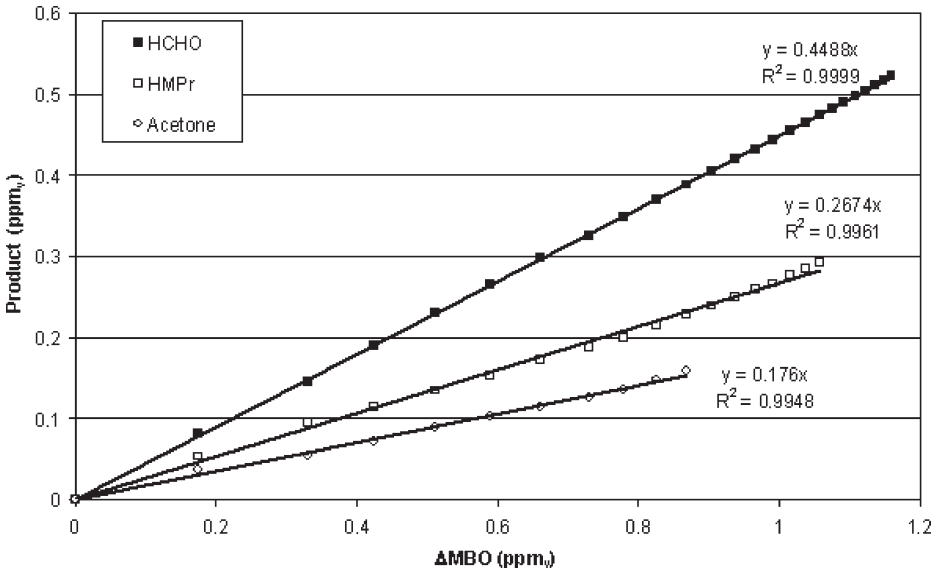

Figure 7 Formation of formaldehyde, HMPr and acetone during a reaction between MBO and ozone in dry condition.

behaviour could be due to the effect of the hydroxyl group and hence could be a common feature of the ozonolysis of α-Hydroxy-alkenes.

The three groups suspected the formation of HMPr, but this work is the first one to be able to quantify it: yields of 0.43 and 0.84 were determined in, respectively, dry and humid conditions. The higher value under humid conditions is explained by an additional primary formation through the decomposition of the larger Criegee intermediate in the

Table VII Production yields observed during ozonolysis of MBO under dry and humid conditions

Product	Yields under dry conditions	Yields under humid conditions	Reference
Formaldehyde	0.44±0.05	0.55±0.03	This work
	0.29±0.03		Alvarado et al. (1999)
	0.47±0.06		Fantechi et al. (1998b)
	0.36±0.09		Grosjean and Grosjean (1995)
HMPr	0.43±0.12	0.84±0.08	This work
Acetone	0.39±0.22	–	This work
	–		Alvarado et al. (1999)
	0.08±0.05		Fantechi et al. (1998b)
	0.23±0.06		Grosjean and Grosjean (1995)
Formic Acid	0.14±0.04	–	This work
Formic anhydride	0.16±0.07	–	This work

Comparison to previous literature.

presence of water *via* the hydroperoxyde channel (Finlayson-Pitts and Pitts 2000), according to the following equations:

$$(CH_3)_2C(OH)C^{\circ}(H)OO^{\circ} + H_2O \rightarrow (CH_3)_2C(OH)CH(OH)OOH$$
$$(CH_3)_2C(OH)CH(OH)OOH \rightarrow (CH_3)_2C(OH)CHO + H_2O_2$$

Acetone yields exhibit a large variability: Fantechi observed a weak yield of 0.08, Grosjean measured a yield of 0.23 and we saw a production yield of 0.39 with an important error of 0.22. A similar variability was observed by Alvarado et al., (1999) using GC–FID when working at 5% humidity, and the acetone yield in the Alvarado et al., (1999) study using FTIR spectroscopy under dry conditions was 0.12. These big differences might be due to the difficulty of monitoring acetone by FTIR (acetone presents a weak IR absorption in the water absorption IR region) and to the very important role of humidity. Indeed, we noticed that acetone production disappears in humid conditions: the Criegee decomposition pathway, developed in Grosjean and Grosjean (1995), that leads to acetone may be sensitive and bypassed as soon as water is present in the environment. Water stabilises the O–H bond in the large Criegee intermediate. This bond can also not be split in the presence of water to produce acetone. A tiny water amount is probably efficient enough to disrupt the acetone-pathway which could explain the high variability of acetone production during the dry experiments. Consequently, this observation means that in usual natural conditions (HR> 1%), no acetone can be formed by the ozonolysis of MBO.

Moreover we noticed a primary formation of formic acid and formic anhydride in dry conditions, and none in humid conditions. This observation is to compare with different evolution pathways nowadays well accepted for the Criegee intermediate in the presence of water (Finlayson-Pitts and Pitts 2000):

$$H_2C^{\circ}OO^{\circ} + H_2O \rightarrow HCOOH + H_2O \quad (a)$$
$$H_2C^{\circ}OO^{\circ} + H_2O \xrightarrow{M} CH_2(OH)OOH \quad (b)$$
$$CH_2(OH)OOH \rightarrow HCHO + H_2O_2 \quad (c)$$
$$CH_2(OH)OOH \rightarrow HCOOH + H_2O \quad (d)$$

In the case of our MBO ozonolysis experiments in CRAC in the presence of water, the pathway that leads to acids (a) would be minor in comparison to the hydroperoxide pathway (b). Indeed no acid production was observed and we did not detect directly peroxide compounds but we noticed an important increase of carbonyl compounds which according to equation (c) may come from a decomposition of the hydroxy–hydroperoxides in solution or on the wall (Neeb et al., 1997; Sauer et al., 1999).

Consequently there are two different production ways occurring under dry and humid conditions. Product yields are reported in Table VII and Figure 7 summarises the mechanism schemes of MBO ozonolysis in dry and in humid conditions. The observed chemistry is so sensitive to humidity that only the humid pathway occurs in natural conditions.

3.2.2 Aerosol production (in CRAC)

A production of fine particles was observed during ozonolysis experiments (see Figure 8): their diameters varied from 30 to 200 nm.

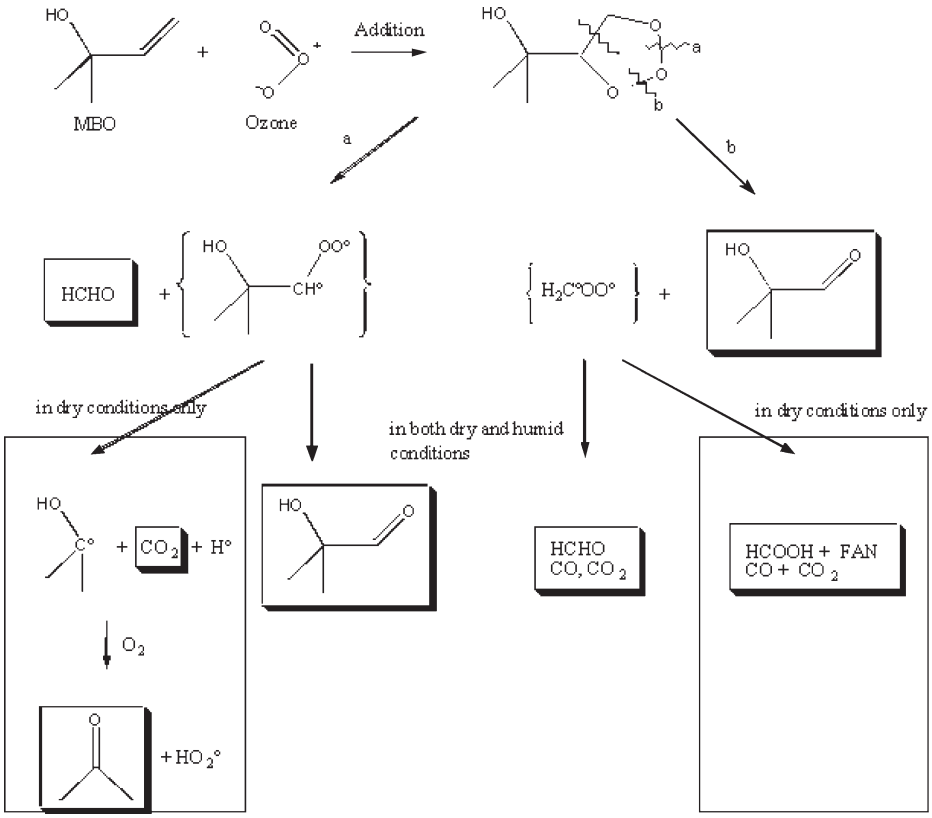

Figure 8 Ozonolysis scheme of MBO under dry and humid conditions. In dry conditions, the possibility that the Criegee intermediates may undergo both reaction channels cannot be ruled out. In humid conditions, it appears that one of the channels disappears (channel on *grey background*).

Mass production yield is defined as the ratio of the amount of SOA formed from the oxidation of MBO to the amount of reacted MBO:

$$Y = \frac{\Delta M_{\mathrm{o}}}{\Delta \mathrm{MBO}},$$

where ΔM_{O} (μg m^{-3}) is the organic aerosol mass formed after the consumption of ΔMBO (μg m^{-3}). SOA production yields are reported for ozonolysis experiments carried in CRAC

Table VIII Secondary organic yields measured during photo-oxidation experiments in EUPHORE and ozonolysis with various relative humidity in CRAC

Experiment	ΔMBO (ppm)	ΔM_{O} (μg m^{-3})	Y
Ozonolysis HR<1%	1.63	74	0.018
Ozonolysis HR=30%	0.76	25	0.009
Ozonolysis HR=30%	0.75	12	0.004
Ozonolysis HR=30%	0.74	21	0.015
Ozonolysis HR=20%	0.89	10	0.003
Ozonolysis HR=20%	0.85	9	0.003

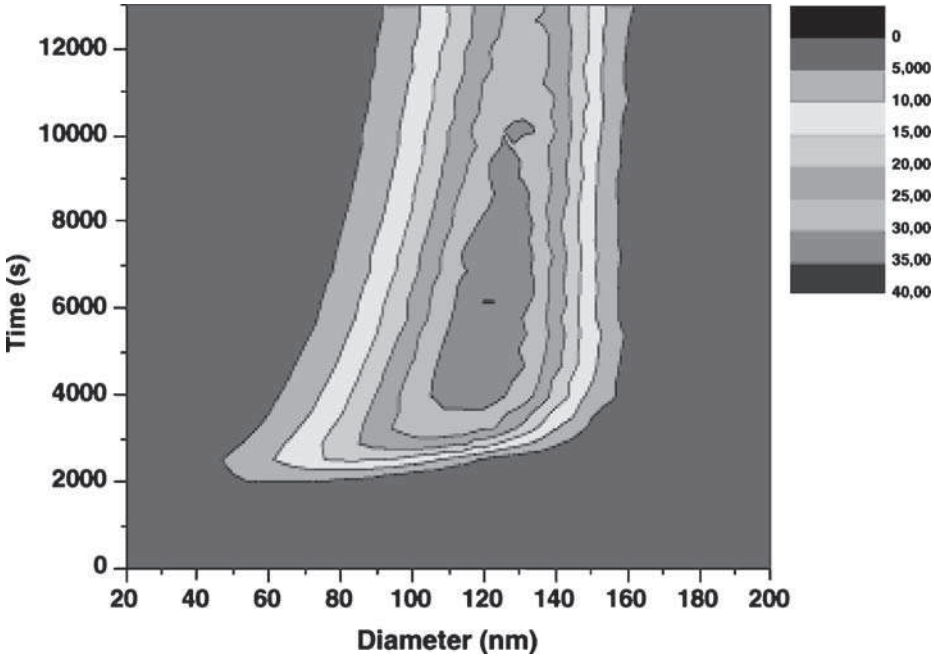

Figure 9 SOA production during a typical MBO ozonolysis in Cork. $[MBO]_0$=1.5 ppm_v, $[O_3]$=3.0 ppm_v. Ozone is added after 2,000 s: the SOA formation is instantaneous.

in Table VIII and were calculated with an aerosol density of 1 (Figures 9 and 10). It was checked that no aerosol production came from the OH-scavenger, CO (whereas an SOA formation was observed with cyclohexane as OH-scavenger). Under dry conditions this yield is equal to 1.8% and decreases to less than 1% under humid conditions. This decrease is consistent with the recent study on gaseous ozonolysis under various humidity conditions made by Sadezki et al., in 2003 on a series of small vinylethers (Sadezki et al., 2003). Indeed they noticed a formation of aerosol under dry conditions and a disappearance of this production in humid conditions.

4 Atmospherical Implications

4.1 Kinetics of MBO global daytime degradation in the troposphere

The rate constant found for MBO+OH reaction leads to a MBO lifetime of 2.5 h, using the commonly accepted value 2×10^6 molecule cm^{-3} as the OH concentration in the troposphere. Compared to the lifetime of MBO with ozone, 1.1 day (Klawatsch-Carrasco et al., 2004), the MBO+OH reaction is much faster. Thus the dominant reaction of MBO during the day is its reaction with OH radicals rather than its ozonolysis.

4.2 Mechanism of MBO global daytime degradation in the troposphere

The kinetics study indicates that the OH reaction is the dominant daytime process in the troposphere. However the mechanistic results obtained about both OH– and ozone-

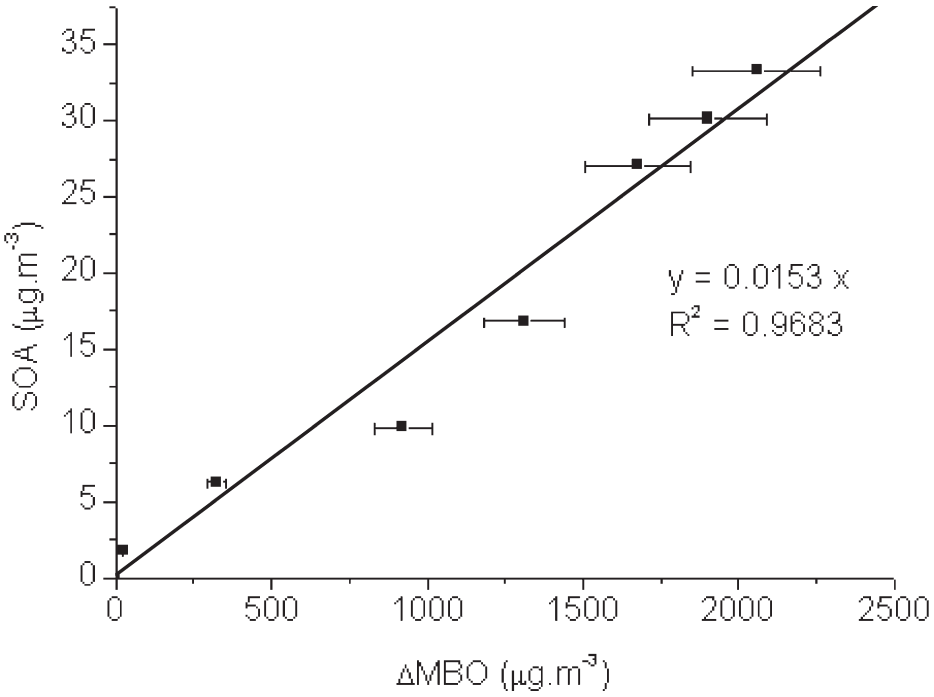

Figure 10 SOA production yield plot during a typical MBO ozonolysis experiment. $[MBO]_0$=1.5 ppm_v, $[O_3]$=3.0 ppm_v.

oxidation of MBO have shown some significant differences (especially concerning the SOA production) which imply that ozonolysis has a non-negligible environmental role in the daytime decomposition of MBO. To validate the mechanisms developed for OH and Ozone reactions, some experiments were driven under realistic conditions in the EUPHORE outdoor simulation chamber: two MBO photo-oxidation experiments were performed, introducing 250 ppb of MBO and, respectively, 50 and 25 ppb of NO, respectively, in the EUPHORE chamber under dry conditions, before submitting the mixture to natural irradiation. Experimental conditions are described in Table IX and a characteristic concentration/time plot is given on Figure 11. As these experiments could be

Table IX Initial conditions for the EUPHORE photo-oxidation experiments

Date of experiment	May 19, 2003	May 20, 2003
Duration of experiment	9:30–16:00 GMT	10:00–16:00 – GMT
Temperature (K)	295	297
Total pressure (mbar)	1,004.9	1,011.1
Atmospherical conditions	Sunny	Sunny
Initial mixing ratios (ppb_v)		
MBO	250	250
NO	50	25

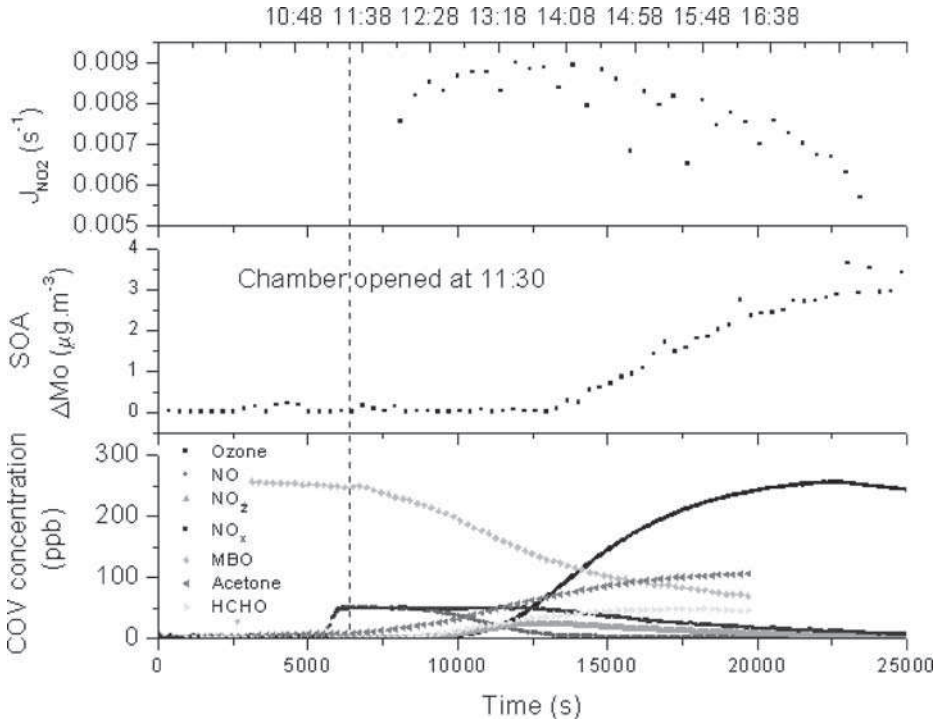

Figure 11 J_{NO2}, SOA yield and concentrations of COV, ozone and NO_x during a photo-oxidation experiment in EUPHORE : $[MBO]_0$=250 ppb, $[NO]_0$=50 ppb, natural irradiation at 11:30.

useful for modellers, reactants, products, NO_x, SOA and ozone concentrations and also J_{NO2} and J_{HCHO} of the $[NO]_0$=50 ppb experiment are provided in supplementary material.

4.2.1 Ozone production

An ozone production was noticed, corresponding to more than one equivalent of disappeared MBO. During the two experiments carried out in EUPHORE, the following yields were measured:

$$[O_3]/[MBO] = 1.40 \text{ with } [NO]_o = 50 \text{ ppb}$$
$$[O_3]/[MBO] = 1.20 \text{ with } [NO]_o = 25 \text{ ppb}$$

4.2.2 Aerosol production

After 1 h of reaction, a small production of fine secondary organic aerosols was observed. This later production was consistent with the later production of ozone in the chamber. Their diameters increased during the experiment from 10 to 100 nm. SOA density was approximated as 1. During the photo-oxidation experiments, aerosol production accounted for 0.5% of the global carbon mass. Despite its weak contribution to the carbon balance, this small formation of secondary aerosol might have an important atmospherical impact in cases where MBO is a massively emitted biogenic compound (Claeys et al., 2004).

4.2.3 Primary VOC formation

FTIR data and DNPH samples showed a production of only four different carbonyl compounds, HMPr, formaldehyde, acetone and glycolaldehyde. Because of the importance of acetone in tropospheric chemistry (Jacob et al., 2002), acetone global production rate was measured for both photo-oxidation experiments. A yield of $\Delta[\text{Acetone}]/\Delta[\text{MBO}] = 0.42 \pm 0.03$ was found in both cases. The important yield of acetone coming from MBO degradation added to the abundance of MBO natural emissions show that MBO is a significant source of acetone in the troposphere.

5 Conclusion

Global daytime reactivity of MBO has been studied under realistic conditions in the outdoor simulation chamber of EUPHORE. Specific reactions of MBO with ozone and with OH radicals have been studied in the indoor simulation chambers of LISA and CRAC. This work allowed us to understand the observations made on the EUPHORE realistic experiments thanks to a specific work realised in LISA and in CRAC on the reactions of MBO with its diurnal aggressors, OH radicals and ozone.

Global degradation of MBO produces around 130% of ozone at realistic NO concentrations (between 25 and 50 ppb). A small production of secondary organic aerosol (Y lower than 1%) was observed which may have an important atmospherical impact in places where MBO is abundantly emitted. The specific studies of reactions with ozone and OH radicals prove that this SOA production only comes from the ozonolysis process.

Concerning the COV produced in gazeous phase, major compounds were identified and quantified, in particular 2-hydroxy-2-methylpropanal (HMPr), formaldehyde, acetone, glycolaldehyde, formic acid and formic anhydride. Formaldehyde and HMPr are formed by both processes, ozonolysis and reaction with OH radicals. Glycolaldehyde comes from the reaction of MBO with OH radicals. Formic acid and formic anhydride come from MBO ozonolysis in dry conditions. Acetone is significantly formed by the reaction of MBO with OH, $R_{\text{acetone}}=0.67$, is also formed by ozonolysis under dry conditions, $R_{\text{acetone}}=0.39$ but its production stops under humid conditions: realistic simulations in EUPHORE showed a global production yield of 0.42. In case MBO is an abundant biogenic product, it has an important role as source of acetone in the troposphere.

Acknowledgments The authors gratefully thank INERIS (Institut National de l'Environnement et des RISques) and PNCA for their financial support. The authors would also like to thank the help of the whole scientific group in EUPHORE.

References

Alvarado, A., Tuazon, E.C., Aschmann, S.M., Arey, J., Atkinson, R.: Products and mechanisms of the gas phase reactions of OH radicals and O3 with 2-methyl-3-buten-2-ol. Atmos. Environ. **33**, 2893–2905 (1999)

Atkinson, R.: Gas-phase tropospheric chemistry of volatile organic compounds: 1. alkanes and alkenes. J. Phys. Chem. Ref. Data **26**, 215–290 (1997)

Atkinson, R., Arey, J.: Gas-tropospheric chemistry of biogenic volatile organic compounds: a review. Atmos. Environ. **37**(suppl 2), S197–S219 (2003)

Atkinson, R., Aschmann, S.M., Carter, W.P.L., Winer, A.M., Pitts, J.N., Jr.: Alkyl nitrate formation from the NO_x–air photooxidations of C_2–C_8 *n*-alkanes. J. Phys. Chem. **86**(11), 4563–4569 (1982)

Atkinson, R., Tuazon, E.C., Aschmann, S.M.: Products of the gas-phase reactions of O3 with alkenes. Environ. Sci. Technol. **29**, 1674–1680 (1995)

Barnes, I., Hjorth, J.: Informal IR intercalibration exercise. Private communication (2004)

Becker, K.H., Hjorth, J., Laverdet, G., Millan, M.M., Platt, U., Toupance, G., Wildt, J.: Design and technical development of the European photoreactor and first experimental results. EV5V-CT92-0059 (1996)

Brauers, T., Finlayson-Pitts, B.: Analysis of relative rate measurements. Int. J. Chem. Kinet. **29**(9), 665–672 (1997)

Carrasco, N., Doussin, J.F., Picquet-Varrault, B., Carlier, P.: Tropospheric degradation of 2-hydroxy-2-methylpropanal, a photooxidation product of 2-methyl-3-buten-2-ol: kinetic and mechanistic study of its photolysis and its reaction with OH radicals. Atmos. Environ. **40**(11), 2011–2019 (2006)

Claeys, M., Graham, B., Vas, G., Wang, W., Vermeylen, R., Pashyinska, V., Cafmeyer, J., Guyon, P., Andreae, M.O., Artaxo, P., Maenhaut, W.: Formation of secondary organic aerosols photooxidation of isoprene. Science **303**, 1173–1176 (2004)

Destaillats, H., Spaulding, R., Charles, M.J.: Ambient air measurements of acrolein and other carbonyls at the Oackland–San Francisco bay bridge Toll Plaza. Environ. Sci. Technol. **36**, 2227–2235 (2002)

Doussin, J.F., Ritz, D., Durand-Jolibois, R., Monod, A., Carlier, P.: Design of an environmental chamber for the study of atmospheric chemistry: new developments in the analytical device. Analusis **25**, 236–242 (1997)

Fantechi, G., Jensen, N.R., Hjorth, J., Peeters, J.: Determination of the rate constants for the gas phase reactions of methyl butenol with OH radicals, ozone and NO_3 radicals. Int. J. Chem. Kinet. **30**(20), 589–594 (1998a)

Fantechi, G., Jensen, N.R., Hjorth, J., Peeters, J.: Mechanistic studies of the atmospheric oxidation of methylbutenol by OH radicals, ozone and NO3 radicals. Atmos. Environ. **32**(20), 3547–3556 (1998b)

Ferronato, C., Orlando, J.J., Tyndall, G.S.: Rate and mechanism of the reactions of OH and Cl with 2-methyl-3-buten-2-ol. J. Geophys. Res. **103**, 25579–25586 (1998)

Finlayson-Pitts, B.J., Pitts, J.N.J.: Chemistry of the upper and the lower atmosphere. Academic, San Diego, California (2000)

Goldan, P., Kuster, W.C., Fehsenfeld, F.C.: The observation of a C5 alcohol emission in a North American pine forest. Geophys. Res. Lett. **20**, 1039–1042 (1993)

Grosjean, D., Grosjean, E.: Rate constants for the gas phase reactions of ozone with unsaturated aliphatic alcohols. Int. J. Chem. Kinet. **26**, 1185–1191 (1994)

Grosjean, E., Grosjean, D.: Carbonyl products of the ozone-unsaturated alcohol reaction. J. Geophys. Res. **100**, 22815–22820 (1995)

Grosjean, E., Grosjean, D.: Gas phase reaction of alkenes with ozone: formation yields of primary carbonyls and biradicals. Environ. Sci. Technol. **31**, 2421–2427 (1997)

Grosjean, E., Grosjean, D.: The gas phase reaction of alkenes with ozone: formation yields of carbonyls from biradicals in ozone–alkene-cyclohexane experiments. Atmos. Environ. **32**, 3393–3402 (1998)

Grosjean, D., Grosjean, E., Williams, M.B.: Atmospheric chemistry of olefins: a product study of ozone–alkene reaction with cyclohexane added to scavenge OH. Environ. Sci. Technol. **28**, 186–196 (1994)

Guenther, A., Nicholas Hewitt, C., Erickson, D., Fall, R., Geron, C., Graedel, T., Harley, P., Klinger, L., Lerdau, M., McKay, W.A., Pierce, T., Scholes, B., Steinbrecher, R., Tallamraju, R., Taylor, J., Zimmerman, P.: A global model of natural volatile organic compound emissions. J. Geophys. Res. **100** (D5), 8873–8892 (1995)

Guenther, A., Geron, C., Pierce, T., Lamb, B., Harley, P., Fall, R.: Natural emissions of non-methane volatile organic compounds, carbon monoxide, and oxides of nitrogen from North America. Atmos. Environ. **34**, 2205–2230 (2000)

Horie, O., Moortgat, G.: Decomposition pathways of the excited Criegee intermediates in the ozonolysis of simple alkenes. Atmos. Environ. **25A**, 1881–1896 (1991)

Horie, O., Crowley, J.N., Moortgat, G.: Methylperoxy self-reaction: products and branching ratio between 223 and 333 K. J. Phys. Chem. **94**, 8198–8203 (1990)

Imamura, T., Lida, Y., Obi, K., Nagatani, I., Nakagawa, K., Patroescu-Klotz, I., Hatakeyama, S.: Rate coefficients for the gas-phase reactions of OH radicals with methylbutenols at 298 K. Int. J. Chem. Kinet. **36**(7), 379–385 (2004)

IUPAC: http://www.iupac-kinetic.ch.cam.ac.uk/ Summary of evaluated kinetic and photochemical data for atmospheric chemistry (2005)

Jacob, D., Field, B.D., Jin, E.M., Bey, I., Li, Q., Logan, J.A., Yantosca, R.M.: Atmospheric budget of acetone. J. Geophys. Res. **107**(D10), 10.1029 (2002)

Jaeglé, L., Jacob, D.J., Brune, W.H., Wennberg, P.O.: Chemistry of HOx radicals in the upper troposphere. Atmos. Environ. **35**(3), 469–489 (2001)

Klawatsch-Carrasco, N., Doussin, J.F., Carlier, P.: Absolute rate constants for the gas-phase ozonolysis of isoprene and methylbutenol. Int. J. Chem. Kinet. **36**(3), 152–156 (2004)

Lightfoot, P.D., Roussel, P., Caralp, F., Lesclaux, R.: A flash photolysis study of the CH3O2+CH3O2 and CH3O2+HO2 reactions between 600 and 719 K: the unimolecular decomposition of methylhydroperoxide. J. Chem. Soc., Faraday Trans. **87**, 3213–3220 (1991)

Meunier, N., Doussin, J.F., Chevallier, E., Durand-Jolibois, R., Picquet-Varrault, B., Carlier, P.: Atmospheric fate of alkoxy radicals: branching ratio of evolution pathways for 1-propoxy, 2-propoxy, 2-butoxy and 3-pentoxy radicals. Phys. Chem. Chem. Phys. **5**, 4834–4839 (2003)

Nash, T.: Chemical status of nitrogen dioxide at low aerial concentration. Ann. Occup. Hyg. **11**(3), 235–239 (1968)

Neeb, P., Sauer, F., Horie, O., Moortgat, G.: Formation of hydroxymethyl hydroperoxide and formic acid in alkene ozonolysis in the presence of water vapour. Atmos. Environ. **31**, 1417–1423 (1997)

Niki, H., Maker, P.D., Savage, C.M., Breitenbach, L.P.: Fourier transform infrared studies of the self-reaction of C2H5O2 radicals. J. Phys. Chem. **86**, 3825–3829 (1982)

Papagni, C., Arey, J., Atkinson, R.: Rate constant for the gas-phase reactions of OH radicals with a series of unsaturated alcohols. Int. J. Chem. Kinet. **33**(2), 142–147 (2001)

Picquet-Varrault, B., Doussin, J.F., Durand-Jolibois, R., Carlier, P.: Kinetic and mechanistic study of the atmospheric oxidation by OH radicals of allyl acetate. Environ. Sci. Technol. **36**, 4081–4086 (2002)

Reisen, F., Aschmann, S.M., Atkinson, R., Arey, J.: Hydroxyaldehyde products from hydroxyl radical reactions of Z-3-hexen-1-ol and 2-methyl-3-buten-2-ol quantified by SPME and API–MS. Environ. Sci. Technol. **37**, 4664–4671 (2003)

Rudich, Y., Talukdar, R., Burkholder, J.B., Ravishankara, A.R.: Reaction of methylbutenol with Hydroxyl radical: mechanism and atmospheric implications. J. Phys. Chem. **99**, 12188–12194 (1995)

Sadezki, A., Mellouki, A., Winterhalter, R., Römpp, A., Moortgat, G.: Aerosol formation by gas-phase-ozonolysis of small vinylethers. EGS–AGU–EUG Joint Assembly: Abstract from the meeting held in Nice, France, 6–11 April 2003, abstract#11652 (2003)

Sauer, F., Schäfer, C., Neeb, P., Horie, O., Moortgat, G.: Formation of hydrogen peroxide in the ozonolysis of isoprene and simple alkenes under humid conditions. Atmos. Environ. **33**, 229–241 (1999)

Spaulding, R., Charles, M.J., Tuazon, E.C., Lashley, M.: Ion trap mass spectrometry affords advances in the analytical and atmospheric chemistry of 2-hydroxy-2-methylpropanal, a proposed photooxidation product of 2-methyl-3-buten-2-ol. J. Am. Soc. Mass Spectrom. **13**, 530–542 (2002)

Taylor, W.D., Allston, T.D., Moscato, M.J., Fazekas, G.B., Kozlowski, R., Takacs, G.A.: Atmospheric photodissociation lifetimes for nitromethane, methyl nitrite, and methyl nitrate. Int. J. Chem. Kinet. **12**(4), 231–240 (1980)

Thuener, L., Bardini, P., Rea, G.J., Wenger, J.: Kinetics of the gas-phase reactions of OH and NO_3 radicals with dimethylphenols. J. Phys. Chem. A **108**(50), 11019–11025 (2004)

Wallington, T.J., Gierczac, C.A., Ball, J.C., Japar, S.M.: Fourier transform infrared study of the self reaction of C2H5O2 radicals in air at 295 K. Int. J. Chem. Kinet. **21**(11), 1077–1089 (1989)

Wayne, R.P.: Chemistry of atmospheres, 3rd edn. Oxford University Press, New York (2000)

Yu, J., Jeffries, H.E., Le Lacheur, R.M.: Identifying airborne carbonyl compounds in isoprene atmospheric photooxidation products by their PFBHA oximes using gas chromatography/ion trap mass spectrometry. Environ. Sci. Technol. **29**, 1923–1932 (1995)

Icarus 213 (2011) 625–635

Contents lists available at ScienceDirect

Icarus

journal homepage: www.elsevier.com/locate/icarus

Nitrile gas chemistry in Titan's atmosphere

Thomas Gautier [a,*], Nathalie Carrasco [a], Arnaud Buch [b], Cyril Szopa [a], Ella Sciamma-O'Brien [a], Guy Cernogora [a]

[a] Université Versailles St. Quentin, UPMC Univ. Paris 06, LATMOS, CNRS, 11 Bvd d'Alembert, 78280 Guyancourt, France
[b] LGPM, Ecole Centrale de Paris, Grande voie des Vignes, 92295 Chatenay-Malabry Cedex, France

ARTICLE INFO

Article history:
Received 6 January 2011
Revised 7 April 2011
Accepted 7 April 2011
Available online 18 April 2011

Keywords:
Prebiotic chemistry
Experimental techniques
Atmospheres, Chemistry
Saturn, Satellites

ABSTRACT

This work presents the first study of the gaseous products resulting from the partial dissociation of methane and nitrogen in the PAMPRE experimental setup simulating Titan's atmospheric chemistry.

Using cryogenic trapping, the gaseous products generated from the chemical reactions occurring in the reactor have been trapped. Analyses of these products by gas chromatography coupled to mass spectrometry have allowed the detection and identification of more than 30 reaction products. Most of them are identified as nitrile species, accompanied by aliphatic hydrocarbons and a few aromatics compounds. The observed species are in agreement with the data from the recent Cassini–Huygens mission as well as from other laboratory setups capable of dissociating nitrogen and methane. This work emphasizes the probable importance of nitrogen-bearing compounds in the chemistry taking place in Titan's atmosphere.

Furthermore, a quantification of mono-nitriles with saturated alkyl chains has been performed relatively to hydrogen cyanide and shows a power law dependence in their concentration. This dependence is consistent with the Cassini-INMS data and Titan's photochemical models.

An empirical relationship has been extracted from our experimental data: $[C_xH_{2x-1}N] = 100x^{-5}$, where x is the number of carbon atoms in the nitrile molecule. This relationship can be directly used in order to foretell the concentration of heavier nitriles induced by chemistry in Titan's atmosphere.

1. Introduction

The dense atmosphere of Titan, Saturn's largest satellite, is mainly made up of nitrogen and methane (Kuiper, 1944). Organic chemical reactions take place in this atmosphere, induced by solar radiation and electrically charged heavy particles coming from Saturn's magnetosphere (Sittler et al., 2009).

This induced organic chemistry is one of the most complex known in the Solar System, and leads to the formation of solid organic aerosols responsible for Titan's brownish color.

These aerosols present a major interest for planetary science. First, knowing how they are formed and what their properties are is a clue to better understanding the radiative transfer in planetary atmospheres. Second, the formation process of organic complex molecules presents de facto a large interest for exobiology.

In order to understand Titan's atmospheric chemistry, one needs to use several complementary methods. First, Earth and space observations of Titan are used to detect the most predominant species in its atmosphere. In particular, the instruments onboard the current Cassini/Huygens mission (NASA/ESA) have revealed new aspects of Titan's chemistry, discovering many heavy molecules, and negative and positive ions in its upper atmosphere (Israel et al., 2005; Hartle et al., 2006; Yelle et al., 2006; Barnes et al., 2009; Vinatier et al., 2010). Second, numerical models are used to study the chemical pathways and mechanisms that could explain these observations (Wilson and Atreya, 2003; Hébrard et al., 2006, 2007; Carrasco et al., 2008; Lavvas et al., 2008; Krasnopolsky, 2009).

Finally, the last approach to study the chemistry in Titan's atmosphere is the experimental simulation in laboratories. Most of these experiments reproduce a gas mixture close to Titan's atmosphere, or at least to a part of its atmosphere, and then deposit energy into this gas mixture to induce chemistry. Different sources of energy can be used to initiate the dissociation of both molecular nitrogen and methane.

Photochemical experiments expose the gas mixture to a light flux. However, this flux is often not sufficient to dissociate molecular nitrogen because UV radiations below 200 nm are stopped by silica windows. In order to induce a nitrogenous chemistry, these experiments often have to introduce nitrogenous reactive species, such as HCN of HC_3N, in the reactive gas mixture (Clarke et al., 2000; Tran et al., 2005; Bar-Nun et al., 2008).

* Corresponding author. Fax: +33 1 80 28 52 90.
E-mail address: thomas.gautier@latmos.ipsl.fr (T. Gautier).

0019-1035/$ - see front matter © 2011 Elsevier Inc. All rights reserved.
doi:10.1016/j.icarus.2011.04.005

In order to dissociate molecular nitrogen, other experiments have been developed using plasma discharges, either Direct Current Plasma (DCP) (Bernard et al., 2003; Somogyi et al., 2005), corona discharges (Ramírez et al., 2005), dielectric barrier discharges (Horvath et al., 2010) or radiofrequency plasmas (Imanaka et al., 2004; Szopa et al., 2006), as the energy source. In this case, the chemistry is induced by electronic impact on methane and molecular nitrogen. The energy distribution of the electrons in the plasma is not so different from the energy spectrum of solar photons (Szopa et al., 2006). Moreover, Robertson et al. (2009) showed that the shape of dayside (photon and electron induced chemistry) and nightside (electron chemistry only) INMS ion mass spectra are similar. This observation suggests that the chemistry found in Titan's ionosphere is more or less similar when initiated by photons or by electrons. It also supports the idea that, experimental plasma setups are relevant tools to simulate Titan's upper atmosphere.

The PAMPRE experimental setup used in this study employs a RadioFrequency Capacitively Coupled Plasma (RF CCP) discharge to dissociate N_2. Alcouffe et al. (2010) have given a wider description of the different plasma experimental setups that have been developed to simulate Titan's atmospheric chemistry and have shown the interest of using RF CCP discharges, which are the only experimental setups where tholins can grow in volume (Bouchoule, 1999), as in Titan's atmosphere.

Previous studies have been done on the plasma physics and on the properties and chemical composition of tholins on PAMPRE experiment (Carrasco et al., 2009; Hadamcik et al., 2009; Alcouffe et al., 2010; Pernot et al., 2010). Recently, the chemistry of the reactive gas mixture and the carbon gas to solid conversion yield in PAMPRE have also been studied (Sciamma-O'Brien et al., 2010).

Here we present the first study of the gas products in PAMPRE, both on their detection and their relative quantification. This study will help to understand the chemistry in the gas phase, highlighting key organic species responsible for the resulting tholin formation.

2. Experimental setup and protocol

2.1. The PAMPRE experiment

The PAMPRE experiment goal is to simulate Titan's atmospheric chemistry, and particularly the chemical reactivity leading to the formation of aerosols, by producing laboratory analogs of these aerosols (Szopa et al., 2006).

The PAMPRE experimental setup configuration used for this study is shown in Fig. 1 and a description of the experimental protocol on PAMPRE can be found in Sciamma-O'Brien et al. (2010).

In the study presented here, all experiments were performed with a continuous 55 sccm N_2–CH_4 gas flow using different methane concentrations. The methane percentages taken into account in the present work are 1%, 4% and 10% of CH_4 in N_2. The 1% and 10% CH_4 concentrations were chosen because they are the extreme values accessible with the PAMPRE setup. The 4% CH_4 concentration was also studied since it corresponds to the maximum tholin production (Sciamma-O'Brien et al., 2010). The pressure in the reactor was approximately 1.7 mbar and the gas temperature was the room temperature.

Using in situ mass spectrometry, Pintassilgo et al. (1999) have shown that in DC N_2–CH_4 discharges, CH_4 is strongly dissociated. In a previous work, the CH_4 consumption in the PAMPRE experiment has been monitored using a mass spectrometer (Sciamma-O'Brien et al., 2010). Unfortunately, in situ mass spectrometry does not allow to measure minor species in the reactor.

On the experimental setup used for the study presented here, as shown in Fig. 1, a cold trap was located at the gas outlet of the reactor. This cold trap is a cylindrical glass coil, with a diameter of 1.3 cm, a length of 1 m and a total volume of 133 cm^3, which is

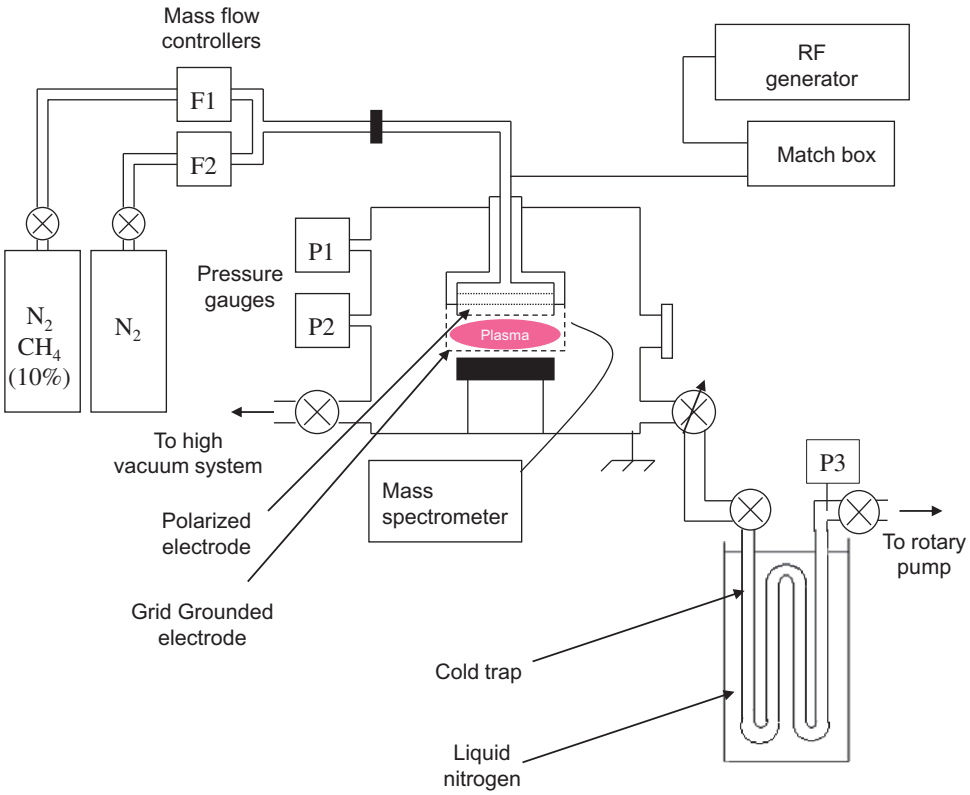

Fig. 1. Schematic of the PAMPRE experimental setup.

immersed in liquid nitrogen. The gas pumped from the reactor flows through this trap where products coming from the reactive gas mixture can condense depending on the pressure and the temperature. Since the trap is cooled by liquid nitrogen, the gas temperature is $T \geqslant 77$ K. The pumping induces a pressure gradient from the reactor ($P = 1.7$ mbar) to the pump such that the pressure in the cold trap is lower than 1.7 mbar. This setup allows the trapping of all the species condensable in these temperature and pressure conditions. A Bourdon pressure gauge measures the pressure in the trap in the range from 0 to 1000 mbar with a resolution of ±10 mbar.

In the study presented here, the trap was heated and then pumped with a turbo pump before each experiment in order to remove water vapor adsorbed on the trap walls. Experiments were 3 h long and repeated at least two times in order to ensure the repeatability of the measurement.

At the end of an experiment, the trap was isolated from the reactor with a gas valve. The pressure inside the trap while it was still immersed in liquid nitrogen was below the limit of detection of the Bourdon gauge. When the trap was warmed up to room temperature, the light species trapped were going back to their gas phase and a solid residue was formed when the trap returns to room temperature. In the present study, only the gas phase present in the cold trap was analyzed. The analysis of the solid residue will be the subject of a future work.

The absence of condensation of both N_2 and CH_4 in the trap was checked with non reactive experiments (plasma off), where a 55 sccm flux of N_2–CH_4 90:10 was injected in the reactor in the same pressure conditions. After a 3 h run the trap was taken out of liquid nitrogen and left at room temperature to warm up. As no pressure increase was observed, neither nitrogen nor methane get trapped.

2.2. Gas phase analysis with gas chromatography–mass spectrometry

The gas trapped was analyzed by gas chromatography coupled to mass spectrometry (GC–MS). The cold trap was connected to a GC–MS device through a six port gas valve to perform direct injection of the trapped gas.

The GC–MS device used in this study was a ThermoScientific GC-Trace coupled to a ThermoScientific DSQ II Mass spectrometer operated in a quadrupole detection mode. The column used for the gas separation was a MXT-QPlot (Restek) 30 m long, 0.25 mm internal diameter and 10 μm stationary phase thickness designed to easily separate volatile compounds up to 5 carbons. For this study, the column temperature was set with a temperature isotherm at 30 °C during 5 min, then a gradient of 5 °C/min from 30 °C to 190 °C and a second isotherm at 190 °C for 5 min. Helium was used as a carrier gas at a constant 1 mL · min^{-1} flow rate. The injector used was an Optic 3 thermal desorber working either in split (1/10) or in splitless mode. The gas phase was trapped in split mode at low temperature (−80 °C) in the injector's liner filled with a mixture of Tenax and Carboseive®. This step allowed concentrating the target species. In order to inject them in the GC, the injector liner was then quickly heated (with a rate of 16 °C min^{-1}) at 250 °C. It operated in splitless mode. The temperature of the detector was set to 200 °C.

Before each injection, a blank experiment was performed under the same analytical conditions without any sample injected. This blank injection allows us to clearly identify potential contaminant species, and discriminate them from chemical species evolving from the sample. No specific contamination was detected in the blank except usual column releases.

3. Results

3.1. Pressure of the gas in the cold trap

When the trap is warmed up, the gas pressure inside the cold trap increases, showing the presence of gas products accumulated during the experiment and condensed in the trap. For the different experiments carried out, this pressure was shown to depend on the methane concentration of the gas mixture injected in the reactor. This indicates that the total amount of condensable species produced changes with the amount of methane introduced in the reactor. The evolution of the total gas pressure measured in the cold trap after warming up to room temperature is given in Fig. 2 as a function of the CH_4 concentration. The evolution of the carbon gas to solid conversion yield obtained from a previous study (Sciamma-O'Brien et al., 2010) is also plotted in this figure. This yield is defined as the ratio between the mass of solid carbon incorporated in the tholins and the mass of reactive gaseous carbon coming from the CH_4 consumption in PAMPRE. It reflects the efficiency of the reactive gas mixture to produce solid aerosols, relatively to the carbon element transfer from reactants (CH_4) to products.

Fig. 2 shows that the highest pressure difference measured between two similar experiments is of 14%, ensuring a satisfying reproducibility of the measurements. Moreover, the pressure linearly increases with the CH_4 concentration. The pressure in the cold trap rises from 60 mbar after an experiment with 1% of CH_4 in the gas mixture up to 500 mbar of gas in the cold trap after an experiment with 10% of CH_4 in the gas mixture. On the other hand, the carbon gas to solid conversion yield linearly decreases with an increasing concentration of methane in nitrogen. For 2% of CH_4 in the experiment, the carbon gas to solid conversion yield is 62% while for 10% of CH_4 in the gas mixture the yield plummets to 12% (Sciamma-O'Brien et al., 2010).

The opposite evolution of the two parameters with the CH_4 concentration in the reactive gas mixture is consistent with the product formation trend in the PAMPRE reactor. At low CH_4 concentrations, gaseous products are essentially converted into solid phase (tholins); the amount of gas remaining is thus low. Inversely, for high CH_4 concentrations, the gas products are not consumed much to create tholins, and stay in the gas phase; the total gas pressure in the trap is then higher.

3.2. GC–MS results

3.2.1. Evolution of the gas phase from 1% to 10% of CH_4 in the experiments

The three chromatograms given in Fig. 3a–c correspond to three experiments, respectively, at 1%, 4% and 10% of CH_4 in N_2. All the peaks have been identified using their elution order and their mass spectra. The peaks of highest intensity seen in these chromatograms can be attributed to nitriles. The main peak is due to hydrogen cyanide (HCN), the second peak in intensity is acetonitrile (CH_3CN) while the two other predominant peaks are attributed to propanenitrile (CH_3CH_2CN) and propenenitrile (CH_2CHCN).

From the analysis of all the chromatograms obtained, whatever the methane concentration, more than 30 species have been detected (cf. Table 1) among which a large amount of nitriles, many hydrocarbons, and a few aromatics, mainly heteroaromatic compounds.

Considering that the MS response is similar for all the detected compounds, whatever the methane concentration in the reactor is, nitrile peaks are always the overriding peaks in the chromatograms, meaning that nitriles are the main species in the gas phase.

For samples produced with 1% and 4% of CH_4 in the experiment, the chromatograms look similar, with just a small increase of the existing peaks. However, for the sample produced with 10% of

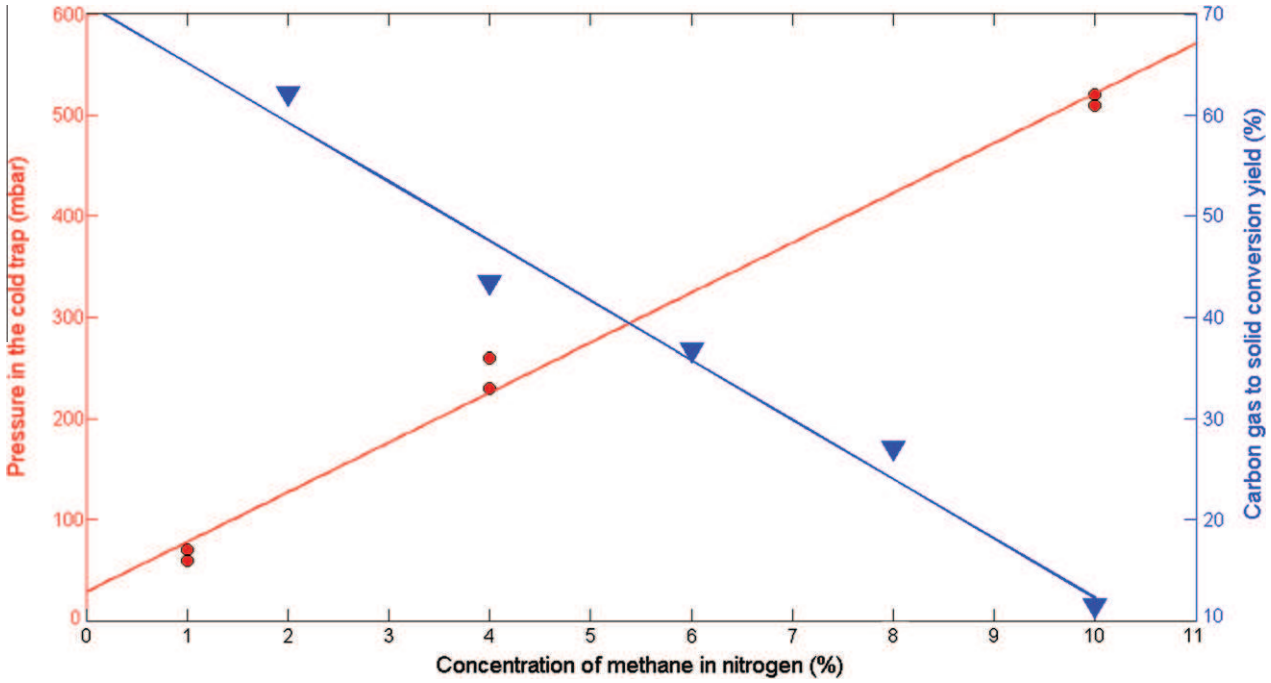

Fig. 2. Evolution of the gas pressure measured in the cold trap after warming up to room temperature (red dots) and of the carbon gas to solid conversion yield (blue triangles, from Sciamma-O'Brien et al. (2010) as a function of CH_4 concentration). (For interpretation of the references to color in this figure legend, the reader is referred to the web version of this article.)

CH_4, new peaks can be observed on the chromatogram. From their retention time and their mass spectra, these peaks can be identified as hydrocarbons. Hydrocarbons containing two carbon atoms (C_2) are eluted at Tr = 5.3 min (ethylene), Tr = 7.2 min (acetylene) and Tr = 8.6 min (ethane). C_3 hydrocarbons are identified at Tr = 17.2 min (propene), Tr = 17.4 min (propane) and Tr = 18.9 min (propyne), while C_4 hydrocarbons are eluted in the range of Tr = 25–27 min. Thanks to pre-concentrated injections performed on a sample coming from an experiment with 10% CH_4 in the reactor, a small signal due to heavier compounds (C_5H_{12}, C_5H_{10}, C_5H_8, C_6H_6) can also be detected for retention time higher than 35 min.

3.2.2. Chemical species detected in the gas phase

The list of all the gaseous compounds detected is given in Table 1.

3.2.2.1. Comparison to Titan. The list of compounds detected in the cold trap with GC–MS and presented in Table 1 is consistent with the currently known list of Titan's atmospheric compounds (Vuitton et al., 2007; Waite et al., 2007; Lavvas et al., 2008; Cui et al., 2009; Robertson et al., 2009). In addition, we have been able to detect some heavy nitriles not detected on Titan, such as butanenitrile (CH_3–$(CH_2)_2$–CN) and pentanenitrile (CH_3–$(CH_2)_3$–CN). The non detection of these molecules on Titan could be explained by the fact that these molecules are expected to be at very low concentrations, far below the current limit of detection of the instruments onboard Cassini/Huygens. In this case, we suggest some minor species to be present in Titan's atmosphere.

3.2.2.2. Comparison to other laboratory studies. It is possible to compare our results with other experimental works containing gas phase analysis. This comparison has been mainly done with experiments closed to PAMPRE experiment, i.e. able to dissociate molecular nitrogen. This criterion limits comparison with plasma experiments (Ramírez et al., 2001, 2005; Bernard et al., 2003). We also included a comparison with the work of Tran et al. (2005), a photochemical experiment, where nitrogenous compounds (such as HCN) were introduced to provide nitrogen to the reactive mixture.

As shown in Table 1, most of the species detected in our experiments are also consistent with the compounds detected in other lab experiments with the same light species detected and with a longer list of heavy nitriles (Ramírez et al., 2001, 2005; Bernard et al., 2003).

However, a few differences are observed between the experimental setups. There are two possible explanations for these differences. First, for experiments capable of dissociating molecular nitrogen, differences observed probably come from the detection methods used. The molecules detected are indeed at very low concentrations and could remain unseen if the separation and detection methods is not optimized to detect them. For example, Tran et al. (2005) detected more heavy compounds than in our study due to their GC column whose stationary phase is optimized for light aromatics detection (Restek RTX-502.2 capillary column). Second, the lack of nitrogenous compounds in some photochemical irradiation experiments (Bar-Nun et al., 2008) can be explained by the fact that molecular nitrogen is not dissociated. Indeed, the bond energy for N_2 is 9.7 eV which means that this molecule needs a radiation with a wavelength lower than 128 nm to be photo-dissociated and to release a nitrogen atom that could be involved in further reactions. Unfortunately, since silica cuts off radiation around 200 nm, if an experimental setup uses silica windows, molecular nitrogen will not be dissociated nor will it be used to form nitrogen-bearing species.

Finally, it is interesting to note that ammonia was detected in our experiments in much lower concentrations than expected (Bernard et al., 2003). One possible explanation for this lack of NH_3 is the use of stainless steel for transfer and injection in the GC–MS, since ammonia is known to adsorb onto it. The ammonia concentration detected in the GC–MS chromatograms might therefore not be representative of the ammonia present in the cold trap. A solution for ammonia detection might be to perform a Siltek® treatment of the stainless steel parts.

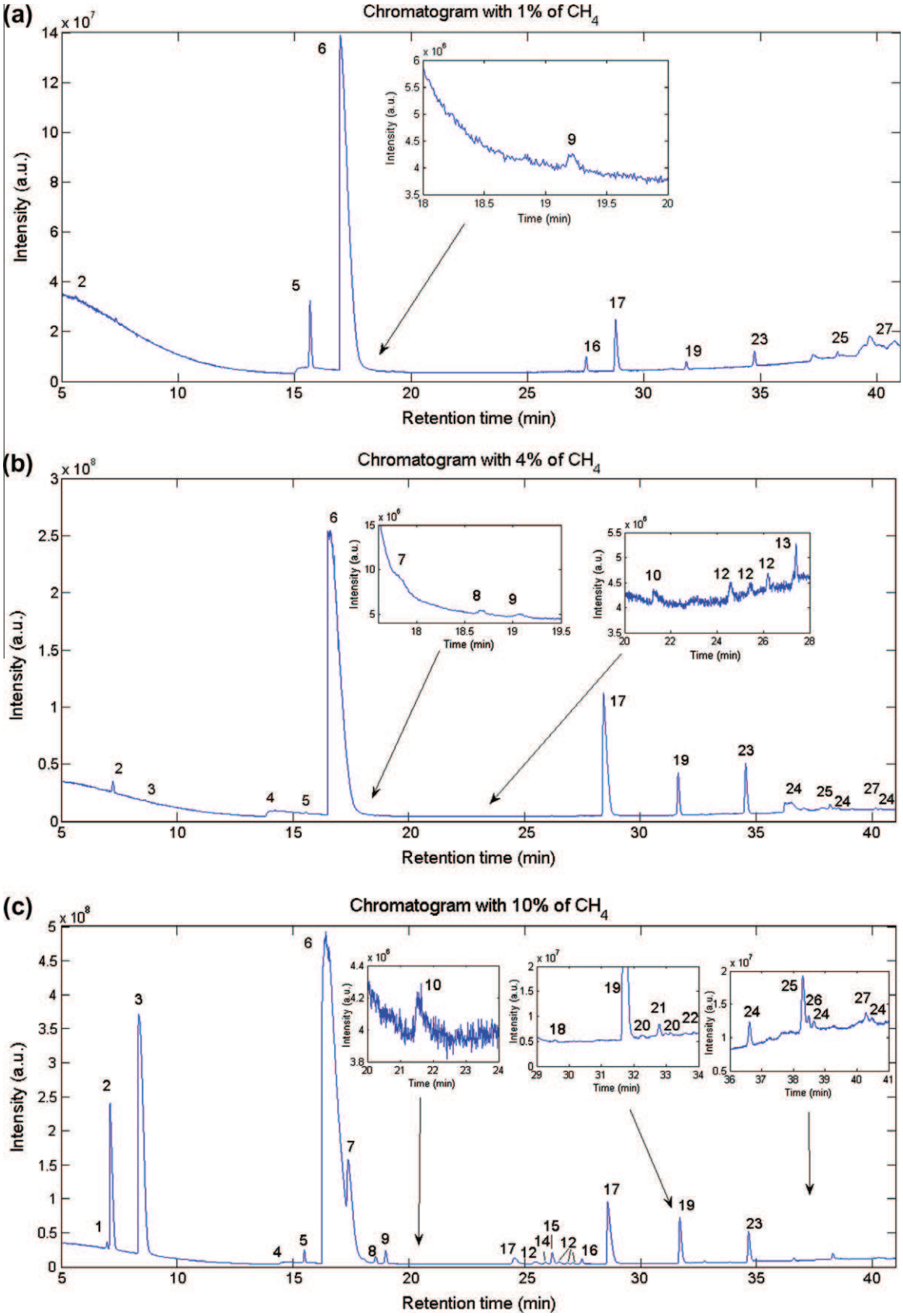

Fig. 3. (a–c) Chromatograms of gas samples trapped during experiments with, respectively, 1% (a), 4% (b) and 10% CH_4 (c) from GC–MS analysis. Peaks are numbered in agreement with Table 1. Minor peaks are shown in the insets.

Table 1
List of gaseous compounds detected in our experiment, in Titan's atmosphere and in other laboratory experiments.

Compounds detected in our experiment	Formula	Peak identification in chromatogram of Fig. 3	Detected in Titan atmosphere	Detected in laboratories experiments
Nitrogenous compounds				
Hydrogen cyanide	HCN	6	a	b,c
Ammonia	NH_3	4	a	b
Ethanedinitrile	C_2N_2	5	a	b,c
Methyl isocyanide	C_2H_5N	13	a	
Acetonitrile	C_2H_3N	17	a	b,c,d
Propiolonitrile	HC_3N	16	a	b,d
2-Propenenitrile	C_3H_3N	19	a	c
Propanenitrile	C_3H_5N	23	a	c
2-Methylpropanenitrile	C_4H_7N	25		c
Butanenitrile	C_4H_7N	27		c
C_4H_5N isomer	C_4H_5N	24	a	
C_5H_7N isomer	C_5H_7N			
Pentanenitrile	C_5H_9N			
Pentanedinitrile	$C_5H_6N_2$			
Butanedinitrile	$C_4H_4N_2$			
Butanenitrile, 3-dimethyl	C_5H_9N			
Hydrocarbons				
Acetylene	C_2H_2	2	a	b,c,d
Ethylene	C_2H_4	1	a	b,c,d
Ethane	C_2H_6	3	a	b,c,d
Allene	C_3H_4	8		b,c
Propyne	C_3H_4	9	a	b,c,d
Propene	C_3H_6		a	c,d
Propane	C_3H_8	7	a	b,c,d
1-Buten-3-yne	C_4H_4	14		c
C_4H_6 isomer	C_4H_6	18	a	c,d
C_4H_8 isomer	C_4H_8	12		c,d
n-Butane	C_4H_{10}	15		c,d
i-Butane	C_4H_{10}	11		c,d
C_5H_8 isomer	C_5H_8	22		c
C_5H_{10} isomer	C_5H_{10}	20		c,d
n-Pentane	C_5H_{12}	21		c,d
Aromatic species				
Tetrazolo[1,5-*b*]pyridazine	$C_4H_3N_5$	26		
Triazine	$C_3H_3N_3$			
Benzene	C_6H_6		a	c,d
Pyrrole	C_4H_5N			
Other species				
Methanol	CH_3OH	10		
Ethanol	C_2H_5OH			
Acetone	C_2H_6O			

a: Cui et al. (2009), Robertson et al. (2009), and Vuitton et al. (2007).
b: Bernard et al. (2003).
c: Ramírez et al. (2001, 2005).
d: Tran et al. (2005).

3.2.2.3. Oxygen containing compounds. A few oxygen-bearing compounds have also been detected (cf. Table 1) in our experiments: three compounds with low peaks areas (less than 0.1% of the HCN peak area). Those can be explained by the presence of remaining micro-leaks due to the use of a low pressure experiment. Leaks have been measured to be lower than 10^{-3} sccm, four orders of magnitude lower than the 55 sccm injected gas flow rate. The oxygen contamination can thus be considered as negligible in this work.

3.2.2.4. Aromatic species. As shown in Table 1, we have also detected aromatic compounds in the cold trap. These aromatic compounds are however less numerous than reported in other laboratory experiments (Ramírez et al., 2001). This could be due to the GC column used in the present work, which was optimized for the detection of light molecules containing approximately up to 6 carbon or nitrogen atoms.

Moreover, the detected aromatic compounds are mainly heteroaromatics, containing at least one nitrogen atom. The main aromatic species detected is tetrazolo[1,5-*b*]pyridazine which seems to be the bountiful aromatic compound in the gas mixture. The topological formulas of this compound and its experimental mass spectrum compared to theoretical mass spectra from NIST database are shown in Fig. 4.

The formation of tetrazolo[1,5-*b*]pyridazine is not well explained yet. A possible hypothesis could be the addition of propenenitrile (C_3H_3N), one of the most abundant molecules detected in the cold trap, with tetrazole (CH_2N_4). Tetrazole is basically formed by a reaction between hydrogen cyanide (HCN) and N_3^+ but its presence still has to be explained in our case, even if N_3^+ is known to be present in nitrogen plasmas (de Petris et al., 2006).

4. Discussion

4.1. The predominance of nitriles

In order to characterize the evolution of the nature of the chemical species detected in the sample as a function of the injected methane concentration, a qualitative ratio ρ has been defined as $=n\_N/n\_CH$. Where n_N is the number of N-bearing compounds and n_CH is the number of hydrocarbons. Even if this ratio characterizes only the number of detected species and does not take into

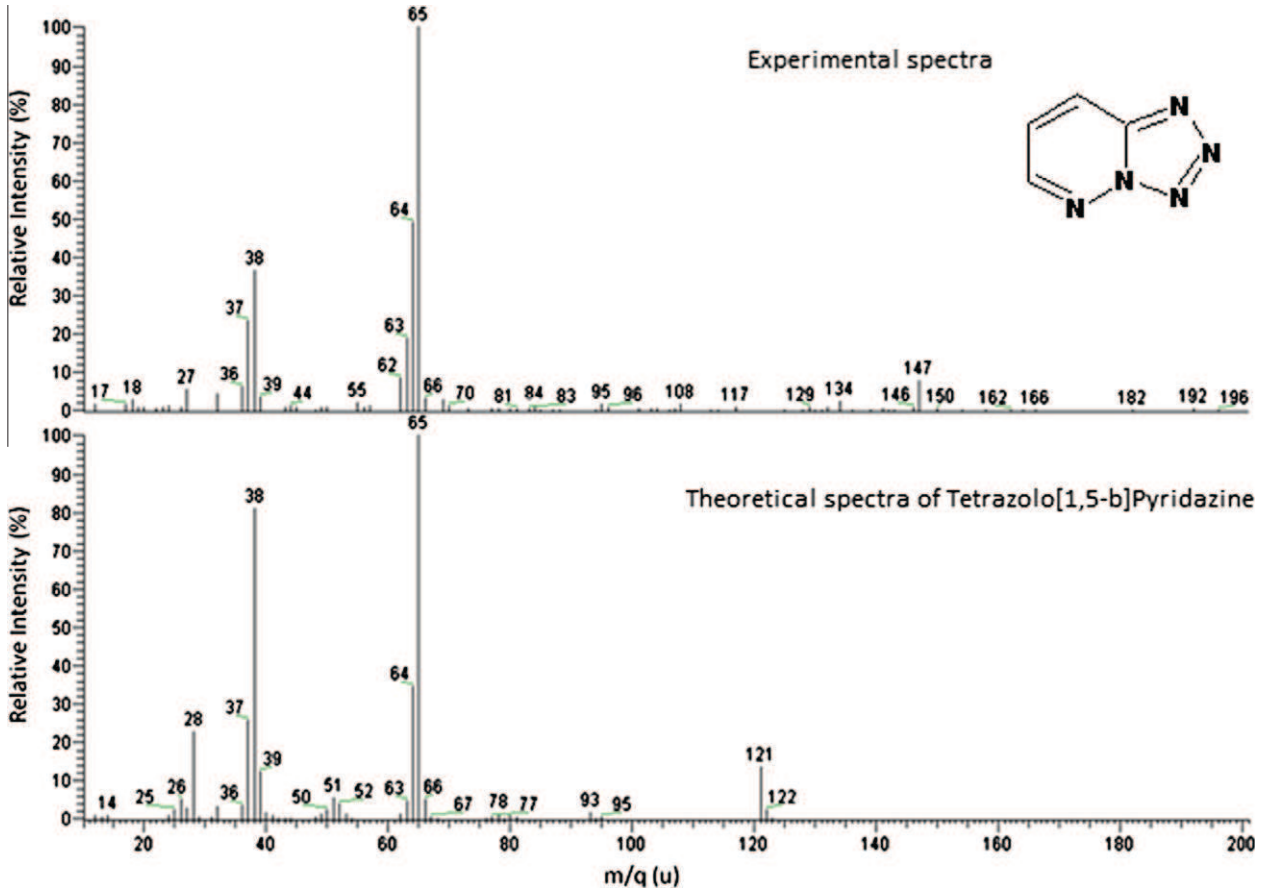

Fig. 4. Experimental (up) and theoretical (down) spectra of tetrazolo[1,5-*b*]pyridazine. The topological scheme of tetrazolo[1,5-*b*]pyridazine is given in the up spectra.

account the relative area of the peaks in the chromatograms, ρ provides a good first-level indicator of the nitrile to hydrocarbon ratio which allows the relative comparison of the results obtained with the three methane concentration chromatograms. The evolution of ρ with the CH_4 concentration is given in Table 2.

As we can see, the value of this ratio shows significant differences between low methane concentrations (1% and 4%) and high methane concentrations (10%). At low CH_4 concentrations the number of nitrile compounds is at least three times higher than the number of hydrocarbons, while at high CH_4 concentrations there are more hydrocarbons than nitriles. This suggests a change in the gas chemistry for the 10% of methane condition, compatible with the gas to solid conversion efficiency studied in Sciamma-O'Brien et al. (2010).

4.2. Discussion on the possible predominance of N-bearing compounds in Titan's aerosols

Even for experiments with ρ values in favor of hydrocarbons (experiments with 10% of methane in the initial mixture), if considering the area of peaks, nitriles are by far the major chemical products in the gas phase. Therefore they are suspected to largely contribute to the chemistry leading to the formation of aerosols in our experiment.

Table 2
Evolution of ρ, the ratio of nitrogen-bearing compounds versus hydrocarbon compounds detected in our experiment as a function of methane concentration of the gas mixture injected in the plasma reactor.

CH_4 concentration	1%	1%	4%	10%	10%
*n*_N	7	11	19	12	16
*n*_CH	2	3	6	15	17
ρ	3.5	3.7	3.2	0.8	0.9

For a long time, Titan's aerosols were considered to be formed by the aggregation of poly-aromatic hydrocarbons (PAH) (Waite et al., 2007). However, for the last few years, several publications have considered that nitrogenous compounds contribute significantly to the aerosol formation process.

This hypothesis is based on several clues. First, the observational data from the Cassini–Huygens mission have shown that there is a large amount of nitrogenous molecules such as nitriles or imines in Titan's atmosphere (Vuitton et al., 2007, 2009; Waite et al., 2007; Yelle et al., 2010). Second, atmospheric chemistry models have also inferred that quite a large amount of nitriles should be present in Titan's atmosphere, even more than hydrocarbons for a given number of atoms (Lebonnois et al., 2001; Hébrard et al., 2006; Lavvas et al., 2008). On the other hand, some observational data analyses have implied that the concentration of nitriles is slightly smaller than the hydrocarbon concentration (Vinatier et al., 2010). Models have also started to formulate hypotheses on the presence of a chemical pathway producing poly aromatic nitrogenous hetero-cycles (PANH), instead of a commonly admitted full PAH pathway in Titan's atmospheric chemistry (Vuitton et al., 2007). This tends to be confirmed by the detection of nitrogen-bearing aromatics in analogs of Titan's aerosols produced in laboratory experiments such as the PAMPRE tholins (Pernot et al., 2010).

4.3. Nitrile reactivity

The laboratory experiments which are capable of dissociating N_2 are known to generate a complex chemistry producing both

hydrocarbons and nitrogenous compounds (Bernard et al., 2003; Imanaka et al., 2004; Tran et al., 2005). Moreover, structural and chemical analyses performed on tholins produced with different laboratory experiments have confirmed that they contain large amounts of nitrogen (Imanaka et al., 2004; Carrasco et al., 2009; Pernot et al., 2010; Sciamma-O'Brien et al., 2010), in agreement with the ACP-Huygens results (Israel et al., 2005).

Despite the detection and the apparent importance of nitrogenous compounds in the formation of tholins (Khare et al., 2002; Hudson and Moore, 2004; Imanaka et al., 2004), the gas chemistry and reactive schemes of nitriles are still largely unknown and largely underestimated in atmospheric models of Titan (Hébrard et al., 2006; Lavvas et al., 2008). The only part of the nitrile chemistry taken into account in some models, deals with reactions between CN radicals or the lightest nitriles and hydrocarbons (Hébrard et al., 2006; Cui et al., 2009).

Even if the agreement between models and observations is not perfect (Hébrard et al., 2007), HCN production is the most understood pathway (Yung, 1987) leading to nitriles in Titan's atmosphere. Several mechanisms have been proposed to produce nitrogen-bearing tholins by polymerization of HCN, CN or CH_3CN (Wilson and Atreya, 2003; Krasnopolsky, 2009), either on a hydrocarbon, to produce a nitrile, or on another nitrile, to produce a dinitrile (Lavvas et al., 2008).

However, it is important to note that even the production of a simple molecule like acetonitrile is still an open question and deserves a particular attention in order to better explain the large densities observed in different regions of Titan's atmosphere. All the recent post-Cassini models use the rate constant from Sato et al. (1999) to describe the kinetics of the reaction between $N(^2D)$ and C_2H_4; but the branching ratios of the reactions have not been quantified yet and can lead to several scenarios implemented in photochemical models. In all cases, this reaction is treated as either the only pathway or at least one of the most important enabling the production of acetonitrile. Wilson and Atreya (2003), Hébrard et al. (2006) and Lavvas et al. (2008) implemented a 100% acetonitrile production pathway, whereas Krasnopolsky (2009) used only a 20% acetonitrile pathway (and 80% for $NH + C_2H_3$). However, the RRKM calculations of Takayanagi et al. (1998) and the molecular crossed-beam experiments of Balucani et al. (2000) predict 2H-azirine and ketene-imine as the major products at low temperature, with a very minor direct production of acetonitrile. It would be useful to do experiments at the temperature range of Titan's atmosphere to try and confirm/quantify if the isomerisation of these two major products towards acetonitrile could explain an efficient production of acetonitrile from the reaction $N(^2D) + C_2H_4$ as suggested by Balucani et al. (2000).

Reactions with CN radical have been widely studied in the last 20 years. Butterfield et al. (1993) have shown that the reactions of CN with allene, butadiene, propylene and propenenitrile can take place in the gas phase. Carty et al. (2001) have confirmed the reaction of CN with allene and they have also added the reaction of CN with methylacetylene. Yang et al. (1992) have studied the reactivity of CN with alkanes (C_2H_6, C_3H_8, C_4H_{10}, C_5H_{12} and C_8H_{18}), while Seki et al. (1996) have studied its reactivity with acetylene and ethanedinitrile. A study of the addition of CN to CH_4, C_2H_6, C_2H_4, C_2H_2 and C_3H_6 can be found in Sims et al. (1993) and the reaction $CN + CH_3CN$ is given in Zabarnick (1989). In addition, Monks et al. (1993) have considered some of the previous reactions in an oxygenated medium, and Hoobler and Leone (1997) have studied the reactions of C_2H with HCN or CH_3CN.

However, due to the lack of knowledge on the nitrile's reactivity, few studies propose other pathways than CN + hydrocarbon to form heavy nitriles. And yet recent CIRS observations compared the nitrile lifetimes at 300 km of altitude predicted by the photochemical model of Wilson and Atreya (2003) with the observed nitrile enrichment in the North polar latitudes of Titan. They have shown an unsuspected specific reactivity of nitriles on Titan (Teanby et al., 2010). Therefore, it is of high priority to study the underestimated reactivity of nitriles, which are known to be very efficient polymerization products in plasma physics (Yu et al., 1988; Lefohn et al., 1998; Bhat and Upadhyay, 2003; Jampala et al., 2008).

Nitriles are rarely considered as reactive molecules. However, knowing how labile the hydrogen in alpha position of a nitrile molecule is (Carey and Sundberg, 2007), it is reasonable to consider that they can be involved in the chemical pathways leading to the production of aerosols in Titan's atmosphere. The energy coming from the solar radiation and/or the Saturn magnetosphere electron bombardment or a chemical reaction with a sufficiently reactive radical could free the alpha hydrogen of a nitrile molecule, as shown in the following scheme. A much more reactive radical would result from these processes, and could play a role in Titan's complex atmospheric chemistry.

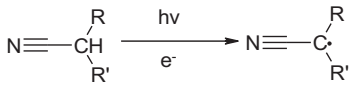

In addition, nitriles could also provide reactive species to form pre-biotic molecules at the surface of Titan or cometary dusts. Particularly, if tholins deposited on Titan's surface could get in contact with liquid water, a hydrolysis reaction would occur, leading to the formation of amino compounds (Khare et al., 1986; Hudson and Moore, 2004; Neish et al., 2010; Ramírez et al., 2010). This contact between tholins and liquid water would be possible since frozen water is abundant at Titan's surface (Tobie et al., 2005). One could expect ice melting from impacts (or cryovolcanism) which may lead to episodic presence of liquid water with a lifetime from 10^2 to 10^4 years (O'Brien et al., 2005).

4.4. Nitrile quantification

4.4.1. Criteria of relative quantification

In the study presented here, a direct quantification of compounds was not possible due to the fact that absolute intensities differed from a chromatogram to another (even for two experiments with the same methane concentration). A quantitative analysis in gas chromatography requires the addition of an internal or external standard in the solute, which was not possible with the configuration of our experimental system. However, by considering each experiment individually, a relative quantification of the nitrile concentrations was achieved.

In order to look for possible growth mechanisms, the area of chromatographic peaks corresponding to nitrile compounds are measured. Only mono-nitriles with a saturated alkyl chain are studied. Dinitriles are excluded because of the two step process they require to be produced. Nitriles with unsaturated radicals are not taken into account either because their formation requires the addition of a CN radical on a pre-existing unsaturated molecule. For example, the formation of propiolonitrile (HC_3N), detected both in Titan's atmosphere and in our experiment, is formed by the addition of CN on acetylene (Seki et al., 1996). In this work we look for new patterns different from the usual CN + hydrocarbons pathway.

Five nitriles correspond to these criteria in our data: hydrogen cyanide (H–CN), acetonitrile (CH_3–CN), propanenitrile (CH_3–CH_2–CN), butanenitrile (CH_3–CH_2–CH_2–CN) and isobutyronitrile ($(CH_3)_2$CHCN).

The chromatographic peak areas of these species are plotted as a function of the number of carbon atoms present in the molecule.

As both butanenitrile and isobutyronitrile contain four carbon atoms, their respective areas are added.

4.4.2. Calibration of the peak areas

As the samples were analyzed through a gas chromatograph coupled with a mass spectrometer, the data collected correspond to peak areas and not directly to the concentration of compounds. To infer the relative concentrations of the nitriles from their area we had to use the ionization cross-section of nitriles.

The mass spectrometer ionizes the molecules by electron impact accelerated at 70 eV. Unfortunately, at this energy, the nitrile ionization cross-sections are still unknown. It is however possible to estimate these cross-sections using the theoretical calculations developed by Fitch and Sauter (1983).

Using their semi-empirical formula the ionization cross-section, Q ($\times 10^{-16}$ cm^2), of a molecule can be calculated based on its atomic composition and on the available experimental ionization cross-sections. This formula is given in the following equation:

$$Q = 0.082 + \sum_{i=1}^{8} \alpha_i n_i \quad (1)$$

where α_i is a coefficient which depends on the type of atom and n_i is the number of atoms for each element. The formula is valid for molecules containing H, C, N, O, F, Cl, Br and I. Coefficients for hydrogen, carbon and nitrogen are, respectively, 0.73×10^{-16} cm^2, 1.43×10^{-16} cm^2 and 1.20×10^{-16} cm^2.

Table 3
Calculated ionization cross-section of the nitriles. The calculation is performed using the formula proposed in Fitch and Sauter (1983).

Compounds	Formula	Q ($\times 10^{-16}$ cm^2)	$\frac{Q_{HCN}}{Q_{RCN}}$
Hydrogen cyanide	HCN	3.442	1
Acetonitrile	C_2H_3N	6.332	0.544
Propanenitrile	C_3H_5N	9.222	0.373
Butanenitrile	C_4H_7N	12.112	0.284
Isobutyronitrile	C_4H_7N	12.112	0.284

Using Eq. (1) we have calculated the ionization cross-section for the five nitriles chosen for the study presented here. They are given in Table 3.

The electron impact ionization cross-sections have an influence on the area of the chromatographic peaks. As a first approximation we consider that the area A of a species s, is directly dependent on the species concentration and on its cross-section: $A_s \propto C_s Q_s$.

As we consider the relative concentrations, the peak area of a hydrocarbon i has to be multiplied by the factor corresponding to the ratio Q_{HCN}/Q_{RCN}. For example, as the cross-section of butanenitrile is approximately four times higher than the one of hydrogen cyanide, the area of the butanenitrile peak has to be divided by four to be compared to the area of the hydrogen cyanide peak.

4.4.3. The nitrile concentration decrease law

After applying this cross-section correction to the areas of the chosen nitrile peaks, the relative nitrile concentrations (HCN area normalized) as a function of the number of carbon atoms in the molecules were plotted.

Fig. 5 shows the relative concentration of the five chosen nitriles seen in Table 3 after correcting their relative concentrations using their respective ionization cross-sections.

The first trend observed on Fig. 5 is the decrease of nitrile concentrations when the number of carbon inside the molecules increases. The shape of this decrease can be modeled with a mathematical power law. The empirical model linked to our data, plotted in Fig. 5, is in good agreement with the experimental data within error bars. Those are estimated at up to 50%, including uncertainties on ionization cross-sections, GC–MS peak areas, reproducibility of the injection protocol in the GC–MS, the production process and trapping in the PAMPRE experiment.

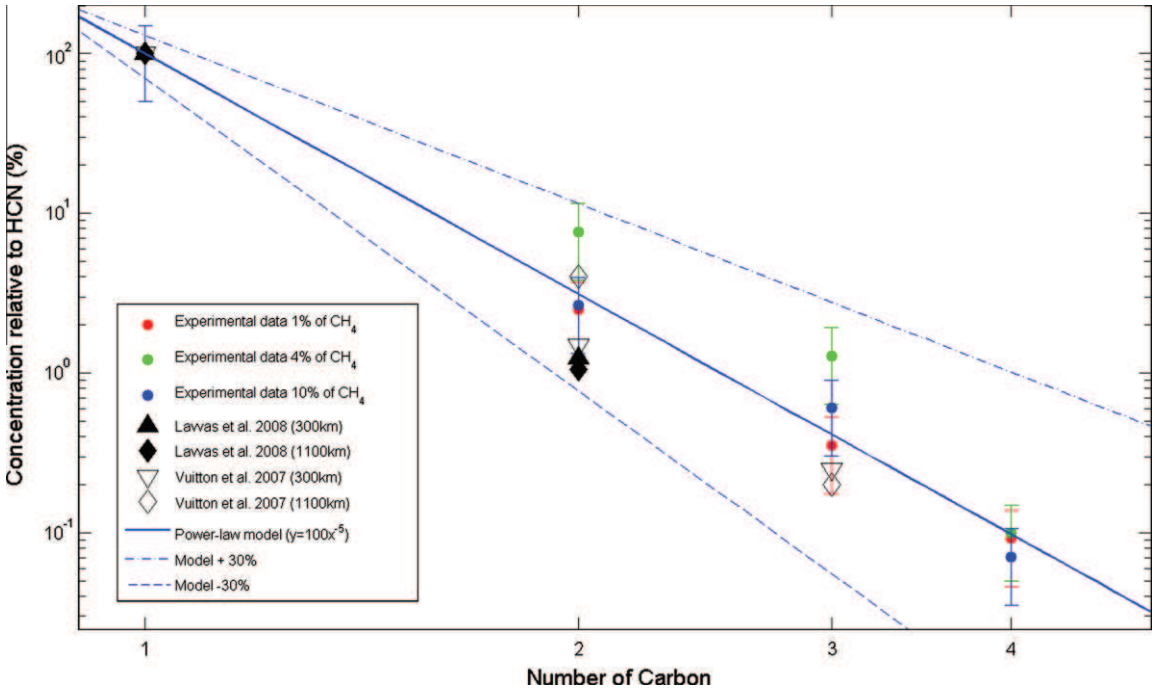

Fig. 5. Relative concentration of the nitriles as a function of the number of carbon in the molecules. The red, green and blue dots represent the experimental data from this work, for experiments with 1%, 4% and 10% of methane in the reactor, respectively. The blue line is the empirical power law model ($y = ax^b$) associated to these experimental data. The dot-dashed line represents the model value plus 30% ($a' = a + 30\%$; $b' = b - 30\%$) while the dashed line is the model value minus 30% ($a'' = a - 30\%$; $b'' = b + 30\%$). The empty black diamonds and triangles are observational data (Vuitton et al., 2007, and reference herein), at 1100 and 300 km from Titan's ground, respectively. The full diamonds and triangles are data from computer modeling (Lavvas et al., 2008) at 1100 and 300 km from Titan's ground, respectively. (For interpretation of the references to color in this figure legend, the reader is referred to the web version of this article.)

This power law decrease shows interdependence between the concentrations of the different nitriles, i.e. the concentration of a $C_xH_{2x-1}CN(x \in \mathbb{N}^*)$ nitrile is first order dependent on the concentration of the $C_{x-1}H_{2x-3}CN$ nitrile.

One can see in Fig. 5 that there are no significant differences between the data sets, whatever the percentage of methane in the experiment. As a consequence a general power law can be extracted from all the experimental data. Eq. (2) gives this power law decrease when HCN is normalized to 100%:

$$[C_xH_{2x-1}N] = 100x^{-5} \quad (2)$$

where x is the number of carbon atoms in a nitrile with saturated carbonaceous radical; $(x \in \mathbb{N}^*)$. Eq. (2) assumes that HCN is normalized to 100%. Using this power law model, it is then possible to estimate the concentration of heavy mono-nitriles with carbonaceous saturated radicals if the concentration of light nitriles is known. As shown in Fig. 5, the experimental data and the associated power law empirical model are also totally consistent with Titan's observational data from INMS (Vuitton et al., 2007) as well as with the results from photochemical models (Lavvas et al., 2008). Eq. (2) can therefore determine the expected concentration of heavy nitriles, not yet detected, in Titan's atmosphere.

Dobrijevic and Dutour (2006) have proposed a power law equation to model the concentration decrease of molecules whose growth comes from the regular addition of a unique monomer. In the same way, we can consider that the power law model we used is also linked to a polymerization scheme of the molecules.

In that case, to come from a $C_{x-1}H_{2x-1}CN$ nitrile to a $C_xH_{2x+1}CN$ nitrile, the required monomer would have to bring one carbon atom and two hydrogen atoms within a linear formula. The intuitive candidate is the methyl fragment, CH_3, which could react with a pre-existing nitrile that lost a hydrogen atom.

Overall, our results highlight that nitriles are reactive compounds, in agreement with the recent CIRS observation by Teanby et al. (2010) and seem to be less inert than implemented in models, where they are mostly considered as chemical reaction sink (Lebonnois et al., 2001; Wilson and Atreya, 2003; Hébrard et al., 2006; Lavvas et al., 2008).

5. Conclusion

Here is presented the first study of the gas phase products in the PAMPRE experiment. We have successfully used a cold trap and GC–MS analysis to deduce the gas composition in a N_2–CH_4 reactive gas mixture simulating Titan's atmosphere.

A large amount of nitriles in the trapped gas mixture has been found, as high as four times the amount of hydrocarbons for a gas mixture with low methane concentration. The main product detected is hydrogen cyanide which has also been detected in large amounts in Titan's atmosphere (Teanby et al., 2007; Vinatier et al., 2010). We have also detected heavier nitriles such as ethanenitrile, propanenitrile and propenenitrile. These heavier nitriles, also detected in Titan's atmosphere, are assumed to be the major compounds in our reactive medium. We have also observed an increase in the ratio between nitriles and hydrocarbons with the decrease of methane concentration in the reactor.

The results of the PAMPRE experiment are consistent with Titan's atmospheric composition, this tends to demonstrate that laboratory experiments, at least those allowing nitrogen dissociation, can be used complementarily to observational data in order to predict both the presence and possible concentrations of compounds which are not yet detected.

On a larger scale, we have detected more than 30 compounds, which, for some of them, had never been detected in experimental simulations before but were expected since they had been observed in Titan atmosphere. Heteroaromatic compounds have also been detected, supporting the hypothesis of PANH pathways for the growth of Titan's aerosols.

The results presented here show the possible importance of nitrogenous compounds in Titan's atmospheric chemistry. With this study we bring more clues to the previously proposed chemical route for aerosol formation in Titan's atmosphere which would predominantly use nitrogen-bearing compounds instead of PAHs (Vuitton et al., 2007; Pernot et al., 2010).

Unfortunately, the nitrile gas chemistry is still mostly unknown, and nitriles are often ignored in Titan atmospheric models even though we know, both from observations and from computational models, that they could be present in large amounts on Titan (Teanby et al., 2007, 2010; Lavvas et al., 2008; Vuitton et al., 2009; Vinatier et al., 2010).

In addition, in the study presented here, we have been able to relatively quantify some of the unsaturated mono-nitriles present in the gas phase. Using this relative quantification we have proposed a power law model for the concentration of radically saturated mono-nitriles, which is (with HCN normalized to 100%) $[C_xH_{2x-1}N] = 100x^{-5}$, where x is the number of carbon atoms in the molecule. With this law, it is possible to estimate the concentration of heavy nitriles due to chemical production (no transport) knowing the concentration of the lighter nitriles.

It will be important in the future to go further and study the possible role of nitriles in Titan's atmospheric chemistry. Indeed, our study suggests that these compounds could have a key role in the formation of organic aerosols in the high atmosphere of Titan, and more generally in the organic chemistry which takes place on Titan. These molecules including nitrogen are also interesting in exobiology since they are known for their reactivity and as precursor of amino acids.

Acknowledgments

This work was financially supported by CNRS (PNP, ANR-09-JCJC-0038 contract) and by the PRES UniverSud. E.S.-O. wishes to thank the CNES for her post-doc position. All the PAMPRE team gratefully thanks Mr. V. Guerrini for the design and the manufacture of the cold trap.

References

Alcouffe, G., Cavarroc, M., Cernogora, G., Ouni, F., Jolly, A., Boufendi, L., Szopa, C., 2010. Capacitively coupled plasma used to simulate Titan's atmospheric chemistry. Plasma Sources Sci. Technol. 19 (1), 015008-1–015008-11.

Balucani, N., Cartechini, L., Alagia, M., Casavecchia, P., Volpi, G.G., 2000. Observation of nitrogen-bearing organic molecules from reactions of nitrogen atoms with hydrocarbons: A crossed beam study of N(2D) + ethylene. J. Phys. Chem. A 104 (24), 5655–5659.

Bar-Nun, A., Dimitrov, V., Tomasko, M., 2008. Titan's aerosols: Comparison between our model and DISR findings. Planet. Space Sci. 56 (5), 708–714.

Barnes, J.W. et al., 2009. VIMS spectral mapping observations of Titan during the Cassini prime mission. Planet. Space Sci. 57 (14–15), 1950–1962.

Bernard, J.-M., Coll, P., Coustenis, A., Raulin, F., 2003. Experimental simulation of Titan's atmosphere: Detection of ammonia and ethylene oxide. Planet. Space Sci. 51, 1003–1011.

Bhat, N.V., Upadhyay, D.J., 2003. Adhesion aspects of plasma polymerized acetonitrile and acrylonitrile on polypropylene surface. Plasmas Polym. 8 (2), 99–118.

Bouchoule, A., 1999. Dusty Plasmas: Physics, Chemistry, and Technological Impact in Plasma Processing. Wiley, 418p.

Butterfield, M.T., Yu, T., Lin, M.C., 1993. Kinetics of CN reactions with allene, butadiene, propylene and acrylonitrile. Chem. Phys. 169, 129–134.

Carey, F., Sundberg, R.J., 2007. Advanced Organic Chemistry, fifth ed. Springer, 1322p.

Carrasco, N., Alcaraz, C., Dutuit, O., Plessis, S., Thissen, R., Vuitton, V., Yelle, R., Pernot, P., 2008. Sensitivity of a Titan ionospheric model to the ion–molecule reaction parameters. Planet. Space Sci. 56 (12), 1644–1657.

Carrasco, N. et al., 2009. Characterization of Titan's tholins: Solubility, morphology and molecular structure revisited. J. Phys. Chem. A 113 (42), 11195–11203.

Carty, D., Page, V.L., Sims, I.R., Smith, I.W.M., 2001. Low temperature rate coefficients for the reactions of CN and C_2H radicals with allene and methyl acetylene. Chem. Phys. Lett. 344, 310–316.

Clarke, D.W., Joseph, J.C., Ferris, J.P., 2000. The design and use of a photochemical flow reactor: A laboratory study of the atmospheric chemistry of cyanoacetylene on Titan. Icarus 147 (1), 282–291.
Cui, J. et al., 2009. Analysis of Titan's neutral upper atmosphere from Cassini Ion Neutral Mass Spectrometer measurements. Icarus 200, 581–615.
de Petris, G., Cartoni, A., Angelini, G., Ursini, O., Bottoni, A., Calvaresi, M., 2006. The N3+ reactivity in ionized gases containing sulfur, nitrogen, and carbon oxides. ChemPhysChem 7 (10), 2105–2114.
Dobrijevic, M., Dutour, I., 2006. A random graphs model for the study of chemical complexity in planetary atmospheres. Planet. Space Sci. 54, 287–295.
Fitch, W.L., Sauter, A.D., 1983. Calculation of relative electron impact total ionization cross sections for organic molecules. Anal. Chem. 55 (6), 832–835.
Hadamcik, E., Renard, J.-B., Alcouffe, G., Levasseur-Regourd, A.C., Szopa, C., 2009. Laboratory light-scattering measurements with Titan's aerosols analogues produced by a dusty plasma. Planet. Space Sci. 57 (13), 1631–1641.
Hartle, R.E. et al., 2006. Initial interpretation of Titan plasma interaction as observed by the Cassini plasma spectrometer: Comparisons with Voyager 1. Planet. Space Sci. 54 (12), 1211–1224.
Hébrard, E., Dobrijevic, M., Bénilan, Y., Raulin, F., 2006. Photochemical kinetics uncertainties in modeling Titan's atmosphere: A review. J. Photochem. Photobiol. C7 (4), 211–230.
Hébrard, E., Dobrijevic, M., Bénilan, Y., Raulin, F., 2007. Photochemical kinetics uncertainties in modeling Titan's atmosphere: First consequences. Planet. Space Sci. 55, 1470–1489.
Hoobler, R.J., Leone, S.R., 1997. Rate coefficients for reactions of ethynyl radical (C_2H) with HCN and CH_3CN: Implications for the formation of complex nitriles on Titan. J. Geophys. Res. 102 (E12), 28717–28723.
Horvath, G., Mason, N., Polachova, L., Zahoran, M., Moravsky, L., Matejcik, S., 2010. Packed bed DBD discharge experiments in admixtures of N_2 and CH_4. Plasma Chem. Plasma Process. 30 (5), 565–577.
Hudson, R.L., Moore, M.H., 2004. Reactions of nitriles in ices relevant to Titan, comets, and the interstellar medium: Formation of cyanate ion, ketenimines and isonitriles. Icarus 172, 466–478.
Imanaka, H., Khare, B.N., Elsila, J.E., Bakes, E.L.O., McKay, C.P., Cruikshank, D.P., Sugita, S., Matsui, T., Zare, R.N., 2004. Laboratory experiments of Titan tholin formed in cold plasma at various pressures: Implications for nitrogen-containing polycyclic aromatic compounds in Titan haze. Icarus 168, 344–366.
Israel, G. et al., 2005. Complex organic matter in Titan's atmospheric aerosols from in situ pyrolysis and analysis. Nature 438 (7069), 796–799.
Jampala, S.N., Sarmadi, M., Manolache, S., Denes, F.S., 2008. Surface functionalization by RF plasma deposition of ethylene diamine, acrylonitrile, and acetonitrile. J. Appl. Polym. Sci. 107 (3), 1686–1695.
Khare, B.N., Sagan, C., Ogino, H., Nagy, B., Er, C., Schram, K.H., Arakawa, E.T., 1986. Amino acids derived from Titan tholins. Icarus 68 (1), 176–184.
Khare, B.N., Bakes, E.L.O., Imanaka, H., McKay, C.P., Cruikshank, D.P., Arakawa, E.T., 2002. Analysis of the time-dependent chemical evolution of Titan haze tholin. Icarus 160, 172–182.
Krasnopolsky, V.A., 2009. A photochemical model of Titan's atmosphere and ionosphere. Icarus 201 (1), 226–256.
Kuiper, 1944. Titan: A satellite with an atmosphere. Astrophys. J. 100 (11), 378–388.
Lavvas, P.P., Coustenis, A., Vardavas, I.M., 2008. Coupling photochemistry with haze formation in Titan's atmosphere, part II: Results and validation with Cassini/Huygens data. Planet. Space Sci. 56 (1), 67–99.
Lebonnois, S., Toublanc, D., Hourdin, F., Rannou, P., 2001. Seasonal variations of Titan's atmospheric composition. Icarus 152 (2), 384–406.
Lefohn, A.E., Mackie, N.M., Fisher, E.R., 1998. Comparison of films deposited from pulsed and continuous wave acetonitrile and acrylonitrile plasmas. Plasmas Polym. 3 (4), 197–209.
Monks, P.S., Romani, P.N., Nesbitt, F.L., Scanlon, M., Stief, L.J., 1993. The kinetics of the formation of nitrile compounds in the atmospheres of Titan and Neptune. J. Geophys. Res. 98 (E9), 17115–17122.
Neish, C.D., Somogyi, A., Smith, M.A., 2010. Titan's primordial soup: Formation of amino acids via low-temperature hydrolysis of tholins. Astrobiology 10 (3), 337–347.
O'Brien, D.P., Lorenz, R.D., Lunine, J.I., 2005. Numerical calculations of the longevity of impact oases on Titan. Icarus 173 (1), 243–253.
Pernot, P., Carrasco, N., Thissen, R., Schmitz-Afonso, I., 2010. Tholinomics – Chemical analysis of nitrogen rich polymers. Anal. Chem. 82 (4), 1371–1380.
Pintassilgo, C.D., Loureiro, J., Cernogora, G., Touzeau, M., 1999. Methane decomposition and active nitrogen in a N_2–CH_4 glow discharge at low pressures. Plasma Sources Sci. Technol. 8 (3), 463–478.
Ramírez, S.I., Navarro-González, R., Coll, P., Raulin, F., 2001. Possible contribution of different energy sources to the production of organics in Titan's atmosphere. Adv. Space Res. 27 (2), 261–270.
Ramírez, S.I., Navarro-González, R., Coll, P., Raulin, F., 2005. Organic chemistry induced by corona discharges in Titan's troposphere: Laboratory simulations. Adv. Space Res. 36 (2), 274–280.
Ramírez, S.I., Coll, P., Buch, A., Brassé, C., Poch, O., Raulin, F., 2010. The fate of aerosols on the surface of Titan. Faraday Discuss. 147, 419–427.
Robertson, I.P. et al., 2009. Structure of Titan's ionosphere: Model comparisons with Cassini data. Planet. Space Sci. 57, 1834–1846.
Sato, K., Misawa, K., Kobayashi, Y., Matsui, M., Tsunashima, S., Kurosaki, Y., Takayanagi, T., 1999. Measurements of thermal rate constants for the reactions of N(2D,2P) with C2H4 and C2D4 between 225 and 292 K. J. Phys. Chem. A103 (43), 8650–8656.
Sciamma-O'Brien, E., Carrasco, N., Szopa, C., Buch, A., Cernogora, G., 2010. Titan's atmosphere: An optimal gas mixture for aerosol production? Icarus 209 (2), 704–714.
Seki, K., Yagi, M., He, M., Halpern, J.B., Okabe, H., 1996. Reaction rates of the CN radical with diacetylene and dicyanoacetylene. Chem. Phys. Lett. 258, 657–662.
Sims, I.R., Queffelec, J.L., Travers, D., Rowe, B.R., Herbert, L.B., Karthäuser, J., Smith, I.W.M., 1993. Rate constants for the reactions of CN with hydrocarbons at low and ultra-low temperatures. Chem. Phys. Lett. 211 (4–5), 461–467.
Sittler Jr., E.C., Ali, A., Cooper, J.F., Hartle, R.E., Johnson, R.E., Coates, A.J., Young, D.T., 2009. Heavy ion formation in Titan's ionosphere: Magnetospheric introduction of free oxygen and a source of Titan's aerosols? Planet. Space Sci. 57 (13), 1547–1557.
Somogyi, A., Oh, C.-H., Smith, M.A., Lunine, J.I., 2005. Organic environments on Saturn's moon, Titan: Simulating chemical reactions and analyzing products by FT-ICR and ion-trap mass spectrometry. J. Am. Soc. Mass Spectrom. 16 (6), 850–859.
Szopa, C., Cernogora, G., Boufendi, L., Correia, J.J., Coll, P., 2006. PAMPRE: A dusty plasma experiment for Titan's tholins production and study. Planet. Space Sci. 54, 394–404.
Takayanagi, T., Kurosaki, Y., Sato, K., Tsunashima, S., 1998. Ab initio molecular orbital calculations for the N(2D) + ethylene reaction. J. Phys. Chem. A 102 (50), 10391–10398.
Teanby, N.A. et al., 2007. Vertical profiles of HCN, HC3N, and C2H2 in Titan's atmosphere derived from Cassini/CIRS data. Icarus 186 (2), 364–384.
Teanby, N.A., Irwin, P.G.J., De Kok, R., Nixon, C.A., 2010. Mappint Titan's HCN in the far infra-red: Implications for photochemistry. Faraday Discuss. 147, 51–64.
Tobie, G., Grasset, O., Lunine, J.I., Mocquet, A., Sotin, C., 2005. Titan's internal structure inferred from a coupled thermal-orbital model. Icarus 175 (2), 496–502.
Tran, B.N., Joseph, J.C., Force, M., Briggs, R.G., Vuitton, V., Ferris, J.P., 2005. Photochemical processes on Titan: Irradiation of mixtures of gases that simulate Titan's atmosphere. Icarus 177 (1), 106–115.
Vinatier, S. et al., 2010. Analysis of Cassini/CIRS limb spectra of Titan acquired during the nominal mission: I. Hydrocarbons, nitriles and CO_2 vertical mixing ratio profiles. Icarus 205 (2), 559–570.
Vuitton, V., Yelle, R.V., McEwan, M.J., 2007. Ion chemistry and N-containing molecules in Titan's upper atmosphere. Icarus 191, 722–742.
Vuitton, V., Lavvas, P., Yelle, R.V., Galand, M., Wellbrock, A., Lewis, G.R., Coates, A.J., Wahlund, J.E., 2009. Negative ion chemistry in Titan's upper atmosphere. Planet. Space Sci. 57 (13), 1558–1572.
Waite, J.H., Young, D.T., Cravens, T.E., Coates, A.J., Crary, F.J., Magee, B., Westlake, J., 2007. The process of tholin formation in Titan's upper atmosphere. Science 316, 870–875.
Wilson, E.H., Atreya, S.K., 2003. Chemical sources of haze formation in Titan's atmosphere. Planet. Space Sci. 51 (14–15), 1017–1033.
Yang, D.L., Yu, T., Wang, N.S., Lin, M.C., 1992. Temperature dependence of cyanogen radical reactions with selected alkanes: CN reactivities towards primary, secondary and tertiary C–H bonds. Chem. Phys. 160, 307–315.
Yelle, R.V., Borggren, N., de la Haye, V., Kasprzak, W.T., Niemann, H.B., Müller-Wodarg, I., Waite, J.J.H., 2006. The vertical structure of Titan's upper atmosphere from Cassini Ion Neutral Mass Spectrometer measurements. Icarus 182 (2), 567–576.
Yelle, R.V., Vuitton, V., Lavvas, P., Klippenstein, S.J., Smith, M.A., Horst, S.M., Cui, J., 2010. Formation of NH3 and CH2NH in Titan's upper atmosphere. Faraday Discuss. 147 (0), 31–49.
Yu, Q., Ye, M., Lu, L., Chen, J., Wang, F., 1988. A study of the polymerization mechanism of acetonitrile in glow discharge. Chin. J. Polym. Sci. 6 (2).
Yung, Y.L., 1987. An update of nitrile photochemistry on Titan. Icarus 72, 468–472.
Zabarnick, S., 1989. Kinetics of $CN(X^2S^+)$ radical reactions with HCN, BrCN and CH3CN. Chem. Phys. 134, 185–191.

Knowledge-based probabilistic representations of branching ratios in chemical networks: The case of dissociative recombinations

Sylvain Plessis,[1] Nathalie Carrasco,[2] and Pascal Pernot[1,3,a)]
[1]*Laboratoire de Chimie Physique, Univ Paris-Sud, UMR 8000, Orsay F-91405, France*
[2]*Laboratoire Atmosphères, Milieux, Observations Spatiales, Université de Versailles Saint-Quentin, UMR 8190, 78280 Guancourt, France*
[3]*CNRS, Orsay F-91405, France*

(Received 11 June 2010; accepted 25 July 2010; published online 5 October 2010)

Experimental data about branching ratios for the products of dissociative recombination of polyatomic ions are presently the unique information source available to modelers of natural or laboratory chemical plasmas. Yet, because of limitations in the measurement techniques, data for many ions are incomplete. In particular, the repartition of hydrogen atoms among the fragments of hydrocarbons ions is often not available. A consequence is that proper implementation of dissociative recombination processes in chemical models is difficult, and many models ignore invaluable data. We propose a novel probabilistic approach based on Dirichlet-type distributions, enabling modelers to fully account for the available information. As an application, we consider the production rate of radicals through dissociative recombination in an ionospheric chemistry model of Titan, the largest moon of Saturn. We show how the complete scheme of dissociative recombination products derived with our method dramatically affects these rates in comparison with the simplistic H-loss mechanism implemented by default in all recent models. © *2010 American Institute of Physics*. [doi:10.1063/1.3479907]

I. INTRODUCTION

Dissociative recombination (DR) of positive ions with free electrons is an important process in highly rarefied and ionized media, such as interstellar clouds,[1–4] upper planetary atmospheres,[5,6] and chemical plasmas.[7–9] DR is the major sink of electrons in ionized media,[10] it is a major pathway for the consumption of ionic species, and it is also an important source of energetic molecules and radicals which can influence significantly the chemical complexification of the system.[8,9] The formation of complex neutral species observed in those media is considered to be largely due to DR.

Models of ion-neutral chemistry generally include DR processes through the reaction rate constant

$$\alpha(T_e) = \alpha_0 \times (T_e/T_0)^{-\beta}, \tag{1}$$

where α_0 is the rate constant at a reference electron temperature T_0 (typically 300 K) and T_e is the electron temperature of interest. When more than one product channel is accessible, the partial rate for channel i is $\alpha_i(T_e)=b_i\times\alpha(T_e)$, where $\{b_i, i=1,N\}$ are the *branching ratios* of the reaction. It is important to note that the global DR rate $\alpha(T_e)$ and the branching ratios $\{b_i\}$ are typically derived from different experiments.

Despite many experimental results in the past years, there are still noticeable difficulties in the modeling of DR processes in complex chemical networks.[11] For instance, the rate of the process depends on the initial state of the ion (electronic and/or rovibrational). In nonthermalized media, as planetary ionospheres, the temperature of electrons is not the only parameter controlling the DR rate and the temperature of ions should also be considered.[10,12] However, within large families of ions, DR rates typically vary within an order of magnitude only and might not be the major source of uncertainty in model predictions.

The main issue in DR modeling is certainly the lack of knowledge about branching ratios. The difficulty of the detection and quantification of neutral fragments, in various isomeric and/or electronic configurations, contributes to this state of affairs. In fact, measured branching ratios have been often proven to be counterintuitive and at odd with the predictions of earlier theories.[13–15] Moreover, data about temperature effects on branching ratios (through collision and/or internal energy) are still very sparse.[11,16,17]

Herbst and co-workers[2,18–20,1,21] extensively explored the impact of DR branching ratios on the chemical composition of interstellar clouds. Based on the theory of Bates,[13–15] they implemented various branching ratios scenario.[2,18,20,1] Herbst and Klemperer[18] first assumed in their model that all products resulting from exoergic channels were produced with equal efficiency, i.e., equal branching ratios. Following Bates,[14] Millar *et al.*[1] based new estimations of branching ratios on the distribution of charges in the parent ion with mitigated success. More recently, as discrepant experimental data about the importance of the H-loss channel became available, they used two alternative scenarios where they attributed a fraction of 0.30 or 0.05 to the H-loss channel, with equipartition among the other channels.[2] An important conclusion of these studies is that branching ratios have a strong impact on steady-state concentrations of neutral species in interstellar clouds. Without a doubt, this can be generalized

a)Electronic mail: pascal.pernot@u-psud.fr.

to other systems where DR drives the fate of ions. Another conclusion is that prediction of DR branching ratios is not yet a routine task.

For the RD of H_3^+ Strasser *et al.*[22] proposed a statistical theory which reproduced nicely existing fragmentation data. However, the transferability of this model to much heavier ions is not straightforward[11] and has not been attempted to our knowledge.

In absence of simple predictive theory, high-level *ab initio* calculations would be the best choice. However, the implication in the process of highly excited electronic states of many open electronic states and the necessity to explore complex potential energy surfaces make it a daunting task. In consequence, accurate quantum or semiclassical calculations are presently limited to very small ions.[17,23–26]

Considering the lack of tractable predictive theories for DR branching ratios of polyatomic ions, experimental data are at the moment the only source of information available to chemical plasma modelers. Several experimental groups made considerable advances in the past decades to produce reference data.[11,16,17] Despite these efforts, we still have very sparse data for molecules with more than four heavy atoms.[16] Even for smaller species, information is often incomplete: For hydrocarbon ions, the distribution of H atoms between fragments is not accessible due to present experimental limitations.[16] This is illustrated in Fig. 1, summarizing the state of knowledge for the products of a middle-sized ion, $C_4H_9^+$. Also, the isomeric form of the parent ion and the isomeric form and electronic state of the neutral products are generally not known.[20] This lack of information about the chemical identity, and therefore the reactivity, of the products of DR can introduce substantial biases in the predictions of chemical models.[27]

It is therefore of utmost importance to be able to incorporate all the knowledge about branching ratios into chemical models. This is not always straightforward, notably when the chemical formulas of the fragments are not fully elucidated.

The present paper addresses the problem of the uncertainty in experimental branching ratios and proposes solutions to enable a realistic implementation of DR in chemical plasma modeling. Probabilistic representations have been designed to account for the various uncertainty patterns identified through an extensive review of literature (Sec. III). In order to deal with incomplete branching ratios data, an innovative representation is based on nested Dirichlet distributions.[28,29] This work extends the previous study by Carrasco and Pernot[30] about the representation of uncertain branching ratios of ion-neutral reactions, where the necessity of a good representation of correlations between these parameters was validated for uncertainty propagation and sensitivity analysis.[27] The theoretical developments are presented in Sec. II A.

The proposed methodology is illustrated on a series of representative ions and applied to the complex ionospheric chemistry of Titan (see Sec. III). In fact, the extreme complexity of DR products formation is in sharp contrast with the fact that none of the ion-neutral coupled models for Titan's ionosphere integrates the multipathway nature of this process.[31–37] With only few exceptions, the present paradigm is to consider the H-loss channel as the only pathway for all H-bearing ions

$$MH^+ + e^- \rightarrow M + H, \tag{2}$$

which is at best a severe approximation. Recent experimental studies have clearly shown that DR could not only break bonds between heavy atoms efficiently but also break more than one bond.[11,16,17] As our probabilistic approach enables to implement a DR scheme accounting for all plausible pathways, we tested it in a ionospheric chemistry model of Titan,[38,27] comparing the results to those of the H-loss approximation.

II. PROBABILISTIC REPRESENTATIONS OF BRANCHING RATIOS

A. Methods

The methodological framework is based on the representation of uncertain parameters by probability density functions (pdfs). These pdfs are then used as inputs in chemical models and processed with Monte Carlo uncertainty propagation (MCUP)[39,40] as follows.

1. Monte Carlo uncertainty propagation

For a model F having as input a vector of uncertain variables $\mathbf{X}=(X_1,\ldots,X_n)$,

$$Y = F(\mathbf{X}) = F(X_1,\ldots,X_n), \tag{3}$$

the probability density on the values of Y is obtained by the Markov integral

$$p(Y=y) = \int d\mathbf{X}\,\delta(y - F(\mathbf{X}))p(\mathbf{X}), \tag{4}$$

where $p(\mathbf{X})$ is the joint pdf of the input variables. Equation (4) can rarely be solved analytically. Instead, we use the Monte Carlo approach which is defined as a standard by supplement 1 to the "Guide to the expression of uncertainty in measurement data."[39] The principle is simple: one generates a set $\{x_{1,i},\ldots,x_{n,i}\}$ of $i=1, N_{\text{run}}$ random draws from the n-dimensional input pdf $p(\mathbf{X})$, and for each element of this set, one computes the value of the model output, generating a representative sample of the output pdf $p(Y)$. This sample $\{y_i\}$ is then used to get statistical estimates of quantities of interest. MCUP has been frequently used in chemical modeling to assess the effect of reaction rates' uncertainty on the concentrations of species.[41–53]

2. Probability density function of the uncertain variables

The inputs for different reactions are typically independent,[54] which enables to factorize the input pdf reactionwise,

$$p(\mathbf{X}) = \prod_r p(\alpha_0^{(r)}, \beta^{(r)}, b_1^{(r)},\ldots,b_{n_r}^{(r)}). \tag{5}$$

For a given DR reaction (r), branching ratios and reaction rates are measured independently, branching ratios are corre-

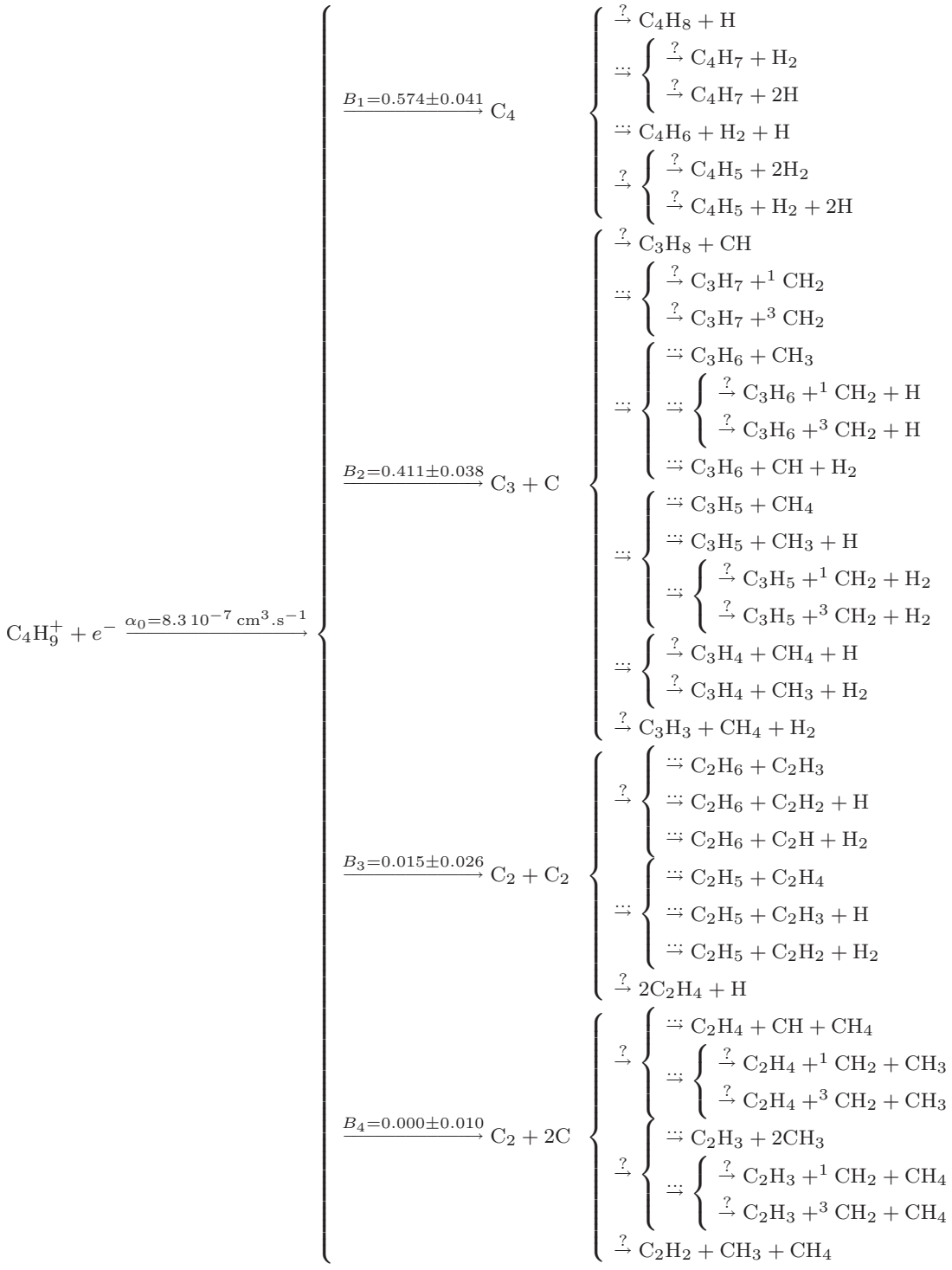

FIG. 1. Tree structure of the putative products for the DR of $C_4H_9^+$. The first level implements available experimental data about the carbon fragmentation pattern (Ref. 16); deeper levels are built according to a list of exoergic channels and the list of species involved in the chemical system of interest. The deep tree structure presented here is obtained according to a heuristic explained in the text.

lated by the sum-to-one constraint, and the rate parameters might also be correlated by the fitting procedure, leading to a further factorization

$$p(\mathbf{X}) = \prod_r p(\alpha_0^{(r)}, \beta^{(r)}) p(b_1^{(r)}, \ldots, b_{n_r}^{(r)}). \quad (6)$$

When treating individual DR processes, we will simplify the notations by omitting the (r) superscript. Our aim in this paper being to study branching ratios and their uncertainties, the DR rate coefficients were fixed at their nominal value, i.e.,

$$p(\mathbf{X}) = \prod_r p(b_1^{(r)}, \ldots, b_{n_r}^{(r)}). \quad (7)$$

In the following, we consider the problem of finding adequate representations for the probability density function of

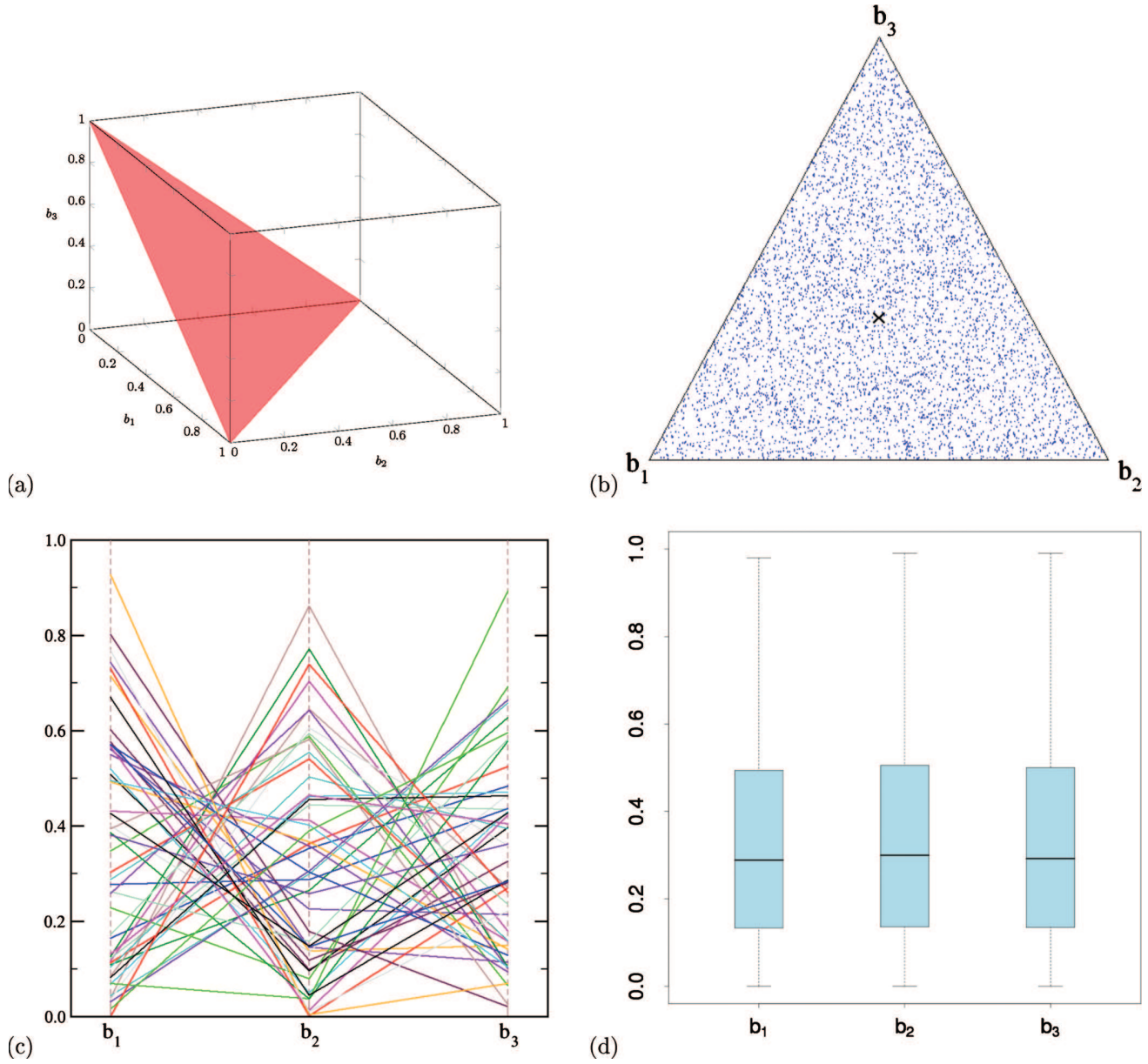

FIG. 2. (a) Visualization of the simplex in a three-dimensional space (b_1, b_2, b_3) and alternative representations of a sample of the uniform distribution within this simplex: (b) ternary graph, (c) parallel graph, and (d) boxplots for the one-dimensional marginal densities $p(b_i)$, $i=1,3$.

individual sets of branching ratios $p(b_1, \ldots, b_n)$, which are consistent with available information and constraints.

B. Space of branching ratios and graphical representations

Branching ratios of a reaction form a *composition*, such as $0 \leq b_i \leq 1$ and $\Sigma_{i=1}^{n} b_i = 1$.[55] The sum-to-one is a major property to be preserved in the representation of branching ratios in chemical networks.[27,30] It introduces a strong negative correlation between the b_i, which cannot be ignored in statistical operations.

The points of a n-dimensional set of branching ratios lie in a subspace of dimension $n-1$ called a *simplex* [see Fig. 2(a)]. In a three-dimensional (3D) space, the simplex is an equilateral triangle. The corner labeled b_i corresponds to the composition $\{b_i=1,\ b_{j\neq i}=0\}$. In this 3D case, probability density functions or representative random samples can be conveniently plotted in a ternary graph, where each point corresponds to an element of the sample [Fig. 2(b)]. For spaces of higher dimensions, we rather use alternative representations such as parallel graphs where the coordinates of each point are drawn on separate parallel vertical axes and linked by a line [Fig. 2(c)]. This kind of graph can convey a lot of information, but makes it difficult to appreciate, for instance, the sampling uniformity in the simplex.

A third representation used in the following is built on the parallel graph basis but displays boxplots of the individual one-dimensional (marginal) densities instead of line sets [Fig. 2(d)]. It is quite convenient to use for comparison of samples, but all information about correlations between the branching ratios is erased.

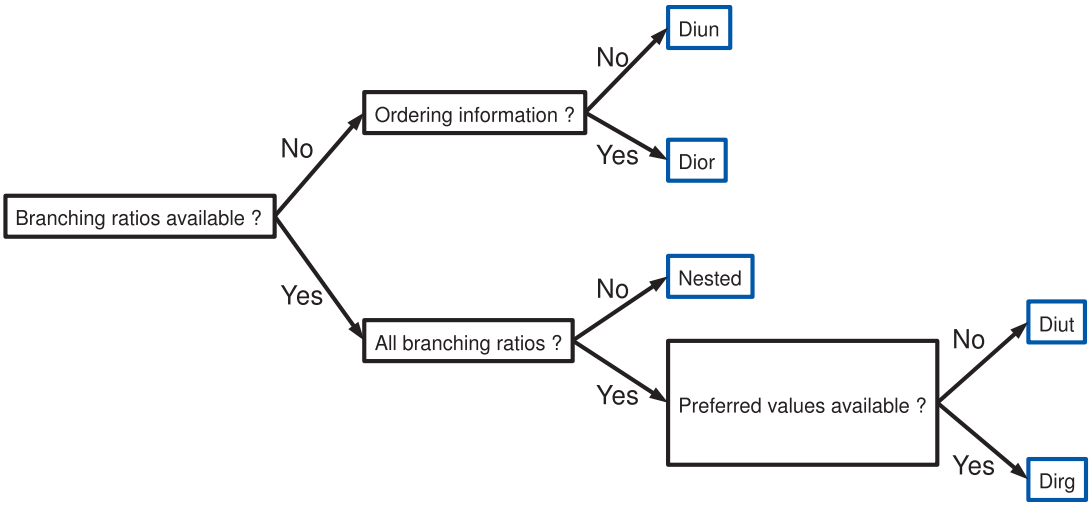

FIG. 3. Decision tree for the choice of a Dirichlet-type distribution.

Another point to have in mind when appreciating these graphs is that the one-dimensional marginal densities from a uniform pdf in a simplex are *not* uniform. It is enlightening to compare the information conveyed by the ternary graph of Fig. 2(b) and the boxplot graph of Fig. 2(d), obtained from identical samples.

C. Elicitation of probability density functions for branching ratios

The design of probability density functions from available information is called *elicitation*.[56] It is a key stage in the MCUP process for which the principle of maximum entropy (PME) provides a reference tool.[57] As there are typically an infinity of pdfs obeying to a limited set of constraints, the PME enables to disambiguate the problem in providing a unique pdf. Standard elicitations based on the PME have been defined, mostly for single variable problems.[39] For instance, if an average value and a standard deviation are available, the reference pdf is a Gaussian/normal distribution. For correlated parameters, the multivariate Gaussian is obtained from a vector of best estimates and a strictly positive variance/covariance matrix. With minimal constraints of positivity and sum-to-one, the PME defines the Dirichlet distribution.[57–59]

A review of DR reactions for ions included in state-of-the-art models of Titan's ionosphere was performed in order to identify representative uncertainty/information patterns for branching ratios. These cases range from sets of preferred values and standard deviations, to intervals, to no information, i.e., unidentified products or unknown branching ratios for known products. All these cases can be successfully handled through distributions in the Dirichlet family and combinations thereof. We consider successively the cases where we have (i) preferred values and the associated uncertainties, (ii) intervals, (iii) no information, (iv) no numerical information but an ordering scheme, and (v) sets of incomplete or heterogeneous data. A decision tree (Fig. 3) has been designed to help the user to choose the appropriate distribution. Sampling methods for these distributions are described in the Appendix.

1. Preferred values and uncertainties: Dirg representation

To sample uncertain branching ratios for ion-molecule reactions, Carrasco and Pernot[30] used the standard Dirichlet distribution (Diri),

$$\{b_1, \ldots, b_n\} \sim \mathrm{Diri}(\mu_1, \ldots, \mu_n; \gamma), \tag{8}$$

where μ_i is the preferred value for branching ratio b_i and γ is a global accuracy factor optimized to reproduce, at best in the least-squares sense, the global relative uncertainty r on the branching ratios proposed in reference databases,[60,61]

$$\gamma = \frac{4}{r^2}\left(\frac{\Sigma_i \mu_i(1-\mu_i)}{\Sigma_i \mu_i \sqrt{\mu_i(1-\mu_i)}}\right)^2 - 1. \tag{9}$$

The Diri distribution represents the fluctuations of quantities independent of each other, under the condition that their sum remains fixed.[58]

This elicitation method reproduces exactly the mean values, but it cannot perfectly reproduce a uniform relative uncertainty for all channels. For dissociative recombination channels, uncertainty statements are often more detailed than a global relative uncertainty; in the best cases, one even has a standard uncertainty per channel, u_i. Being isotropic in the $(n-1)$-simplex [see Fig. 4(a)], the standard Dirichlet distribution cannot properly account for this information, and we found necessary to use a more flexible distribution.

Generalization of the Dirichlet distribution is an active research area in statistics.[62–64] We use here the generalization proposed in Ref. 64. Compared to the Dirichlet distribution, the generalized Dirichlet distribution

$$\{b_1, \ldots, b_n\} \sim \mathrm{Dirg}(\mu_1, \ldots, \mu_n; u_1, \ldots, u_n) \tag{10}$$

enables more anisotropy in the $(n-1)$-simplex, through a differentiated treatment of the generating gamma distributions

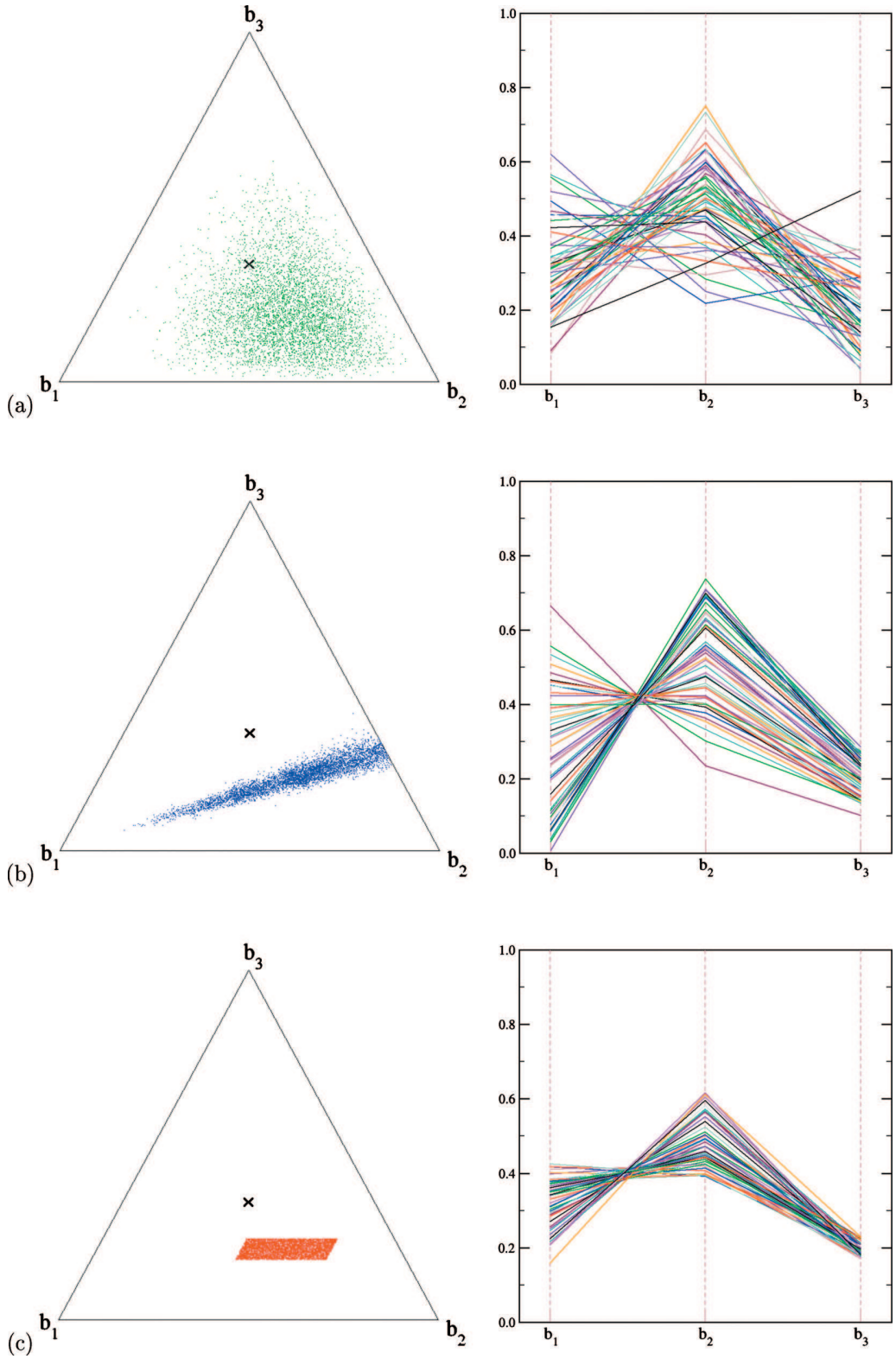

FIG. 4. Ternary (left) and parallel (right) graphs of samples of Dirichlet-type distributions for a set of three branching ratios $\{b_1, b_2, b_3\}$ to represent the following information $b_1 = 0.30 \pm 0.30$, $b_2 = 0.50 \pm 0.04$, and $b_3 = 0.20 \pm 0.01$: (a) Diri(0.3,0.5,0.2;13.7), (b) Dirg(0.3,0.5,0.2;0.3,0.04,0.01), and (c) Diut([0.00,1.00],[0.38,0.62],[0.17,0.23]).

(see Appendix). Here again, the sum-to-one constraint prevents to fully preserve the input uncertainties u_i, but we found this sampling technique to be satisfactory for our purpose.

As an example, considering a set of three branching ratios ($b_1 = 0.30 \pm 0.30$, $b_2 = 0.50 \pm 0.04$, and $b_3 = 0.20 \pm 0.01$) a comparison of samples in the two-dimensional simplex for the corresponding Diri(0.3,0.5,0.2; 13.7) [the value $\gamma = 13.7$

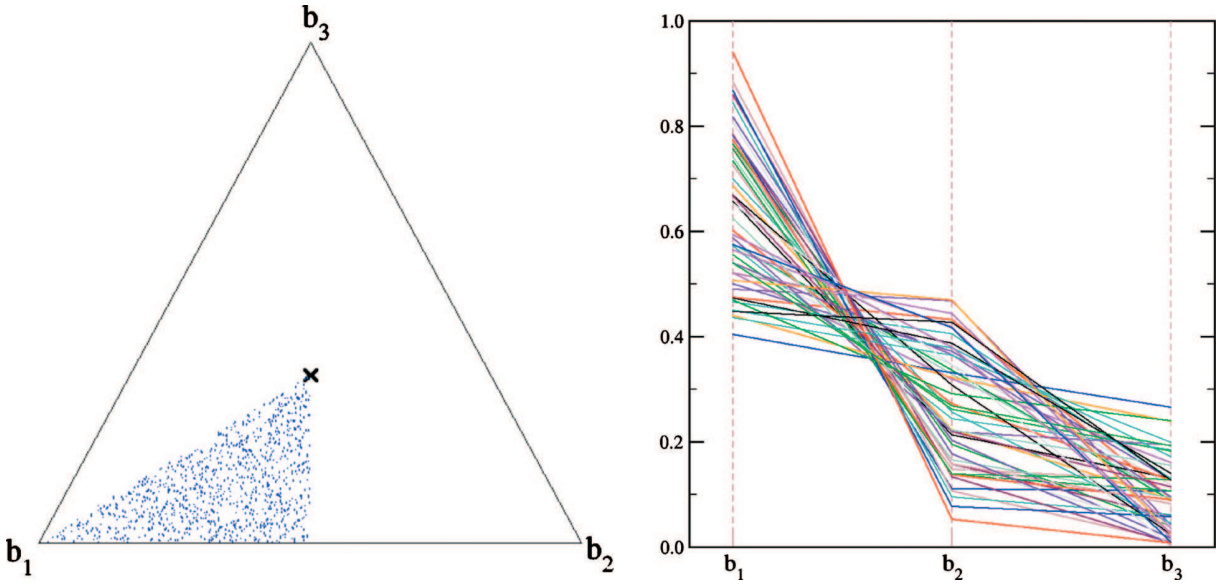

FIG. 5. Dirichlet distributions for a set of three branching ratios $\{b_1,b_2,b_3\}$ when only ordering information $(b_1 \geq b_2 \geq b_3)$ is available: Dior(3).

results from Eq. (9)] and Dirg(0.3,0.5,0.2; 0.3,0.04,0.01) distributions is shown in Figs. 4(a) and 4(b), as ternary graphs and parallel graphs. One can see how, starting from the same information, the Dirg distribution enables an anisotropic sampling more representative of the data constraints than the Diri distribution.

2. Intervals: Diut representation

In some instances branching ratios are defined by limits, without explicit reference to a preferred value: $b_i \in [b_i^{\min}, b_i^{\max}]$. The corresponding distribution is called Diut (from Dirichlet uniform truncated) and noted

$$\{b_1, \ldots, b_n\} \sim \text{Diut}([b_1^{\min}, b_1^{\max}], \ldots, [b_n^{\min}, b_n^{\max}]). \quad (11)$$

As an example, for comparison of Diut sampling with Dirg, we build intervals from the mean values μ_i and standard uncertainties u_i provided in the previous example, using 3σ intervals, i.e., $b_i = \mu_i \pm u_i \rightarrow b_i \in [\mu_i - 3u_i, \mu_i + 3u_i]$. The corresponding distribution is therefore Diut([0.00,1.00],[0.38,0.62],[0.17,0.23]); a sample is shown in Fig. 4(c). It can be seen that the initial interval constraints cannot be globally verified within the simplex, leading to reduced intervals for some variables. In this example, the interval for b_1 is much smaller than prescribed. This is a consequence of the prevailing constraint that the variables should have a null probability to be *outside* the prescribed intervals, i.e., the smaller intervals impose their rule. This type of elicitation should thus be avoided when the prescribed intervals have very different ranges $(b_i^{\max} - b_i^{\min})$.

3. No information: Diun representation

In the absence of information about a set of n branching ratios, one uses a *uniform* pdf over the $(n-1)$-dimensional simplex, i.e., a distribution which does not favor any value or set of values [see Fig. 2(b)]. The uniform Dirichlet (Diun) can be obtained as a special case of the Diri distribution,

$$\{b_1, \ldots, b_n\} \sim \text{Diun}(n) \equiv \text{Diri}(1/n, \ldots, 1/n; n). \quad (12)$$

Note that the Diri-type notation for the Diun distribution is preserved for use in the case of nested distributions, as shown below.

4. No information, except for an order constraint: Dior representation

Statistical and/or thermodynamical considerations are sometimes used to order the putative branching ratios of a set of channels. In such cases where the only information is provided by an ordering of the branching ratios $b_1 \geq b_2 \geq \cdots \geq b_n$, we use a uniform Diun sampling and reorder the outputs to conform with the constraint:

$$\{b_1, \ldots, b_n\} \sim \text{Dior}(n) = \text{sort}(\text{Diun}(n)). \quad (13)$$

Figure 5(b) presents the Dior distribution for three variables, with $b_1 \geq b_2 \geq b_3$.

5. Heterogeneous data sources or incomplete information about branching ratios subsets: Nested Dirichlet

In some instances, the full set of branching ratios for a reaction comes from separate experiments, and in many instances, the set of branching ratios is incomplete, with total indetermination between subsets of products. Such cases cannot be handled by any of the elementary distributions presented above and require a specific treatment.

Let us consider an example where one experiment measured the relative efficiencies of the productions of $M_1 + M_2$ (B_1) and M_3 $(B_3 = 1 - B_1)$. Another experiment, independent of the first one, was able to measure the branching ratios between M_1 (B_{11}) and M_2 $(B_{12} = 1 - B_{11})$. Each experiment comes with its own set of uncertainty ΔB_i, which should be preserved as well as possible when generating branching ratios for the whole set of products. A schematic representation of this information would be

$$I^+ + e^- \begin{cases} \xrightarrow{B_1 \pm \Delta B_1} \begin{cases} \xrightarrow{B_{11} \pm \Delta B_{11}} M_1 \\ \xrightarrow{B_{12} \pm \Delta B_{12}} M_2 \end{cases} \\ \xrightarrow{B_3 \pm \Delta B_3} M_3 \end{cases} . \quad (14)$$

The final branching ratios for M_1, M_2, and M_3 can be computed from both data sets

$$\begin{aligned} \mu_1 &= B_1 \times B_{11}, \\ \mu_2 &= B_1 \times B_{12}, \\ \mu_3 &= B_3. \end{aligned} \quad (15)$$

An option to calculate the uncertainty on the final branching ratios is to use the standard law of combination of variances,[65] i.e.,

$$\frac{u_i}{\mu_i} = \sqrt{\left(\frac{\Delta B_1}{B_1}\right)^2 + \left(\frac{\Delta B_{1i}}{B_{1i}}\right)^2}; \quad i = 1,2, \quad (16)$$

and to transform the nested scheme [Eq. (14)] into a "one-level" scheme,

$$I^+ + e^- \begin{cases} \xrightarrow{\mu_1 \pm u_1} M_1 \\ \xrightarrow{\mu_2 \pm u_2} M_2 \\ \xrightarrow{\mu_3 \pm u_3} M_3 \end{cases} , \quad (17)$$

with the distribution

$$\{b_1, b_2, b_3\} \sim \mathrm{Dirg}(\mu_1, \mu_2, \mu_3; u_1, u_2, u_3). \quad (18)$$

We stress out that this method is not reliable when large uncertainties are involved, as is often the case for DR branching ratios. As the original correlations between the pathways are wiped out, the structure of the distribution is affected, with unpredictable effects on uncertainty propagation and sensitivity analysis.[27,30]

In order to ensure the preservation and proper treatment of the initial information tree, we propose to use a nested Dirichlet distribution,[28,29]

$$\{b_1, b_2, b_3\} \sim \mathrm{Dirg}(B_1 \otimes \mathrm{Dirg}(B_{11}, B_{12}; \Delta B_{11}, \Delta B_{12}), B_3 ; \Delta B_1, \Delta B_3), \quad (19)$$

reproducing the tree structure of the data [Eq. (14)]. We use the $\otimes$ symbol to emphasize that the previous notation does imply a specific function composition, i.e., the values sampled from the external Dirg distribution *do not* depend on the values sampled from the internal distribution. In practice, both sets of random numbers are sampled independently, and then, the necessary products are performed according to Eq. (15).

This construction becomes mandatory when the set of branching ratios contains subsets with total uncertainty. In our example, let us assume that only the set $\{B_1, B_3\}$ is characterized by experimental data, and that the subset of products $\{M_1, M_2\}$ is inferred from energetics considerations without information on the values of the branching ratios $\{B_{11}, B_{12}\}$. This structure can be represented by the distribution

$$\{b_1, b_2, b_3\} \sim \mathrm{Dirg}(B_1 \otimes \mathrm{Diun}(2), B_3; \Delta B_1, \Delta B_3). \quad (20)$$

Figure 6 shows the difference between the nested Dirichlet sampling and the one-level sampling [Eq. (18)] with the values $B_1 = 0.6 \pm 0.1$, $B_3 = 0.4 \pm 0.05$, and $B_{11} \in [0,1]$, $B_{12} \in [0,1]$. It compares samples of the distributions

$$\{b_1, b_2, b_3\} \sim \mathrm{Dirg}(0.6 \otimes \mathrm{Diun}(2), 0.4; 0.1, 0.05) \quad (21)$$

and

$$\{b_1, b_2, b_3\} \sim \mathrm{Dirg}(0.30, 0.30, 0.40; 0.18, 0.18, 0.05), \quad (22)$$

where the parameters are derived using Eqs. (15) and (16) and $B_{11} = B_{12} = 0.5$ as mean value and $\Delta B_{11} = \Delta B_{12} = \sqrt{1/12}$ as standard deviation for the unit square distribution.[39] Due to the large and dominant uncertainty on b_1 and b_2, the one-level model [Eq. (22)] is unable to preserve the accurate information about b_3, and enables a too high proportion of M_3, incompatible with the initial data. In contrast, this accurate information about b_3 is preserved by the nested Dirichlet representation, along with the indetermination between b_1 and b_2.

The nested Dirichlet approach is very flexible and offers a very powerful technique: (i) to preserve the statistical independence of complementary experimental information about branching ratios and (ii) to implement partial knowledge into kinetic modeling. All the Dirichlet-type distributions presented above can be nested, to any level, as required by experimental data.

III. APPLICATIONS

This work was motivated by the study of the impact of uncertain chemical parameters on the predicted densities of ions and neutral species in Titan's ionosphere.[27,30,38,52,66,67] In a first part, we present the guidelines we followed to build our database of dissociative recombinations for Titan's ionosphere. This is illustrated by representative examples of individual reactions extracted from the database. In a second part, we turn to the model of Titan's ionospheric chemistry and compare the production rates of neutral species calculated with the "full model," as enabled by the Dirichlet approach, with the simplistic H-loss scenario, generated as a subset of the previous one.

A. A database of DR for Titan's ionosphere

Because uncertainty about branching ratios is not readily available in reference databases or review articles, a thorough review of literature has been done to build the data set used in this work. The focus has been set on the ions identified in Titan's ionosphere, as listed in Table II.

The starting points for our literature search were the UMIST database,[68] the OSU database,[69] the dissociative recombination database of the molecular physics group of Stockholm University,[70] and the review articles by Florescu-Mitchell and Mitchell[16] and Adams *et al.*[71] A search of various bibliographic databases was performed to find the most recent references. The full data set, including DR rate constants and the relevant references, is provided as Supplementary Material.[72]

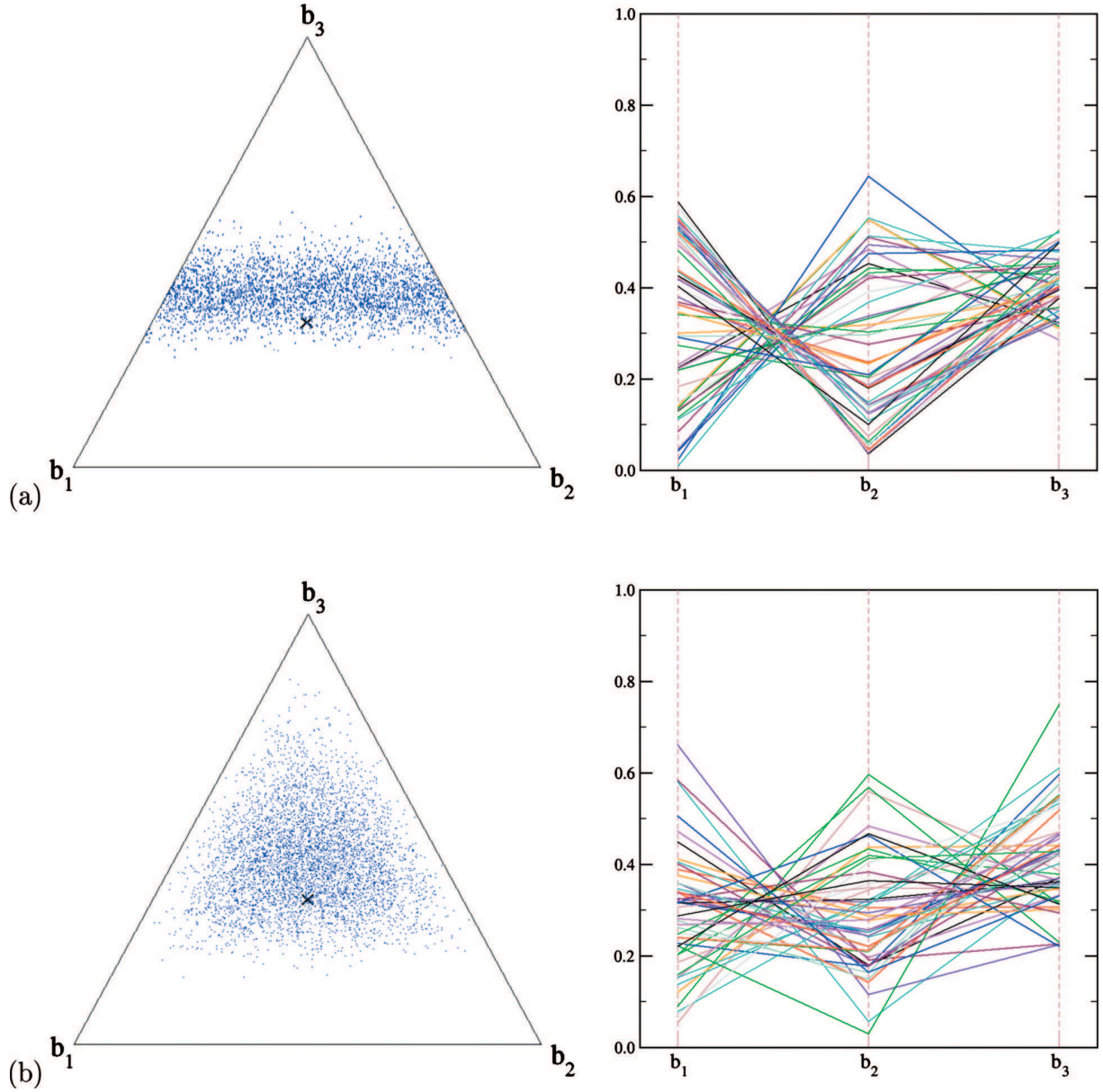

FIG. 6. Comparison of two representations for the consolidation of complementary branching ratios information (see text for details): (a) $\{b_1,b_2,b_3\} \sim \mathrm{Dirg}(0.6 \otimes \mathrm{Diun}(2),0.4;0.1,0.05)$ and (b) $\{b_1,b_2,b_3\} \sim \mathrm{Dirg}(0.30,0.30,0.40;0.18,0.18,0.05)$.

1. Rate constants

The present article being focused on branching ratios and their uncertainties, the DR rate coefficients were taken at their nominal value in the following simulations. The various issues in the treatment of uncertainty of DR rate constants will be treated in a future article. The guidelines we followed to establish the nominal values for both rate parameters α_0 and β in Eq. (1) are described here.

a. DR rate at reference temperature: α_0

- When a single reference value was available, it was taken at face value.
- When several reference values were found:

(1) with discrepant values: the most recent was considered;

(2) with compatible values: the mean value of a loguniform distribution covering all values was used. This was retained to compensate the absence of uncertainty statement in some references.

- When no reference values were available, we used the mean values of loguniform distributions covering intervals with limits defined by existing rates for similar ions:

(1) for light species (less than three heavy atoms) the interval is $[5\times10^{-8},1\times10^{-6}]$ $\mathrm{cm}^3\cdot\mathrm{s}^{-1}$, and the nominal value is 2.24×10^{-7} $\mathrm{cm}^3\cdot\mathrm{s}^{-1}$, e.g., NH_2^+;

(2) for heavy species, presenting generally enhanced reaction rates, the interval is $[5\times10^{-7},3\times10^{-6}]$ $\mathrm{cm}^3\cdot\mathrm{s}^{-1}$,

and the nominal value is 1.22×10^{-6} $cm^3\cdot s^{-1}$, e.g., $C_3H_5^+$, $C_4H_7^+$,…

b. Temperature dependence: β

- When a single reference value was available, it was taken at face value.
- When several reference values were found, we used the mean of a uniform interval covering these values, i.e., $\beta=(\beta_{min}+\beta_{max})/2$.
- When no reference values were available, the mean value of the largest interval as defined by the theoretical values of β for direct and indirect processes was used, i.e., $\beta=(0.5+1.5)/2=1$.

We want to emphasize that these choices can certainly be improved. Evaluation by committees of experts, as in other fields of chemical kinetics, would be most welcome. Moreover, our deliberate use of intervals as the basis of reference value evaluation is motivated by our needs to consider uncertainties in these rate parameters for future work.

2. Branching ratios

Information on branching ratios is typically sparser than on reaction rates, and it is exceptional to have to consider conflicting data. The assignments are therefore mostly based on the rules defined in the decision tree (Fig. 3). However, the following set of considerations is used in order to define the structures of the (nested) Dirichlet distributions.

a. Maximum number of fragments. In absence of experimentally characterized products, one should consider all the exoergic channels and state a total lack of knowledge on the corresponding branching ratios (Diun distribution). It is not possible to make further hypothesizes with respect to the relative stability of the products. From Ref. 16, we know for instance that the measured branching ratios have no definite correlation with the exoergicity of the pathways. An issue in building a list of exoergic pathways is the number of fragments that can be accepted in each pathway. For instance, on the basis of their previous results, for $C_3H_7^+$ Ehlerding *et al.*[73] stopped at a three body breakup pattern, even though some four body channels are opened ($C_3H_3+H_2+2H$, $C_2H_2+CH_3+2H$). Other authors considered also four body breakup patterns in their analysis: CD_3CDO^+,[74] CD_3CND^+,[75] and CH_2CHCNH^+.[76] In the present treatment, we favored exhaustivity and enabled four body breakups when possible.

b. H_2 *vs* 2H. An empirical rule appears throughout the database of branching ratios: the loss of 2 H atoms is generally more probable than the loss of a H_2 molecule. The only measured exception are NH_4^+ and to some extent $C_2D_5^+$. As showed by Strasser *et al.*[77] through statistical modeling of the branching ratios of H_3^+, a fraction of the observed H atoms might come from the fragmentation of the H_2 product, which is created with enough internal energy to breakup through predissociative states. This rule can be used to reduce uncertainty by nesting both pathways within a Dior distribution.

c. Heavy fragments as a basis for nesting. A corollary of the previous rule is that we are often induced to nest together pathways involving the same heavy fragment (e.g., X+2H and $X+H_2$). For hydrocarbons, and in the absence of experimental values, we adopted this as a general guideline to ensure an equilibrated treatment of the heavy fragments. This rule becomes ambiguous for N-bearing molecules and was not generalized to them.

The impact of these rules on the production rates of neutral species is discussed in the next sections.

It is to be noted that by default, all branching ratios are given for zero collision energy. If these data were to be used for systems where this is not representative, the list of open dissociation channels might have to be reconsidered and an additional uncertainty/bias factor should be attached to the measured data. At the moment, we have no information on how this contribution could be designed: It is probably very ion-dependent.

B. Case studies

1. CH_2^+

a. Information. Larsson and collaborators[78] measured the branching ratios for the DR of CH_2^+ in the CRYRING storage ring, and reported preferred values with uncertainty for all the pathways: $b_1(C+H_2)=0.12\pm0.02$, $b_2(C+2H)=0.63\pm0.06$, and $b_3(CH+H)=0.25\pm0.04$.

b. Representation. As we have the complete information on branching ratios and their uncertainties, this is a straightforward case where a Dirg distribution is well adapted,

$$\{b_1,b_2,b_3\}\sim \mathrm{Dirg}(0.12,0.63,0.25;0.02,0.06,0.04). \quad (23)$$

A sample of this distribution can be seen in Figs. 7(a) and 7(b).

2. NH_2^+

a. Information. This is an interesting case where we have to combine two sets of branching ratios coming from different experiments. The main channels have been measured first $B_1(N+H_2)=0.04\pm0.03$, $B_2(N+2H)=0.58\pm0.09$, and $B_3(NH+H)=0.38\pm0.06$.[79,80] In a second stage, the spin state of N through the second channel was elucidated: $B_{21}(({}^4S)N+2H)=0.53\pm0.04$, $B_{22}(({}^2D)N+2H)=0.45\pm0.05$, and $B_{23}(({}^2P)N+2H)=0.02\pm0.02$.[80]

b. Representation. Separately, both sets of data can be handled with Dirg distributions. The global data/uncertainty pattern can be preserved via a nested Dirichlet structure,

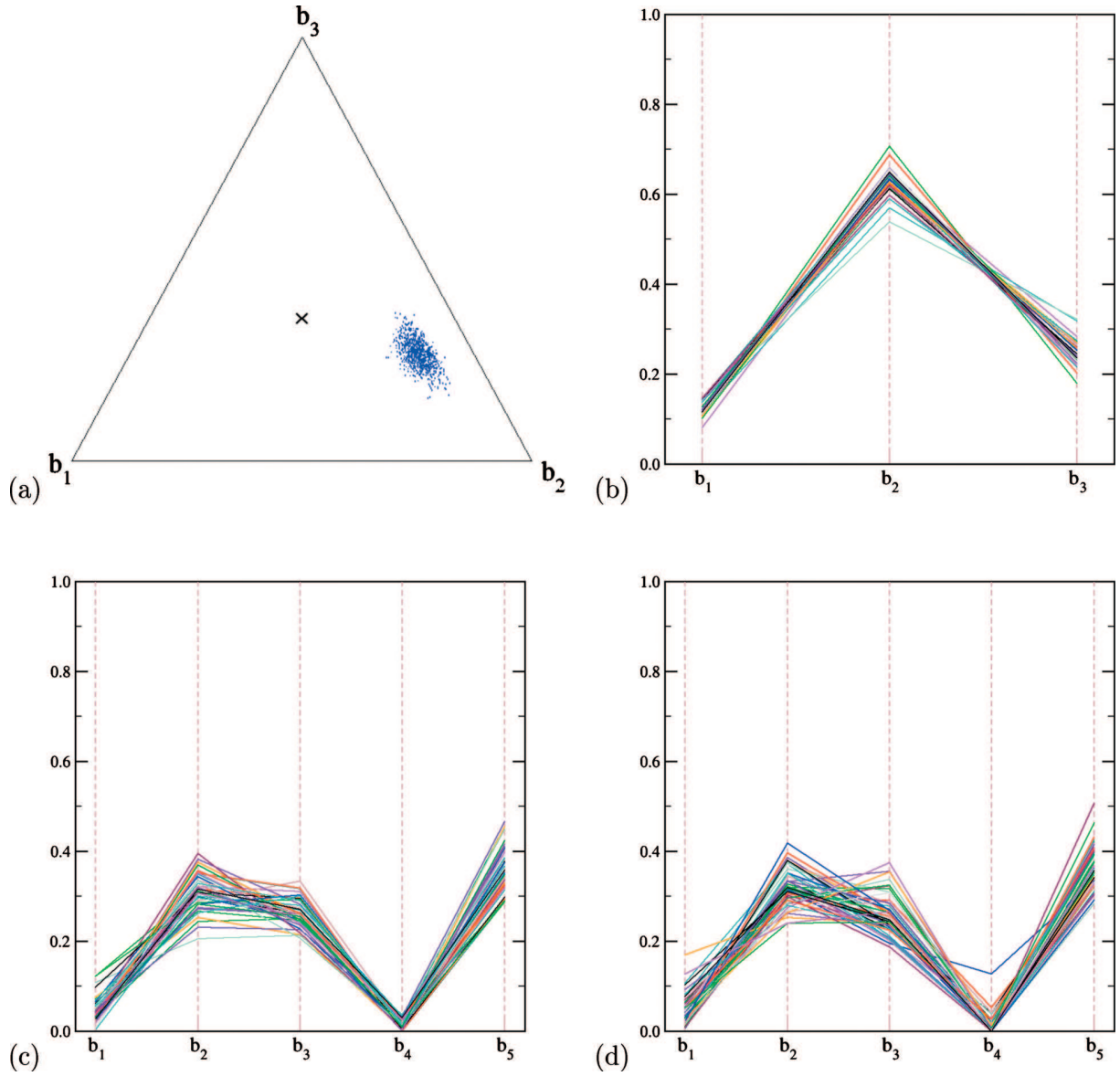

FIG. 7. Samples of uncertain branching ratios for some species of interest: [(a) and (b)] CH_2^+ with nested Dirg and [(c) and (d)] NH_2^+ with nested (c) Dirg and (d) one-level Dirg.

$$\{b_1,\ldots,b_5\} \sim \text{Dirg}(0.04,0.58 \otimes \text{Dirg}(0.53,0.45,0.02;0.04,0.05,0.02),0.38;0.03,0.09,0.06). \tag{24}$$

For comparison, the one-level representation with uncertainties calculated through the standard law of combination of variances [Eq. (16)] would be

$$\{b_1,\ldots,b_5\} \sim \text{Dirg}(0.04,0.31,0.26,0.01,0.38;0.03,0.05,0.05,0.02,0.06). \tag{25}$$

Samples from both distributions are shown in Figs. 7(c) and 7(d). As expected for small standard deviations, both representations look similar. A closer inspection reveals differences for b_3 and b_4, for which the one-level distribution overestimates the dispersion. To be fully consistent, in the absence of information of the spin state distribution of N in the first channel, one could also use a nested Diun(3) distribution over three spin state channels.

3. N_2H^+

a. Information. This is a case where the values of branching ratios are stated as intervals,[81]

$$N_2H^+ + e^- \longrightarrow \begin{cases} \xrightarrow{b_1 \in [0.95,1.00]} N_2 + H \\ \xrightarrow{b_2 \in [0.00,0.05]} NH + N \end{cases}. \tag{26}$$

b. Representation. As the ranges of the intervals are similar, one can use a Diut representation

$$\{b_1,b_2\} \sim \text{Diut}([0.95,1.00],[0.00,0.05]). \tag{27}$$

As in the previous example, an additional nesting level could be introduced in the second channel to account for the unresolved spin states of N.

4. $C_3H_2^+$

This small ion has partially unspecified products and requires the use of a Nested Dirichlet representation.

a. Information. One has measurements for $B_1(C_3)$ and $B_2(C_2+C)$.[82,83] For the C_3 pathway, three exoergic channels are considered with unknown branching ratios (C_3+H_2), (C_3+2H), and (C_3H+H), and for the C_2+C pathway, two channels are invoked (C_2H+CH) and (C_2H+C+H), also with unknown proportions.

b. Representation. A *straight* representation of the information provides the following scheme:

$$C_3H_2^+ + e^- \longrightarrow \begin{cases} \xrightarrow{B_1=0.875\pm0.017} \begin{cases} \xrightarrow{B_{11}\in[0,1]} C_3 + 2H\,(b_1) \\ \xrightarrow{B_{12}\in[0,1]} C_3 + H_2\,(b_2) \\ \xrightarrow{B_{13}\in[0,1]} C_3H + H\,(b_3) \end{cases} \\ \xrightarrow{B_2=0.125\pm0.021} \begin{cases} \xrightarrow{B_{21}\in[0,1]} C_2H + CH\,(b_4) \\ \xrightarrow{B_{22}\in[0,1]} C_2H + C + H\,(b_5) \end{cases} \end{cases}, \tag{28}$$

and the corresponding Nested Dirichlet distribution is

$$\{b_1,\ldots,b_5\} \sim \mathrm{Dirg}(0.875 \otimes \mathrm{Diun}(3), 0.125 \otimes \mathrm{Diun}(2); 0.017, 0.021). \tag{29}$$

Implementation of the "$2H \geq H_2$" rule leads to a further nesting pattern,

$$C_3H_2^+ + e^- \longrightarrow \begin{cases} \xrightarrow{B_1=0.875\pm0.017} \begin{cases} \xrightarrow{B_{11}\in[0,1]} \begin{cases} \xrightarrow{B_{111}\in[0,1]} C_3 + 2H\,(b_1) \\ \xrightarrow{B_{112}\leq B_{111}} C_3 + H_2\,(b_2) \end{cases} \\ \xrightarrow{B_{12}\in[0,1]} C_3H + H\,(b_3) \end{cases} \\ \xrightarrow{B_2=0.125\pm0.021} \begin{cases} \xrightarrow{B_{21}\in[0,1]} C_2H + CH\,(b_4) \\ \xrightarrow{B_{22}\in[0,1]} C_2H + C + H\,(b_5) \end{cases} \end{cases}, \tag{30}$$

and the updated distribution

$$\{b_1,\ldots,b_5\} \sim \mathrm{Dirg}(0.875 \otimes \mathrm{Diri}(0.5 \otimes \mathrm{Dior}(2), 0.5; 2), 0.125 \otimes \mathrm{Diun}(2); 0.017, 0.021). \tag{31}$$

Note that for the needs of nesting within a uniform distribution, we used the notation Diri(0.5,0.5;2) to represent $\{B_{11}, B_{12}\} \sim \mathrm{Diun}(2)$.

We want to emphasize that in the absence of experimental data, the choice of a nesting scheme is not without consequences. The average probability of a product depends on the number of channels where it occurs. In the first case [Eq. (28)], one will produce C_3 and C_3H with mean probability $B_1 \times 2/3$ and $B_1 \times 1/3$, respectively, whereas in the second case [Eq. (30)], the mean probabilities are $B_1 \times 1/2$ each. However, this effect is strongly compensated by the dispersion of the samples due to uniform sampling, as shown in Fig. 8.

5. $C_2H_4^+$

This small ion had all its pathways experimentally characterized.[84] Starting from an aggregated version of the data, we use it to show what can be expected from the nested Dirichlet representation, as used above for $C_3H_2^+$.

a. Information. The full information available is[84]

$$C_2H_4^+ + e^- \longrightarrow \begin{cases} \xrightarrow{b_1=0.11\pm0.07} C_2H_3 + H \\ \xrightarrow{b_2=0.66\pm0.06} C_2H_2 + 2H \\ \xrightarrow{b_3=0.06\pm0.03} C_2H_2 + H_2 \\ \xrightarrow{b_4=0.10\pm0.04} C_2H + H_2 + H \\ \xrightarrow{b_5=0.01\pm0.01} CH_4 + C \\ \xrightarrow{b_6=0.02\pm0.02} CH_3 + CH \\ \xrightarrow{b_7=0.04\pm0.02} 2CH_2 \end{cases}. \tag{32}$$

Mock-up data are generated by aggregating the $C_2(B_1)$ and $C+C(B_2)$ pathways and using representative measurement uncertainties: $B_1 = 0.93 \pm 0.02$ and $B_2 = 0.07 \pm 0.03$.

b. Representation. The complete experimental data shown above can be represented by a flat Dirg distribution, as in the case of CH_2^+. A sample is represented in Fig. 9. Starting from the aggregated data, we build a nested representation based on our set of empirical rules (as they have not been measured, we did not include spin isomers of CH_2),

$$\mathrm{C_2H_4^+} + e^- \longrightarrow \begin{cases} \xrightarrow{B_1=0.93\pm0.02} \begin{cases} \xrightarrow{B_{11}\in[0,1]} \mathrm{C_2H_3} + \mathrm{H}\,(b_1) \\ \xrightarrow{B_{12}\in[0,1]} \begin{cases} \xrightarrow{B_{121}\in[0,1]} \mathrm{C_2H_2} + 2\mathrm{H}\,(b_2) \\ \xrightarrow{B_{122}\le B_{121}} \mathrm{C_2H_2} + \mathrm{H_2}\,(b_3) \end{cases} \\ \xrightarrow{B_{13}\in[0,1]} \mathrm{C_2H} + \mathrm{H_2} + \mathrm{H}\,(b_4) \end{cases} \\ \xrightarrow{B_2=0.07\pm0.03} \begin{cases} \xrightarrow{B_{21}\in[0,1]} \mathrm{CH_4} + \mathrm{C}\,(b_5) \\ \xrightarrow{B_{22}\in[0,1]} \mathrm{CH_3} + \mathrm{CH}\,(b_6) \\ \xrightarrow{B_{22}\in[0,1]} 2\mathrm{CH_2}\,(b_7) \end{cases} \end{cases} . \tag{33}$$

The corresponding nested Dirichlet distribution is

$$\{b_1,\ldots,b_7\} \sim \mathrm{Dirg}(0.93 \otimes \mathrm{Diri}(1/3,1/3 \otimes \mathrm{Dior}(2),1/3;3),0.07 \otimes \mathrm{Diun}(3);0.02,0.03). \tag{34}$$

A sample of this distribution is represented in Fig. 9 and compared to the original experimental data. The nested Dirichlet representation partitions correctly the probability between the C_2 ($\{b_1,\ldots,b_4\}$) and C+C ($\{b_5,\ldots,b_7\}$) pathways. The $\{b_1,\ldots,b_4\}$ space is sampled uniformly, except for the "$b_2 \geq b_3$" constraint. Although this might be difficult to perceive from the one-dimensional marginal densities (boxplots), this sample *does contain* the sample representing the experimental data. This comparison illustrates an essential feature of our method: It is not expected to be predictive, but rather comprehensive/exhaustive, in the sense that it is designed to contain the "correct" branching ratios in agreement with the input data.

6. $CH_2NH_2^+$

a. Information. There are no data about the DR rate and fragmentation pattern for this ion, which has been recently postulated as a main contributor to the formation of ammonia in Titan's ionosphere through its NH_2 fragment.[85]

b. Representation. We consider a uniform distribution over the heavy fragments with exoergic pathways, with an additional nesting for both isomers of HCN,

$$\mathrm{CH_2NH_2^+} + e^- \longrightarrow \begin{cases} \xrightarrow{B_1\in[0,1]} \mathrm{CH_3N} + \mathrm{H} \\ \xrightarrow{B_2\in[0,1]} \mathrm{CH_2} + \mathrm{NH_2} \\ \xrightarrow{B_3\in[0,1]} \begin{cases} \xrightarrow{B_{31}\in[0,1]} \mathrm{HCN} + \mathrm{H_2} + \mathrm{H} \\ \xrightarrow{B_{32}\in[0,1]} \mathrm{HNC} + \mathrm{H_2} + \mathrm{H} \end{cases} \\ \xrightarrow{B_4\in[0,1]} \mathrm{CN} + 2\mathrm{H_2} \end{cases} , \tag{35}$$

with distribution

$$\{b_1,\ldots,b_5\} \sim \mathrm{Diri}(1/4,1/4,1/4 \otimes \mathrm{Diun}(2),1/4;4). \tag{36}$$

7. HCCCNH+

a. Information. Geppert *et al.*[86] measured partial branching ratios for the deuterated molecule $DCCCND^+$, providing probabilities $B_1=0.52\pm0.05$ for channels $\{DC_3N+D,\ C_3N+D_2\}$ and $B_2=0.48\pm0.05$ for $\{DCN+CD_2,\ CN+C_2D_2\}$. An additional and important information is that isotope effects are expected to be small,[86] i.e., we can transpose this information to the hydrogenated ion $HCCCNH^+$. The experimental setup does not allow them to distinguish between isomers, and Osamura *et al.*[87] showed that there exist interconversion barriers low enough to enable the formation of different isomers of HC_3N. They also indicate that the formation of HC_3N is more likely than HC_2NC.

b. Representation. The information about this system can be translated into the following scheme:

$$\mathrm{HCCCNH^+ + e^- \longrightarrow}\begin{cases}\xrightarrow{B_1=0.52\pm0.05}\begin{cases}\xrightarrow{B_{11}\in[0,1]}\begin{cases}\xrightarrow{B_{111}\in[0,1]}\begin{cases}\xrightarrow{B_{1111}\in[0,1]}\mathrm{HC_3N + H}\\ \xrightarrow{B_{1112}\in[0,1]}\mathrm{C_3NH + H}\end{cases}\\ \xrightarrow{B_{112}\le B_{111}}\begin{cases}\xrightarrow{B_{1121}\in[0,1]}\mathrm{C_2NCH + H}\\ \xrightarrow{B_{1122}\in[0,1]}\mathrm{HC_2NC + H}\end{cases}\end{cases}\\ \xrightarrow{B_{12}\in[0,1]}\mathrm{C_3N + H_2}\end{cases}\\ \xrightarrow{B_2=0.48\pm0.05}\begin{cases}\xrightarrow{B_{21}\in[0,1]}\begin{cases}\xrightarrow{B_{211}\in[0,1]}\mathrm{HCN + C_2H}\\ \xrightarrow{B_{212}\in[0,1]}\mathrm{HNC + C_2H}\end{cases}\\ \xrightarrow{B_{22}\in[0,1]}\mathrm{CN + C_2H_2}\end{cases}\end{cases} . \quad (37)$$

In the branch B_{111}, we explicited isomers based on the position of the H atom, as proposed by Osamura *et al.*[87] Note that without explicit information about isomers of C_3N (branch B_{12}), we did not introduce additional species.

The expression of the distribution becomes very intricate and illegible and is not presented here. It involves a Dirg distribution a the first level, and then sequentially nested two-elements Diun distribution, at the exception of branches B_{111} and B_{112} which are nested into a Dior node.

C. Titan ionospheric chemistry

Prior to arrival of Cassini in Titan's atmosphere it was thought that only relatively small compounds, with masses lower than 100 u (maximum mass chosen for the ion-neutral mass spectrometer instrument, INMS), would be detected in the upper atmosphere by the Cassini orbiter, with small contributions of heavy species. However both the INMS and the Cassini plasma spectrometer (CAPS) sensors revealed a large amount of heavy positive ions in the ionosphere, with significant ion densities above 100 u.[88–90] Waite *et al.*[89] suggested that chemical growth in the upper atmosphere is initiated by the ion-neutral chemistry, in agreement with the work of Carrasco *et al.*[91] showing the important role of the condensation reactions (bond rearrangement reactions) for ion growth. These latter processes are very important to understand the organic complexification of the compounds in the upper atmosphere, which cannot be explained only by protonation of neutrals as suggested earlier by Vuitton *et al.*[92]

A few heavy neutrals, among them benzene, and numerous negatively charged species have been detected by INMS and CAPS in significant amounts in the thermosphere. The abundance of benzene in Titan's upper atmosphere raises up numerous issues. This stable aromatic compound constitutes another key species toward organic growth and has been observed in Titan atmosphere by different instruments: the Infrared Space Observatory,[93] the composite infrared spectrometer on board Cassini,[94] and the neutral INMS mass spectrometer.[95] The upper atmospheric chemistry seems to produce efficiently high amounts of benzene, with mole fractions of about $\sim 10^{-6}$ cm^{-3}, larger than in the stratosphere $\sim 10^{-10}$–10^{-9}.[96] This production, specific to the thermosphere, is suspected to be due to the electron recombination of the positive ion $C_6H_7^+$. More generally, the production of all the heavy species (neutral or negatively charged) is presently understood as coming from the ultimate electron recombination of heavy positive ions. Unfortunately, as described previously, the products from these dissociative processes are poorly known, and only the H-loss coproducts are implemented in the recent models.[31–36]

Exceptions to this exclusive implementation of the

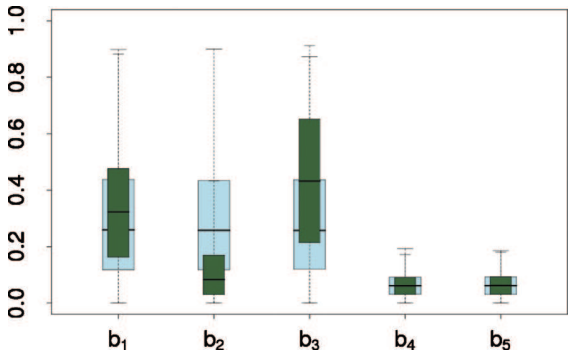

FIG. 8. Influence of the nesting pattern on the distribution of branching ratios $\{b_1,\ldots,b_5\}$ for the DR of $C_3H_2^+$; (blue/light) flat representation of the subchannels; (green/dark) nesting of auxiliary information.

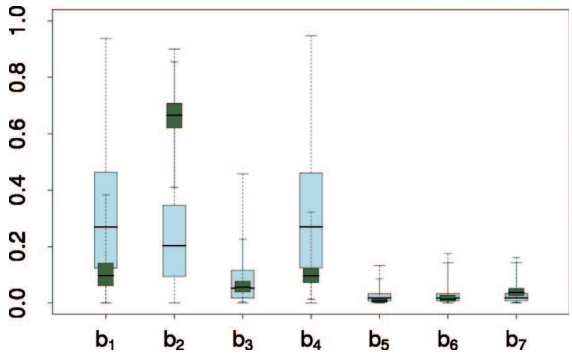

FIG. 9. Comparison of branching ratios $\{b_1,\ldots,b_7\}$ for the DR of $C_2H_4^+$, as measured (dark green boxplots) and recovered from an aggregated version of these data (light blue boxplots).

TABLE I. Comparison of the DR treatment of Krasnopolsy (Ref. 37) and the available literature for some representative ions.

Reaction	No. of open channels	Selected channels (b_i) by Krasnopolsky[a]	Measured contribution of selected channels
$HCNH^+ + e^-$	4	HCN+H (1.0)	0.26–0.41[b]
$C_4H_3^+ + e^-$	14	C_3H_2+CH (1.0)	0.00–0.07[c]
$C_4H_5^+ + e^-$	15	C_3H_4+CH (0.7)	0.00–0.11[c]
		C_4H_4+H (0.3)	0.00–0.51[c]
$CH_4^+ + e^-$	8	CH_3+H (1.0)	Unknown

[a]Reference 37.
[b]Reference 97.
[c]Reference 16.

H-loss channels exist but are often introduced *ad hoc*. For instance, Krasnopolsky[37] used in his coupled model 32 DR, with only one having several branching ratios: $C_4H_5^+ + e^-$ has two channels, with branching ratios different from the measured values (Table I). Another exception to the H-loss scenario is $C_4H_3^+$, condemned by this author to dissociate through a unique CH-loss channel, which is known to account for less than 7% of the measured products.[16] Another oddity concerns the major ion of Titan's ionosphere, $HCNH^+$, for which the selected H-loss channel (HCN+H) accounts at best for 40% of the products of this ion.[97] Let us also mention that a few ions have been implemented with a "H_2-loss" process, neglecting the *a priori* more favorable "2H-loss" process, without theoretical or experimental evidence ($CHCCNH^+$, CH_3CNH^+, and $C_3H_5^+$).[97]

In astrochemistry and ionospheric chemistry, it is well acknowledged that the "benefit" of the H-loss mechanism is to produce large neutral species.[19,98] This choice therefore introduces a bias toward the production of heavy neutrals by deprotonation of heavy ions, enforcing ion-molecule reactivity as the main engine for molecular complexification. Considering that major ions in Titan's ionosphere are protonated species (e.g., $HCNH^+$ and $C_2H_5^+$), the H-loss DR mechanism is singularly producing stable neutral molecules (HCN and C_2H_4). This deprives the chemical system of an important source of highly energetic radicals.

The previous examples show that the treatment of DR in coupled ionospheric models deserves further attention. It is therefore important to check how a more complete implementation of the present knowledge about DR products can improve on the H-loss paradigm. We focus here on the production rates of neutral species from stationary ion densities. Implementing a fully coupled ionospheric model is beyond the scope of this study.

1. The kinetic model

The production rate v_M for a neutral species M through DR is

$$v_M = \frac{d[M]}{dt} = \sum_r \left[\alpha_0^{(r)} \times \left(\frac{T_e}{300} \right)^{-\beta^{(r)}} \times [I^+]_r \times d_e \times \sum_{j=1}^{n_r} b_j^{(r)} \times \nu_{j,M} \right], \quad (38)$$

where $[M]$ is the concentration of the neutral species of interest, $\alpha_0^{(r)}$ is the thermal rate constant at 300 K of DR r, $\beta^{(r)}$ is the power parameter of DR r, $[I^+]_r$ is the density of the ion destroyed by DR r, d_e is the electron density, $b_j^{(r)}$ is the jth branching ratio of DR r, and $\nu_{j,M}$ is the stoichiometric coefficient of the neutral species in channel j.

a. Initial conditions. The production rates were calculated with ionic densities taken from the T19 flyby INMS ionic day spectrum at 1100 km of altitude from peak assignments in Refs. 89 and 98 (see Table II). Electron density d_e is equal to the sum of the ions densities.[99] A representative value of the electrons temperature (570 K) at 1100 km has been used.

b. Chemical schemes. Our "full scheme" implements DR for the ions listed in Table II. This scheme includes a detailed treatment for 58 ions, corresponding to 448 partial reactions, forming 62 different neutral species. The H-loss scheme was obtained by pruning the full scheme from irrelevant pathways and ensuring adequate normalization of the remaining branching ratios. This scheme comprises 63 partial reactions producing a subset of 48 neutral species. Note that for some ions, more than one H-loss pathways are possible (due to products isomers or spin states), and that the detailed branching ratios for all species not bearing H have been maintained. Differences observed between both models can therefore be attributed to H-bearing species only.

2. Impact of nesting schemes

The full model was run with two extreme nesting patterns: a flat pattern where all nesting options were ignored, except for the spin states of CH_2, and our working pattern, with implementation of the nesting rules defined in Sec. III A 2. The ratios of the production rates of neutral species by the flat (v_M^{flat}) and the full, nested, (v_M^{full}) mechanisms are shown in Fig. 10. As a control, we also calculated the ratio $v_M^{\text{full}}/v_M^{\text{full}}$ using two different Monte Carlo samples. The 50% symmetric probability interval corresponding to the inner part of our boxplots has been plotted in Fig. 10 to enable a visual appreciation of the statistical significance of the deviations of production rates ratios from 1. For $v_M^{\text{full}}/v_M^{\text{flat}}$ the median production rates of all neutral species vary by less than a factor 2, which is much smaller than the global uncertainty on the production rates of most species. Statistically, the choice of a nesting pattern can thus be considered as a secondary effect.

3. Comparison of DR models

The ratios of the production rates of neutral species by the H-loss ($v_M^{\text{H-loss}}$) and the full (v_M^{full}) mechanisms are shown in Fig. 10. It is to be noted first that the effects observed here are much larger than those due to the choice of a nesting scheme. The differences between production rates for the H-loss and full models can thus be considered as independent from the implementation details of the full model.

The H-loss mechanism favors 15 species among the 45 neutrals common to both schemes, all of which are stable neutral species. Among these 15 significantly overestimated species, 7 are nitrogen-containing species:

TABLE II. Peak assignment of the T19 flyby. Spectrum values taken from Ref. 89 and assignment from Ref. 98. In absence of data about their DR, species in italics have not been considered in the model.

m/z (u)	Density (cm^{-3})	Ions and predicted fractional contribution					
12	4.31	C^+	1.000 00				
13	6.44	CH^+	1.000 00				
14	20.15	N^+	0.800 00	CH_2^+	0.200 00		
15	60.62	NH^+	0.000 99	CH_3^+	0.999 01		
16	17.87	CH_4^+	0.993 10	NH_2^+	0.006 90		
17	90.47	CH_5^+	0.998 54	NH_3^+	0.001 46		
18	155.35	NH_4^+	1.000 00				
25	7.11	C_2H^+	1.000 00				
26	9.80	$C_2H_2^+$	0.999 54	CN^+	0.000 46		
27	59.42	$C_2H_3^+$	0.551 95	HCN^+	0.448 05		
28	3258.69	$HCNH^+$	0.955 18	N_2^+	0.027 72	$C_2H_4^+$	0.017 10
29	582.39	$C_2H_5^+$	0.974 22	N_2H^+	0.025 26	H_3CN^+	0.000 52
30	1271.59	$CH_2NH_2^+$	1.000 00				
31	30.08	$C_2H_7^+$	0.947 78	$CH_3NH_2^+$	0.052 22		
32	5.71	$CH_3NH_3^+$	1.000 00				
36	2.37	C_3^+	1.000 00				
37	2.83	C_3H^+	1.000 00				
38	11.97	C_2N^+	0.998 65	$C_3H_2^+$	0.001 35		
39	2318.55	$C_3H_3^+$	0.821 89	$CHCN^+$	0.178 11		
40	110.60	CH_2CN^+	0.821 23	$C_3H_4^+$	0.178 77		
41	630.96	$C_3H_5^+$	0.983 18	CH_3CN^+	0.016 82		
42	786.41	CH_3CNH^+	0.999 55	$C_3H_6^+$	0.000 45		
43	52.69	$C_3H_7^+$	0.965 77	$C_2H_3NH_2^+$	0.034 23		
44	5.06	$C_3H_8^+$	1.000 00				
45	0.79	$C_3H_9^+$	1.000 00				
49	0.40	C_4H^+	1.000 00				
50	36.02	$C_4H_2^+$	0.998 78	C_3N^+	0.001 22		
51	209.77	$C_4H_3^+$	0.998 87	$CHCCN^+$	0.001 13		
52	1083.38	$CHCCNH^+$	0.996 20	$C_4H_4^+$	0.003 64	$C_2N_2^+$	0.000 16
53	146.29	$C_4H_5^+$	0.852 26	$HC_2N_2^+$	0.128 01	$C_2H_3CN^+$	0.019 73
54	755.55	CH_2CHCNH^+	0.999 97	$C_4H_6^+$	0.000 03		
55	63.10	$C_4H_7^+$	1.000 00				
56	67.00	$C_2H_5CNH^+$	0.999 98	$C_4H_8^+$	0.000 02		
57	4.67	$C_4H_9^+$	1.000 00				

- Stable nitriles such as HC_3N, CH_3CN, and C_3H_3N. The chemistry of nitriles is a present major concern for the better understanding of Titan's aerosol formation. Vuitton *et al.*[98] deduced unsuspected high densities of nitriles in the upper atmosphere from an ion mass spectrum analysis measured by the Cassini INMS instrument, and proposed that these are very plausible aerosol precursors. From the Huygens ACP experiment, Israël *et al.*[100] identified -CN groups as one major constitutive function in the aerosol composition. Moreover, recent works on Titan's laboratory analogs analysis also highlighted patterns involving an unsaturated C,N combination for tholin molecular growth.[101,102] However, photochemistry and neutral-neutral chemistry of nitriles have already been identified as incomplete and to be improved (see the review of Hébrard *et al.*[50]). Here, we point out that the H-loss model tends to exaggerate the nitrile production rates in Titan's upper atmosphere. As an example, Vigren *et al.*[75] showed that the dissociative recombination of CD_3CND^+ led to 35% of bond rupture between heavy atoms.
- One imine, the methanimine CH_3N. Balucani *et al.*[103] identified this species as a good candidate for polymerization or copolymerization in Titan's atmosphere, suggesting new paths for nitrogen rich aerosols production. According to their experimental and theoretical studies, methanimine would also be produced by the reaction between $N(^2D)$ and ethane. It would thus be important to compare these two methanimine production pathways in a complete ion-neutral Titan's atmospheric model.
- Three excited isomers of HC_3N: C_3NH, C_2NCH, and HC_2NC, possibly produced by the DR of HC_3NH^+.[87] These very reactive nitrogen-bearing species are not known to be produced by any other process in Titan's atmosphere. Moreover their own reactivity remains completely unknown. As a matter of fact, these three reactive species are very possibly produced in Titan's atmosphere, are very reactive, nitrogen-containing, but their becoming in Titan's atmosphere is completely un-

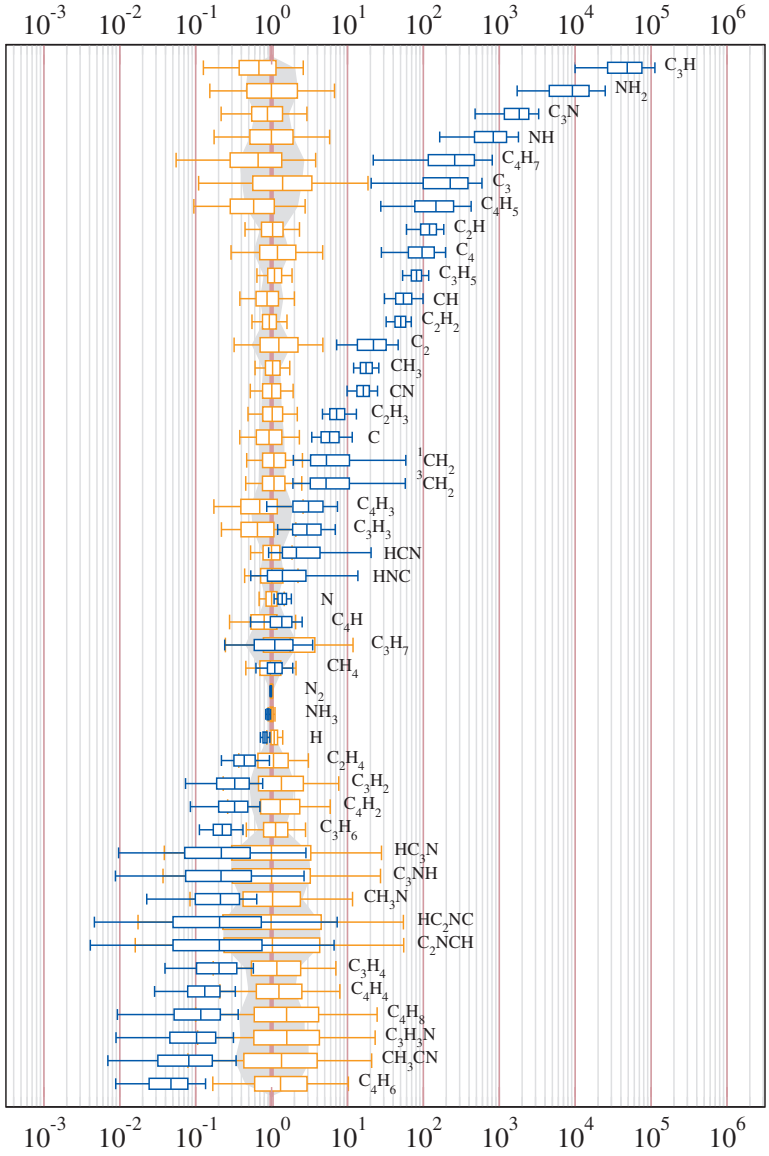

FIG. 10. Comparison of the production rates of neutral species between different DR model implementations: (brown) ratio $v_M^{\text{full}}/v_M^{\text{flat}}$ between the nested and flat versions of the "full" model (see text); (blue) ratio $v_M^{\text{full}}/v_M^{\text{H-loss}}$ between the full and "H-loss" models. The gray zone depicts the intrinsic dispersion due to the Monte Carlo estimation of production rates ratios: symmetric 50% probability interval for the ratio $v_M^{\text{full}}/v_M^{\text{full}}$ estimated from two independent samples.

known. This highlights a challenging case for Titan's chemistry understanding.

The production rates of six species are indifferent to the choice of DR mechanism, among them are N_2, H (logically well represented in a H-loss mechanism), and ammonia. Considering the poor knowledge on the dissociative recombination of larger protonated amines, an enhancement of the production rate of ammonia could be expected when more data are available.

The most salient feature of this comparison is that the full mechanism enhances significantly the production rate for 24 of the 41 species common to both schemes. The enhancement factor goes from 2–3 to 10^4. We consider below a few cases which are of high interest for Titan's atmospheric chemistry.

- One major result of this simulation is that the H-loss mechanism does not account for the rich reactivity enhancement due to the formation of radicals by DR. The H-loss model strongly underestimates the production rates of radicals in comparison with the stable neutral species (except C_3H_7 which is not significantly modified): 16 of the 24 underestimated species are radicals. This may affect the neutral growth pathways. Their underestimation by DR processes may lead to improper neutral production rates in photochemical models. A first example is the methyl radical CH_3, an important node in the Titan neutral chemical network for hydrocarbon neutral growth. Its DR production rate is underestimated by a factor of 10 in the H-loss mechanism, which might be significant for night chemistry. Another striking example is the C_4H_y family or radicals. Those are the main compounds presently taken into account as "soot" in the photochemical models to initiate aerosol

nucleation in the stratosphere, whereas their production rates by DR in the H-loss mechanism are largely underestimated, with factors above 100 for C_4H_5 and C_4H_7.

- Nitrogen atom production rate is also slightly enhanced in the full model. Actually the increase itself is not important, but the spin states of these atoms are not systematically well-quantified in the DR studies and cannot be therefore presently taken into account in the DR models, except maybe through a Diun construction as we did for the spin states of CH_2. Yet, the long-lived metastable $N(^2D)$ atoms undergo efficient reactions with all the abundant stable neutrals in Titan's atmosphere, whereas the ground state $N(^4S)$ atoms are almost not reactive.[104] Their respective production from DR pathways have then to be carefully measured in order to be compared to molecular nitrogen dissociation production.
- The production rate of C_2H_2 is underestimated in the H-loss model by a factor of a few tens. C_2H_2 is a saturated hydrocarbon invoked to explain polymerization mechanisms in Titan's stratosphere.[37,105–107] An additional production rate by the DR full mechanism could thus be important in comparison with the neutral production rates in coupled ion-neutral chemistry models.
- It is also to be noted that H_2 is not formed through the H-loss scenario. The underestimation of H_2 could also have an important impact in the models, this species being suspected to participate to heterogeneous reactions with the aerosols.[108–110]

For all these compounds, we highlight here the importance of the calculation of their production rates with a full-DR model instead of a simplified H-loss model to be properly compared with the neutral production rate contribution in coupled ion-neutral chemistry models.

IV. CONCLUSION

Important results about the distribution of products of dissociative recombination have been gathered by several teams in the past years. Although partial, this information deserves to be considered in detailed chemical models of ionized media. However, the nominal approach of chemistry modeling is not able to cope consistently with partial data. We have shown that a probabilistic approach based on nested Dirichlet distributions, encompassing plausible cases in conformance with experimental data, enables to deal with this situation. An inconvenience of this approach is the additional computational cost of Monte Carlo simulations, but in such conditions of uncertainty, deterministic modeling is unarguably a poor option.

Distributions of the Dirichlet family are generic tools for sum-to-one variables, easy to implement in a Monte Carlo uncertainty propagation framework, providing a flexible treatment of the available data about branching ratios. We have shown that they enable to unlock the modeling of complex chemical networks involving partially known dissociative recombination products. The representation of uncertain branching ratios proposed in this work is compact, self-contained, and suited for implementation in kinetics databases such as the KInetic Database for Astrochemistry.[111]

When compared to the H-loss mechanism still in use in many ionospheric chemistry models for Titan, the Dirichlet modeling provides a spectacular enrichment in the chemodiversity and in the production rates of highly reactive neutral radicals. Where the H-loss scenario, forming mainly stable neutral species, can be considered as damping the reactivity of neutral species, the full model can be seen as boosting this reactivity and contributing to molecular growth through radical chemistry. The effect of these radicals on the chemistry of neutral species has now to be quantified by implementation of the enhanced DR scheme in a ion-neutral coupled model (work in progress).

V. SUPPLEMENTARY MATERIAL

The database of DR rate constants and branching ratios elaborated for this article and used in the applications is provided in a separate document, with additional notes and complete references.[72]

ACKNOWLEDGMENTS

The authors thank J. B. Mitchell, K. Béroff, and M. Chabot for fruitful discussions.

APPENDIX: SAMPLING OF DIRICHLET-TYPE DISTRIBUTIONS

We present here the basic techniques to generate random samples of Dirichlet-type distributions used in this article. A FORTRAN code and R interface to generate random samples from these distributions are available by simple request to the contact author.

1. The Dirichlet distribution: Diri

The Dirichlet distribution is efficiently sampled using sum-normalized gamma random numbers:[30,112]

(1) Independent random values $x_1,\ldots,x_n$ are drawn from standard gamma distributions, defined by a single parameter α_i,

$$\mathrm{Sgamma}(\alpha_i) = \frac{1}{\Gamma(\alpha_i)} x_i^{\alpha_i - 1} e^{-x_i}, \quad \text{where} \quad \alpha_i = \mu_i \times \gamma, \tag{A1}$$

where $\Gamma(.)$ is the gamma function,[113] and

(2) the x_i are normalized

$$b_i = \frac{x_i}{\sum_{j=1}^{n} x_j}. \tag{A2}$$

2. The generalized Dirichlet distribution: Dirg

For each branching ratio, one defines two parameters, α_i (shape parameter) and β_i (scale parameter) through

$$\alpha_i = \left(\frac{\mu_i}{u_i}\right)^2 \quad \text{and} \quad \beta_i = \frac{\mu_i}{u_i^2}, \tag{A3}$$

one generates n independent random samples $x_1, \ldots, x_n$, from gamma distributions

$$\text{gamma}(\alpha_i, \beta_i) = \frac{\beta_i^{\alpha_i}}{\Gamma(\alpha_i)} x_i^{\alpha_i - 1} e^{-\beta_i x_i}, \tag{A4}$$

and one normalizes them [Eq. (A2)].

3. Uniform Dirichlet: Diun

The recipe is to generate n independent random samples $x_1, \ldots, x_n$, from unit-scaled exponential distributions $\exp(1) = e^{-x_i}$ and normalize them [Eq. (A2)].

4. Truncated uniform Dirichlet: Diut

In order to obtain a uniform sampling in a subspace of the simplex, it is possible to start from the uniform Diun distribution and use a rejection algorithm. This approach becomes very inefficient for small intervals and/or high dimensions. Efficient direct generation of uniform samples on restricted spaces is an active research area in experimental design.[114,115] A direct algorithm based on conditional distributions, proposed by Fang and Yang,[116] has been used in this work.

5. Nested Dirichlet

Practical implementation is based on the building of a tree structure in which one generates at each node the random numbers for its children nodes and then calculates the probabilities of the terminal leaves by recursive products along the tree branches.

[1] T. J. Millar, D. J. DeFrees, A. D. McLean, and E. Herbst, Astron. Astrophys. **194**, 250 (1988).
[2] E. Herbst and H.-H. Lee, Astrophys. J. **485**, 689 (1997).
[3] W. D. Geppert, W. D. Thomas, A. Ehlerding, J. Semaniak, F. Österdahl, M. af Ugglas, N. Djurić, A. Paál, and M. Larsson, Faraday Discuss. **127**, 425 (2004).
[4] W. D. Geppert, R. Thomas, A. Ehlerding, F. Hellberg, F. Österdahl, M. Hamberg, J. Semaniak, V. Zhaunerchyk, M. Kaminska, A. Källberg, A. Paál, and M. Larsson, J. Phys.: Conf. Ser. **4**, 26 (2005).
[5] J. L. Fox, J. Phys.: Conf. Ser. **4**, 32, 2005.
[6] D. L. Huestis, S. W. Bougher, J. L. Fox, M. Galand, R. E. Johnson, J. I. Moses, and J. C. Pickering, Space Sci. Rev. **139**, 63 (2008).
[7] M. Masuzaki and T. Tsuzuki, Phys. Lett. A **38**, 441 (1972).
[8] D. C. Schram, Pure Appl. Chem. **74**, 369 (2002).
[9] D. C. Schram, R. A. B. Zijlmans, O. Gabriel, and R. Engeln, J. Phys.: Conf. Ser. **192**, 012012 (2009).
[10] C. H. Sheehan and J. P. St.-Maurice, Adv. Space Res. **33**, 216 (2004).
[11] R. D. Thomas, Mass Spectrom. Rev. **27**, 485 (2008).
[12] J. L. McLain and N. G. Adams, Planet. Space Sci. **57**, 1642 (2009).
[13] D. R. Bates, Phys. Rev. **78**, 492 (1950).
[14] D. R. Bates, Astrophys. J. **306**, L45 (1986).
[15] D. R. Bates, Astrophys. J. **344**, 531 (1989).
[16] A. I. Florescu-Mitchell and J. B. A. Mitchell, Phys. Rep. **430**, 277 (2006).
[17] M. Larsson and A. E. Orel, *Dissociative Recombination of Molecular Ions* (Cambridge University Press, Cambridge, 2008).
[18] E. Herbst and W. Klemperer, Astrophys. J. **185**, 505 (1973).
[19] E. Herbst Astrophys. J. **222**, 508 (1978).
[20] S. Green and E. Herbst, Astrophys. J. **229**, 121 (1979).
[21] E. T. Galloway and E. Herbst, Astrophys. J. **376**, 531 (1991).
[22] D. Strasser, J. Levin, H. B. Pedersen, O. Heber, A. Wolf, D. Schwalm, and D. Zajfman, Phys. Rev. A **65**, 010702 (2001).
[23] D. Talbi, A. Le Padellec, and J. B. A. Mitchell, J. Phys. B **33**, 3631 (2000).
[24] A. P. Hickman, R. D. Miles, C. Hayden, and D. Talbi, Astron. Astrophys. **438**, 31 (2005).
[25] D. Talbi, Chem. Phys. **332**, 298 (2007).
[26] H.-G. Yu, J. Chem. Phys. **128**, 194106 (2008).
[27] N. Carrasco, C. Alcaraz, O. Dutuit, S. Plessis, R. Thissen, V. Vuitton, R. Yelle, and P. Pernot, Planet. Space Sci. **56**, 1644 (2008).
[28] B. Null, The Nested Dirichlet distribution: properties and applications, Working paper, Department of Management Science and Engineering, Stanford University, October 2008.
[29] G.-L. Tian, M.-L. Tang, K. C. Yuen, and K. W. Ng, Comput. Stat. Data Anal. **54**, 394 (2010).
[30] N. Carrasco and P. Pernot, J. Phys. Chem. A **111**, 3507 (2007).
[31] C. N. Keller, T. E. Cravens, and L. Gan, J. Geophys. Res. **97**, 12117 (1992).
[32] N. G. Keller, V. G. Anicich, and T. E. Cravens, Planet. Space Sci. **46**, 1157 (1998).
[33] M. Banaszkiewicz, L. M. Lara, R. Rodrigo, J. J. Lopez-Moreno, and G. J. Molina-Cuberos, Icarus **147**, 386 (2000).
[34] E. H. Wilson and S. K. Atreya, J. Geophys. Res. **109**, E06002 (2004).
[35] V. De La Haye, "Corona formation and heating efficiencies in Titan's upper atmosphere: Construction of a coupled ion, neutral and thermal structure model to interpret the first INMS Cassini data," Ph.D. thesis, The University of Michigan, 2005.
[36] V. De La Haye, J. H. Waite, Jr., T. E. Cravens, I. P. Robertson, and S. Lebonnois, Icarus **197**, 110 (2008).
[37] V. A. Krasnopolsky, Icarus **201**, 226 (2009).
[38] N. Carrasco, O. Dutuit, R. Thissen, M. Banaszkiewicz, and P. Pernot, Planet. Space Sci. **55**, 141 (2007).
[39] BIPM, IEC, IFCC, ISO, IUPAP, and OIML, "Evaluation of measurement data—Supplement 1 to the GUM: Propagation of distributions using a Monte Carlo method," International Organization for Standardization (ISO) Technical Report No. 101, 2008.
[40] J. C. Helton, J. D. Johnson, C. J. Sallaberry, and C. B. Storlie, Reliab. Eng. Syst. Saf. **91**, 1175 (2006).
[41] A. M. Thompson and R. W. Stewart, J. Geophys. Res. **96**, 13089 (1991).
[42] M. Dobrijevic and J. P. Parisot, Planet. Space Sci. **46**, 491 (1998).
[43] B. D. Phenix, J. L. Dinaro, M. A. Tatang, J. W. Tester, J. B. Howard, and G. J. McRae, Combust. Flame **112**, 132 (1998).
[44] G. E. Moore and R. J. Londergan, Atmos. Environ. **35**, 4863 (2001).
[45] D. Bose, M. V. V. S. Rao, T. R. Govindan, and M. Meyyappan, Plasma Sources Sci. Technol. **12**, 225 (2003).
[46] M. Dobrijevic, J. L. Ollivier, F. Billebaud, J. Brillet, and J. P. Parisot, Astron. Astrophys. **398**, 335 (2003).
[47] M. T. Reagan, H. N. Najm, P. P. Pebay, O. M. Knio, and R. G. Ghanem, Int. J. Chem. Kinet. **37**, 368 (2005).
[48] V. Wakelam, F. Selsis, E. Herbst, and P. Caselli, Astron. Astrophys. **444**, 883 (2005).
[49] V. Wakelam, E. Herbst, and F. Selsis, Astron. Astrophys. **451**, 551 (2006).
[50] E. Hébrard, M. Dobrijevic, Y. Bénilan, and F. Raulin, J. Photochem. Photobiol., A **7**, 211 (2006).
[51] E. Hébrard, M. Dobrijevic, Y. Bénilan, and F. Raulin, Planet. Space Sci. **55**, 1470 (2007).
[52] M. Dobrijevic, N. Carrasco, E. Hébrard, and P. Pernot, Planet. Space Sci. **56**, 1630 (2008).
[53] E. Hébrard, N. Carrasco, Z. Peng, M. Dobrijevic, and P. Pernot, "Photochemical modeling of Tital atmosphere at the 10 percent uncertainty horizon," Faraday Discuss. (in press).
[54] An exception would be the case where a group of rate constants has been adjusted simultaneously to fit some data, leading to correlated uncertainties. However, there is no traceability for such cases in reference chemical reactions databases.
[55] J. Aitchison, *The Statistical Analysis of Compositional Data*, Monographs on Statistics and Applied Probability (Chapman and Hall, London, 1986).
[56] A. O'Hagan, Department of Probability and Statistics, University of Sheffield Research Report No. 557/05, 2005. Invited article for a volume entitled Bayesian Statistics and its Applications.
[57] J. N. Kapur, *Maximum Entropy Models in Science and Engineering* (Wiley, New York, 1989).
[58] M. Evans, N. Hastings, and B. Peacock, *Statistical Distributions*, 3rd ed.

(Wiley-Interscience, New York, 2000).
[59] M. O. Vlad, M. Tsuchiya, P. Oefner, and J. Ross, Phys. Rev. E **65**, 011112 (2001).
[60] V. G. Anicich, J. Phys. Chem. Ref. Data **22**, 1469 (1993).
[61] V.G. Anicich, JPL Publ. **03–19**, 1 (2003).
[62] T.-T. Wong, Appl. Math. Comput. **97**, 165 (1998).
[63] A. Ongaro, S. Migliorati, and G. S. Monti, Proceedings of the CODA-WORK'08, La Universitat, Girona, May 2008.
[64] J. W. Lingwall, W. F. Christensen, and C. S. Reese, Environmetrics **19**, 618 (2008).
[65] BIPM, IEC, IFCC, ILAC, ISO, IUPAC, IUPAP, and OIML, "Evaluation of measurement data–Guide to the expression of uncertainty in measurement (GUM)," International Organization for Standardization (ISO) Technical Report No. 100, 2008.
[66] N. Carrasco, E. Hébrard, M. Banaszkiewicz, M. Dobrijevic, and P. Pernot, Icarus **192**, 519 (2007).
[67] E. Hébrard, M. Dobrijevic, P. Pernot, N. Carrasco, A. Bergeat, K. M. Hickson, A. Canosa, S. D. Le Picard, and I. R. Sims, J. Phys. Chem. A **113**, 11227 (2009).
[68] J. Woodall, M. Agúndez, A. J. Markwick-Kemper, and T. J. Millar, Astron. Astrophys. **466**, 1197 (2007).
[69] E. Herbst, see: http://www.physics.ohiostate.edu/eric/research.html for gas-phase model.
[70] Molecular Physics Group, see: http://mol.physto.se/DRdatabase/ for dissociative recombination database.
[71] N. G. Adams, V. Poterya, and L. M. Babcock, Mass Spectrom. Rev. **25**, 798 (2006).
[72] See supplementary material at http://dx.doi.org/10.1063/1.3479907 for the full dataset of branching ratios, along with DR rate constants and the relevant references.
[73] A. Ehlerding, S. T. Arnold, A. A. Viggiano, S. Kalhori, J. Semaniak, A. M. Derkatch, S. Rosen, M. af Ugglas, and M. Larsson, J. Phys. Chem. A **107**, 2179 (2003).
[74] E. Vigren, M. Kaminska, M. Hamberg, V. Zhaunerchyk, R. D. Thomas, J. Semaniak, M. Danielsson, M. Larsson, and W. D. Geppert, Phys. Chem. Chem. Phys. **9**, 2856 (2007).
[75] E. Vigren, M. Kaminska, M. Hamberg, V. Zhaunerchyk, R. D. Thomas, M. Danielsson, J. Semaniak, P. U. Andersson, M. Larsson, and W. D. Geppert, Phys. Chem. Chem. Phys. **10**, 4014 (2008).
[76] E. Vigren, M. Hamberg, V. Zhaunerchyk, M. Kaminska, R. D. Thomas, M. Larsson, T. J. Millar, C. Walsh, and W. D. Geppert, Astrophys. J. **695**, 317 (2009).
[77] D. Strasser, L. Lammich, S. Krohn, M. Lange, H. Kreckel, J. Levin, D. Schwalm, Z. Vager, R. Wester, A. Wolf, and D. Zajfman, Phys. Rev. Lett. **86**, 779 (2001).
[78] A. Larson, A. Le Padellec, J. Semaniak, C. Stromholm, M. Larsson, S. Rosen, R. Peverall, H. Danared, N. Djuric, G. H. Dunn, and S. Datz, Astrophys. J. **505**, 459 (1998).
[79] L. Vikor, A. Al-Khalili, H. Danared, N. Djurić, G.-H. Dunn, M. Larsson, A. Le Padellec, S. Rosén, and M. Af Ugglas, Astron. Astrophys. **344**, 1027 (1999).
[80] R. D. Thomas, F. Hellberg, A. Neau, S. Rosén, M. Larsson, C. R. Vane, M. E. Bannister, S. Datz, A. Petrignani, and W. J. van der Zande, Phys. Rev. A **71**, 032711 (2005).
[81] C. D. Molek, V. Poterya, N. G. Adams, and J. L. McLain, Int. J. Mass. Spectrom. **285**, 1 (2009).
[82] G. Angelova, O. Novotny, J. B. A. Mitchell, C. Rebrion-Rowe, J. L. Le Garrec, H. Bluhme, A. Svendsen, and L. H. Andersen, Int. J. Mass. Spectrom. **235**, 7 (2004).
[83] J. B. A. Mitchell, G. Angelova, C. Rebrion-Rowe, O. Novotny, J. L. Le Garrec, H. Bluhme, K. Seiersen, A. Svendsen, and L. H. Andersen, J. Phys.: Conf. Ser. **4**, 198 (2005).
[84] A. Ehlerding, F. Hellberg, R. Thomas, S. Kalhori, A.A. Viggiano, S.T. Arnold, M. Larsson, and M. af Ugglas, Phys. Chem. Chem. Phys. **6**, 949 (2004).
[85] R. Yelle, V. Vuitton, P. Lavvas, M. Smith, S. Horst, and J. Cui, AAS/Division for Planetary Sciences Meeting Abstracts, September 2009, Vol. 41, p. 17.07.
[86] W. D. Geppert, A. Ehlerding, F. Hellberg, J. Semaniak, F. Osterdahl, M. Kaminska, A. Al-Khalili, V. Zhaunerchyk, R. Thomas M. af Ugglas, A. Kallberg, A. Simonsson, and M. Larsson, Astrophys. J. **613**, 1302 (2004).
[87] Y. Osamura, K. Fukuzawa, R. Terzieva, and E. Herbst, Astrophys. J. **519**, 697 (1999).
[88] D. Young, J. Berthelier, M. Blanc, J. Burch, A. Coates, R. Goldstein, M. Grande, T. Hill, R. Johnson, V. Kelha, D. Mccomas, E. Sittler, K. Svenes, K. Szego, P. Tanskanen, K. Ahola, D. Anderson, S. Bakshi, R. Baragiola, B. Barraclough, R. Black, S. Bolton, T. Booker, R. Bowman, P. Casey, F. Crary, D. Delapp, G. Dirks, N. Eaker, H. Funsten, J. Furman, J. Gosling, H. Hannula, C. Holmlund, H. Huomo, J. Illiano, P. Jensen, M. Johnson, D. Linder, T. Luntama, S. Maurice, K. Mccabe, K. Mursula, B. Narheim, J. Nordholt, A. Preece, J. Rudzki, A. Ruitberg, K. Smith, S. Szalai, M. Thomsen, K. Viherkanto, J. Vilppola, T. Vollmer, T. Wahl, M. Wuest, T. Ylikorpi, and C. Zinsmeyer, Space Sci. Rev. **114**, 1 (2004).
[89] J. H. Waite, D. T. Young, T. E. Cravens, A. J. Coates, F. J. Crary, B. Magee, and J. Westlake, Science **316**, 870 (2007).
[90] R. Brown, J.-P. Lebreton, and H. Waite, *Titan from Cassini-Huygens* (Springer, New York, 2009).
[91] N. Carrasco, S. Plessis, and P. Pernot, Int. J. Chem. Kinet. **40**, 699 (2008).
[92] V. Vuitton, R. V. Yelle, and M. J. McEwan, Icarus **191**, 722 (2007).
[93] A. Coustenis, A. Salama, B. Schulz, S. Ott, E. Lellouch, T. Encrenaz, D. Gautier, and H. Feuchtgruber, Icarus **161**, 383 (2003).
[94] A. Coustenis, R. K. Achterberg, B. J. Conrath, D. E. Jennings, A. Marten, D. Gautier, C. A. Nixon, F. M. Flasar, N. A. Teanby, B. Bézard, R. E. Samuelson, R. C. Carlson, E. Lellouch, G. L. Bjoraker, P. N. Romani, F. W. Taylor, P. G. J. Irwin, T. Fouchet, A. Hubert, G. S. Orton, V. G. Kunde, S. Vinatier, J. Mondellini, M. M. Abbas, and R. Courtin, Icarus **189**, 35 (2007).
[95] J. H. Waite, H. Niemann, R. V. Yelle, W. T. Kasprzak, T. E. Cravens, J. G. Luhmann R.L. McNutt, W.-H. Ip, D. Gell, V. De La Haye, I. Muller-Wordag, B. Magee, N. Borggren, S. Ledvina, G. Fletcher, E. Walter, R. Miller, S. Scherer, R. Thorpe, J. Xu, B. Block, and K. Arnett, Science **308**, 982 (2005).
[96] V. Vuitton, R. V. Yelle, and J. Cui, J. Geophys. Res. **113**, E05007 (2008).
[97] J. Semaniak, B.F. Minaev, A.M. Derkatch, F. Hellberg, A. Neau, S. Rosen, R. Thomas, M. Larsson, H. Danared, A. Paal, and M. af Ugglas, Astrophys. J., Suppl. Ser. **135**, 275 (2001).
[98] V. Vuitton, R. V. Yelle, and V. G. Anicich, Astrophys. J. **647**, L175 (2006).
[99] Note that there is a running controversy about a systematic discrepancy factor of about 3 between ion densities measured by INMS and those measured by the CAPS instrument (Ref. 90). Whereas in our model the absolute production rates of neutrals species by DR scale as the squared value of this factor, all the results presented in this work are based on ratios of production rates, and therefore totally independent of it.
[100] G. Israël, C. Szopa, F. Raulin, M. Cabane, H. B. Niemann, S. K. Atreya, S. J. Bauer, J.-F. Brun, E. Chassefière, P. Coll, E. Condé, D. Coscia, A. Hauchecorne, P. Millian, M.-J. Nguyen, T. Owen, W. Riedler, R. E. Samuelson, J.-M. Siguier, M. Steller, R. Sternberg, and C. Vidal-Madjar, Nature (London) **438**, 796 (2005).
[101] N. Carrasco, I. Schmitz-Afonso, J.-Y. Bonnet, E. Quirico, R. Thissen, O. Dutuit, A. Bagag, O. Laprévote, A. Buch, A. Giulani, G. Adandé, F. Ouni, E. Hadamcik, C. Szopa, and G. Cernogora, J. Phys. Chem. A **113**, 11195 (2009).
[102] P. Pernot, N. Carrasco, R. Thissen, and I. Schmitz-Afonso, Anal. Chem. **82**, 1371 (2010).
[103] N. Balucani, F. Leonori, R. Petrucci, M. Stazi, D. Skouteris, M. Rosic, and P. Casavecchia, "Formation of nitriles and imines in the atmosphere of Titan: Combined crossed-beam and theoretical studies on the reaction dynamics of excited nitrogen atoms N(2D) with ethane," Faraday Discuss. (in press).
[104] N. Balucani, A. Bergeat, L. Cartechini, G. G. Volpi, P. Casavecchia, D. Skouteris, and M. Rosi, J. Phys. Chem. A **113**, 11138 (2009).
[105] S. Lebonnois, E. L. O. Bakes, and C. P. McKay, Icarus **159**, 505 (2002).
[106] S. Lebonnois, Planet. Space Sci. **53**, 486 (2005).
[107] P. P. Lavvas, A. Coustenis, and I. M. Vardavas, Planet. Space Sci. **56**, 67 (2008).
[108] S. Lebonnois, E. L. O. Bakes, and C. P. McKay, Icarus **161**, 474 (2003).
[109] H. L. DeWitt, M. G. Trainer, A. A. Pavlov, C. A. Hasenkopf, A. C. Aiken, J. L. Jimenez, C. P. McKay, O. B. Toon, and M. A. Tolbert, Astrobiology **9**, 447 (2009).
[110] E. Sciamma-O'Brien, N. Carrasco, C. Szopa, A. Buch, and G. Cernogora, Icarus **209**, 704 (2010).
[111] V. Wakelam, American Astronomical Society Meeting Abstracts, May 2009, Vol. 214, p. 402.15.

[112] A. Gelman, J. B. Carlin, H. S. Stern, and D. B. Rubin, *Bayesian Data Analysis* (Chapman and Hall, London, 1995).
[113] M. Abramowitz and I. A. Stegun, *Handbook of Mathematical Functions with Formulas, Graphs, and Mathematical Tables* (Dover, New York, 1964).
[114] T. J. Santner, B. J. Williams, and W. I. Notz, *The Design and Analysis of Computer Experiments* (Springer-Verlag, New York, 2003).
[115] G.-L. Tian, H.-B. Fang, M. Tan, H. Qin, and M.-L. Tang, J. Multivariate Anal. **100**, 1854 (2009).
[116] K.-T. Fang and Z.-H. Yang, Stat. Probab. Lett. **46**, 113 (2000).